GEMINI CATIONIC SURFACTANT-BASED DELIVERY SYSTEMS FOR NON-INVASIVE CUTANEOUS GENE THERAPY

A Thesis Submitted to

the College of Graduate Studies and Research

in Partial Fulfillment of the Requirements

for the Degree of Doctor of Philosophy

in the College of Pharmacy and Nutrition

University of Saskatchewan

Saskatoon, Saskatchewan

By

Ildiko Badea

PERMISSION TO USE

In presenting this thesis in partial fulfillment of the requirements for a Postgraduate degree from the University of Saskatchewan, I agree that the Libraries of this University may make it freely available for inspection. I further agree that permission for copying of this thesis in any manner, in whole or in part, for scholarly purposes may be granted by Dr. Marianna Foldvari who supervised my thesis work or, in her absence, by the Dean of the College of Pharmacy and Nutrition. It is understood that any copying, publication or use of this thesis or parts thereof for financial gain shall not be allowed without my written permission. It is also understood that due recognition shall be given to me and to the University of Saskatchewan in any scholarly use which may be made of any material in my thesis.

Requests for permission to copy or to make other use of material in this thesis in whole or part should be addressed to:

Dean of the College of Pharmacy and Nutrition

University of Saskatchewan

Saskatoon, Saskatchewan, S7N 5C9

ABSTRACT

Gene transfer represents an important advance in the treatment of both genetic and acquired diseases. Topical gene therapy involves administration of the genetic material onto the surface of skin and mucosal membranes. Cationic gemini surfactants (*m*-*s*-*m*, where *m* represents the carbon atoms in the alkyl tail and *s* represents the carbon atoms in the spacer) are a novel category of delivery agents with especially high potential for polynucleotides. This is due to their structural versatility, ability to bind and condense DNA, and relatively low toxicity.

The objectives were to design, construct and characterize a cationic, non-viral gemini surfactant-based delivery system for an IFN-γ coding plasmid suitable for cutaneous gene therapy and to evaluate this novel therapeutic approach in a Tsk (tight-skin scleroderma) mouse model to determine its clinical feasibility.

The delivery systems were characterized by microscopy, dynamic light scattering (DLS), circular dichroism (CD) and small angle X-ray scattering (SAXS). *In vitro* gene expression was evaluated in PAM 212 keratinocyte culture. The extent of topical delivery of the plasmid using nanoparticle and nanoemulsion formulations was evaluated by measuring IFN-γ levels in CD1, IFN-γ-deficient and Tsk mice. The effect of transgene expression on collagen synthesis was evaluated in Tsk animals by real-time PCR.

The *in vitro* plasmid–gemini–lipid (PGL) system showed heterogeneous particle size (100-200 nm small particles and 300-600 nm aggregates). Electrostatic interactions

between the DNA and PGL systems shifted the negative ζ-potential of the DNA (-47 mV) to positive values (30-50 mV). At the same time, condensation of the DNA, and formation of Ψ^- DNA was indicated by the increase of the overall negative signal in the CD spectra, due to the flattening of the 290 nm peak and shift of the 260 nm peak into the negative region in a structure-dependent manner. Lipid organization of the DNA–DOPE system, in the absence of gemini surfactants, shows hexagonal structure, while addition of gemini surfactant at +/- charge ratio of 10 caused lamellar phase organization. For short spacers (n=3-6), additional *Pn3m* cubic phase also appear to be present.

In vitro transfection efficiency in the 12-n-12 series was found to be dependent on the length of the spacer between the two positively charged head groups, with the n=3 spacer showing the highest activity. The PGL systems with 12-3-12 and 12-4-12 led to significantly higher transgene expression compared to the other surfactants of the series. The transfection efficiency significantly correlated with the surface area occupied by one molecule (a). The effect of the tail length influenced the transfection efficiency, with longer tails being associated with higher protein expression. The highest *in vitro* transfection efficiency was recorded with the 18:1-3-18:1 surfactant (1.4±0.3 ng/5x10^4 cells).

In vivo, high levels of IFN-γ expression were detected in the skin of animals treated with both nanoparticle (359±239 pg/cm^2) and nanoemulsion (607±411 pg/cm^2) formulations compared to topical naked DNA (136±125 pg/cm^2). IFN-γ levels in the skin of animals injected with 5 μg DNA were 256±130 pg/cm^2. IFN-γ levels in the lymph nodes were higher for the nanoparticle formulation (433±456 pg/animal)

compared to nanoemulsion (131±136 pg/animal) suggesting different delivery pathway of the two formulations.

IFN-γ expression was at high levels in the skin of Tsk mice after 4-day and 20-day treatments (472±171 and 345±276 pg/cm^2). Both 4-day and 20-day treatments reduced the procollagen type I α1 mRNA levels for the topical treatment (64 and 70% reduction) and intradermal injection (58 and 72% reduction). Intercellular adhesion molecule-1 (ICAM-1) was upregulated by 50% in both topically treated and injected animals after 20-day treatment.

Here, it has been demonstrated that cationic gemini surfactant-based delivery systems are able to transfect epidermal cells *in vivo*, and the transgene IFN-γ expression is sufficient to cause significant reduction of collagen in an animal model of scleroderma. It has been shown for the first time that topical gene therapy is a feasible approach for the modulation of excessive collagen synthesis in scleroderma-affected skin.

ACKNOWLEDGEMENTS

I would like to thank my supervisor, Dr. Marianna Foldvari for her professional and moral support and guidance. I thank the members of the advisory committee, Drs. Ronald Verrall, Adil Nazarali, Suresh Tikoo, Alan Rosenberg and Maria Baca-Estrada for their guidance.

I thank Dr. Shawn Wettig for technical assistance regarding small-angle X-ray scattering. I thank Mukasa Bagonluri, Deborah Michael and McDonald Donkuru for technical support. I also thank Martin Abu, Drs. Praveen Kumar and Martin King from PharmaDerm Laboratories Ltd. (Saskatoon, SK) for their insights; Drs. Shawn Babiuk and Donna Mahony from Vaccine and Infectious Disease Organization (Saskatoon, SK) for assistance regarding molecular biology techniques. The atomic force and confocal microscopy images were obtained with the technical assistance of Jason Maley and Dr. Sophie Brunet from the Saskatchewan Structural Sciences Centre (Saskatoon, SK).

I recognize the following institutions: Vaccine and Infectious Disease Organization (Saskatoon, SK), PharmaDerm Laboratories Ltd. (Saskatoon, SK) and the National Synchrotron Light Source (Brookhaven National Laboratory, NY) for the use of instruments and equipment.

The work presented here was supported by grants from the Canadian Institute of Health Research and the Natural Science and Engineering Research Counsel of Canada.

DEDICATION

I dedicate this work to my husband, Dr. Alin Badea and my daughter, Andreea Badea.

TABLE OF CONTENTS

LIST OF TABLES

LIST OF FIGURES

LIST OF ABBREVIATIONS

AAV	adeno-associated virus
AFM	atomic force microscopy
CD	circular dichroism
cDNA	complementary DNA
CMC	critical micellar concentration
CMV	cytomegalovirus
CTGF	connective tissue growth factor
Dc-chol	3ß-[N-(N',N'-dimethylaminoethane)-carbamoyl]cholesterol hydrochloride
DLPE	dilauroylphosphatidylethanolamine
DLS	dynamic light scattering
DMPE	dimiristoylphosphatidylethanolamine
DODAB	dioctadecyldimethylammonium bromide
DODAC	dioctadecyldimethylammonium chloride
DOPE	dioleylphosphatidylethanolamine
DOSPA	2,3-dioleyloxy-N-[2(sperminecarboxyamido)ethyl]-N,N-dimethyl-1-propaniminium bromide
DOTAP	1,2-dioleoyl-3- (trimethylammonium) propane
DOTMA	N-[1-(2,3-dioleyloxy)propyl]-N,N,N-trimethylammonium chloride
DPPC	dipalmitoyl phosphatidylcholine
DPPE	dipalmitoylphosphatidyl ethanolamine
DPyPE	diphytanoylphosphatidylethanol-amine
DSC	differential scanning calorimetry
DSPE	distearoylphosphatidylethanolamine
ELISA	enzyme-linked immunosorbent assay
EMC	endomyocarditis
FACS	fluorescence activated cell sorting
FRET	fluorescence resonance energy transfer
GFP	green fluorescent protein
GM-CSF	granulocyte-macrophage colony-stimulating factor
HMGB	high-mobility group box
ICAM	intercellular adhesion molecule
IFN	interferon
IL	interleukin
IRES	internal ribosomal recognition sequence
Jak/ STAT	Janus kinase/signal transducer and activator of transcription
LUV	large unilamellar vesicle
MACAF	monocyte chemotactic and activating factor
MLV	multilamellar vesicle
NC	nonionic/cationic liposome
NE	nanoemulsion
NP	nanoparticle
ODN	antisense oligonucletode
PC	phosphatidylcholine
PCR	polymerase chain reaction
PDGF	platelet-derived growth factor

PECAM	platelet endothelial cell adhesion molecule
PEG	polyethylene glycol
PEI	polyethylenimine
PG	plasmid–gemini complex
PGL	plasmid–gemini–DOPE system
PLL	poly-L-lysine
PSS	progressive systemic sclerosis
RT-PCR	reverse-transcription PCR
SAXD	small-angle X-ray diffraction
SAXS	small-angle X-ray scattering
SC	stratum corneum
SSc	systemic sclerosis
STAT	signal transducer and activator of transcription
TEM	transmission electron microscopy
TGF	transforming growth factor
TNF	tumour necrosis factor
Tsk	tight skin mouse
UCL	ultradeformable cationic liposomes
VEGF	vascular endothelial growth factor
WAXD	wide-angle X-ray diffraction
YB	Y box-binding protein

I. INTRODUCTION

I.1. General view on gene therapy

Gene transfer represents an important advance in the treatment of both genetic and acquired diseases. Gene therapy relies on the efficient transfer of DNA, RNA fragments or chimeric DNA-RNA molecules into cells. The goal is to correct a genetic mutation, create a new function by inserting a gene, or block gene overexpression. The modification can be permanent (best achieved by chromosomal insertion) or transient in the targeted cell or tissue. Genetic immunization is based on the delivery of DNA encoding for a foreign protein and its expression in cells. The *in situ* generated protein has the potential to induce both cell-mediated and humoral immune responses [1, 2]. The recombinant genetic material is carried by vectors of viral or non-viral type. Viral vectors include adenoviruses, adeno-associated virus or retroviruses. The efficiency of delivery of viral vectors is higher than non-viral systems, and this method can integrate the genes into chromosomes, causing permanent modification in the cell. Unfortunately, the immunogenicity of these carriers restricts their use. Moreover, the size of the inserted gene is limited (low packaging capacity), and large-scale production is difficult and costly. The non-viral vectors, plasmids and oligonucleotides, are transferred into cells via physical methods or chemical delivery agents. These vectors do not pose the safety issues of the viruses and are easy to prepare, but their efficiency is low, and can induce only transient gene expression. The successful introduction of recombinant

genetic material into mammalian cells and expression of these genes modifying cellular phenotypes in the1970s led to the recognition of the potential of this technique as a therapeutic tool. The early methods included chromosome transfer (cell fusion, chromosome-and microcell-mediated gene transfer), viral vectors (DNA and RNA viruses), physical methods (microinjection and electroporation) and chemical agents (calcium phosphate precipitation, polyethylene glycol and liposomes) [3]. The first successful treatment was reported in 1990 at the National Institute of Health. The patient was treated for adenosine deaminase deficiency causing severe immunodeficiency. In past decades, research has focused on genetic diseases such as cystic fibrosis [4], hemophilia [5, 6], sickle cell anemia, and Gaucher's disease. Important achievements can be mentioned in the treatment of acquired diseases (cancer, neurological disorders, cardiological disorders) as well [7]. Genodermatoses such as epidermal fragility, keratinization, hair, pigmentation disorders and cancer are candidates for topical gene therapy [8, 9].

A major setback for gene therapy occurred in 1999, when a patient suffering from ornithine transcarboxylase deficiency died from multiple organ failure in a clinical trial involving gene therapy. Moreover, in 2002 two children treated for X-linked severe combined immunodeficiency disease developed leukemia-like syndrome (http://ornl.gov/sci/techresources/). Due to these events, the question was posed: Is gene therapy a feasible approach? Recent advances such as mapping of human and animal genomes, development of new therapeutic tools such as small interfering RNAs, improved delivery systems, better designed *in vitro* and *in vivo* experiments, use of new analytical tools, such as synchrotron radiation, RNA and DNA microarrays and combination of these with advanced computational systems, will provide the answer.

Currently, 520 ongoing clinical trials in the US (http://www.clinicaltrials.gov/) are focusing on both gene therapy and genetic immunization. Although most are oriented towards cancer therapy, some trials are exploring treatment options for other genetic or acquired diseases. Some of the trials involve *ex vivo* methods. For example, genetically modified fibroblasts producing human nerve growth factor are intracerebrally injected in Alzheimer's patients in order to reduce neuronal atrophy (Clinical Trials.gov ID: NCT00017940). Patients with homozygous familial hypercholesterolemia can be treated with autologous hepatocytes transduced with a normal low-density lipoprotein receptor gene (Clinical Trials.gov ID: NCT00004809). Gaucher's disease is caused by the absence of glucocerebrosidase due to a genetic deficiency inducing glycocerebroside accumulation in macrophages. *Ex vivo* transduction of bone marrow stem cells with retroviruses containing the human glucocerebrosidase gene and transplantation in patients could provide the necessary enzyme levels (Clinical Trials.gov ID: NCT00001234). Systemic administration of DNA is involved in several clinical trials. Duchenne muscular dystrophy (DMD) is a fatal muscle degenerative disorder, caused by mutations in the dystrophin gene. Antisense oligonucleotides can be used to restore the production of dystrophin by exon skipping and improve muscle survival and function (Clinical Trials.gov ID: NCT00159250). Patients with diabetic neuropathy and macrovascular disease can be treated by intramuscular administration of a plasmid containing the cDNA for vascular endothelial growth factor (Clinical Trials.gov ID: NCT00056290). In another study, human clotting factor IX (inserted in adeno-associated virus vector) will be injected into the liver of patients suffering from severe hemophilia B (Clinical Trials.gov ID: NCT00076557).

Topical gene therapy involves administration of the genetic material onto mucosal membranes (lungs, conjunctiva, oral and rectal cavities) and the surface of the skin. Cystic fibrosis transmembrane conductance regulator gene (CFTR) can be delivered to the cells lining the nose of cystic fibrosis patients using cationic liposome mediated gene transfer (Clinical Trials.gov ID: NCT00004471) or adenovirus vector (Clinical Trials.gov ID: NCT00004779). Platelet-derived growth factor-B (*PDGF-B*) gene can improve the healing of chronic wounds especially frequent in diabetic patients. Injection of the genetic material into the wound can generate PDGF-β, improving the clinical appearance of chronic wounds compared to previous methods of direct application of wound-healing substances (Clinical Trials.gov ID: NCT00065663 and NCT00000431). Particle bombardment of unaffected skin with DNA (gp100 and granulocyte macrophage colony stimulating factor (GM-CSF) cDNA) coated gold beads is a therapeutic option for malignant melanoma patients. The two proteins, gp100 and GM-CSF, can help the body build immune response and kill the tumour cells (Clinical Trials.gov ID: NCT00003897).

Presently, no clinical trials use gene delivery to intact skin for treatment of skin disorders. However, research in the last decade is progressing towards improvement of the delivery systems and extension of gene therapy to genodermatoses.

I.2. DNA delivery systems

I.2.1. Naked DNA

There are many advantages of using DNA-based drugs (therapeutic genes) compared to the delivery of proteins. Proteins are relatively unstable molecules and require intact tertiary and quaternary structure for their activity, whereas DNA is more stable and only chemical alterations can cause loss of potency, as nucleic acid sequence is most important for its function [10]. Using plasmid DNA for delivery of the therapeutic genes could yield sustained protein expression at the site of application. Although biologically active interferon (IFN)-γ in a liposomal system could be delivered through skin [11], the short half life of the cytokine might require frequent administration, whereas DNA application could generate proteins for a longer period of time. Since the size of the gene is not a limiting factor in plasmid vectors, several therapeutic genes could be inserted in the same backbone, and expressed concomitantly at the target site.

The discovery of plasmid vector systems as a tool in molecular biology was an important breakthrough in gene therapy. Potentially infectious polyoma virus DNA was inserted into plasmids and the recombinant DNA was tested in mouse cells and mice. The injected plasmid did not cause infection in mice. Moreover, live *E.coli* containing the recombinant polyoma virus plasmid DNA were also unable to induce infection by either ingestion in a food source or parenteral injection [12].

The capability of plasmids to generate proteins was tested by microinjection into *Xenopus laevis* oocyte nuclei [13-15]. The ability of the transgene to integrate into the

host genome of mouse eggs [16] and cultured mammalian cells [17, 18] was also demonstrated. Although, early studies show that gene expression can only be achieved by nuclear injection [19], it was later demonstrated that plasmid injected into the cytoplasm could also be expressed [20]. Further studies demonstrated transfection with circular plasmids led to transient gene expression, and only a few copies integrated into the chromosomal DNA. The reference gene, chloramphenicol acetyltransferase (CAT), expression declined from 10 units/g tissue at 24 hours to 4.6 units at 72 hours. No CAT activity could be detected after 96 hours [21].

Subsequently, the use of DNA-based drugs for therapeutic purposes emerged and studies demonstrated that proteins could be generated *in vivo*. Studies with non-fasting male Wistar rats injected intravenously with liposome-encapsulated plasmid containing the gene for rat insulin I showed that the gene penetrates mainly the liver and spleen, causing significant reduction of the glucose level and a simultaneous increase in the blood insulin level. The effect lasted for about 10 hours [22]. Integration and even longer expression can be achieved by the use of viral vectors (up to 48 hours) [23, 24] or use of linear double stranded DNA [25].

DNA molecules are negatively charged, high molecular weight compounds, an impediment in the spontaneous transfection procedure. Poor expression is due to membrane barriers and enzymatic processes. In a recent review, several barriers were identified in the efficient delivery of DNA-based drugs after intravenous administration:(1) physicochemical properties, such as the size of the DNA–cationic lipid complexes and the strength of the interaction; (2) interaction with blood components such as albumin; (3) recognition by the immune system and phagocytosis; (4) permeation through blood vessels; (5) slow uptake by target cells; (6) endosomal

release; (7) cytoplasmic stability; and (8) nuclear localization [26, 27] and immune response triggered by the foreign genetic material [28, 29]. A detailed description of transfection barriers is offered by Varga et al. [30]. Researchers recognized that due to these drawbacks delivery issues would arise when the genetic material was used as a therapeutic drug.

Structural characteristics of DNA could be the starting point in the design of delivery systems. There are three known conformations of DNA: A-, B- and Z-DNA. B-DNA is considered the native form of DNA, since its X-ray diffraction pattern is similar to the DNA found in intact sperm heads. A- and Z-DNA have been found only in certain biological contexts such as sporulation, protein binding, salt concentration, or environmental conditions such as salt concentration and relative humidity. Parameters such as the diameter of the DNA double strand, helical sense, the shape of major and minor grooves, helix pitch and rise (Figure I.1) are specific for each conformation (Table I.1) [31]. These parameters are essential for modeling purposes. In order to design cationic delivery agents, knowing the sterical arrangement of the phosphate groups is important. Di- and polycationic agents could bind adjacent phosphates of the helix rise (at a distance of 3.32Å for the B-DNA) or helix pitch (at 33.2 Å) depending on the distances between the positively charged moieties. The width and depth of the minor and major grooves could determine the properties of the groove-binding agents. The major groove of the B-DNA is wide and deep, and the minor groove is narrow and shallow.

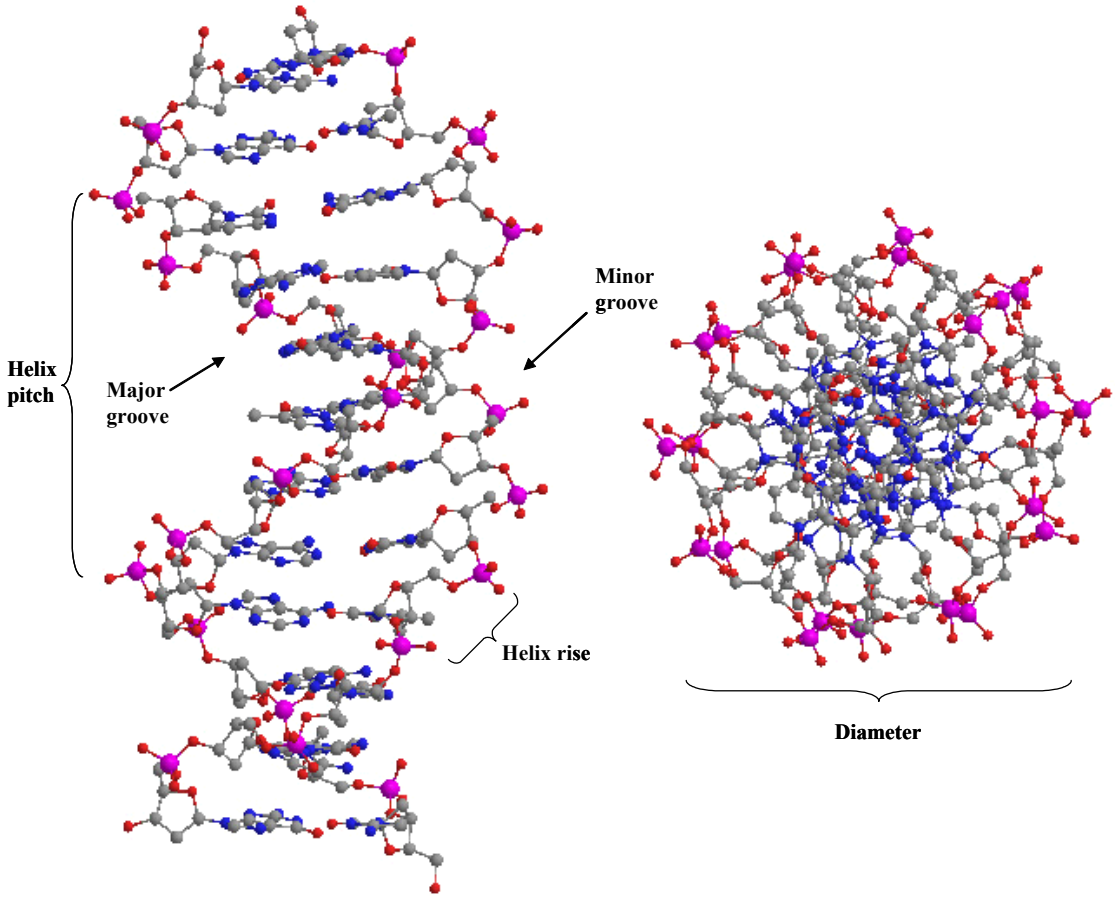

Figure I.1. The structure of B-DNA represented by stick-and-ball model.

The view on the left is perpendicular to the axis, and on the right is down the axis. Carbon atoms are gray, oxygen atoms red, nitrogen atoms blue and phosphorus atoms pink, respectively. The structure is derived from PDB structure 264D (http://www.rcsb.org)

Table I.1. Properties of A-, B- and Z-DNA conformations.

Property [31]	**A-Form**	**B-Form**	**Z-Form**
Helical sense	Right-handed	Right-handed	Left-handed
Repeating helix unit	1 base pair	1 base pair	2 base pairs
Rotation/base pair (degrees)	33.6	35.9 +/- 4.2	-60/2
Mean base pairs/turn	10.7	10.0 +/- 1.2	12
Inclination of base normals to helix axis (degrees)	+19	-1.2 +/- 4.1	-9
Rise/base pair along helix axis (Å)	2.3	3.32 +/- 0.19	3.8
Pitch/turn of helix (Å)	24.6	33.2	45.6
Mean propeller twist (degrees)	+18	+16 +/- 7	~0

After intravenous injection, foreign DNA is destroyed by scavenger cells, with the half life of naked plasmid being less than 10 minutes [32]. One of the first delivery attempts involved direct injection of the plasmid into cells. In this case, the barriers to protein expression were the destruction of the DNA by the endonucleases and penetration through the nuclear pores into the nucleus. This method required specialized equipment and personnel, and was not feasible for clinical application.

Injection of naked DNA into various tissues (muscle, skin, tumour) showed protein expression could be achieved at the site of injection. When the plasmid is injected into the tissue, some cells are pierced thereby facilitating the penetration of the plasmid leading to high protein levels around the injection sites. For example, recent studies demonstrate direct injection of naked plasmid containing genes of several cytokines such as interleukin (IL)-4, IL-6, IL-10, transforming growth factor (TGF)-β1, monocyte chemotactic and activating factor (MACAF), GM-CSF, tumour necrosis factor (TNF)-α and IFN-γ into the skin markedly increase levels of these cytokines at the site of injection. IL-4, IL-6 and IL-10 were also detected in the serum levels high enough to exert biological effect [33]. This demonstrates that direct injection can be used as a delivery tool for plasmid DNA into the tissue. Another example is the application of naked DNA onto damaged tissue. Platelet-derived growth factor A and B chain genes were inserted in plasmid vectors and used in lyophilized collagen pads to treat experimentally induced ischemic dermal ulcer in rabbit. By applying the pads on the wounds, the DNA can directly enter the cells of the damaged tissue. The volume of granulation tissue formation as well as epithelization and wound closure were evaluated after 10 days. A significant increase in new granulation tissue formation was observed when the collagen pads contained 1 mg plasmid versus empty collagen pads.

Application of pads loaded with 2 mg plasmid caused another 15% increase over the 1-mg plasmid pads [34]. One of the practical applications of this study would be in chronic wound healing. Another study demonstrated that injection of naked DNA can result in delivery to the circulatory system, a useful feature for application in peripheral arterial occlusive disease [35]. Gene therapy can be employed as a potential treatment for myocardial and lower limb ischemia. Plasmid DNAs encoding for three isotypes of the angiogenic cytokine vascular endothelial growth factor were injected into ischemic skin flaps in rat. The flap survival and angiogenesis were assessed after 7 days. The results show significant flap survival in one of the isotypes, suggesting that plasmid transfection could be used as a supplementary tool in reconstructive surgery [36].

Increasing the ionic strength in the phosphate buffered saline (PBS) vehicle (1.5x and 3x PBS) used for injecting DNA led to higher transfection efficiency in mice after intradermal injections than using physiological buffer [37]. The physiological effect of the delivered DNA is dose dependent; inadequate concentrations are not able to generate enough protein, but very large doses also have a negative effect on protein expression. In a study using two plasmids coding for keratinocyte growth factor and insulin-like growth factor, three different doses of DNA (0.22 μg, 2.2 μg and 22 μg) were injected into the skin. Therapeutic parameters characteristic for wound healing were monitored, and the highest therapeutic effects for both plasmids were found at the 2.2 μg dose [38].

Although the direct injection method is not feasible for all candidates for gene therapy, it is the most frequently employed method in current clinical trials. For example, therapeutic protein is generated for treatment of angina (ClinicalTrials.gov identifier: NCT00090714) by cardiac injection of plasmid carrying the VEGF gene. Human clotting factor IX gene inserted into adeno-associated virus (AAV) vector

injected into the liver was approved for testing in hemophilia B patients (ClinicalTrials.gov identifier NCT00076557). Direct injection into tumour tissue of genes coding for cytokines (IL-2, IL-12), immunostimulatory proteins, and antigens was proposed for treatment of melanoma, breast, ovary, colorectal, liver and renal cancers.

I.2.2 Lipid-based delivery systems for DNA

In order to treat certain diseases where direct injection of the genetic material is not feasible (e.g., metastatic tumours, genodermatoses with extensive lesions, conditions affecting the brain) or non-invasive methods are preferred (pediatric and geriatric patients, mass vaccination), new delivery systems are necessary in order to efficiently deliver DNA to the site of action. The role of delivery systems is to overcome cellular and molecular obstacles without invasive intervention [39]. The cell membrane is a common barrier whether viral or non-viral carriers are used. Macromolecules penetrate the cell membrane by endocytosis. Targeted receptor-mediated uptake, achieved by conjugation of the delivery vectors with targeting moieties, could direct delivery to certain cells or tissues. Intracellular trafficking can also pose challenges. If not protected, the genetic material can be destroyed in the lysosomes. Polymers are used for their buffering capacity. They facilitate extravasation by increasing membrane permeabilization, allowing the DNA to pass into the cytoplasm. The endonucleases present inside the cell can also destroy the foreign DNA. Cationic agents can shield the DNA from the effect of DNase. In order to increase the penetration of the genes into the cell nucleus, nuclear localization peptides can be used to guide the transport of DNA in the cytoplasm. Transcription, translation and plasmid dilution can also hinder protein expression. Pharmacokinetic models can be utilized to evaluate which are the rate

limiting steps in protein expression. Factors such as complex internalization, endosomal escape, DNA unpacking, nuclear pore targeting, nuclear import, plasmid degradation, dilution, and protein production have been evaluated. Computational models of known agents can help to predict the effect of various compounds. Unfortunately, *in vitro* modeling does not always correlate with *in vivo* results.

Liposomes, discovered by Alec Bangham, were used as membrane models [40], and later as drug delivery vehicles [41]. In the 1980s the potential of the liposomes as delivery agents for macromolecules, e.g., DNA, was also evaluated [42]. By liposomal encapsulation, the therapeutic index of the drugs can be increased and specific cells can be targeted [43]. Certain types of lipid-based delivery systems can efficiently deliver DNA into the cell *in vivo*. Liposomes having relatively low cellular toxicity can be used for the transfection of various cell types; the efficiency is based on physical and chemical characteristics of the building elements of the liposomes.

By using cationic lipids, electrostatic interactions take place between the positive charges in the delivery agent and the negative charges on the phosphate backbone of the DNA. The phosphate groups of the DNA are neutralized by the positively charged lipids and the DNA is compacted thereby facilitating the transfer through cell membranes. Cationic lipids can also protect DNA against degradation by endonucleases. The cationic to anionic charge ratio (+/- ratio) plays an important role in the evaluation of delivery efficiency of various agents. A wide variety of cationic lipids has been described in the literature as macromolecular delivery agents. Several synthetic positively charged 2,3-dialkyloxypropyl quaternary ammonium compounds have been described in the literature to increase transfection efficiency of plasmid DNA *in vitro* [44-48]. Plasmid DNA–alkylphospholipid (APL) lipoplexes containing DODAB (Table I.2) injected into

tumours significantly reduced tumour size compared to naked DNA and Lipofectin–DNA complexes [49]. Moreover, intravenous preinjection of 3-tetradecylamino-N-tert-butyl-N'-tetradecyl propionamidine cationic liposomes followed by intravenous injection of plasmid-liposome complexes increased transfection efficiency 40 times, due to the inhibitory effect of the liposomes on the TNFα, which plays a role in triggering immune responses [50]. In addition to the classical approach of the monovalent quaternary ammonium compounds, such as DODAP and DOTAP (Table I.2), and cationic derivatives of cholesterol, new compounds such as reducible cationic lipids, disulphide-bond bearing lipids, acid-labile cationic lipids and glycine betaine derivatives were also tested in order to overcome the barriers of DNA delivery. Reducible cationic lipids bearing disulfide bonds improve the release of the DNA in the cytoplasm, where the bond is cleaved, the DNA is released and the transfection efficiency is improved 1000 fold [51]. Cationic lipids with acid-labile vinyl ether linkage are stable at neutral pH, but degrade in the acidic environment of the endosomes, promoting the escape of the DNA into the cytosol and increasing transfection 2-3 fold compared to the DOTMA-cholesterol system (Table I.2). The *in vivo* transfection efficiency of the two delivery systems in tumours was comparable [52]. Cationic cholesterol-derivative (Dc-chol), formulated in liposomes or emulsions was used to transfer DNA into the cells. The advantage of the compound lies in its high transfection efficiency and low cellular toxicity *in vitro*. The presence of serum reduced the transfection efficiency of the liposomal formulation, but had no effect on the emulsion-type formulations [53]. The transfection ability of the Dc-chol emulsion in the presence of serum makes these types of formulations suitable for parenteral administration. Another cationic sterol-derivative (dexamethasone–spermine) increased DNA delivery *in vitro* 10-fold at a +/- charge ratio

of 6, compared to Lipofectamine. The advantage of the system *in vivo* was the intrinsic anti-inflammatory property of the corticosteroid [54]. Ultradeformable cationic liposomes (UCL) prepared with DOTAP (Table I.2) showed *in vitro* transfection efficiency comparable with Lipofectamine, and were able to deliver plasmid DNA to the liver, kidney and lungs after transdermal application [55]. Some cationic lipids, especially monovalent lipids, present relatively high cytotoxicity and therefore their *in vivo* use is limited. Natural glycine betaine compounds covalently linked to acyl chains by enzymatically hydrolysable peptide and ester bonds showed reduced cytotoxicity and also improved transfection efficiency by 40% compared to commercial agents in cultured hepatocytes [56].

The efficiency of the cationic lipids as delivery systems can be augmented by incorporating neutral lipids in the delivery systems. Injected intramuscularly, DOTAP (Table I.2) containing liposomes (dehydration/rehydration vesicles) entrapping plasmid DNA encoding for hepatitis B surface antigen triggered IgG production at significantly higher levels than naked DNA. The magnitude of the immune response was dependent on the nature of the helper lipid, the highest being with phosphatidylcholine (PC)–DOPE–DOTAP vesicles compared to dipalmitoyl phosphatidylcholine (DPPC) or cholesterol-containing liposomes [57].

A helper lipid, added to the cationic lipid–DNA complexes, can increase both the stability of the delivery system and its *in vitro* and *in vivo* transfection efficiency. For example, solid nanoparticles having a cetylpalmitate core and containing positively charged lipids, such as cetylpyridimium chloride, CTAB, dimethyldodecyl ammonium bromide or DOTAP (Table I.2), transfected mammalian cells more efficiently than DNA–PEI (Table I.2) complexes. *In vivo* efficiency was not reported in this publication

[58]. Creating highly stable particles (no aggregation and polydispersity) under 100 nm in size can be achieved by template-driven assembly of the nanoparticles. For this purpose, detergents with an alkyl chain of 12-18 carbons and an isothiuronium head group are cleaved in controlled conditions to reveal a reactive thiol group. Accumulated on the DNA template, these groups form disulfide-linked lipids containing two alkyl chains. Complex formation was evaluated by fluorescence assay, particle size and ζ potential measurements, electron microscopy and thin layer chromatography. Fibroblasts from monkey kidney (CV-1 cells) transfected with the complexes showed high efficiency when combined with fractured dendrimers to increase cell association of the complexes [59].

A comparison of several helper lipids (dilauroylphosphatidylethanolamine (DLPE, C12:0), dimiristoylphosphatidylethanolamine (DMPE, C14:0), dipalmitoyl-phosphatidylethanolamine (DPPE, C16:0), diphytanoylphosphatidylethanolamine (DPyPE, C16:0 branched), distearoylphosphatidylethanolamine (DSPE, C18:0), and dioleylphosphatidylethanolamine (DOPE, C18:1)) showed that branched and unsaturated species combined with cationic lipids act in "physical synergism" to increase transfection efficiency [60].

Co-lipids such as DOPE have been widely used for their membrane-active properties, namely the ability to induce hexagonal lipid conformation [61, 62]. DOPE has been associated with a variety of cationic compounds such as cationic lipids [63-72], cholesterol derivatives [71, 73, 74] and poly-L-lysine [75].

The role of the cationic lipids, as presented here, is (1) compaction of the DNA molecule so it can penetrate through the cell membranes, (2) protection of the genetic material inside the cells from degradation by endonucleases, and (3) release of the free

DNA to cross the nuclear membrane. However, as mentioned above, the transfection efficiency of the cationic lipid-based delivery systems is much lower than the viral vectors. Several ways can improve gene expression. In the literature, three areas are targeted: (1) compaction of the DNA and penetration of the cell membrane, including tissue-specific targeting, (2) escape from the endosomes and dissociation of the complexes, and (3) nuclear targeting. New delivery agents could target peptides to facilitate the uptake by certain cells, fusogenic peptides and lipids to increase membrane permeability, acid-labile compounds and polymers to facilitate lysosomal escape, biodegradable compacting agents to help DNA unpacking, and nuclear targeting sequences to direct the DNA towards the nucleus.

The first step of efficient gene expression is the efficient transport of the macromolecule through the cell membrane. Peptides such as sequences of Tat protein from human immunodeficiency virus (HIV) and adenine nucleotide translocator (Ant) protein can promote cellular uptake of macromolecules. Poly(3-guanidinopropyl methacrylate), a polycationic agent that mimics the effect of these peptides, was able to deliver DNA into cells at higher efficiency compared to polyarginine-based agents. This compound can introduce the genetic material into the cells due to its penetration and DNA-compaction properties [76]. Another example of increased cellular uptake is fusogenic liposomes formulated with anionic 1,2-dioleyl-phosphoethanolamine-N-dodecanoyl (N-C12-DOPE) and DOPC encapsulating spermine-compacted DNA. These complexes efficiently transfected OVCAR-3 cells *in vitro* and ovarian cancer cells *in vivo* after intraperitoneal injection. This agent also showed significantly lower toxicity than cationic delivery agents [77]. Another delivery approach is cross-linked delivery systems. Short peptides containing multiple cysteine residues are able to form disulfide

bonds after binding the DNA, and increase the condensation of the DNA molecule. The transfection efficiency of cross-linked peptides was 5-60 times higher than non-cross-linked peptides *in vitro* [78, 79]. Monovalent surfactants can form multivalent cationic sheaths on a DNA template, using cysteine-based detergent to avoid aggregation [80].

Targeting naturally endocytosed receptors on the cell surface, such as integrin, is an attractive approach for enhanced gene delivery. PLL–molossin (Table I.2), a fusion peptide derived from American pit viper, coupled with a 16-lysine residue is one such ligand. For efficient delivery, exposing the cells to chloroquine (a buffering agent that inhibits lysosomal enzymes) to facilitate escape of the genetic material from the endosomes is necessary. Since efficient transfection of cells can be achieved after a fairly long contact time with the transfection agent, and additional chloroquine exposure of 8-10 hours, this method is suitable only for *ex vivo* delivery. The organs are exposed to the PLL–mollossin–DNA system followed by addition of chloroquine before transplantation [81]. One of the applications of this technique is in chronic allograft rejection whereby targeting vascular smooth muscle cells with non-viral vectors *ex vivo* could arrest or reverse the graft rejection [82].

Tissue-specific delivery can be achieved with TerplexDNA, created by complexation of plasmid DNA with stearyl-PLL and low-density lipoprotein (LDL). Increased cellular delivery into the heart and protein expression (elevated for up to 30 days) were observed. Levels of protein were significantly lower with naked DNA and lasted for only 5 days [83]. Similarly, after systemic administration of TerplexDNA in mice, protein expression persisted in major organs for 35 days versus naked DNA for only 7 days [84]. Mannose receptor-mediated gene transfer, a liver-targeting method, was carried out by intravenously injecting plasmid DNA complexed with mannosylated

PLL. These complexes selectively accumulated in the liver, measured by the amount of ^{32}P-labelled DNA, and achieved the highest protein expression compared to all other major organs [85]. Galactose-modified polyornithine had a similar effect, with 60% of the radioactivity of the ^{32}P-labelled DNA accumulating in the liver. Gene expression in the hepatocytes was higher with galactose-modified polyornithine compared to DOTMA–cholesterol liposome-encapsulated DNA [86]. Lipid-linked targeting peptides (RGD-DOPE), selected to deliver genes into epithelial cells, were able to increase transfection efficiency of the DOTMA-cholesterol-DNA complexes 10 fold. This improvement is important as it demonstrates that specifically designed peptides are able to target certain cell types (e.g., tumour cells) and increase the uptake of DNA, leading to higher transgene expression [87].

The release of DNA from endosomes and dissociation from the cationic components of the delivery system are important factors in efficient gene expression. Only free DNA can penetrate into the nucleus through the nuclear pores. Histidine-rich polylysine can complex DNA and facilitate DNA unpacking in the cytoplasm [88]. A similar effect can be achieved when poly-L-lysine (PLL) is coupled to nicotinic acid [89]. These compounds bind H^+ ions at low pH in the endosome/lysosome, facilitating the escape of genetic material from the vesicles (sponge effect). Unfortunately, quantitative comparison is not feasible since all experiments used different vectors, conditions and assays to evaluate plasmid delivery and gene expression. Similar roles have been described for dendritic PLL (DPK) of 6th generation. DPK was able to transfect cells comparably to the commercial agent. The probable mechanism of uptake of the complexes was macropinocytotic engulfing, and the release from the endosomes was mediated by the sponge-effect (the protonable moieties confer buffering capacity to

the molecule, causing swelling and rupture of the endosome) of the DPK [90]. Polyethylenimine (PEI) (Table I.2), a cationic polymer, efficiently absorbs on the surface of DNA and protects against endonucleases [91]. It acts as a proton sponge, thus facilitating release of the DNA from the endosomes [92]. PEI mediated gene transfer into pancreatic tumour disseminated into the peritoneal cavity due to the permeability of the peritoneal tissue [93]. Increased expression was observed when the DNA was complexed with linear PEI compared to the branched counterparts [94, 95]. Moreover, association with anti-platelet endothelial cell adhesion molecule (PECAM-1 or CD31) of the PEI–DNA complexes increases targeting of the pulmonary endothelium, with minimal systemic toxicity after intravenous administration [95]. Incorporation of receptor-targeting ligand into PEI–DNA complexes shielded with polyethylene glycol (PEG) enhances delivery of the genetic material to the tumour cells [96]. Combinations of polycation-condensed DNA with liposomal encapsulation are believed to further increase the uptake and expression efficiency of the plasmid [77, 97].

Fusogenic peptides (composed of short sequences of amino acids containing glutamates) derived from influenza virus hemagglutin increased 3-4 fold the transfection efficiency of Lipofectamine, a cationic lipid used for integrin receptor-targeted delivery of the PLL–mollossin–DNA vector. The mechanism of action probably relies on the more effective escape of the complexes from the endocytic vesicles [98].

Efficient intracellular trafficking of the DNA released form the endosomes is necessary for increased gene expression. Intradermal injection of DNA, complexed with high-mobility group box 1 (HMGB1) protein (having a DNA binding domain and a nuclear localization signal) and encapsulated into liposomes, increased gene expression 10 fold due to enhanced nuclear targeting [99].

Complex systems have been created to overcome cellular barriers and increase gene expression. New design approaches such as the "modular design" [100] combining different targeting strategies could be important in the future of non-viral gene therapy. For example, using cationic lipids such as DOPE to facilitate DNA uptake can be associated with targeting moieties such as transferrin to promote endocytosis [101]. Fusogenic peptides (influenza hemagglutin peptide) increase the escape of the DNA from endosomes/lysosomes [76, 102]. Combination with an integrin-targeted non-viral DNA vector (polylysine-molossin) can further improve gene expression [98]. *In vivo*, the delivery of genetic material can be further increased by preinjecting the animals with cloroquine, followed by the PLL–molosin–DNA system [103]. These examples illustrate that multicomponent systems including agents that condense and protect the genetic material, target specific cells, facilitate cellular uptake, enhance release from endosomes and mediate intracellular trafficking towards the nucleus are the future of non-viral gene delivery. The efficiency of these systems might approach that of viral delivery without the high toxicity.

Table I.2. Cationic gene delivery agents and adjuvants

Generic name	Chemical name	Chemical formula	Characteristics	Ref.
Monovalent cationic lipids				
CTAB	Hexadecyltrimethylammonium bromide	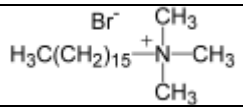	cationic, single chained	[104]
DODAC	Dioctadecyldimethylammonium chloride	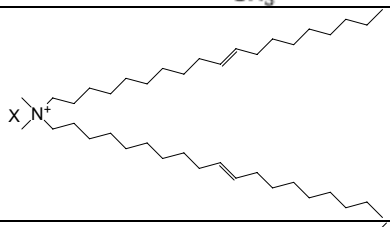	cationic, double chained	[105, 106]
DODAB	Dioctadecyldimethylammonium bromide	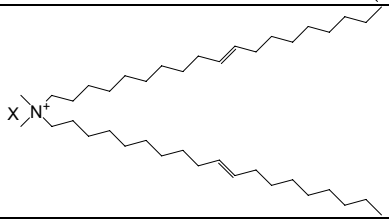	cationic, double chained	[105]
DOTMA	N-[1-(2,3-dioleyloxy)propyl]-N,N,N-trimethylammonium chloride	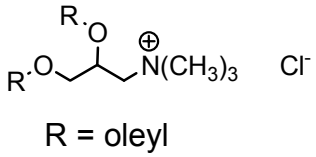	cationic, double chained, ether links, compaction and penetration of DNA	[44]
DOTAP	(2,3-bis-octadec-9-enoxyloxy-propyl)-trimethyl-ammonium chloride	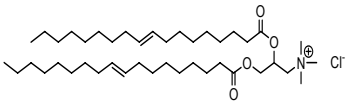	cationic, double chained, ester links, compaction and penetration of DNA	[107]
DMRIE	1,2-dimyristyloxypropyl-3-dimethyl-hydroxyethyl ammonium bromide	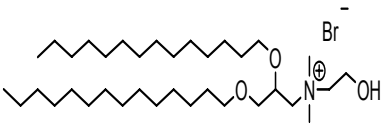	cationic, double chained, compaction and penetration of DNA	[47]
GAP-DLRIE	N-(3-aminopropyl_-N,N-dimethyl-2,3(bis-dodecyloxy)-1-propanimidium bromide	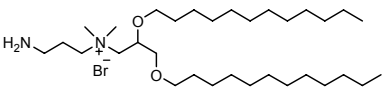	cationic, compaction and penetration of DNA	[48]
RPRs	reducible lipids	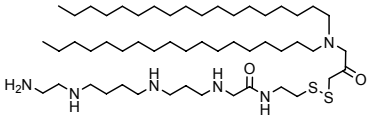	cationic, reduction-sensitive disulfide bond, improved DNA	[51]

			release in the cytoplasm	
BCAT	O-(2R-1,2-di-O-(1'Z, 9'Z-octadecadienyl)-glycerol)-3-N-(bis-2-aminoethyl)-carbamate	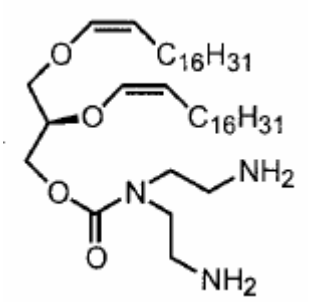	cationic, acid-labile, increase endosomal escape	[52]
BPDAB	bis[2-(11-phenoxyundecanoate)ethyl]-dimethylammonium bromide	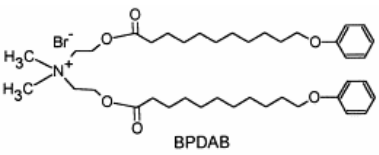 BPDAB	cationic, compaction and penetration of DNA	[45]
HADAB	*N*-hexadecyl-*N*-(10-[*O*-(4-acetoxy)-phenylundecanoate] ethyl) dimethyl ammonium bromide	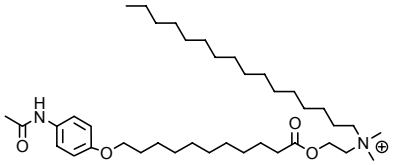	cationic, compaction and penetration of DNA	[45]
BBDAB	bis[2-(11-butyloxyundecanoate) ethyl] dimethylammonium bromide	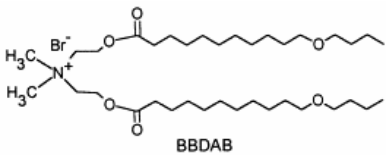 BBDAB	cationic, compaction and penetration of DNA	[45]
Guanidinylated deriv.	N,N-di-n-octadecyl – N-(2-guanidinyl) ethyl-N-methyl ammonium chloride	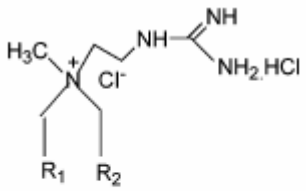 **1**, $R_1 = R_2 = n\text{-}C_{13}H_{27}$; **2**, $R_1 = R_2 = n\text{-}C_{15}H_{31}$; **3**, $R_1 = R_2 = n\text{-}C_{17}H_{35}$	cationic, compaction and penetration of DNA	[108]

Steroid structures				
Dc-chol	3ß-[N-(N',N'-dimethylaminoethane)-carbamoyl]cholesterol hydrochloride	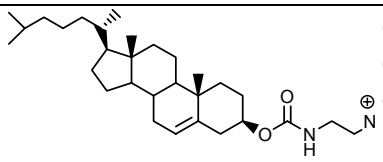	cationic, cholesterol derivative	[109]
DS	dexamethasone-spermine	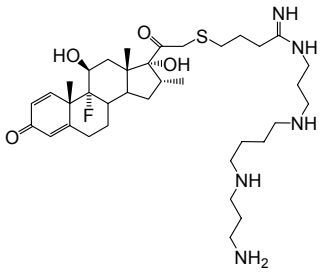	polycationic, antiinflamatory	[54]
Polycationic delivery agents				
DOSPA	2,3-dioleyloxy-N-[2(sperminecarboxy amido)ethyl]-N,N-dimethyl-1-propaniminium bromide	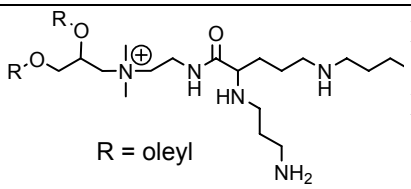	polycationic, compaction and penetration of DNA	[48, 105]
PLL	Poly-L-lysine	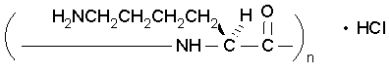	polycationic, compaction and penetration of DNA	[21]
DPK 6th generation	Dendritic poly-L-lysine	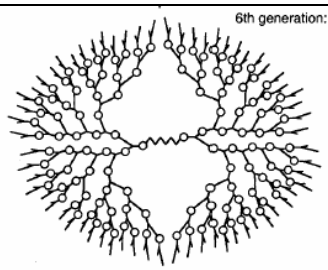	polycationic, compaction and penetration of DNA	[90]
Poly histidine	Poly-histidine-PEG conjugates	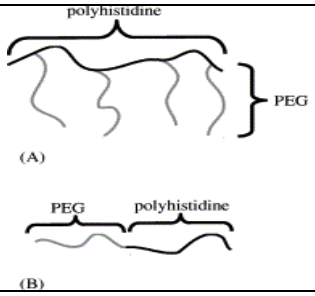	polycationic, compaction and protection of DNA	[110]
Poly ornithine	Polyornithine	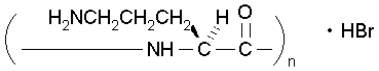	polycationic, compaction and penetration of DNA	[86]

Polymeric agents				
PEI	Polyethyleneimine	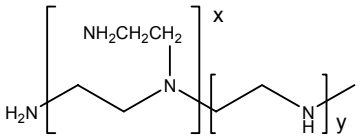	polycationic, compaction and penetration of DNA	[93]
pGuaMA	poly(3-guanidinopropyl methacrylate)	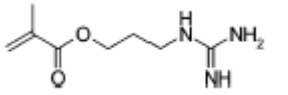	polycationic, penetration of DNA	[76]
Chitosan	Polysaccharide built mainly of D-glucosamine	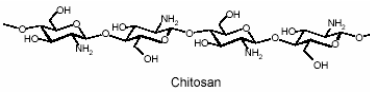 Chitosan	Condensation of DNA	[111-113]
GBs	glycine betaine derivatives	glycine betaine compounds covalently linked to acyl chains by enzymatically hydrolysable peptide and ester bonds	cationic, enhanced DNA unpacking reduced cytotoxicity	[56]
Prot-amine	arginine and lysine rich protein	-	polycationic, compaction and penetration of DNA	[114]
Amino acid derivatives as adjuvants				
Cross-linked systems	peptides of cysteine and lysine, ± histidine or tryptophan	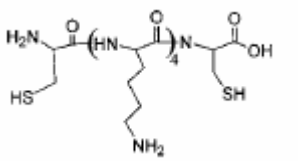	stabilizes lysine-conjugated DNA via cysteine residues	[78]
H5WYG	histidine-rich peptide	-	adjuvant for PLL complexed DNA, increases escape from endosomes	[88]
Fuso genic peptides	fusogenic peptide of influenza virus haemagglutinin	-	adjuvant for PLL complexed DNA, increases escape from endosomes	[98]
Nicotine	Nicotinylated PLL	-	increases escape from endosomes	[89]
Tf	Transferrin	-	receptor binding ligand, increased targeting for PEI-DNA system	[96]
PECAM-1	antiplatelet endothelial cell adhesion molecule 1	-	receptor binding ligand, increased targeting for PEI-DNA system	[95]

Molossin	a 15-amino acid moiety for targeting cellular integrins, derived from snake venom	-	targeting vector fused with PLL	[81]
RDG	lipopeptide	-	receptor binding ligand, increased targeting for cationic lipid-DNA system	[87]
HMGB-1	High mobility group box -1	-	protein having DNA binding domain and nuclear localization signal	[99]
Sugar-based receptor targeting agents				
Mannose	Mannosylated PLL	-	mannose receptor targeting	[85]
Galactose	Galactosylated polyornithine	-	galactose receptor targeting	[86]

I.2.3. Novel cationic gemini surfactants as delivery agents in gene therapy

Cationic gemini surfactants (Figure I.2) are a novel category of delivery agents with potential use in gene therapy. Since the description of these agents in 2000 by Menger [115], only a few publications have described their transfection efficiency *in vitro*. Based on their versatility, high potential for combinatorial chemistry, modeling, ability to bind and condense DNA, and relatively low toxicity, the gemini surfactants may have the potential to be used not only *in vitro*, but also *in vivo* as delivery agents for macromolecules.

Cationic gemini surfactants are molecules with two ionic head groups attached to their hydrocarbon tails and connected with a spacer or linker [115]. These compounds are capable of compacting DNA and have several advantages compared to classic monovalent surfactants: lower cellular toxicity [116], lower critical micellar concentration (generally one or two orders of magnitude), higher efficiency in reducing surface tension, greater tendency to self-assemble, and greater variety due to the nature of the spacers separating the two quaternary nitrogen atoms. This variety contributes to flexibility in designing suitable delivery systems for different target cells [117].

Figure I.2. General structure of gemini surfactants.

The two hydrophobic alkyl chains (tail) with charged head groups (ion) are connected with a carbon spacer [115]. By modification of the spacer length and chemical nature (saturation degree and length) of the tail by combinatorial chemistry, a great variety of surfactants tailored for specific needs could be generated.

Table I.3. Gemini surfactants used as delivery agents for genetic material

Surfactant category	Chemical structure	Head spacer	Tail	Ref.
Alkyl *m-s-m* surfactants	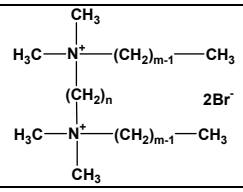	Alkyl	Alkyl	[117]
Substituted *m-s-m* surfactants	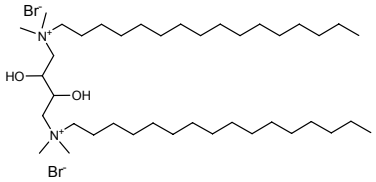	Hydroxyl substituted	Alkyl	[118]
Ester-linked *m-s-m* surfactants	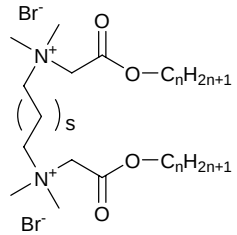	Alkyl	Carboxylated	[119]
Tetraalkyl	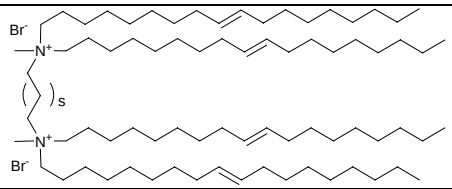	Alkyl	Alkyl	[120]
Sugar-based	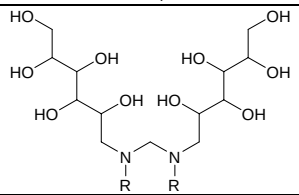	Sugar	Alkyl	[121, 122]
Peptide-based (GS)	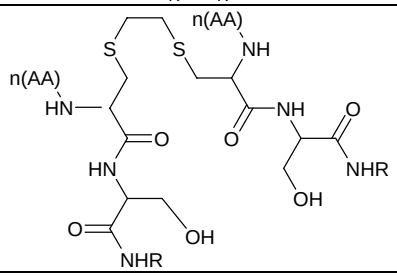	Peptide (lysine)	Alkyl	[123, 124]
Peptide-based (DSN)	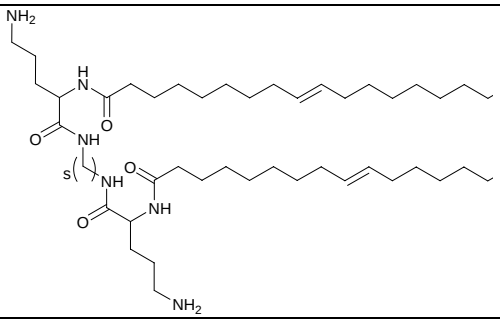			[125]

Tartaric acid based	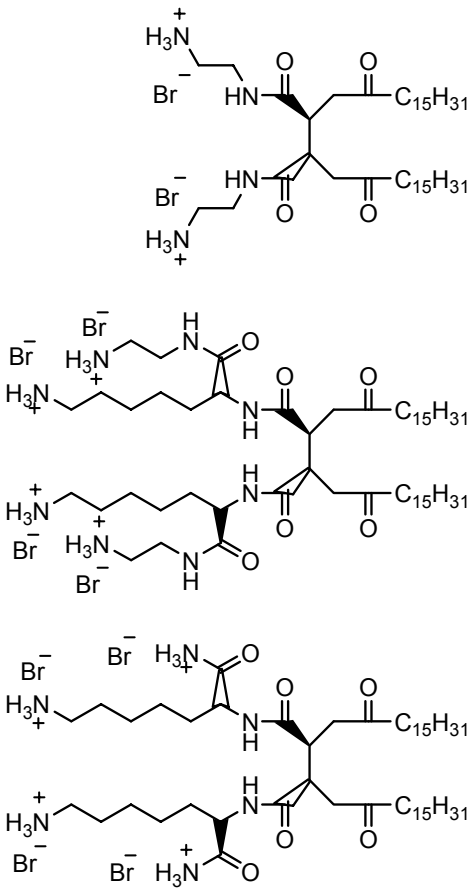	Tartraric acid derivative	Alkyl	[126]

DNA compaction by gemini compounds depends on both the nature of the head group (effective head group area, valence) and the length and saturation of the hydrophobic tail. The optimal aggregation of these surfactants can be expressed by the surfactant parameter, N_s,

$$N_s = \frac{v}{la_0} \qquad \text{(I.1)}$$

where v = volume of alkyl tail, l = length of alkyl tail, and a_0 = surface area occupied by the head-group. An Ns value, indicating the preferred curvature of the structure, of 0.3 is typical for spherical micelle organization (highly curved), whereas Ns = 1 represents planar bilayer formation and Ns > 1 applies to inverted micelles. Gemini surfactants efficiently compact DNA when the spacer length s is <4 or >10. Intermediate spacer lengths are less effective. Increase of the tail length from 12 to 18, hence hydrophobicity, also improves the compaction of plasmid DNA [127]. Contrary to the previously described principle regarding cationic transfection agents where higher compaction correlates with better transfection efficiency, Rosenzweig et al. [116] found the 16-6-16 surfactant transfected BHK cells more efficiently than the 16-2-16 and 16-3-16 compounds. The presence of helper lipid in up to a 1:2 weight ratio to the gemini agent inhibited or substantially reduced cell transfection. Although these compounds present various morphological structures (lamellar for the compounds with saturated cetyl tail and micellar or mixed for the oleyl tail), the effect on DNA and interaction with biological membranes have not been explored. More recently, the role of helper lipids as DNA stabilizing agents for the gemini surfactants with C10, C12 and C14 tails was demonstrated [119]. The transfection efficiency (expressed as number of cells expressing the reporter gene) was comparable to the commercial GenePorter agent.

Measuring the adiabatic compressibility, an indicator of the micelle formation process of the gemini surfactants, the authors demonstrated that the gemini surfactants showed lower isentropic compressibilities compared to monocationic counterparts due to the ability of the gemini surfactant to form chain associations before the critical micellar concentration (CMC) is reached. The transfection efficiency was inversely proportional to the CMC. Differential scanning calorimetry indicated that these surfactants were active at the membrane surface, rather than affecting the phospholipids bilayers.

Another group of cationic alkyl gemini derivatives with two oleyl tails attached to each positively charged nitrogen and a C3 or C6 spacer has shown the ability to deliver DNA *in vitro*. The surfactant having a spacer of 6 carbons (Table I.3) was able to transfect cells at higher efficiency compared to its monovalent counterpart, DODAC (Table I.2), especially at +/- charge ratios greater than 2. This effect was due to the ability of the surfactant to induce non-bilayer phase transition in the lipid bilayer. The presence of the helper lipid DOPE increased the transfection efficiency about ten-fold [120]. Gemini surfactants having sugar spacers in their head groups and two palmitoyl or oleyl tails were able to transfect CHO-K1 cells at comparable levels to Lipofectamine. The cationic nitrogen atoms were separated by either 4 or 6 carbon spacers [121]. Peptide-based gemini transfection agents having C12, C16 saturated or C18:1 unsaturated tails were used *in vitro* to evaluate transfection efficiency. Consistent with the findings of Karlsson et al. [125], increasing tail lengths were associated with higher transfection efficiencies. The nature of the head-group was also important. Three lysine residues linked through the ϵ-amino group (GS surfactants; see Table I.3), rather than α-nitrogen, were found to yield the highest transfection of CHO-DG44 cells [124]. The optimal concentration of the delivery agent was 10 μM. The amide linkage in the

headgroups is biodegradable, conferring lower cytotoxicity to these molecules [123]. L-tartaric acid derivatives were tested in CHO-K1 cells to determine their transfection efficiency. Cellular toxicity creates difficulties in the evaluation of these compounds as transfection agents [126].

Overall, gemini surfactants demonstrate great potential for gene delivery. Due to the low CMC compared to their monovalent counterparts, these surfactants associate more readily in aqueous environments, bind DNA with higher efficiency creating higher local concentrations around the negatively charged macromolecule, and thus are efficient in lower concentrations. Their lower toxicity compared to monocationic surfactant also contributes to their usefulness *in vivo*. Their versatility is attributed to the length and nature of the hydrophobic tails (length of carbon chain, degree of saturation and symmetrical or asymmetrical nature) and nature of head group (i.e., length of the alkyl spacer and nature of the functional substitutes). These chemicals can generally be easily synthesized at low cost, a major advantage for industrial drug manufacturing.

I.3. Structural requirements for efficient DNA delivery systems

Physico-chemical characterization of delivery systems is important in order to better understand the mechanism of delivery. An abundance of assays have tried to explain the relationship between physical and chemical behaviour and efficiency, from classical encapsulation assessments by zeta potential measurements, fluorescence measurements, gel electrophoresis [128, 129] and electron microscopy (EM) [130] to differential scanning calorimetry (DSC) [45], circular dichroism (CD) [131], synchrotron X-ray scattering [132] and X-ray diffraction [133, 134] studies.

An efficient DNA delivery system has to fulfill several criteria: ability to bind DNA and create complexes of a certain size and morphology, neutralize surface charges to facilitate cellular uptake, induce changes in the DNA structure favorable for efficient delivery, protect the genetic material against intracellular degradation, and ability to undergo polymorphic phase changes.

Particle size and the morphology of the complexes are generally important characteristics of the DNA delivery. Sternberg et al. [135] studied the relationship between the morphology and size of cationic lipids. DNA/DDAB/DOPE complexes presented higher *in vitro* transfection efficiency compared to complexes containing DOPE. The size of the particles was 100-300 nm with a tendency for fusion of the liposomes upon standing due to the ability of the DOPE to form non-bilayer structures [135]. DNA condensed with a spermine derivative (alpha-galacto-omega-spermine bolaamphiphile–GalSper) formed particles with a bimodal distribution of 100 and 800 nm. Addition of DOPE further increased the size to 1100 nm. The DNA/GalSper/DOPE lipoplexes transfected HepG2 cells compared to DNA/GalSper complexes [136]. The effect of the size of the particles upon the mechanism of uptake, fusion [44, 137] or endocytosis [39, 138] has been debated in the literature, although the combination of two pathways has not been excluded [139]. Recent publications shed light on the uptake of cationic delivery particles larger than 100nm (the optimal size for endocytosis). Although the main process of internalization into the cells was endocytosis, lipoplex-cell fusion could also occur, as evidenced by the reduced gene expression caused by the addition of fusion inhibitors [140]. Moreover, DNA could induce changes in the lipid organization of cationic vesicles. DNA addition to cationic liposomes induced fusion of the vesicles [141]. Small-angle X-ray scattering (SAXS) measurements of mixtures of

Dc-Chol/DOPC and DOTAP/DOPE vesicles indicate no fusion, explained by the repulsion of particles due to electrostatic charges. However, addition of DNA to the mixture of the two types of vesicles caused changes in the SAXS pattern indicating lipid mixing.

The morphology of the liposomes might also modulate the transfection efficiency. Multilamellar vesicles (MLV) transfect cells more efficiently than large unilamellar vesicles (LUV) [66, 118, 142], and are taken up by cells more efficiently [143]. Zabner et al. describe heterogeneous morphology of cationic lipid/DNA complexes that efficiently deliver DNA *in vitro* [39].

Another important feature that influences transfection efficiency is the +/- charge ratio. A wide variety of optimal charges is described in the literature. Generally, the cationic agent/DNA complexes show increasing transfection efficiency with increasing charge only to a certain point (optimal charge ratio), after which efficiency decreases. This decline might be due to the relative toxicity of the cationic lipid. Wang et al. found the transfection efficiency of monocationic alkyl acyl carnitine derivatives was optimal at +/- ratios of 5, and cell survival drastically decreased at values of 8-32. Two studies on airway epithelial cells demonstrate that a +/- charge ratio >1 is required in this type of cell. An early transfection experiment shows the optimal +/- charge ratio using cationic DMRIE is 1.25 [144]. In a recent publication, a novel cationic cholesterol derivative at a +/- charge ratio of 2.8 effectively transfected three different epithelial cell lines in the presence of eqimolar DOPE. At this charge ratio, the DNA was fully associated with the liposomes (gel-retardation assay) and presented maximum compaction (dye exclusion) [145]. Cationic gemini lipids, formulated with various amounts of DOPE at a +/- charge ratio of 3 showed transfection efficiency comparable to a commercial agent [119].

DOTAP-containing liposomes were mixed with DNA at increasing +/- charge ratios and the charged particles separated from the excess of empty liposomes. These cationic lipoplexes with +/- charge ratios of 2-4 showed more compact structure than the mixtures before separation. The isolated fraction of positively charged liposomes demonstrated higher transfection efficiency compared to the neutral or negatively charged fractions, low cytotoxicity and resistance to inhibitory effect of serum. The negatively charged complexes (+/- charge ratios of 0.25-0.5) showed moderate transfection efficiency [146]. In some cases, +/- charge ratios <1 were optimal for delivery of genetic material in certain tumours [147-149] or brain cells [150].

In the majority of cases, the ζ-potential of the particles in the delivery system is positive in order to achieve optimal transfer through the cell membrane. The positive overall surface charge is necessary for interaction of the particles loaded with the genetic material with the cell membrane. In the case of the cationic lipid DC-6-14/DOPE complexes, a +13mv ζ-potential and a +/- charge ratio of 1.5 were optimal for high transgene expression [140]. The transfection efficiency of cationic cholesterol derivatives in the presence of DOPE as helper lipid paralleled the ζ-potential (values of +9 to +33mV), with increasing ζ-potential inducing higher levels of reporter gene expression [151]. In addition to the positive surface charge of cationic lipids, the surface charge density of the particles is another parameter indicating the degree of interaction with the cell membrane and the transfection efficiency. This parameter can be controlled by the addition of neutral lipids. For example, substituted alkyl gemini derivatives with a low cationic/neutral lipid ratio (0-0.25) transfected cells inefficiently. The protein expression gradually increased between molar rations of 0.25-0.5, then remained unchanged with further increase of the proportion of the cationic lipid [118]. Lin et al.

[152] expanded the concept to monovalent and polyvalent cationic compounds, demonstrating that the transfection efficiency of all studied cationic agents (DOTAP, DOSPA amd DMRIE) as a function of surface charge density (σ_M – the average charge per unit surface area of the lipid membrane) fitted into a universal curve. For all compounds, σ_M values between 0.0015 e/Å^2 and 0.012 e/Å^2 were optimal, rendering universality to this parameter for cationic liposomes with lamellar structure [152].

Cationic lipids induce changes in the structure of the DNA, imposing a conformation advantageous for transmembrane delivery of the genetic material. Monocationic (DMRIE, DOTAP) or polycationic (DOSPA) lipids aided by DOPE as helper lipid induced changes in the original CD spectrum of the B-DNA, inducing the formation of Ψ^- form, a more organized, highly compacted DNA structure. CD spectra of the newly created structure showed depression of the 270-280-nm peak. A more pronounced depression was present with the DOTAP/DOPE vesicles, correlating with the highest transfection efficiency [131, 153].

A key factor in understanding the mechanism by which cationic lipids are able to deliver DNA into the cells and facilitate the release from the endosomes is the interaction between the lipid and the DNA. Cationic lipids of various composition assume lamellar or non-bilayer (hexagonal) structure. Koltover et al. demonstrated that DOTAP/DNA formulations present modifications of the Bragg reflections in the scattering pattern measured by SAXS as increasing amounts of DOPE are added to the system. In the absence of DOPE, a lamellar structure (L_α) is detected, where the DNA is sandwiched between two bilayers [154]. The thickness of bilayer–DNA unit was 57 Å [155]. Addition of DOPE gradually changed the scattering profile to a hexagonal arrangement (H_{II}), due to the membrane-bending shape of the molecule. In this

conformation, the DNA strands are surrounded by the inverted lipid molecules, packed in cylindrical units, with a unit spacing of 67 Å [154]. DNA–cationic liposome (containing CTAB or sodium octylsulfate) interaction with linear DNA (~700bp) was studied by cryo-transmission electron microscopy (TEM) and SAXS, demonstrating that DNA strands were intercalated between double layers of the liposomes, with the thickness of one DNA-bilayer unit being 60 Å [156]. Comparison of scattering patterns of DODAB (two tails) and CTAB (single tail) complexed with linear dsDNA indicated a lamellar structure for the double-tailed surfactant and hexagonal for the single-tailed compound [157], but no correlation with their transfection efficiency was presented. Small- and wide-angle X-ray diffraction (SAXD and WAXD) studies of DNA–cationic gemini surfactant–helper lipid complexes demonstrate that both DNA and lipid undergo major structural changes. At increasing cationic surfactant/helper lipid molar ratios, a non-linear decrease of the repeat period of the lamellar lipid phase was observed (meaning a decrease in the bilayer thickness), accompanied by a modification of the DNA-DNA interhelical distances [133]. The structural periodicity of DOTAP/DNA complexes was demonstrated to be a function of +/- charge ratio and ionic strength, as indicated by fluorescence resonance energy transfer (FRET) studies. A short DNA/lipid distance (18-21Å) was observed at +/- charge ratios of 3 or above [158], consistent with calculations of the water gap (28 Å) based on SAXS measurement of a lamellar system [154]. At lower charge ratios, the DNA lipid distance increased proportionally with the decrease of charge ratio. Similar structural organization was described by Tarahovsky et al. [159] as revealed by electron microscopic visualization of thermostable DNA–cationic lipid complexes. These complexes, with a lamellar periodicity of 60-65 Å, transfected cells more efficiently compared to thermolable complexes [159],

demonstrating that complexes assuming lamellar lipid organization are able to transfect cells efficiently. At the other end of the spectrum, Zuhorn et al. [160] indicated the presence of hexagonal phase is crucial for efficient cellular delivery and endosomal escape of the DNA. When pyridinium-based cationic lipid SAINT-2 was mixed with DOPE, the structural organization showed hexagonal conformation and cell transfection was effective, while SAINT-2/DPPE complexes with mixed lamellar-hexagonal structure showed 2-3 fold lower efficiency.

Since both lamellar and hexagonal structures can facilitate DNA delivery, lipid/DNA organization in the formulation may not be the basic requirement for efficient transgene expression, but rather the ability of the system to adopt various phases according to their milieu. For example, it has been shown that unsaturated cationic pyridinium derivative/DOPE/DNA mixtures form lamellar structure in water but hexagonal conformation in HEPES saline buffer [70]. Other formulations might have similar behaviour: lamellar in formulation and hexagonal in biological media (intercellular fluid, endosomal lumen). Another aspect that could be explored is the ability of the delivery systems to induce membrane fusion and phase transition, regardless of their original phase characteristics. For example, fusion of a lamellar delivery system with the lamellar endosome and lipid mixing could yield a new composition, favouring hexagonal conformation [61]. Moreover, addition of DNA to a mixture of two liposomes induces fusion and lipid reorganization [141]. Foldvari et al. [161] showed that efficient cell transfection can be achieved due to the ability of the gemini cationic lipid/DOPE/DNA systems to adopt polymorphic structures coexisting with lamellar phases.

In conclusion, effective cationic lipid delivery systems have the following properties: (1) they interact with the DNA, creating complex structures, (2) they are generally efficient in +/- charge ratios >1, (3) their surface charge density, as a universal indicator of the transfection efficiency, is greater than 0.0015 e/Å^2 but lower than 0.012 e/Å^2, (4) they can induce changes in the native structure of DNA, yielding highly compacted particles able to penetrate through biological membranes, and (5) they adopt or induce hexagonal or polymorphic phase as a basic criterion of cellular uptake and escape from endosomes.

As these various examples have revealed, not only the chemical nature of the transfection agents plays a role in the delivery of the genetic material, but also the physical properties; their ability to induce changes in the structure of the DNA, the type and strength of interaction with the DNA, chain packing, size, morphology and ζ-potential of the particles are aspects that contribute to successful gene delivery. Modeling of the cationic lipid–DNA complexes can lead to further understanding of the requirements governing the efficient gene delivery, such as phase behavior, packing capabilities and electrostatic interactions [162-164]. Characterization of the cationic lipid-based formulations and correlation with transfection efficiency using multifactorial design can help in selecting various delivery systems and predicting the suitability of new compounds for gene delivery [165]. Further research should capitalize on corroboration of experimental results and mathematical models in order to select delivery agents suitable for dermal and transdermal delivery.

I.4. Skin as a target organ

The skin (Figure I.3) is probably the most accessible of somatic tissues for drug delivery. The molecular characterization of several cutaneous disorders reveals the potential of using gene therapy in these diseases [107, 166-168].

Cutaneous absorption is limited by the stratum corneum (SC), the outer protective layer of the skin. This highly lipophilic barrier consists of several layers of flattened keratinized cells, which are continuously replaced from the epidermis. Most drugs penetrate the stratum corneum by passive diffusion, described by Fick's law:

$$J = -\frac{Dk_1}{e}\Delta C \qquad \text{(I.2)}$$

where: J = flux (quantity of drug penetrating per unit area in unit time);

ΔC = drug concentration difference above and below the membrane (stratum corneum);

D = diffusion constant of the drug in stratum corneum;

k_1 = partition coefficient of the drug between stratum corneum and vehicle; and

e = thickness of the stratum corneum.

The partition coefficient depends on the solubility of the drug and its oil/water partitioning coefficient [169]. The total amount of drug absorbed depends on the drug concentration in the vehicle, dosage regimen, site and area of application, and application method (e.g., occlusion, rubbing, etc). The brick-and-mortar model for the stratum corneum presumes it is built of protein-rich cell layers, separated by intercellular lipids [170].

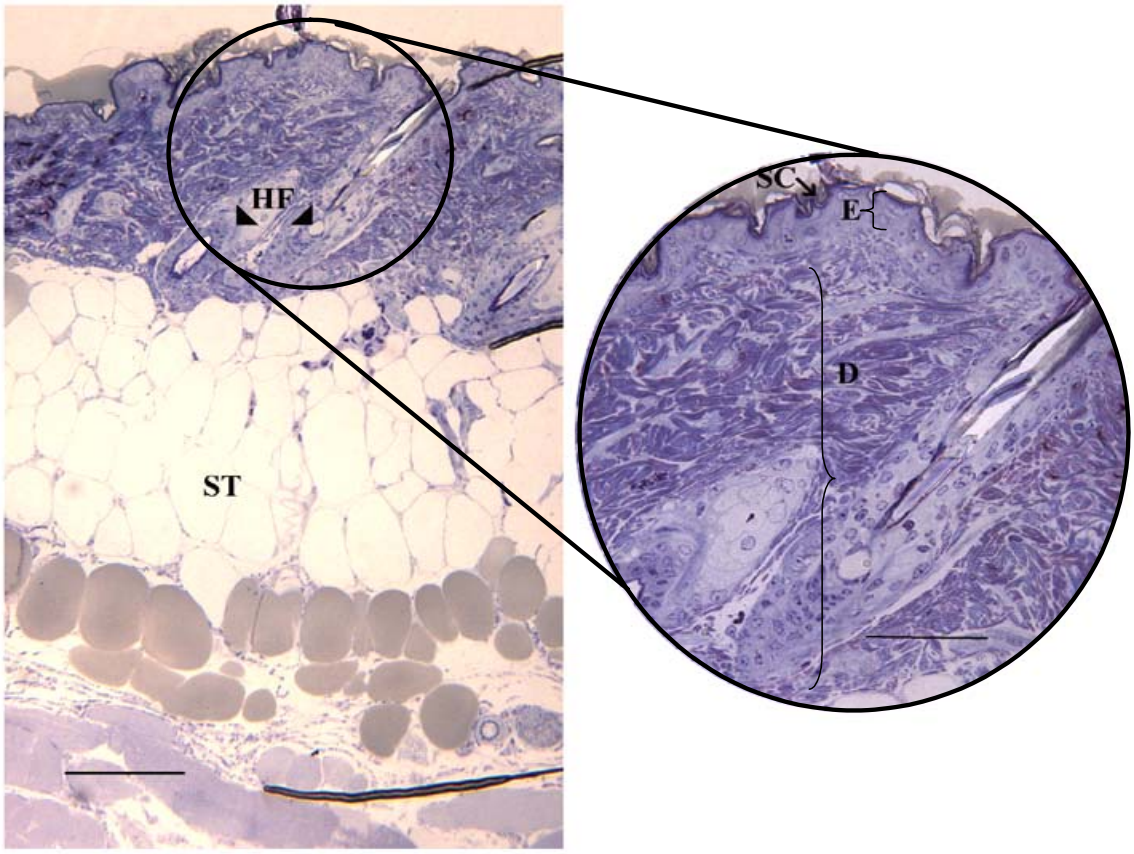

Figure I.3. Light micrograph of murine skin stained with 1% toluidine blue.

The skin is composed of three distinct layers, each with specific functions. The epidermis (E) is a stratified, continuously renewing layer. Keratinocytes, Langerhans' cells, melanocytes and Merkel cells reside in the epidermis. The outermost layer, the horny layer or stratum corneum (SC with arrow), functions as a barrier and thus limits drug penetration into the skin. The dermis (D) confers mechanical strength to the skin. Fibroblasts, macrophages and mast cells are supported by the extracellular matrix. Nerve endings, vascular network (blood and lymph vessels), apocrine and eccrine glands and hair follicles (HF with arrowheads) are located in the dermis. The subcutaneous tissue (ST) is a fatty layer that plays a role in thermoregulation and cushioning against mechanical injuries. Bar 100 μm, bar inset 50 μm.

Depending on the physicochemical characteristics of the drug, the two main pathways of permeation through the skin are intercellular, involving penetration along the lipid channels, and intracellular, through the cellular content. By this model the mechanism of enhancers can also be explained [171]. Penetration enhancers can enhance drug diffusion into the skin by increasing the permeability of the stratum corneum. Polar enhancers such as dimethylsulfoxide, propylene glycol, and surfactants increase the hydration of the statum corneum, thus favour the delivery of hydrophilic drugs, whereas nonpolar solvents (e.g., hexamethyldisiloxane, isopropyl palmitate, and oleic acid) perturb the lipid bilayer structure [172]. Combination of polar-nonpolar permeation enhancers can increase drug penetration by affecting both the "bricks" and "mortar" in the model. Cutaneous and percutaneous absorption of drugs depends on physicochemical characteristics of the drug (solubility, particle size, oil/water partitioning coefficient), the nature of vehicle or delivery system, and skin-related factors such as site of application, age and skin condition. *In vitro* and *in vivo* models exist for quantitative evaluation of drug absorption. The *in vitro* methods include study of drug penetration in diffusion cells using intact or stripped skin (human or animal) as the membrane. *In vivo* absorption is studied in animal models and humans. Percutaneous absorption is measured as the amount of drug either in the receiving chamber of the diffusion cell or in serum. Cutaneous delivery is defined as the amount of drug in the whole skin, and in the separated stratum corneum, epidermis and dermis. *In vivo*, the biological response can also be monitored [173].

Delivery of genetic material is greatly hindered by the large molecular weight, low diffusion constant, and highly hydrophilic nature of DNA. However, keratinocytes can be transfected efficiently and sufficient protein can be expressed ("bioreactor"

concept), making topical administration an attractive approach for gene therapy (Figure I.4) [174]. In a review, Vogel describes two ways of using keratinocytes for expressing immunogenic and therapeutic proteins. One is *ex vivo* transfection, when keratinocytes removed from the patient are genetically modified, then grafted back for long-term expression. The other is an *in vivo* approach, based on direct delivery of genetic material into the skin cells using various delivery systems to achieve transient gene expression [175]. As mentioned previously, subcutaneous injection of plasmid DNA containing genes of several cytokines (e.g., IL-4, IL-6, IL-10, TGF-β1, MACAF, GM-CSF, TNF-α and IFN-γ) resulted in markedly increased levels of these cytokines at the site of injection; IL-4, IL-6 and IL-10 concentrations reached high enough serum levels to exert a biological effect [33]. Intradermally injected plasmid was taken up by keratinocytes relatively readily, as shown with rhodamine-labeled plasmid, but gene expression depended on the ability of the genetic material to enter the nucleus [176].

Keratinocytes are part of the immune system and are able to secrete cytokines and growth factors, such as IL-1, IL-6, IL-12, IL-15, IL-18, TNF-α, GM-CSF, IL-7 and vascular endothelial growth factor (VEGF). The interactions among the cytokines, chemokines and growth factors are complex (Figure I.4). For instance, IL-18 increases the Th1 responses triggered by IL-12, a cytokine responsible for triggering IFN-γ secretion of the lymphocytes. Expression of HLA DR on human keratinocytes strongly suggests the immunocompetent nature of the keratinocytes [177]. The interactions among immune elements might play important roles in the development of scleroderma, and could be the target for treatment options with the aim being the restoration of the Th1/Th2 balance [178]. Evidence suggests targeting dendritic cells is a potential application of gene delivery to achieve a long-lived immune response [179-181].

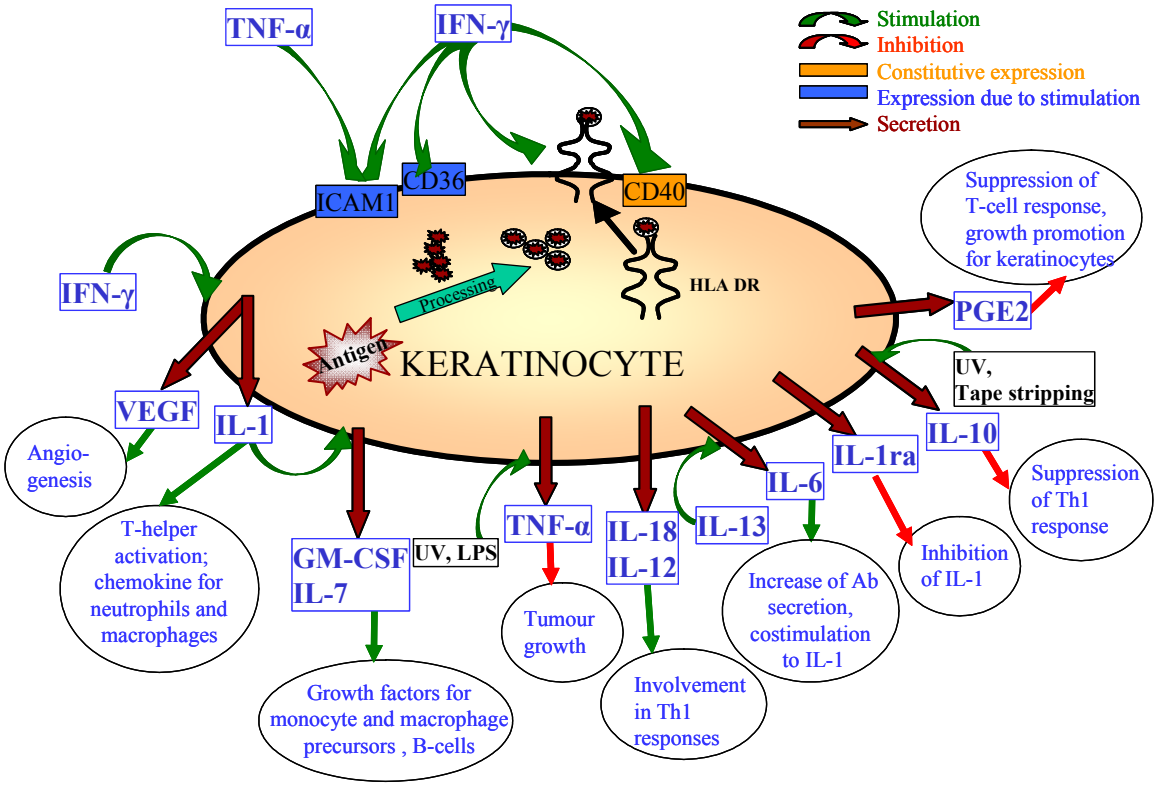

Figure I.4. Schematic representation of the function of keratinocytes and interaction with immune cells.

Major histocompatibility complex class II molecules (HLA DR), CD36, CD40 and intercellular adhesion molecule 1 (ICAM-1) are expressed constitutively or as a result of external stimulation in keratinocytes. Pro-inflammatory cytokines such as IL-1, IL-6, IL-7, IL-12, IL-18 and TNF-α are secreted by keratinocytes when stimulated by chemotactants, such as IL-1, ultraviolet (UV) light, bacterial lipopolysacharides (LPS), or mechanical injury. These cytokines regulate T-cell proliferation and antibody secretion by B-cells. Prostaglandin E_2 (PGE_2), IL-1 receptor antagonist (IL-1ra) and IL-10 are some of the down-regulatory cytokines modulating the immune response in the skin. Growth factors such as the vascular endothelial growth factor (VEGF), granulocyte-macrophage colony-stimulating factor (GM-CSF) and IL-7 are involved in cell proliferation and tissue regeneration [182].

Epidermal stem cells are attractive targets for long-lasting gene therapy. Transduction of this cell population could induce prolonged protein expression in the skin, a useful feature for the treatment of genetic diseases [183, 184]. Although viral vectors are more efficient for the delivery of genes, they are toxic, highly immunogenic and more difficult to prepare. Also, viral vectors can only be loaded with relatively small genes (e.g., AAV can package only 2.4kb double stranded DNA) [185]. Despite the fact that non-viral approaches at present have lower efficiency, they have the advantages of low immunogenicity and easy preparation [26].

I.5. Topical gene delivery

Some hindrances to systemic administration, such as the passage through epithelial cells of the circulatory system to the target organs and interaction with elements of the blood are not present when DNA is applied topically. However, several major obstacles to topical gene delivery remain. The stratum corneum, the outer protective layer of the skin, presents a barrier difficult to penetrate by the large DNA molecules [27]. Furthermore, once DNA passes through this barrier, it meets the defense mechanism of the skin, represented by the dendritic cells in the epidermis; these powerful antigen-presenting cells recruit scavenger cells from the blood circulation. The uptake of the DNA into target cells (i.e., keratinocytes or fibroblasts) in the skin requires passage through the cell membrane, another rate-limiting step impeding gene expression. Escape from the endosomes and intracellular degradation can also diminish the amount of the DNA available for nuclear transport. Figure I.5 presents the barriers to efficient DNA delivery and protein expression.

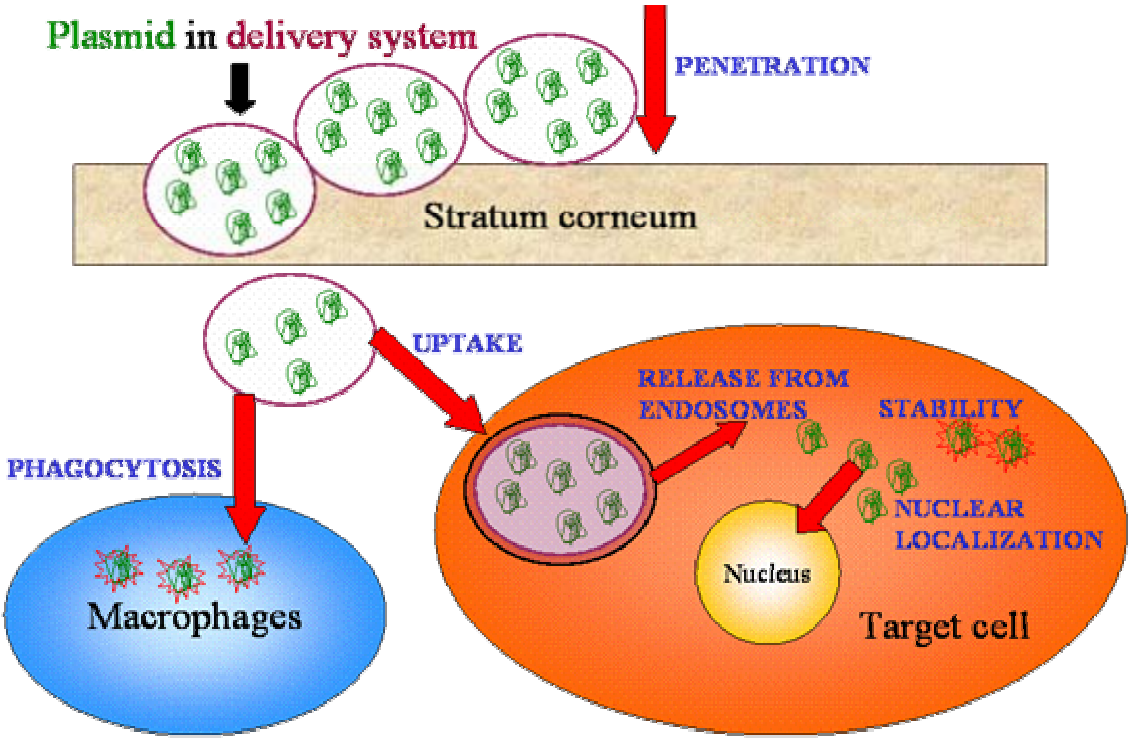

Figure I.5. Schematic representation of the obstacles to the delivery of DNA-drugs and protein expression in the skin.

The figure demonstrates limited and slow penetration through the stratum corneum, phagocytosis, slow uptake by the target cells, lack of release from endosomes, instability in cytoplasm and lack of nuclear uptake.

Although several studies demonstrate the efficiency of lipid-mediated delivery of the DNA *in vitro* [44, 186, 187], including delivery into keratinocytes [188, 189] and fibroblasts [190, 191], little is known about the cutaneous delivery of the liposomal plasmid DNA. There are two ways to deliver DNA into the skin: *ex vivo* by insertion of genes into keratinocytes removed from the patient and reinsertion after transgene expression [192, 193], or *in vivo*, involving direct introduction of the genetic material into the skin followed by local or systemic gene expression [27, 175].

Gene expression in intact skin was achieved *ex vivo* by cutaneous delivery of a cationic liposome-DNA system. The DOTAP-DNA complexes were incubated in Franz cells with intact excised skin for 6 hours, followed by a 24-hour incubation to allow gene expression. The β-galactosidase expression was 16 fold higher in the skin treated with the liposomal DNA compared to the naked plasmid [194].

In vivo delivery of DNA could be achieved in various ways: by invasive intradermal injection [195-197], jet propulsion or biolistic delivery [180, 198, 199], or non-invasive topical DNA application [200]. All these methods can be associated with physical or chemical enhancement. Physical methods include electroporation, sonophoresis and iontophoresis. Chemical formulations, including lipid-based delivery systems, can aid topical DNA delivery.

Early studies demonstrated the feasibility of topical DNA delivery using reporter genes in liposomal formulation [107, 201]. Liposomal delivery systems containing DOTAP delivered the β-galactosidase expression gene into the skin, and protein was detected in epidermis, dermis and hair follicles [107].

Typically, studies demonstrated delivery after the skin permeability was increased in some way. Stratum corneum was removed by stripping the skin with

cellotape [55], adhesive glue [202], brushing with firm bristles [203] or treating with depilatory agents that remove the upper cornified layer of the skin [166]. Microneedles create superficial damage in the stratum corneum, allowing direct access of the DNA molecules to the epidermis, enabling delivery and enhanced expression 2800-fold by the "dip and scrape" method compared to intact skin [203-205]. Although the method is semi-invasive, no pain was associated with the use of microneedles in human volunteers [206]. Thus, this might be an attractive method for vaccination in pediatric population.

Delivery of genetic material into the skin first found application in vaccine therapy. Of the 715 clinical trials in the world, 6.7% are focusing on vaccine development [http://www.wiley.co.uk/genetherapy/clinical/].

Fan et al. [200] demonstrated that naked DNA can penetrate the unaltered skin and elicit immune responses. Topical vaccination in mice with aqueous solution of HBsAg expression plasmid elicited antigen-specific immune responses. The magnitude of antibody production was about half the response following intramuscular injection. The hair follicles played an important role in the DNA delivery, since transgene expression could not be detected in hairless animals [200], and thus penetration through the intact stratum corneum was not achieved. Although naked DNA could generate enough protein to trigger immune responses, therapeutic feasibility of the method is questionable. For gene therapy, larger amounts of the therapeutic proteins need to be generated, and application of plasmids might not involve a hairy skin surface. Cationic nanoparticles and ethanol-in-fluorocarbon microemulsion [207, 208] were also used for dermal delivery of genetic materials, and the immune response to the generated protein was biased to Th1-type in the microemulsion system. Topical application of antigen-coding DNA in lipid-based delivery systems also elicit immune responses. Application

of biphasic lipid vesicles containing plasmid encoding for the bovine herpesvirus type-1 glycoprotein D (pgD) was followed by 5 fold higher antibody titers compared to control animals, and similar in magnitude to intradermal injection of a lower dose plasmid. The topical biphasic formulation triggered a Th2 type of response, whereas the intradermal injection elicited Th1 type [209]. This fact confirms the route of administration might be important for tailoring vaccination strategies. Although no clinical trials involve non-viral cutaneous gene delivery for therapeutic purposes, efforts are being made to create efficient non-invasive delivery systems and devices.

Nonionic/cationic liposomes (NC) are able to enhance transfection *in vivo*, facilitating the delivery of plasmid DNA into the skin, mostly into perifollicular cells. Protein levels after delivery of plasmid DNA encoding for IL-1 receptor antagonist (IL-1ra) were four fold greater compared to naked DNA (165 pg/cm^2 vs. 32.5 pg/cm^2). Expression of transgenic protein can correct perturbance in cytokine production, which is the cause of several diseases affecting the skin. Liposomal delivery of IL-1ra and expression of protein in the cells inhibited the pathological effects of the endogenous IL-1 in skin cells, provided the levels of the antagonist are 10-100 fold higher than the cytokine levels [210]. Similar findings were shown in another study where the ability of nonionic and nonionic/cationic liposomes to deliver plasmids DNA into the skin was twice as high compared to polymer compounds and polyethylene glycols, with peak expression at 24 hours [168].

Transgene expression was reported following topical application of plasmid DNA in nanoemulsions of polyoxyethylene 20 sorbitan monooleate, sorbitan monooleate and olive oil. C57 BL/6J mice and hairless Skh-hr-1 mice were treated with plasmid DNA encoding for human interferon-α2 and the protein expression found to be

significantly higher in the hairy mice. Although the mechanism of transfection is unclear, the uptake of the genetic material seems more active in the hair follicles [211].

In most publications, the relative differences between different formulations compared to naked DNA or control vehicle were assessed, but the specific gene expression levels actually obtained as well as levels required for successful treatment were not examined. In some articles, either the activity of reporter genes (measured in light emission units) [166, 212] or immune response against reporter genes, such as β-galactosidase [200, 207] or messenger RNA expression [55], were presented. However, performing quantitative comparisons on the amounts of protein expressed is possible in some cases. For example, Wu et al. [211] indicate application of 10 μg plasmid coding for human interferon α2 (pNGVLhuIFN α2) on four consecutive days (total DNA dose: 40 μg) in a nanoemulsion formulation in mice generates approximately 100 pg protein/cm^2 skin. Chiotti et al. [213] show levels of expression of human interleukin-1 receptor antagonist (IL-1ra) of approximately 165 pg/cm^2 in hamster ear, after topical application of 2x350 μg plasmid DNA for three days. Similar protein levels were obtained in another study using the gene gun, by administering 5 μg/site of murine interleukin-12 (IL-12) coding plasmid on 4 sites, 1.5 x 1.5 cm^2 skin surface, covering an intradermal tumour. The IL-12 level was 266±27.8 pg in the epidermal layer, this level of expression being sufficient to exert a biological effect, causing tumour regression in mice [214]. Although further experiments are necessary to evaluate the biological implications of these protein levels, the use of the non-viral DNA delivery as a therapeutic tool might be feasible. Moreover, these protein levels are comparable to those generated using lentiviral vectors. Siprashvili and Khavari [215] showed that after intradermal injection of 5 μg of GRE-Epo lentivirus in human skin grafts transplanted on

mice, human erythropoietin (Epo) levels of 25mIU/mL were achieved, corresponding to 357 pg protein. The generated Epo was sufficient to exercise biological effect causing an increase in hematocrit from 40-45% to 60-65% [215]. Although direct comparison cannot be made, the protein levels achieved by intradermal injection of lentivectors (357 pg Epo/mL) and non-viral topical delivery systems (165 pg IL-1ra/cm^2 skin and 266 pg IL-12/cm^2 skin) are in the same range, proving once more the potential of non-viral vectors and topical delivery systems in gene therapy.

DNA delivery can be achieved by physical delivery methods, such as iontophoresis and electroporation. These methods alone or in conjunction with chemical delivery systems, such as liposomes, could efficiently increase transgene expression. Iontophoresis used for the delivery of antisense oligonucletodes (ODNs) targeting IL-10 for treatment of atopic dermatitis induced a decrease in cytokine levels, accompanied by physical improvement, such as reduction of inflammation, erythema and scaling at the site of application, but not distant locations [216]. The mechanism of penetration and delivery is electromigration and electroosmosis [217]. Electroporation produces transient perturbation of lipid bilayers in the skin by cavitation. Since the created transmembrane potential is larger than that of the resting membrane, electroporation causes dielectric breakdown of membrane and creates hydrophilic pores for drug delivery [218]. Immune response to hepatitis B increased significantly in pigs injected intradermally with plasmid DNA coding for the antigen together with electroporation compared with animals injected intradermally, without electroporation [219].

The mechanism of the interaction of the liposomes with the skin [220], as well as the potential application of this technology for *in vitro* and *in vivo* delivery of the macromolecules such as proteins and peptides [11, 221-223], has been described.

Structural and functional differences exist among proteins, peptides and DNA. The transdermal delivery of these compounds requires different conditions and their fate in cells is different. Understanding the mechanism of the lipid-mediated cutaneous delivery of DNA may lead to increased possibilities for the use of DNA in gene therapy.

Novel approaches, such as targeting dendritic cells, can be achieved with specifically designed plasmids, driven by dectin-2 promoter, characteristic only for Langerhans' cells. Reporter genes carried by such vectors were expressed in the dendritic cells only. If certain antigen-coding genes are delivered by this type of system, the immune response to the generated antigen can be modulated [224].

Topical application of liposomal DNA transfects hair follicles in a cycle-dependent manner, being the most efficient in the anagen phase of the hair growth [225]. Topically applied fluorescent-labelled plasmid was retained in hair follicles of hair-bearing skin, but was not detected in skin lacking normal hair follicles [200].

Topical delivery of genetic material is gaining importance for both therapy and immunization. The accessibility of the application site, ease of administration, non-invasiveness, uptake of the DNA by specialized cells and the "bioreactor" nature of the skin are the advantages of this delivery approach. However, barriers such as penetration through the stratum corneum, the protective layer of the skin, and slow and still inefficient delivery into the viable cells have to be overcome. The mechanism of delivery needs to be elucidated for the majority of promising dermal and transdermal delivery systems. Physico-chemical characterization of the formulations, interactions with the skin lipids and cells, and correlations between the properties and efficiency could lead to improved gene delivery.

I.6. Localized scleroderma as a potential target for topical gene therapy

I.6.1 General description of the clinical problem

Scleroderma or progressive systemic sclerosis (PSS) is a chronic disease manifested by the excessive deposition of collagen (both type I and type III) in skin and connective tissue, vascular abnormalities and autoimmunity. Sclerotic fibroblasts (myofibroblasts) are capable of multiple *in vitro* passages, thus their accumulation might be responsible for the fibrosis characteristic for the disorder [226]. These fibroblasts produce excessive collagen even in the absence of the immune stimulus, suggesting the dysfunction of some regulatory genes associated with phenotypic selection (i.e., the subpopulation of fibroblasts producing excessive collagen is amplified at the expense of the normal fibroblasts). The stimulus for the excessive collagen production originates from immune mechanisms (Figure I.6).

The development of sclerosis consists of three major steps: (1) cellular infiltration and vascular damage due to external stimuli or genetic factors, (2) inflammation due to the activation of monocytes and T-cells, and (3) fibrosis [227]. Almost all activated T-cells are predominantly $CD4^+$ cells in the skin. The number of T-cells expressing the $CD8^+$ cell surface marker found on suppressor cells is diminished. The levels of both TGF and IL-4 are increased in the blood. Activated T cells produce TGF-β, IL-4 and lymphotoxin that stimulate fibroblast growth.

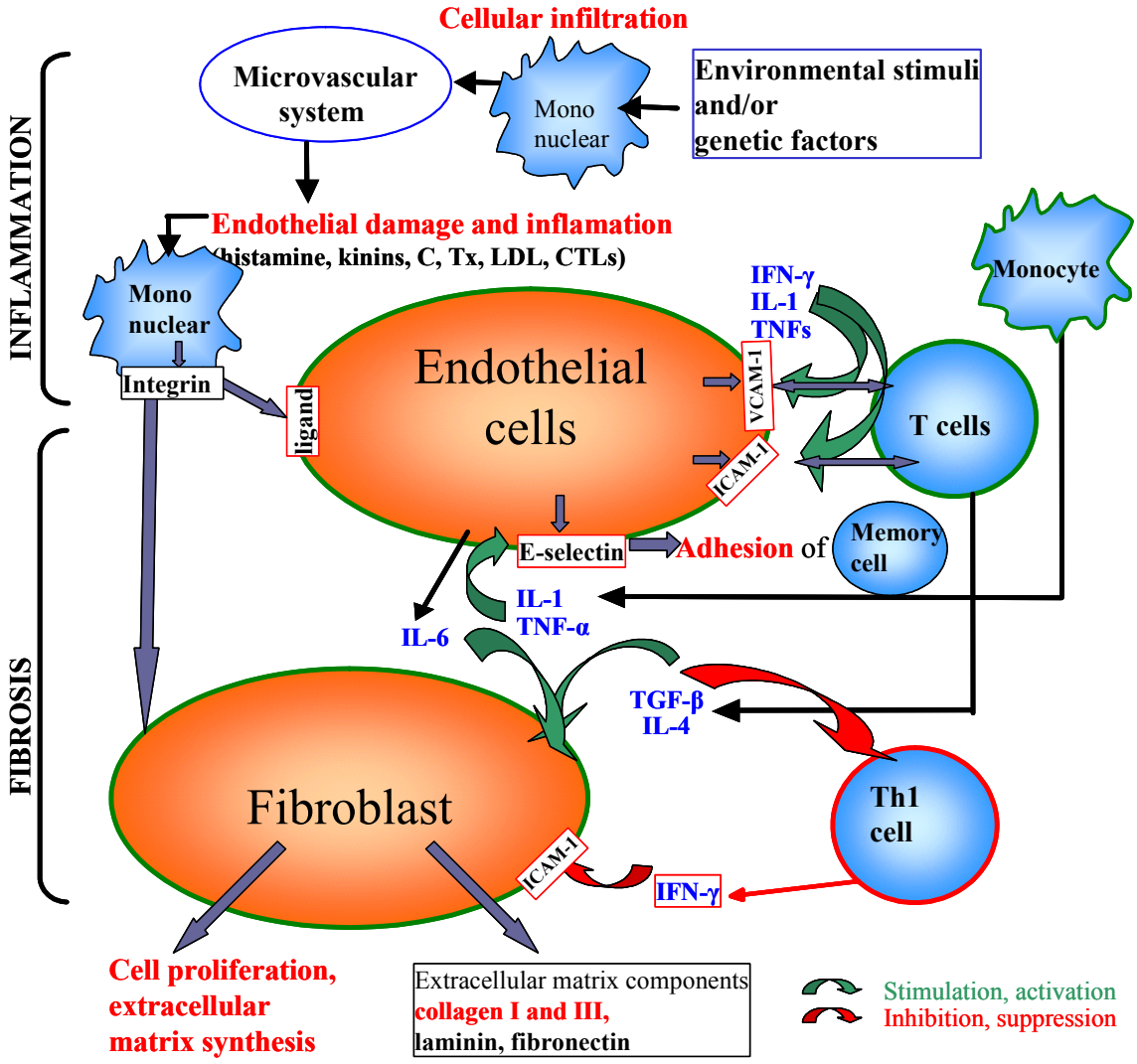

Figure I.6. Pathogenesis model of scleroderma.

IFN-γ gene therapy may have an effect on four groups of pathophysiological markers of scleroderma: (1) collagen and extracellular matrix components, (2) cell proliferation, (3) cell adhesion molecules, and (4) cytokines [227, 228].

TGF-β selectively induces the connective tissue growth factor (CTGF), platelet-derived growth factor (FDGF) and metalloproteinase-3, all increasing the mitogenic activity in fibroblasts [229]. TGF-β stimulates the synthesis of several extracellular matrix proteins, such as collagens, fibronectin, tenascin, tissue inhibitor of metalloproteinase-1 and plasminogen inhibitor-1, and induces TGF-β secretion in fibroblasts (autoinduction). The fibrosis is induced through the Smad pathway (Figure I.7); the intracellular Smads (e.g., Smad3) are activated by the binding of the TGF-β to its receptor on the surface of the fibroblast. The Smads than translocate into the nucleus, where they activate or repress gene transcription (e.g., activation of procollagen type I α gene, *COL1A2*) via the p300/CBP cofactor [230]. The profibrotic activity of IL-4 results in increased production of extracellular matrix via signal transducer and activator of transcription 6 (STAT6) protein. This protein binds a STAT (signal transducers and activator of transcription) responsive element facilitated by the p300/CBP cofactor (Figure I.7). STAT6 might also activate transcription of the *TGFβ* [231]. T-cells produce factors such as IL-6 and IFN-γ that suppress fibroblast growth and collagen synthesis. IFN-γ directly suppresses collagen synthesis in two ways (Figure I.7): through Janus kinase (Jak)/ STAT1 signaling and the Y box-binding protein (YB-1) pathway. The IFN-γ blocks *COL1A2* promoter activity by the JAK/STAT1α activation. The activated STAT1α competes with the TGF-β-activated Smad3 for the limited amount of the cellular cofactor p300/CBP, blocking the transcription of *COL1A2* [232]. The second pathway involves the activation of YB-1, which directly interacts with the promoter region of the *COL1A2*, blocking its transcription. Additionally, the YB-1 binds mRNA in the cytoplasm, which could constitute yet another way to block collagen synthesis at the translational level [233]. Moreover, IFN-γ directly stimulates prostaglandin

production (another fibroblast growth inhibitor) in monocytes. Monocytes play an important role in the fibrosis; they express on their surface antigens characteristic of activated cells, and produce reduced amounts of interleukin-1 (IL-1) as demonstrated by monocytes removed from patients suffering form systemic sclerosis [227]. Depending on which cytokines are predominant, upregulation or suppression of the tissue fibrosis is controlled by the immune system; presence of IL-4 and IL-10 inhibits secretion of IFN-γ by Th1 cells, thus fibrosis is favoured. Conversely, if the IFN-γ is present, Th2 cells are inhibited, and production of IL-4 and IL-10 is blocked [234]. Recent evaluation of the cytokine balance in scleroderma patients revealed the presence of IL-4, IL-10 and TGF-β (induced by IL-4) characteristic of Th2 immune responses, agents that induce tissue fibrosis. Altered B-cell activity might also contribute to the response shift, by activation of Th2 lymphocytes [178]. Since the clinical presentation of the disease has multiple components, research groups are focusing on the evaluation of the pathological markers as possible treatment targets.

The pathological markers of sclerosis are: (1) vascular infiltration and cell damage, (2) imbalance of the cell mediated and humoral immune responses, (3) abnormal response of the fibroblasts to the immune stimulus, (4) increased number of activated mast cells, and (5) increased levels of cytokines. Immunohistochemistry and electron microscopy reveal that both type I and III collagen species are increased in scleroderma-affected skin, where the ratio of the two collagens is 5:1, similar to the normal skin [235].

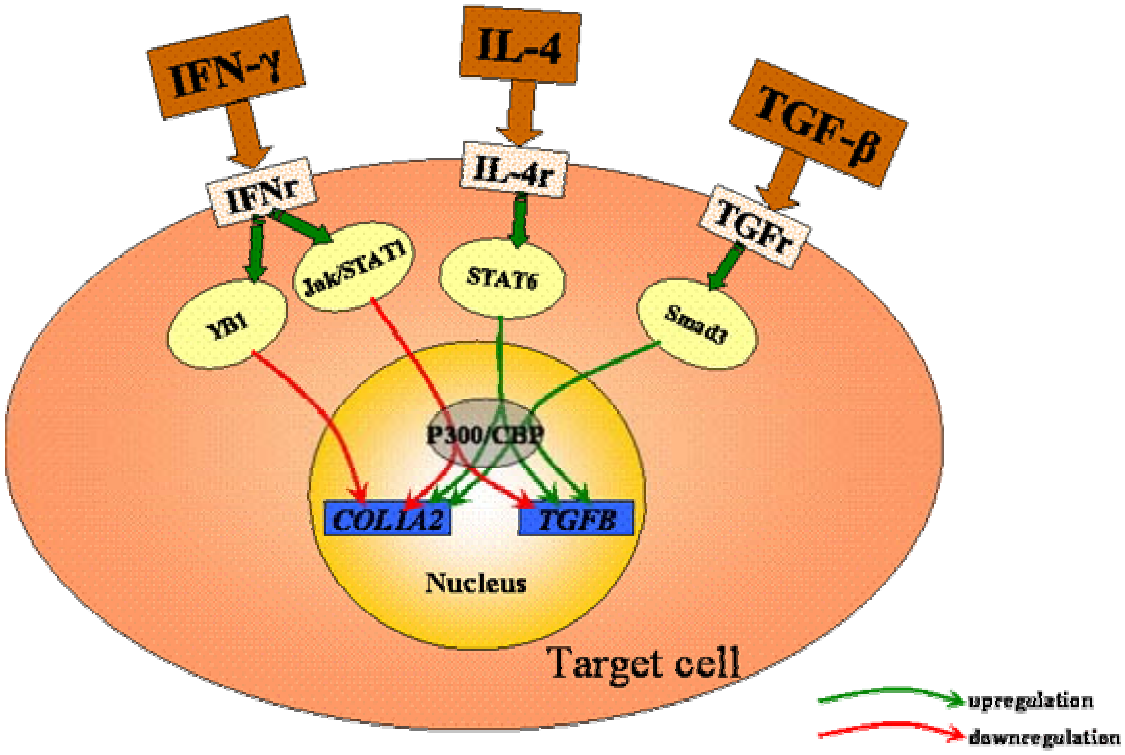

Figure I.7. Schematic representation of the role of IFN-γ, IL-4 and TGF-β in the regulation of collagen synthesis.

IFN-γ supresses gene transcription directly via the YB1 pathway and indirectly by inhibition of the P300/CBF protein [233]. IL-4 and TGF-β both stimulate *COL1A2* transcription via STAT6 and Smad3 pathways [231, 232]. Additionally, TGF-β autoinduces additional TGF-β production by fibroblasts through stimulation of the *TGFB* gene.

Localized forms of scleroderma, including morphea (patches of scleroderma) and linear scleroderma (linear bands of sclerodermatous tissue) are the most frequent form of scleroderma [229] (Figure I.8). In morphea, the lesions are confined to the skin, and occur as plaques (morphea en plaque) or indurated papular lesions (guttate morphea). As the disease evolves, more extensive lesions appear, the subcutaneous tissue is replaced by dense collagenous tissue, a process that can progress to involve deeper tissues including muscle and fascia [228]. Morphea is also characterized by the absence of visceral involvement, and coexistence with systemic scleroderma is infrequent [229]. Skin involvement in the systemic sclerosis presents similar clinical signs to the localized scleroderma, and the two conditions are histopathologically identical, thus treatment approaches could be applied for both localized scleroderma and the skin in systemic sclerosis.

I.6.2. Animal models of scleroderma

To study the cutaneous modifications in scleroderma, different animal models have been developed and used by research groups. One model, the tight skin-1 (Tsk1) mouse, has been proposed due to increased collagen synthesis in the skin and accumulation in the dermis. The morphological changes are caused by a spontaneous mutation of fibrillin-1 gene (*FBN1*) on chromosome 2. Homozygous Tsk1+/+Tsk1 embryos die *in utero*, but the heterozygous Tsk1+/+pa animals are viable and present the pathological changes characteristic of scleroderma [236].

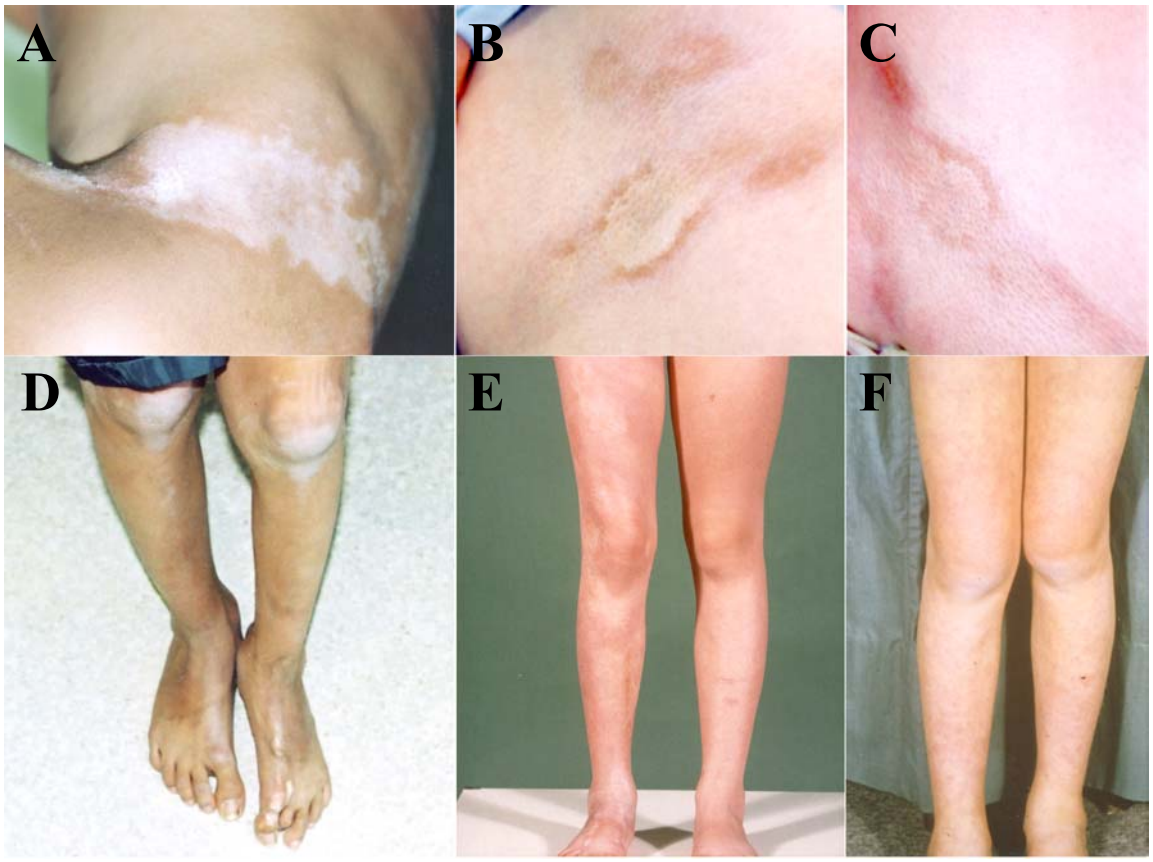

Figure I.8. Clinical presentation of morphea and linear scleroderma.

The lesions might appear on any area of the body. Lesions on the face and scalp, although less common, can be quite disfiguring when they occur. The morphea plaques are indurated, hyper- or hypopigmented with erythematous and/or violaceous halo (Panels A-C). The size of the lesions can vary considerably in size. Panels D-F are representative of linear scleroderma. (Courtesy of Dr. Alan Rosenberg).

The mutation is inherited as an autosomal dominant trait. Electron microscopic evaluation reveals increased thickness of the dermis and denser packing of the fibrills compared to normal mice [237]. Osborn et al. indicate both increased thickness of the skin and twice the collagen content of the normal animals for both one and six month old Tsk1 mice [238]. High levels of TGF-β are detected in the early stages of development (first 16 days) paralleled by increased collagen synthesis in the skin of Tsk mice [239, 240]. The presence of immune cells and autoimmune antibodies in the mutated strain has also been demonstrated [241]. Altered B-cell function in the Tsk1 mice could be the leading cause for the cytokine imbalance and presence of autoimmunity [178]. Recent studies question the morphological changes in the Tsk1 mice, demonstrating the lack of differences in skin thickness and collagen content compared to pa+/+pa animals [242, 243]. However, with all its imperfections, the presence of pathological markers such as immune cells and cytokines similar to scleroderma patients proves the usefulness of the model. In the Tsk2 model, the mutation of *FBN2* on chromosome 1 leads to the mononuclear infiltration and apparition of tight skin [244]. Autoimmunity has also been demonstrated in this model [245].

Dermal sclerosis can be induced by injection of bleomycin, an anti-tumour agent. Side effects such as Raynoud's phenomenon, lung and cutaneous fibrosis are frequent in the bleomycin treatment. Experimentally, scleroderma-like symptoms can be induced by injecting more than 1 μg bleomycin subcutaneously for 3-4 weeks in mice. The animals presented cutaneous changes (increased thickness of the dermis, excessive collagen I production), persistent for 6 weeks after the last treatment. Myofibroblasts present in the dermis can be reduced by anti-TGF-β antibody treatment. Immunological markers of scleroderma (immune cells, cytokines, chemokines) are found in the bleomycin-treated

animals [246]. The bleomycin-induced scleroderma has been useful for the study of the pathogenesis in scleroderma. Using the model for scleroderma therapy might pose questions such as characterization of the individual lesions, duration of the sclerotic modifications and of the treatment, and spontaneous remission of the lesions.

The murine sclerodermatous graft-versus-host disease model is a useful tool in evaluation of the cellular and molecular mechanisms in the apparition and progression of scleroderma, as well as the key elements in the abrogation of excessive collagen synthesis. The model is especially useful for the study of rapidly progressing disease (months instead of years), since early recognition of the rapidly progressing scleroderma (before the appearance of irreversible tissue damage) improves the treatment outcome [247].

The relaxin gene knockout model provides useful information on the evolution of progressive sclerosis, and the possibility of treatment with relaxin. Relaxin-deficient mice show age-related increases in collagen deposition that can be reversed by administration of relaxin at the early stages of the excessive collagen deposition (at the age of one month), but are not affected at advanced dermal scarring [248]. Transgenic mice overexpressing negative-type II TGF-β receptor were developed to study the effect of TGF-β on cell growth [249]. An interesting approach of using the murine sclerodermatous graft-versus-host disease model capitalizes on the similarities in the immunological make-up and fibrotic processes between the model and human progressive scleroderma. The model is useful for the study of cellular and molecular processes involved in scleroderma [247]. The necessity of bone marrow transplants for each animal could represent a hindering factor in the therapeutic studies, where a relatively large number of well-characterized animals are required.

I.6.3 Current treatment options and clinical challenges

The clinician is faced with significant challenges in the treatment of systemic sclerosis (SSc) due to the various clinical manifestations, the presence of the autoimmune components and the diversity of the laboratory features. In a recent review [250], the cited treatment options are directed to alleviate the clinical signs of the disease: 1) vascular therapy is attempted by Ca-channel blockers, angiotensin-converting enzyme (ACE) inhibitors, antiplatelet drugs, prostaglandins, phosphodiesterase inhibitors, and nitroglycerin; 2) autoimmune therapy is initiated with methotrexate, cyclophosphamide, and antithymocyte globulin followed by mycophenolate mofetil (an immunosuppressive agent); and 3) antisclerotic therapy, such as prostacyclin, ecteinascidin, atorvastatin, integrin and UV radiation is administered to slow the progress of disease in the early inflammatory stages. Encouraging results in the prevention of the progression of the autoimmune component have been shown using high-dose immunosuppressive agents and stem-cell replenishment in early stages of diffuse scleroderma [251]. The treatment consists of total body irradiation, and administration of cyclophosphamide, antithymocyte globulin and autologous stem cells [252]. Pulmonary hypertension, digital ulceration and the Raynaud phenomenon (a vasospastic process affecting the blood vessels of fingers, toes, nose and ears) may be controlled by bosentan, an endothelin-1 antagonist compound [253-255]. Thalidomide, an agent known to increase $CD8^+$ T cells in HIV infected patients, can be used in the treatment of SSc. Oral administration of the drug increased the plasma levels of IL-12, a potent inducer of IFN-γ, and improved healing digital ulcers in scleroderma patients [256]. Collagen type I synthesis can be inhibited by halofuginone (an anticancer drug that specifically inhibits the synthesis of collagen type I). Additionally, intraperitoneal

injection of this agent reduces the number of cells producing collagen [257]. Clinical signs of localized scleroderma can also be successfully improved by UVA irradiation resulting in decreased morbidity [258]. Current treatment possibilities for localized scleroderma also include topical corticosteroids, calcitriol and calcipotriene, methoxsalen followed by UVA exposure and methotrexate. All these treatments improve the clinical appearance, but do not cure the disease [259, 260]. Current clinical trials by the US National Institutes of Health (Table I.4) are mainly oriented towards the improvement of clinical aspects of the disease, rather than causal treatment.

Novel approaches for decreasing the fibrosis include modulation of cytokine expression in the sclerotic tissue. TGFβ, IFN-γ, IL-4, endothelin, CTGF are some of the targets [261]. Imiquimod, an IFN-γ inducer, was successfully used to clinically improve signs of morphea. Topically applied imiquimod 5% cream induced Th1 type response and induced regression of morphea plaques in patients [262]. Animal studies in tight-skin mice, the genetic model for scleroderma, indicate administration of IL-12 coding plasmid significantly reduces skin thickness and production of IL-4, and increases IFN-γ levels at a dosing regimen of 100 μg plasmid injected once every three weeks for 21 weeks [263]. The same effect can be achieved by blocking the endogenous TGF-β signaling with anti-TGF-β antibodies or TGF-β1 antisense oligonucleotide [264]. Zhou et al. [265] analyzed fibroblasts from scleroderma patients and found increased SPARC (secreted protein, acidic and rich in cystein) levels. This protein regulates the assembly and deposition of extracellular matrix components, and its modulation might contribute to the control of the disease. IFN-γ decreases collagen production *in vitro* in overproliferative fibroblasts from hypertrophic scars and *in vivo* improves the clinical

Table I.4. Ongoing clinical trials sponsored by the US National Institutes of Health or other agencies in 2005

Study	Agent	Characteristics	Form of scleroderma	Sponsor/ Phase (ClinicalTrials.gov Identifier)
Oral Type I Collagen for Relieving Scleroderma	Drug: bovine type I collagen	Daily oral dose of bovine type I collagen	Diffuse systemic scleroderma	National Institute of Arthritis and Musculoskeletal and Skin Diseases (NIAMS) Phase II (NCT00005675)
Safety and Value of Self Bone Marrow Transplants Following Chemotherapy in Scleroderma Patients	Drug: fludarabine, cyclophosphamide, thymoglobulin Procedure: leukapheresis, self bone marrow transplant	Safety and value of self bone marrow transplants after chemotherapy	Systemic Sclerosis	National Institute of Arthritis and Musculoskeletal and Skin Diseases (NIAMS) University of Pittsburgh Cancer Institute Amgen Genzyme Phase I (NCT00040651)
Efficacy and Safety of Oral Bosentan on Healing/Prevention of Digital (Finger) Ulcers in Scleroderma	Drug: bosentan	Prevention and healing effects of bosentan versus placebo on digital ulcers	Scleroderma patients with or without digital ulcers at baseline	Actelion Phase III (NCT00077584)
Scleroderma: Cyclophosphamide or Transplantation (SCOT)	Procedure: self blood cell transplantation Drug: high-dose immunosuppressive therapy: cyclosphosphamide, equine antithymocyte globulin, methylprednisolone, growth colony stimulating factor	Comparison of two treatments: 1- high-dose immunosuppressive therapy followed by self blood cell transplantation 2- high-dose pulse IV cyclophosphamide	Severe systemic sclerosis	National Institute of Allergy and Infectious Diseases (NIAID) Phase II/III (NCT00114530)

Efficacy and Safety of Oral Bosentan in Pulmonary Fibrosis Associated with Scleroderma	Drug: bosentan	Possibility of oral administration of bosentan	Diffuse or limited systemic sclerosis associated by significant interstitial lung disease	Actelion Phase II/III (NCT00070590)
Safety, Tolerability, and Pharmacokinetics of CAT-192 (Human Anti-TGF-Beta1 Monoclonal Antibody) in Patients with Early Stage Diffuse Systemic Sclerosis	Drug: human anti-transforming growth factor beta-1 monoclonal antibody	Evaluation the safety, tolerability, and pharmaco-kinetics of repeated treatments with CAT-192	Early stage diffuse systemic sclerosis	Genzyme Cambridge Antibody Technology Phase I/II (NCT00043706)
Rapamycin Vs Methotrexate in Diffuse SSc	Drug: rapamycin Drug: methotrexate	Determination of safety of the rapamycin compared to methotrexate	Diffuse systemic sclerosis	University of California, Los Angeles Phase I/II (NCT00241189)

Ultraviolet B (UVB) Light Therapy in the Treatment of Skin Conditions With Altered Dermal Matrix	Procedure: UVB irradiation	Evaluation the effectiveness of high dose UVB light therapy	Keloid (or hypertrophic scar), scleroderma, acne keloidalis nuchae, old burn scars, granuloma annulare or related conditions in subjects with darkly pigmented skin	University of Michigan Phase II/III (NCT00129428)
Treatment of Early Systemic Sclerosis by Bosentan	Drug: bosentan	Inhibition of fibroblast activity early in the disease course	Systemic sclerosis	Rikshospitalet University Hospital Phase I/II (NCT00226889)
Imiquimod in Children with Plaque Morphea	Drug: imiquimod	Pilot study to assess to potential efficacy and relative safety of Imiquimod	Children with morphea (localized scleroderma)	The Hospital for Sick Children Phase IV- not recruiting yet (NCT00147771)
Imiquimod 5% Cream in Plaque-Type Morphea: A Pilot, Prospective Open-Label Study	Drug: imiquimod 5% cream (Aldara)	Safety and efficacy of imiquimod 5%	Morphea	University of Alberta 3M Pharmaceuticals Phase III- not recruiting yet (NCT00230373)

Safety and Efficacy of Pletal (Cilostazol) for the Treatment of Juvenile Primary and Secondary Raynaud's Phenomenon	Drug: cilostazol (Pletal)	Safety and effectiveness of cilostazol to lessen the severity of the symptoms and decrease the number of secondary Raynaud's episodes in juvenile patients	Raynaud's Disease	Otsuka America Pharmaceutical Phase IV (NCT00048776)
Phase III Randomized, Double-Blind, Placebo-Controlled Study of Oral Iloprost for Raynaud's Phenomenon Secondary to Systemic Sclerosis	Drug: iloprost	Evaluation of the safety and efficacy of oral iloprost	Raynaud's Disease secondary to systemic sclerosis	National Center for Research Resources (NCRR) University of Pittsburgh Phase III (NCT00004786)
Phase II Pilot Study of Cyclophosphamide and Rabbit Anti-Thymocyte Globulin as Salvage Therapy in Patients With Diffuse Systemic Sclerosis	Drug: anti-thymocyte globulin, cyclophosphamide	Determination of the toxicity of cyclophosphamide and rabbit anti-thymocyte globulin	Diffuse systemic sclerosis	Fred Hutchinson Cancer Research Center Phase II (NCT00016458)

Stem Cell Transplant to Treat Patients with Systemic Sclerosis	Drug: cyclo-phosphamide, mesna, growth colony stimulating factor Procedure: leukopheres is, total body irradiation	Discovery if stem cell transplantation can help patients with systemic sclerosis	Systemic sclerosis	Baylor College of Medicine The Methodist Hospital Phase I (NCT00058578)

Source: http://clinicaltrials.gov/ct/gui/

signs of overproliferative skin conditions such as scleroderma, morphea and keloids [266, 267].The mechanism by which the collagen synthesis is reduced is complex [268]. *In vivo* studies on experimentally induced scleroderma in mice demonstrate that after injecting the sclerotic agent (bleomycin), subcutaneous administration of $5x10^5$U/mL IFN-γ for three weeks reduces the hydroxyproline content of the skin significantly by up to 72% [269]. Delivery of IFN-γ to the skin could provide the required amount of drug at the target site without systemic exposure. After injection of gene expression vectors of eight human cytokines (IL-4, IL-6, IL-10, TGF-β1, TNF-α, MACAF, GM-CSF and IFN-γ) into rat skin, transgenic cytokine expression in keratinocytes and serum were assessed. All cytokines were expressed in the keratinocytes (20-200pg/μg protein). The interleukins and TGF-β, but not the other cytokines, were detected in the sera of the animals [33]. These findings demonstrate that the kerationocytes in the epidermis can be used to express genes introduced via plasmid vectors. The generated proteins might exhibit local or systemic effects.

Early clinical studies indicated significant decrease of the skin thickness score and the area score in systemic sclerosis after intramuscular IFN-γ administration (100-500 μg/m^2 three times weekly for 18 weeks) [270]. More recent studies indicate mixed results and the side effects are common, mainly with flu-like symptoms [271]. The poor clinical results might be attributed to the low levels of IFN-γ in the tissues affected by sclerosis, due to its short half-life of only 1-3 to 30 minutes [272, 273], and the presence of the side effects might be associated with the systemic administration of the protein-based treatment. Injection of 100 μg IFN-γ subcutaneously in the periphery of localized lesions did not produce the desired effect of reducing the size or fibrosis in the existent lesions, but was able to prevent the apparition of new lesions. The reason might be that

IFN- γ inhibits the synthesis of collagen, but has no effect on collagen-degrading enzymes [274]. The invasive administration of the therapeutic protein and the tissue damage caused might also have triggered an unwanted cytokine cascade.

Currently, approved treatment options for IFN- γ do not include localized scleroderma. Accepted indications for the recombinant human IFN-γ1b are in reduction of frequency and severity of infections associated with chronic granulomatous disease and as adjuvant in severe malignant osteopetrosis [275]. Due to its antiproliferative, antifibrotic, antitumour and antimicrobial properties, IFN-γ opens new perspectives in clinical dermatology [276]. New applications include viral infections, as adjuvant in IFN-α treatment in human papillomavirus infections [277], bacterial infections due to its Th1/Th2 modulatory effect in leishmaniasis [278], and mycobacterial infections [279]. Other potential topical applications include atopic dermatitis [280], decrease of fibroblast proliferation in hypertrophic scars [281] and malignant melanoma [282].

Treatment of scleroderma with IFN-γ could have several advantages compared to other treatment options. Through the YB1 pathway, IFN-γ directly inhibits the *Col1A2* transcription. Moreover, due to its inhibitory action on the p300/CBP cofactor, IFN-γ neutralizes the effect of both IL-4 and TGF-β on fibroblasts and inhibits the transcription of both *Col1A2* and *TGFB* in the target cells. Anti IL-4 or TGF-β would abolish only the mediation through either STAT6 or Smads, leaving the other pathways open. A disadvantage of blocking the TGF-β is that it can affect not only the hypertrophied skin but other tissues such as vascular walls, cartilages and ligaments. The same disadvantage is valid for systemic halofuginone treatment that reduces the collagen-producing cells [283]. In fibrotic disorders, the number of fibroblasts decreases with the progression of the disease and many of them differentiate into myofibroblasts, which are characterized

by excessive extracellular matrix synthesis, synthesis of tissue inhibitor of metalloproteinase (inhibits collagen degradation), increased reactivity to TGF-β, and decreased sensitivity to IFN-γ [284, 285]. Due to its effect on fibroblast proliferation IFN-γ could expand the number of healthy fibroblasts and restore the normal collagen homeostasis in the dermis. IFN-γ can also play a role in the restoration of the immune balance by stimulation of the Th1 cells.

Relaxin could be considered as an alternative treatment option to decrease of collagen in the skin. Relaxin is a polypeptide with hormone function secreted by the ovary in high amounts during pregnancy. One of its functions is to reduce collagen synthesis during pregnancy in order to soften the birth canal. In fibroblasts derived from scleroderma patients, both relaxin and IFN-γ reduced collagen synthesis, and when used in combination relaxin augmented the effect of IFN-γ [286].

For localized scleroderma, the topical application of IFN-γ protein or the encoding gene has several advantages such as ease of self-administration, good patient compliance, maximum effect at site of application without increased plasma concentration, avoidance of RES clearance and controlled release of the macromolecular drug. In addition, the treatment can easily be terminated at the point where clinical assessment confirms the remission of the sclerotic lesions on the skin.

Administration of plasmids coding for IFN-γ could have several advantages over protein administration: (1) generation of the biologically active protein in the skin, using the bioreactor function of the keratinocytes, (2) increase of the half-life by sustained gene expression, (3) possibility of insertion of two or more genes in the same vector (i.e., *IFN-γ* and *Relaxin*), and (4) reduction of systemic side effects, due to the dermal localization of the generated protein [33].

II HYPOTHESIS

The main hypothesis is that IFN-γ coding plasmid can be delivered into the skin after topical application using gemini surfactant-based delivery systems and IFN-γ will be expressed in the skin.

Sub-hypothesis 1: Gemini surfactants will be suitable DNA-complexing biomaterials for topical gene delivery.

Sub-hypothesis 2: IFN-γ expressed within the skin will have an impact on the pathophysiological markers of localized scleroderma in a mouse model.

III. RATIONALE

The skin is the largest somatic organ in the body. It is easily accessible, and represents an attractive site for treatment of various dermatological and systemic disorders. Previous studies demonstrate that keratinocytes can act as a bioreactor. The bioreactor concept means that transfected keratinocytes continuously express the desired therapeutic protein for a specific period of time. The duration of gene expression is modulated by the transfer vector; viral vectors tend to incorporate the foreign gene into the genomic DNA causing long-term expression, while non-viral carriers (plasmids) do not have the ability to insert DNA into the chromosomes, and the gene expression is transient. Moreover, keratinocytes are immunocompetent cells able to express surface antigens and secrete (constitutively or stimulated) cytokines, chemokines and growth factors that modulate the cell-mediated and humoral immune responses. Conversely, fibroblasts are not part of the immune cells, thus are void of the ability to express surface antigens and participate in immunological processes.

Localized scleroderma is a cutaneous disorder characterized by excessive collagen deposition in the skin. The disease is progressive, and in severe cases can cause severe disfiguration. The etiology of the disease is unknown. Current antifibrotic treatment options are limied, and include iloprost (prostacyclin), a vasodilator, Ecteinascidin 743, a compound with antitumour activity, atorvastatin, a drug used to treat hyperlipidemia, with some immunomodulatory properties, and UV radiation. Evaluation of the efficacy of the treatments is difficult due to (1) the skin softens

spontaneously after a maximal degree of fibrosis, (2) the treatment started at advanced stages of sclerosis resolves the sclerosis slowly, (3) the degree of skin sclerosis is not correlated with the overall disease stage, and (4) the evaluation of skin score is subjective [250].

Extracellular IFN-γ can inhibit the excessive collagen production in fibroblasts by direct action (YB1 pathway) and by interference with the P300/CBP cofactor. This inhibition blocks the profibrotic effect of IL-4 and TGF-β, with both STAT6 and Smad pathways needing the P300/CBP protein in order to activate *COL2A1* transcription. At the same time, autoinduction of TGF-β is also inhibited by IFN-γ at the transcriptional level.

In pathological conditions, IFN-γ is effective in reducing excessive deposition of collagen both *in vitro* in fibroblasts, grown in three dimensional collagen lattices, and *in vivo* in clinical studies with scleroderma patients. However, due to clinical side effects, systemic use of IFN-γ for scleroderma may not be possible.

To locally treat scleroderma, the keratinocytes in the epidermis can transiently express IFN-γ from plasmid DNA. By establishing an appropriate treatment regimen, therapeutic protein levels could be reached directly in the skin, and the length of therapy could be decided based on the clinical appearance of the lesions (remission of the plaques), reduction of skin thickness score and increase of the elasticity of the skin.

By developing an effective topical non-invasive dosage form for IFN-γ coding plasmid and providing a sustained supply of IFN-γ within the skin, a more effective approach for the management of the cutaneous form of scleroderma can be achieved.

Cationic lipids are able to bind DNA and neutralize the surface charges of the phosphate backbone of the molecule. By this interaction, the plasmid is compacted and

can penetrate through biological membranes. Intracellularly, the cationic surfactants protect the DNA against degradation by endonucleases. The nature of the cationic surfactant and the presence of helper lipids that enhance permeation by temporarily perturbing lipids cell membranes and the stratum corneum will determine the *in vitro* and *in vivo* transfection efficiency of the delivery system. Physico-chemical characterization of the delivery systems, and study of their interaction with the plasmid and biological membranes, could lead to development of topical formulations with improved efficiency.

Several strategies could be explored in order to increase transgene expression and achieve therapeutic protein levels: (1) optimization of the plasmid construct (i.e., appropriate backbone and promoter region), (2) optimization of the delivery system (effect on the genetic material, such as compaction and protection, and on the stratum corneum and cell membranes), and (3) use of permeation enhancers to facilitate the penetration of the plasmid DNA into the skin in order to reach target cells.

In this project we will assess:

(1) formulation development and characterization for *in vitro* and *in vivo* gene delivery;

(2) quantitative aspects of DNA plasmid delivery by *in vitro* and *in vivo* experiments;

(3) the efficiency of topical delivery; and

(4) the therapeutic role of the IFN-γ in scleroderma-affected skin (Tsk tight skin mouse model).

IV. PRIMARY OBJECTIVE

The primary objective is to investigate the feasibility of delivering plasmid DNA coding for IFN-γ into skin using a novel cationic gemini delivery system and to evaluate the level of expression of IFN-γ in normal, IFN-γ-deficient and disease (scleroderma) mouse models.

V. SPECIFIC OBJECTIVES

V.1 To prepare and characterize lipid-based DNA delivery systems

a. Purify and characterize plasmids designed for mammalian expression of the IFN-γ gene, to be used for delivery studies *in vitro* (in murine keratinocyte cell line) and *in vivo* in mice.

b. Prepare novel gemini surfactant–DNA complexes, for *in vitro* and *in vivo* delivery.

c. Evaluate physicochemical characteristics and pharmaceutical properties of the delivery agents by light, atomic force and electron microscopy, circular dichroism, size and ζ (zeta) potential measurements, dye binding and small angle X-ray scattering.

d. Evaluate the relationship between physicochemical properties of cationic gemini delivery systems and their efficiency *in vitro* and *in vivo.*

V.2 To develop methods suitable for evaluation of DNA delivery in vitro *and* in vivo

a. Optimize PAM 212 keratinocyte cell culture, transfection, sample collection and detection methods.

b. Develop topical treatment regimens, sample collection and analysis methods.

c. Set-up and validate enzyme-linked immunosorbent assay (ELISA), fluorescence activated cell sorting (FACS) and fluorescent microscopy for protein detection, and polymerase chain reaction (PCR) and reverse transcription PCR (RT-PCR) methods for skin homogenate to determine the amount of plasmid DNA and mRNA in the skin.

V.3 To evaluate the rate and extent of DNA delivery

a. Quantify by PCR the delivered plasmid into the skin in an animal model by comparing the quantity of the amplified fragment to known amount of templates.

c. Determine the protein expression by ELISA and fluorescent microscopy.

d. Evaluate the effect of IFN-γ in a localized scleroderma model (tight skin mouse).

VI. MATERIALS AND METHODS

VI.1 Plasmids

The plasmid pIRES2.EGFP (Clontech, Palo Alto, CA) contains the gene encoding for the enhanced green fluorescent protein (GFP) fused with internal ribosomal recognition sequence (IRES), preceded by a multiple cloning site for gene insertion. The gene of murine IFN-γ, containing the sequence coding for 155 amino acids of the murine IFN-γ [287], was obtained by restriction digest with Bgl II from the pSLRSV.IFN plasmid. The pGT plasmid (kindly supplied by Dr. R. Pontarollo, VIDO, Saskatoon, SK), a vector designed for gene therapy, has the CpG motifs removed and contains the human cytomegalovirus (CMV) promoter, kanamycin resistance site. The murine cytomegalovirus promoter [288] was obtained from the pLMCMVgDt plasmid (kindly supplied by Dr. S. Tikoo, VIDO, Saskatoon, SK) by PCR, having the two primers designed in such way that the promoter included a Kpn I and a Pst I site.

a. pGTmCMV plasmid was obtained by replacing the human CMV promoter in the pGT vector with the murine CMV promoter.
b. pIRES.IFN-GFP plasmid contains the IFN-γ gene inserted into the multiple cloning site of the pIRES2.EGFP vector at the Bgl II- BamH I site. The plasmid was grown in *dam⁻/dcm⁻* E.coli and the IFN-γ–IRES–GFP coding sequence cut with Bgl II and Xba I.

c. pGT.IFN plasmid was constructed by inserting the IFN-γ gene into the Bgl II site of the pGT vector.
d. pGTmCMV.IFN plasmid was created by inserting the IFN-γ gene into the Bgl II site of the pGTmCMV vector.
e. pGT.IFN-GFP was obtained by inserting the IFN-γ–IRES–GFP fragment into Bgl II and Xba I sites of the pGT vector.
f. pGTmCMV.IFN-GFP was constructed by inserting the IFN-γ–IRES–GFP fragment into Bgl II and Xba I sites of the pGTmCMV vector.

Primers were designed and two fragments of the pIRES.IFN-GFP plasmid, one containing the gene of IFN-γ and one containing the IRES-GFP construct, were sequenced with automated sequencer (PBI/NRC, Saskatoon, SK) and compared with sequences retrieved from GenBank (NCBI databases).

Reagents were purchased from Invitrogen Life Technologies (Carlsbad, CA), and restriction enzymes from Amersham Pharmacia Biotech (Baie d'Urfe, QC).

VI.2 Formulation development for in vitro *transfection*

For transfection, a group of eleven gemini surfactants [115] were used (Figure IV.1).

1.5 mM aqueous solutions of the gemini cationic surfactants were prepared. The solutions were filtered through 0.2 μm Acrodisc® filters (Pall Gelman, Ann Arbor, MI).

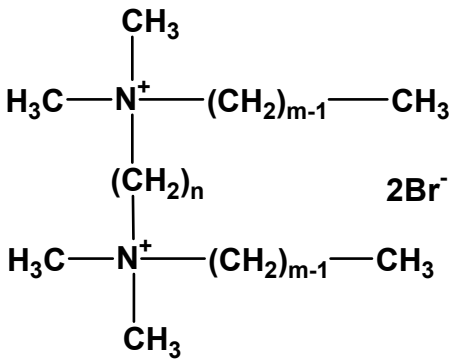

Figure IV.1. Structure of gemini surfactants.

The head group is composed of two positively charged nitrogen atoms each containing two methyl groups, a saturated hydrocarbon chain of 12 (m=12) or 16 (m=16) or an unsaturated carbon chain of 18 (m=18:1) carbon atoms, connected by a saturated carbon spacer of n carbon atoms (Table VI.1).

Table VI.1. Numerical designation for the gemini surfactants.

n	m	Chemical name	Symbol
3	12	1,3 propanediyl-bis(dimethyl-dodecylammonium) bromide	12-3-12
4	12	1,4 butanediyl-bis(dimethyl-dodecylammonium)bromide	12-4-12
6	12	1,6 hexanediyl-bis(dimethyl-dodecylammonium)bromide	12-6-12
8	12	1,8 octanediyl-bis(dimethyl-dodecylammonium)bromide	12-8-12
10	12	1,10 decanediyl-bis(dimethyl-dodecylammonium)bromide	12-10-12
12	12	1,12 dodecanediyl-bis(dimethyl-dodecylammonium)bromide	12-12-12
16	12	1,16 hexadecanediyl-bis(dimethyl-dodecylammonium)bromide	12-16-12
3	16	1,3 propanediyl-bis(dimethyl-hexadecylammonium)bromide	16-3-16
2	18:1	1,2 ethanediyl-bis(dimethyl-oleylammonium) bromide	18:1-2-18:1
3	18:1	1,3 propanediyl-bis(dimethyl-oleylammonium) bromide	18:1-3-18:1
6	18:1	1,2 hexanediyl-bis(dimethyl-oleylammonium) bromide	18:1-6-18:1

Lipid vesicles were prepared using sonication techniques. 1,2 dioleyl-*sn*-glycero-phosphatidylethanolamine (DOPE) (Avanti Polar Lipids, Alabaster, AL) and α-tocopherol (Spectrum, Gardena, CA) in 1:0.2 weight ratios were dissolved in 100% ethanol (Commercial Alcohols Inc., Brampton, ON) at 10 mg lipid/mL in a round bottom flask. The solvent was evaporated by rotary evaporation (Rotavapor RE111 BÜCHI Laboratoriums-Technik AG, Switzerland) at 100 rpm at 55^{o}C, producing a thin film deposited on the walls of the flask. Traces of organic solvent from the lipid were removed with high vacuum overnight. Glass beads were added to the flask and the lipid was resuspended at 1 mmol concentration in 9.25% isotonic sucrose (Spectrum) solution (pH= 9). The suspensions were bath-sonicated (Branson 2200, Cleansonic, Orange, VA) for 3 hours at 55^{o}C. The suspensions were filtered through 0.45 μm Acrodisc® filters.

The plasmid–gemini complexes (PG) were prepared as follows: 0.2 μg plasmid was mixed with an aliquot of gemini surfactant solution added to obtain a 5, 10, 20 or 40 +/-charge ratio and incubated at room temperature for 15 minutes prior to transfection. The plasmid–gemini–DOPE systems (PGL) were prepared by mixing the plasmid (0.2 μg/well) with the gemini surfactant solution (5, 10, 20 or 40 +/- charge ratio) and incubating at room temperature for 15 minutes. To this mixture, 25 μL of DOPE vesicles was added. Cells were transfected after a 30-minute incubation at room temperature.

VI.3 Transfection of PAM 212 cells with plasmid constructs

VI.3.1 Transfection using Lipofectamine

PAM 212 murine keratinocyte cells (kindly provided by Dr. S. Yuspa, NCI, Bethesda, MA) were grown to 90% confluency in 75-cm^2 tissue culture flasks in

supplemented MEM, prepared from minimal essential media (MEM) (Gibco BRL, Burlington, ON) with Antibiotic Antimycotic Solution (Sigma, Oakville, ON) 1:100 dilution, and 10% fetal bovine serum (FBS) (Cansera, Etobicoke, ON). The day before transfection, $5x10^4$ cells/well were seeded on 24-well plates (Greiner Labortechnik GmbH, Germany). For fluorescence imaging, the cells were grown on 13-mm diameter cover slips (Canemco, St. Laurent, QC) overnight at 37°C with 5% CO_2 in an incubator (Sanyo Electric Co. Ltd., Japan) to 70-80% confluency. The supplemented MEM was replaced with MEM one hour prior to transfection. The cells were transfected with the following plasmids: pSLRSV, pSLRSV.IFN, pIRES.GFP, pIRES.IFN-GFP, pGT, pGT.IFN, pGT.IFN-GFP, pGTmCMV, pGTmCMV.IFN and pGTmCMV.IFN-GFP, using Lipofectamine PLUS® (Invitrogen Life Technologies, Carlsbad, CA). For each well, 0.2 μg plasmid was used. The transfection method followed the manufacturer's protocol and was optimized for the PAM 212 cells. Briefly, 0.2 μg plasmid was mixed with 10 μL Plus reagent in 25 μL MEM and incubated at room temperature for 15 minutes. Four μL of Lipofectamine reagent mixed with 25 μL of MEM was added to the plasmid. After incubating the mixture for 15 minutes at room temperature, it was added dropwise to cells covered with 200 μL of fresh MEM. The plates were incubated for 5 hours at 37°C in a CO_2 incubator, then the transfection mixture was replaced with supplemented MEM, and the incubation continued for 24 hours, after which the supernatants were collected. Media on the cells was replaced with fresh media. After another 24-hour incubation period, the second supernatants were collected and stored at -20°C.

VI.3.2 Transfection of PAM 212 cells with pGTmCMV.IFN-GFP plasmid using PG and PGL systems

PAM 212 murine keratinocyte cells were prepared for transfection as described earlier. The transfection mixtures were prepared as described earlier, and then added to the cells dropwise. The plates were incubated for 5, 6, 8, 10 or 24 hours at 37^{o}C in a CO_2 incubator. The transfection mixture was replaced with supplemented MEM and the plates further incubated for 24 hours. The supernatants were collected and stored at -20^{o}C. For positive control, the cells were transfected with Lipofectamine PLUS® as described above.

VI.4 Topical formulations

Three dermal delivery systems were prepared with the 12-3-12, 16-3-16 and 18:1-3-18:1 gemini surfactants. A cationic nanpoarticle formulation (NP) was prepared with DOPE 10 mg/mL, 1,2 dipalmitoyl-*sn*-glycero-phosphatidylcholine (DPPC) (Sigma) 10 mg/mL, the gemini surfactant 10 mg/mL, and diethylene glycol monoethyl ether (Gattefossé, Saint-Priest, France) 25 mg/mL, containing 25 μg of plasmid in 50 μL of formulation (NP12, NP16, NP18 formulations). As a comparison, cholesteryl 3β-(-N-dimethylamino-ethyl carbamate) (Dc-chol, Sigma) was used in a nanoparticle formulation: DOPE 10 mg/mL, DPPC 10 mg/mL, Dc-chol 10 mg/mL, and diethylene glycol monoethyl ether 25 mg/mL (NPDc formulation). The applied dose was 25 μg plasmid in 50 μL formulation. The nanoparticle formulation prepared with the 16-3-16 surfactant (NP16) was further improved for application on the Tsk mice (to overcome the barriers created by the morphological changes in the skin, such as increased thickness and rigidity). The new formulation (NP16-PDM) had the following

composition: DOPE 25 mg/g, purified phoshatidylcholine from soybean lechitin 25 mg/g, and the 16-3-16 gemini surfactant 10 mg/g formulation. Two permeation enhancers were added: an in house synthesized amino acid derivative (PDM 27) 10 mg/g, and propylene glycol 70 mg/g. The plasmid concentration was increased to100 μg in 100 μg formulation. All nanoparticle formulations contained α-tocopherol as an antioxidant agent. A cationic nanoemulsion (NE) was prepared with PEG-8 caprylic/capric glycerides 200 mg/mL, polyglyceryl-3-isostearate 200 mg/mL, octyldodecyl myristate 400 mg/mL (all ingredients from Gattefossé) and the gemini surfactant 10 mg/mL. The topical formulations were characterized (by visual appearance such as consistency, colour, transparency, atomic force microscopy (AFM), TEM, size and ζ-potential measurement).

VI.5 Topical treatment

The animal experiments were approved by the University of Saskatchewan Committee on Animal Care and Supply Protocol Review. Four different strains of mice were used: 8-10-week old female CD1 mice (Animal Resource Center, University of Saskatchewan, Saskatoon, SK), 8-10-week old female IFN-γ-deficient mice (B6.129S7-*IFNg*^{tm1Ts}/J, The Jackson Laboratory, Bar Harbor, ME) and 4-8-week old female Tsk- mice (B6.Cg-*Fbn1*^{Tsk}+/+Pldn^{pa}/J, The Jackson Laboratory). The animals were anesthetized with isoflurane and close-shaved one day prior to treatment. For the short-term treatment regimen, the topically treated groups of CD1, IFN-γ-deficient and Tsk animals were anesthetized with acepromazine/ketamine (5 mg/100 mg per kg) injected intraperitoneally. The shaved area was cleaned with distilled water and was dried using sterile gauze. Nanoparticle and nanoemulsion formulations (50 μL containing 25 μg

pGTmCMV.IFN-GFP plasmid for each animal) were painted on the shaved area using a pipette, and covered with Parafilm for 2-3 hours (Figure IV.2). For the CD1 mice the treatments were repeated at 24 and 48-hour intervals. Each animal received a total dose of 75 μg pGTmCMV.IFN-GFP plasmid. The IFN-γ deficient and Tsk animals were treated for four days, receiving a total dose of 100 μg pGTmCMV.IFN-GFP plasmid. For the 20-day treatment of the Tsk mice, the animals were anesthetized with isoflurane. On the shaved back area, 100 mg formulation was applied then covered with Parafilm and sealed with Op-site. The animals were placed in individual restrainers for 2 hours. The treatment was applied once daily for five days per week and lasted for 4 weeks. The animals were reshaved once weekly. Each animal received 500 μg pGTmCMV.IFN-GFP plasmid per week. In the injected CD1 animals were intradermally treated on their backs at three locations with NE plasmid formulation (5 μg plasmid/site), low and high concentration of aqueous plasmid solution (2.5 and 5 μg plasmid/site) or phosphate buffered saline pH=7.2 (PBS). The total dose for the animals injected with NE-DNA formulation was 15 μg plasmid per animal and for the injected DNA solutions was 7.5 μg plasmid (low dose) and 15 μg plasmid per animal (high dose). The Tsk mice for the 4-day treatment were injected intradermally on their shaved back once 24 hours prior to sample collection at four locations (2.5 μg plasmid/site, total dose 10 μg) For the 20-day treatment the animals were injected intradermally with 2.5 μg plasmid at four locations twice weekly, for a total duration of four weeks. The total dose was 20 μg plasmid per week. The control animals were shaved and left untreated. Blood, skin biopsies, lymph nodes from inguinal and axillary sites and spleen were harvested 24 hours after the last treatment.

A B

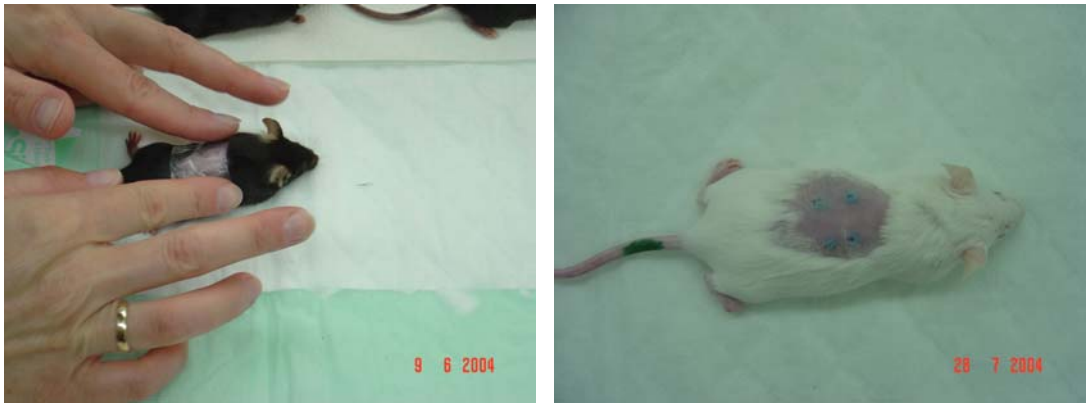

Figure IV.2. Topical and intradermal treatment of the animals.

A – Mice treated with topical nanoparticle and nanoemulsion formulation (illustrated on an IFN-γ-deficient mouse). The treatment area (2x2cm) was shaved one day prior to the first application. The skin was cleaned with sterile gauze and purified water. The formulations were painted on the shaved area, covered with parafilm and sealed with Op-site. The animals were immobilized for 2-3h (anesthesia or restraining cages) to allow absorption of the formulation.
B – Mice injected intradermally with nanoparticle formulation, plasmid solution or PBS (illustrated on a CD1 mouse). The shaved area (2x2cm) was cleaned with sterile gauze and purified water before the injections. The injection sites are visualized with trypan blue dye.

VI.6 Sample processing

Plasma was separated by centrifugation from blood collected from animals by cardiac puncture, and stored at -20°C. The skin was rinsed with distilled water using sterile gauze and the treated areas were excised. The samples were snap-frozen in liquid nitrogen, and stored at -80°C. The axillary and inguinal lymph nodes were collected, snap-frozen in liquid nitrogen, and stored at -80°C. The skin was homogenized under liquid nitrogen using a biopulverizer. The device was thoroughly cleaned, disinfected with 70% ethanol and dried in a laminar flow hood under UV light for 15 minutes between the recoveries from different groups to avoid cross-contamination. The lymph nodes were homogenized in microfuge tubes with disposable pellet pestles (Kontes, VWR, Mississauga, ON).

The homogenized skin samples dedicated for ELISA and the lymph nodes were resuspended in 500 µL protein resuspension buffer (PBS containing leupeptin 10 µg/mL (Sigma) and soybean trypsin inhibitor 20 µg/mL (Sigma)). The homogenates were vortexed for 1 minute, sonicated for 30 seconds and kept on ice for 1 minute. This cycle was repeated three times. All samples were centrifuged at 16,000*g* for 15 minutes. The supernatants, free of cell debris, were collected and stored at -20°C.

The homogenized skin samples dedicated for plasmid quantification by PCR were resuspended in proteinase K solution (200 µg/mL), incubated for 2 hours at 56°C, heated for 10 minutes to 95 °C, chilled on ice for 10 minutes and centrifuged at 16000*g* at 4°C for 20 minutes. The supernatants were collected and used for PCR.

The total RNA from skin homogenates was isolated using RNeasy Lipid Tissue Mini Kit (Qiagen, Mississauga, ON) according to the manufacturer's protocol.

Approximately 20 mg of skin from each animal was used. To the tissue, 500 μL Qiazol Reagent was added, and the samples further homogenized with a Pro200 rotor-stator homogenizer (Pro Scientific Inc., Oxford, CT). Another 500 μL of Qiazol Reagent was added and incubated for 5 minutes at room temperature to dissociate the nucleoprotein complexes. The RNA was extracted after adding 200 μL chloroform (Sigma) by shaking the samples vigorously for 15 seconds by hand. After two minutes of incubation, the samples were centrifuged at 12000*g* for 15 minutes at 4^{o}C. The mixture separated into a bottom phenol-chloroform layer, an intermediate film and a top aqueous layer containing the total RNA. The clear supernatant (~600 μL) was carefully transferred into a fresh tube, and the RNA precipitated with 600 μL of 70% ethanol (prepared with endonuclease-free purified water; Gibco). The samples were added onto the binding membrane in 6-700 μL portions and centrifuged at 8000*g* at room temperature for 20 seconds. The flow-through was discarded after each centrifugation. The membrane was washed consecutively with 700 μL RW1 wash buffer and twice with 500 μL RPE wash buffer. The membrane was dried by centrifugation at 12000*g* for 1 minute. The binding columns were transferred into fresh microfuge tubes. The RNA was eluted twice with 30 μL of purified water by centrifugation at 12000*g* at room temperature for 1 minute. The total RNA was quantified and integrity verified using Agilent 2100 Bioanalyzer (Agilent Technologies, Palo Alto, CA). The single- and double-stranded DNA was digested from RNA samples (1 μg total RNA) with DNase I (1U/μL) and incubated for 15 minutes at room temperature to complete the reaction. The DNase I was inactivated by addition of 25 mM EDTA. Samples were heated for 10 minutes at 65^{o}C, when the RNA samples were ready to be used in reverse transcription prior amplification. First-strand cDNA was synthesized using Superscript II for RT-PCR. RNA sample (1 μg), 20 μM

Oligo$(dT)_{12\text{-}18}$ and 10 mM dNTPs were mixed and heated at 65^{o}C for 5 minutes, then quickly chilled on ice. The contents of the tube were collected by brief centrifugation. First strand buffer, 0.1 M DTT and RNase inhibitor (40 U/μL) were added. The contents of tubes were mixed gently and incubated at 42 ^{o}C for 2 minutes. Superscript II was added and mixed by pipetting up and down. After 50 minutes of incubation at 42^{o}C, the enzyme was inactivated by heating at 70^{o}C for 15 minutes. The cDNA was used for real-time PCR and PCR to quantify the mRNA.

VI.7 ELISA

ELISAs were performed using round bottom 96-well plates (Immulon II, Dynatech Laboratories, Chantilly, VA). The plates were coated with 50 μL/well capture antibody: rat anti-mouse IFN-γ (2 μg/mL) in coating buffer (0.05 M $NaHCO_3$, pH=9.6) and incubated for 24 hours at 4^{o}C. The wells were blocked with 1% bovine serum albumin (BSA) (New England Biolabs, Mississauga, ON) in PBS at room temperature for one hour. Recombinant murine IFN-γ standard was used at a 2000 pg/mL concentration and was consecutively diluted one in four with 1% BSA solution on plates. 1% BSA solution was used as a blank control. The supernatants from cell cultures, as well as the skin and lymph homogenates and the serum from mice, were diluted one in four on plates. The plates were incubated overnight at 4^{o}C. Biotinylated rat anti-mouse IFN-γ (0.5 ng/mL in 1% BSA solution) was added. The plates were incubated for 2 hours at room temperature. The streptavidin-alkaline phosphatase conjugate (Invitrogen Life Technologies, Carlsbad, CA) was added in 1:1000 dilution, and incubated for 1 hour at room temperature. The 4-nitrophenyl phosphate di(tris) salt 1 mg/mL in PNPP buffer (1% diethanolamine, 0.5 mM $MgCl_2$, pH=9.8; Sigma) was used

to develop the assay. Optical density of the samples was measured at 405 nm, using a Benchmark Microplate Reader (BioRad, Mississauga, ON) instrument and the concentration of the IFN-γ was calculated from a standardized IFN-γ curve. Antibodies and recombinant murine IFN-γ were purchased from Pharmingen, Mississauga, ON.

VI.8 Bioassay

The murine IFN-γ was tested for biological activity based on the reduction of the viral cytopathic effect [27]. The protocol, cells, virus and antibody were kindly supplied by Dr. C. Havele, University of Saskatchewan, SK. On a 96-well flat bottom plate (Greiner Labortechnik GmbH, Germany) $5x10^4$ L929 cells (ATTC# CCL-1) grown in RPMI-1640 medium supplemented with 10% FBS, 0.1 mM 2-mercaptoethanol (Sigma, Burlington, ON), 0.8 mM sodium pyruvate (Sigma) and antibiotic-antimycotic solution (Sigma) 1:100 dilution were plated together with 1:2 serial dilutions of the supernatants from PAM 212 cells transfected with pGTmCMV.IFN-GFP. The plates were incubated for 24 hours in a CO_2 incubator. The media were replaced with a 100-fold dose of the TCD_{50} (tissue culture dose 50) of endomyocarditis (EMC) virus [289] in 100 µL media. The TCD_{50}, determined by Karber assay, defines the dose of virus required to cause death of 50% of the cells in culture. The cells were incubated with virus and the endpoint determined as the moment when the virus caused the death of 100% of cells untreated with IFN-γ. The wells were washed with PBS, the cells fixed for 15 minutes in 4% formaldehyde (Sigma) and stained with 0.05% crystal violet (Sigma) solution in 20% methanol for 15 minutes. The plates were washed and dried. Before measuring, 100 µL methanol/well was added to the plates. The absorbance was read at 595 nm on automated plate reader ($PowerWave_x$, Biotech Instruments Inc., Winooski, VT). To

verify the non-specific antiviral effect, monoclonal antibody against IFN-γ activity XMG1.2 [290] was added to the supernatants. Standard recombinant murine IFN-γ (Pharmingen, Mississauga, ON) was also included in the assay.

VI.9 PCR

For the detection of the plasmid DNA, four primers were designed for nested PCR. The external primers were: sense (pKanEF) 5'–*ACT CAC CGA GGC AGT TCC AT*-3' and antisense (pKanER) 5'–*GGT AGC GTT GCC AAT GAT GT*–3', amplifying a 540-bp fragment of the pGTmCMV.IFN-GFP plasmid. The internal primers were: sense (pKanIF) 5'–*ATG GCA AGA TCC TGG TAT CG*–3' and antisense (pKanIR) 5'–*TTA TGC CTC TTC CGA CCA TC*–3', which amplify a 459-bp fragment from the previous reaction. All primers were purchased from Invitrogen Life Technologies, Carlsbad, CA. Thirty five μL of supernatant from skin homogenate were used for the amplification with the external primers, and 2 μL of the PCR product were used for amplification with the internal primers. Standard dilutions were prepared with the pGTmCMV.IFN-GFP plasmid at 10^2, 10^3, 10^4, 10^5 and 10^6 copies/PCR reaction. PCR Reagent System (Invitrogen Life Technologies, Carlsbad, CA) was used for the reactions. The PCR mixtures were prepared according to the manufacturer's protocol.

PCR to detect murine procollagen type Iα2 from cDNA was performed using custom primers: forward primer: 5'–CCA GGC CAA CAA GCA TGT CT–3', reverse primer: 5'–GTC AGC ACC ACC AAT GTC CA–3', amplifying a 400-bp fragment. For each reaction, 2 μL of cDNA were mixed with 1 μL of each primer (10 pmol/μL) and 22.5 μL of PCR Supermix (Invitrogen). Glyceraldehyde-3-phosphate dehydrogenase (Gapdh) primers were used for the housekeeping gene (452-bp fragment). The PCR

conditions were: hot start for 4 minutes at 94°C, denaturation at 94°C for 45 seconds, annealing at 56°C for 30 seconds, extension for 30 seconds at 72°C and final extension at 72°C for 7 minutes. The reaction was carried out in thirty cycles. A Techne Genius unit (Techne Incorporated, Princeton, NJ) was used. Band intensities were quantified using AlphaImager software.

VI.10 Real-time PCR

The cDNA was used to run real-time PCR using RT^2 Real-time™ gene expression kit and primer sets for mouse procollagen type Iα1 (NCBI RefSeq Accession # NM 007742) amplifying 122 bp fragments and mouse ICAM-1 (NCBI RefSeq Accession # NM 010493) amplifying 185 bp fragments. Glyceraldehyde-3-phosphate dehydrogenase (Gapd; NCBI RefSeq Accession # NM 008084), a ubiquitous gene was used as housekeeping gene (two primer sets amplifying 203 and 128 bp fragments) (Superarray, Frederic, MD). SYBR green was used to quantify double-stranded DNA. The reactions were carried out under the following conditions: hot start for 15 minutes at 94°C, denaturation at 94°C for 30 seconds, annealing at 56°C for 30 seconds, extension at 72°C for 30 seconds in 40 cycles and final extension at 72°C for 7 minutes, followed by melting curve between 45-100°C in 1°C increments for 10 seconds. The quantification was based on the ratio between the gene of interest detected in the treated and untreated animals, standardized to the housekeeping gene [291]:

$$ratio = 2^{-[\Delta Cp_{sample} - \Delta Cp_{control}]} \quad \text{(VI.1)}$$

where ΔCp_{sample} is the Cp deviation of untreated–treated of the target gene transcript; and $\Delta Cp_{control}$ is the Cp deviation of untreated–treated of the reference gene transcript.

The increase or decrease in the mRNA levels of the genes of interest was expressed as percentage of the control animals:

$$\%change = ratiox100 \quad \text{(VI.2)}$$

To confirm the size of the product, the fragments were separated by 2% agarose gel electrophoresis at 10 V/cm voltage.

VI.11 Fluorescence activated cell sorting (FACS)

PAM 212 cells were seeded on 6-well plates (Costar, Corning, NY) at $1x10^6$ cells/well density and grown to 60-80% confluency. The supplemented MEM was changed to MEM one hour prior to transfection. The transfection mixtures were prepared with 1 μg pGTmCMV.IFN-GFP, using the 16-3-16 gemini surfactant at 5, 10, 20 or 40 +/- charge ratios, as described earlier, keeping the concentration of the reagents constant. The supernatants were collected and stored at -20°C. The cells were detached using Versene solution containing 0.05% trypsin (Sigma), centrifuged at 4°C and 1000*g* for 5 minutes, washed twice with PBS and resuspended in Fa-cola (PBS with 0.2% gelatin and 0.03% Na azide). Triplicate samples were pooled. The cell sorter was calibrated with non-transfected cells and 10^4cells were counted of each sample.

VI.12 Microscopy

VI.12.1 Fluorescent, light and confocal microscopy

Cells were grown in 24-well plates on cover slips and transfected with plasmids, as described. Twenty-four hours after transfection, the cells were washed twice with PBS and mounted on cover slips. Skin samples snap-frozen in liquid nitrogen were

embedded in Tissue-Tek O.C.T. Compound (Canemco), and cut in 7 μm thick sections. They were mounted on poly-D-lysine-coated microscope slides. Phase contrast and fluorescent images were registered using an Axiovert 200M inverted microscope (Zeiss, Germany), with LD-A Plan 40X objective lens. The excitation and emission wavelengths for GFP were 488 nm and 507 nm, respectively (FITC filter). Autofluorescence was detected with a rhodamine filter (excitation at 570 nm, emission at 590 nm). Confocal one-photon images were collected from whole skin biopsies using an argon ion laser source and a Zeiss LSM410 microscope. A baseline measurement (autofluorescence) was performed at a 488 nm excitation wavelength and a 630-680 nm emission band, and the laser intensity adjusted. GFP fluorescence was measured using the same settings with a 514-560 nm band filter. The two obtained images were merged. The skin samples for light microscopy were fixed in 4% paraformaldehyde solution and embedded in paraffin. Sections of 7 μm thickness were stained with hematoxylin-eosine.

VI.12.2 Atomic force microscopy (AFM)

Atomic force microscopy images were obtained using a Pico SPM instrument (Molecular Imaging Inc., Tempe, AZ), with MAC-mode, and MI MAC cantilever type II (K=1.2-5.5N/m). The PG complexes were spread on the surface of freshly cleaved mica (Grade V-4, SPI Supplies, West Chester, PA), and incubated for 30 seconds or 15 minutes at room temperature. The PGL systems, topical nanoparticles or nanoemulsion (10 μL each) were spread on the surface of freshly cleaved mica, and incubated for 15 minutes at room temperature. The excess formulation was removed with lint free absorbent tissue, and the surface dried with N_2. A 4x4 μm area was scanned for the PGL systems, and nanoemulsion, and a 35x35 μm area for the topical nanoparticles.

VI.12.3 Transmission electron microscopy (TEM)

Transfection mixtures and topical formulations were prepared as described earlier. Carbon coated 300-mesh copper grids were discharged with UV light for 10 minutes prior to use. A 20 μL aliquot of sample was dropped on the grid and incubated for 15 seconds. The liquid was blotted with absorbent tissue. The specimens were stained with either 1% phosphotungstic acid (PTA) or 2% uranyl acetate (UA) for 15 seconds, and blotted with tissue. The dried samples were examined with a Philips CM 10 electron microscope at an accelerating voltage of 60 kV, and pictures taken on 3 ¼" x 4" Kodak Electron Microscope Film 4489.

VI.13 Dye-binding assay

Plasmid pGTmCMV.IFN-GFP (final concentration of 20 μg/mL) was complexed with the gemini surfactants at a +/- charge ratio of 10 in the presence or absence of DOPE as described for *in vitro* transfection on 96-well plates, with samples prepared in triplicates. Ethidium bromide (Sigma) was added to the samples at 0.1 μg/mL final concentration. The samples were incubated for 10 minutes at room temperature. Fluorescence excitation was carried out at 530 nm and emission measured at 590 nm using a BioTek FL600 plate reader (BioTek Instruments, Winooski, VT). The relative fluorescence of the PG complexes was expressed as a percentage of the fluorescence of a 20 μg/mL plasmid solution. The fluorescence of the PGL systems was compared to a plasmid–DOPE mixture.

VI.14 Circular dichroism (CD)

Aqueous gemini surfactant solutions and the DOPE suspension were prepared as for *in vitro* transfection and degassed at 37^{o}C in a bath sonicator. Plasmid pGTmCMV.IFN-GFP (20 μg/mL) and gemini surfactant were mixed at a +/- charge ratio of 10 using water or DOPE liposomes as a vehicle. The samples were incubated for 10 minutes at room temperature before measurements were carried out. Spectra were obtained by using an Applied Photo Physics π* 180 instrument (Leatherhead, UK) with a 1 nm slit, at 37^{o}C.

VI.15 Size and ζ-potential measurement by dynamic light scattering (DLS)

An aqueous solution of pGTmCMV.IFN-GFP plasmid was prepared at 500 μg/mL concentration. The transfection mixture with the pGTmCMV.IFN-GFP plasmid (20 μg/mL final concentration in the formulation), gemini surfactants (charge ratios of +/- 0.1 to 10) and DOPE vesicles was prepared as described earlier for transfection of PAM 212 keratinocytes. A control mixture was prepared by replacing the plasmid DNA with water. Topical nanoparticle and nanoemulsion formulations of the pGTmCMV.IFN-GFP plasmid (500 μg/mL) using the 12-3-12, 16-3-16, 18:1-3-18:1 gemini surfactants and Dc-chol were prepared as described under "Topical formulations". Blank formulations without plasmid were also prepared. The size of the particles was measured with a Nano ZS instrument (Malvern Instruments, Worcestershire, UK). Samples were run in triplicates, and represented as average ± SD.

VI.16 Small angle X-ray scattering (SAXS)

Transfection mixtures were prepared as for *in vitro* transfection experiments and concentrated 5 times under vacuum to a final DNA concentration of 200 μg/mL. Topical nanoparticle, and nanoemulsion formulations were prepared, similar to samples described above in the "Topical formulation" section. Samples were loaded into 1.5 mm borosilicate capillaries (Charles Supper, Natick, MA). Stratum corneum isolated from human skin was incubated with topical nanoparticles and nanoemulsion at 4^{o}C for 24 hours. The samples were rinsed three times with 400 μL purified water (Gibco) and introduced in borosilicate capillaries. Scattering was measured for 15-30 seconds using the synchrotron light source (Beam X21A, National Synchrotron Light Source, Brookhaven, NY). Beamline X21 is based on a wiggler source, with a helium gas-cooled Si(111) monochromator selecting the photon energy. The X-ray beam was focused by a toroidal mirror into the experimental station. Three pairs of precision slits, positioned at 4 m, 1 m, and 5 cm upstream of the sample, defined the beam. The scattering pattern was recorded using a 13 cm Mar CCD detector (Mar USA, Evanston, IL) at 1.26 m (calibrated with the scattering pattern of Ag-behenate) downstream of the sample. The measurements were performed with 12KeV X-rays and the data covered a q-range from 0.008 $Å^{-1}$ to 0.5 $Å^{-1}$. All beam paths were under vacuum, except at the sample position, where the sample was in air. Kapton windows terminated the vacuum beam paths. The data were recorded at room temperature. All spectra were processed to remove background contributions by subtracting the scattering profile obtained for a capillary containing water only. The scattering profiles obtained for the formulation-treated stratum corneum have been analyzed using PRIMUS and PEAK software obtained from the EMBL Biological X-ray Scattering Group in Hamburg, Germany [292]

(http://www.embl-hamburg.de/ExternalInfo/Research/Sax/). The radial averaged data files of samples were input into the PRIMUS program and the DNA solution file was used as background correction for each data file. The background corrected data were then used as input files in the PEAK program using 1.24 as the X-ray wavelength. The features observed were fit as separate peaks and the structural parameters associated with the peak obtained directly from the fit. The results of this fit are (1) the d-spacings (d):

$$d = \frac{2\pi}{q_{max}} \tag{VI.3}$$

where q_{max} is the position of the peak maximum, (2) the long range order parameter (L):

$$L = \frac{\lambda}{\beta \cos\theta} \tag{VI.4}$$

where λ is the wavelength of the incident X-rays, θ is the scattering angle corresponding to q_{max}, and β is the full width at half max of the peak (in radians), and (3) the degree of disorder (Δ/d):

$$\Delta / d = \frac{1}{\pi}\left(\frac{\beta d}{\lambda}\right)^{\frac{1}{2}}. \tag{VI.5}$$

VI.17 Statistics

Statistical analysis was done with SPSS 13.0 software, using ANOVA (Tukey's multiple comparison test), non-parametric analysis (Kruskal-Wallis test) and Pearson's correlation. Significant differences between the experimental groups were established at the $p<0.05$ level of significance.

VII. RESULTS AND DISCUSSION

VII.1 Plasmid constructs and evaluation of their in vitro *transfection efficiency*

In the first phase of this project, a suitable plasmid encoding IFN-γ was constructed. Initially, several plasmids were designed and constructed, based on the pGT backbone, CMV promoters and the two genes of interest (IFN-γ and GFP). The plasmids were characterized and tested *in vitro* with Lipofectamine Plus, a commercial transfection agent, in order to evaluate differences caused by the nature of the backbone and promoters. The expression of the IFN-γ was quantified by ELISA and antiviral assay (in order to verify bioactivity) and the GFP was identified by fluorescence microscopy.

VII.1.1 Plasmid constructs

The different vectors used for the initial selection exhibit different features (Table VII.1). The promoter region for the pSLRSV contains the Rous sarcoma virus (RSV) promoter. The pIRES and pGT plasmids contain the human cytomegalovirus (hCMV) promoter, while the pGTmCMV contains the murine CMV (mCMV). All plasmids contain a bovine growth hormone polyadenylation signal (polyA) and an origin of replication (Ori) for propagation in *E. coli*. The antibiotic resistance site (ABR), ampicillin (Amp) for pSLRSV and kanamycin (Kan) for the other vectors, ensures clonal selection.

Table VII.1. Characteristics of the cloned plasmids.

Plasmid	Promoter	Gene(s)	IRES	PolyA	Ori	ABR	Source
pSLRSV	RSV	Null	No	Yes	Yes	Amp	Gift (VIDO)
pSLRSV	RSV	IFN-γ	No	Yes	Yes	Amp	Gift (VIDO)
pIRES.GFP	hCMV	GFP	Yes	Yes	Yes	Kan	Clontech
pIRES.IFN-GFP	hCMV	IFN-γ, GFP	Yes	Yes	Yes	Kan	Cloned
pGT	hCMV	Null	No	Yes	Yes	Kan	Gift (VIDO)
pGT.IFN	hCMV	IFN-γ	No	Yes	Yes	Kan	Cloned
pGT.IFN-GFP	hCMV	IFN-γ, GFP	Yes	Yes	Yes	Kan	Cloned
pGTmCMV	mCMV	Null	No	Yes	Yes	Kan	Cloned
pGTmCMV.IFN	mCMV	IFN-γ	No	Yes	Yes	Kan	Cloned
pGTmCMV.IFN-GFP	mCMV	IFN-γ, GFP	Yes	Yes	Yes	Kan	Cloned

The gene for IFN-γ is inserted in all plasmids with the appropriate ligation to the multiple cloning sites (MCS). IRES was inserted into the pIRES, pGT and pGTmCMV vectors. The IRES sequence is a feature of picornaviruses such as encephalomyocarditis virus (ECMV), and initiates mRNA translation at this site [293]. In eukaryotic cells, translation occurs by the scanning mRNA from the 5' end until an initiation codon is reached, thus one expression cassette allows the expression of one gene. If the IRES sequence is inserted into the expression cassette of a vector after the stop codon of the first open reading frame (ORF), the ribosomes attach to the mRNA at the 5' end and the IRES site, translating the two ORFs simultaneously, eliminating the need of co-transfection of the cells with two different vectors. The two proteins are not fusion products, thus their biological function is unaltered. Therfore, the pGTmCMV.IFN-GFP plasmid (Figure VII.1), containing the genes coding for IFN-γ and GFP in such a bicistronic system was constructed as described in the "Materials and methods" section.

The murine cytomegalovirus promoter was obtained from pLMCMVgDt plasmid by PCR, having the two primers designed in such way that the promoter included a Kpn I and a Pst I site. The IFN-γ gene was obtained by restriction digest with Bgl II from the pSLRSV.IFN plasmid [294], which contained the sequence coding for 155 amino acids of murine IFN-γ. The gene was inserted into the MCS of the pIRES.GFP vector at the Bgl II–BamH I site. The plasmid was grown in *dam*$^{-}$/*dcm*$^{-}$ E.coli and the IFN-γ–IRES–GFP coding sequence cut with Bgl II and Xba I. The pGTmCMV plasmid was obtained by replacing the human CMV promoter in the pGT vector with the murine CMV promoter.

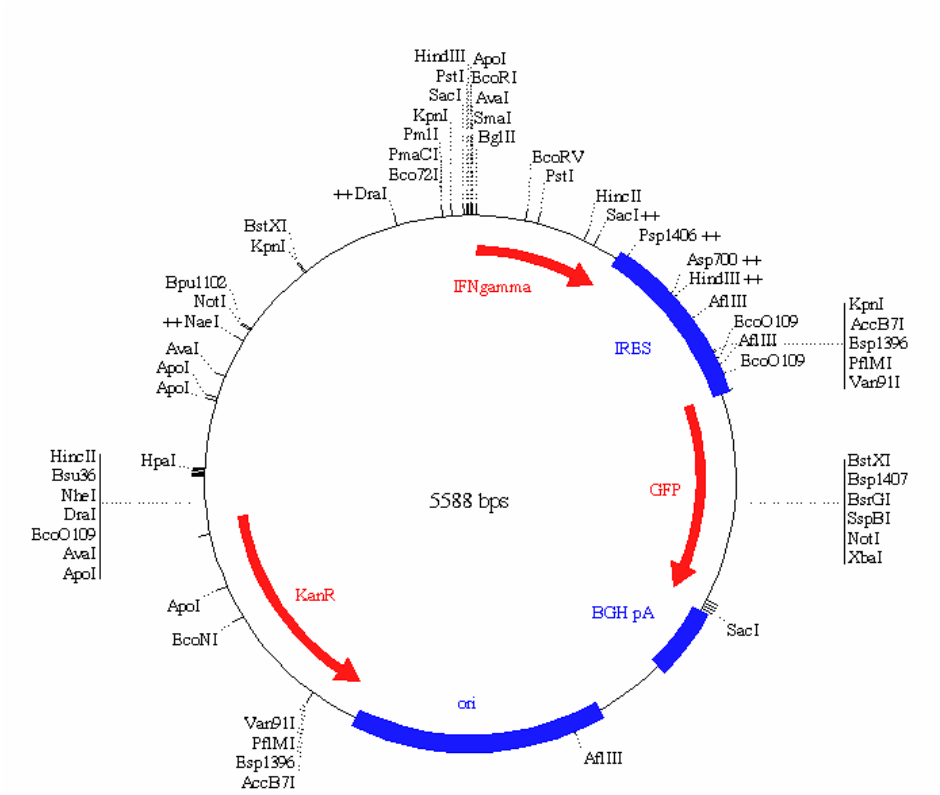

Figure VII.1. pGTmCMV.IFN-GFP plasmid.

The genes coding for IFN-γ and GFP, in a bicistronic system, were inserted into the Bgl II–Xba I site of the pGTmCMV vector. The pGTmCMV plasmid was obtained by replacing the human CMV promoter in the pGT vector with the murine CMV promoter. The plasmid also features bovine growth hormone polyadenylation sequence (BGHpA), Col E1 plasmid replication region (ori) and the selection marker in E. coli host of kanamycin resistance (KanR).

The pGTmCMV.IFN-GFP was constructed by inserting the IFN-γ–IRES–GFP fragment into the Bgl II–Xba I site of the pGTmCMV vector. All structures were verified by restriction digest and agarose gel electrophoresis. As a result of the preliminary testing of the intermediary plasmids in PAM 212 cells, the plasmids used for *in vitro* and *in vivo* experiments were the plasmids containing the murine CMV promoter (pGTmCMV) and the coding plasmid derived from this vector, pGTmCMV.IFN-GFP. There are several benefits for using this plasmid. The backbone is designed for gene therapy, with the immunogenic CpG motifs removed, thus it could be used for a sustained period without triggering immune reactions. The species-specific mCMV promoter features a strong enhancer region [288], thus it could yield strong gene expression in the murine keratinocytes PAM 212 and in the skin of different mouse strains. The IRES sequence permits co-expression of two individual proteins. According to the literature, IL-7 and the low-affinity nerve growth factor receptor (LNGFr) gene were both expressed in cells transfected with a bicistronic system [295]. In our case, the expression of the two genes allows both quantification of the therapeutic protein, IFN-γ, and localization of gene expression at the cellular and tissue level of the marker protein GFP. Two other plasmids, the pGT and pGT.IFN-GFP plasmids were kept as back-up plasmids.

VII.1.2 Evaluation of gene expression

VII.1.2.a IFN-γ expression assessed by ELISA

The expression of the IFN-γ gene was tested in PAM 212 murine keratinocyte cell culture. ELISA of the cell supernatants showed high expression of IFN-γ 24 hours after transfection with pGTmCMV.IFN-GFP plasmid, compared to the null plasmid (Figure VII.2).

The pGT backbone (in pGT.IFN and pGTmCMV.IFN plasmids) increased the IFN-γ expression significantly ($p<0.05$) compared to the pSLRSV backbone (pSLRSV.IFN) and the pIRES vector (pIRES.IFN-GFP). The highest transfection efficiency was observed with the pGTmCMV.IFN-GFP plasmid (158±5 ng IFN-γ/$5x10^4$ cells, n=3). No significant differences were noted between using the CMV promoter of human or murine type. No IFN-γ was secreted by the cells transfected with the null plasmids. IFN-γ expression was sustained and could be detected at 48 hours, which is significant given the short biological half-life of the protein, 0.5 and 4.5 hours (biphasic elimination) for murine recombinant IFN-γ [296].

VII.1.2.b Biological activity of the IFN-γ

IFN-γ inhibits multiplication of several DNA and RNA viruses in host organisms. Contrary to the IFN-α family, which inhibits mRNA translation, IFN-γ can block viral replication at the transcriptional level [297].

The biological activity of the IFN-γ was tested by antiviral assay. The EMC virus infected the L929 cells, causing cell lysis (Figure VII.3 Panel L929-EMC).

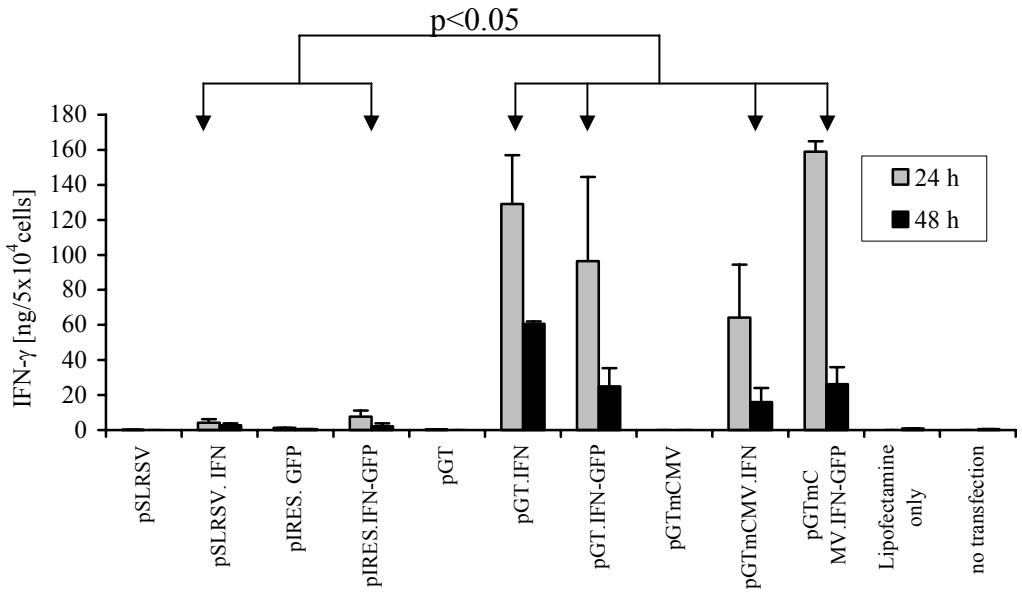

Figure VII.2. IFN-γ expression in PAM 212 cells.

Cells were transfected with 0.2 μg of the following plasmid constructs: pSLRSV, pSLRSV.IFN, pIRES.GFP, pIRES.IFN-GFP, pGT, pGT.IFN, pGT.IFN-GFP, pGTmCMV, pGTmCMV.IFN and pGTmCMV.IFN-GFP, using Lipofectamine Plus Reagent.
Results are shown as mean (n=3), error bars represent standard deviation.

Addition of IFN-γ expressed from pGTmCMV.IFN-GFP by transfection of PAM 212 cells prevented cell death in a concentration-dependent manner (Figure VII.3, top row). The IFN-γ concentration in the supernatant was 240±79 ng/mL (~140 ng/5x10^4cells, n=3), compared to null plasmid where no activity could be detected (results not shown). The detected quantity was consistent with the ELISA assay. When the IFN-γ was blocked with the monoclonal antibody XMG1.2 against IFN-γ activity, no cytoprotective activity was detected (Figure VII.3, bottom row). Antiviral assay confirmed that the IFN-γ gene inserted into the pGTmCMV vector was expressed, and able to exercise biological activity (i.e., cytoprotection against viral infection) in cell culture.

VII.1.2.c GFP expression by fluorescence microscopy

The GFP expression followed the pattern of IFN-γ expression, with the cells transfected with pGTmCMV.IFN-GFP presenting stronger fluorescence than those transfected with pIRES.IFN-GFP (data not shown). The null plasmids did not show any fluorescence even though cells were exposed to a 3-times more intense beam than the GFP-coding plasmids. Figure VII.4 shows the merged images of cells transfected with pGTmCMV.IFN-GFP (Figure VII.4A) and pGTmCMV (Figure VII.4B).

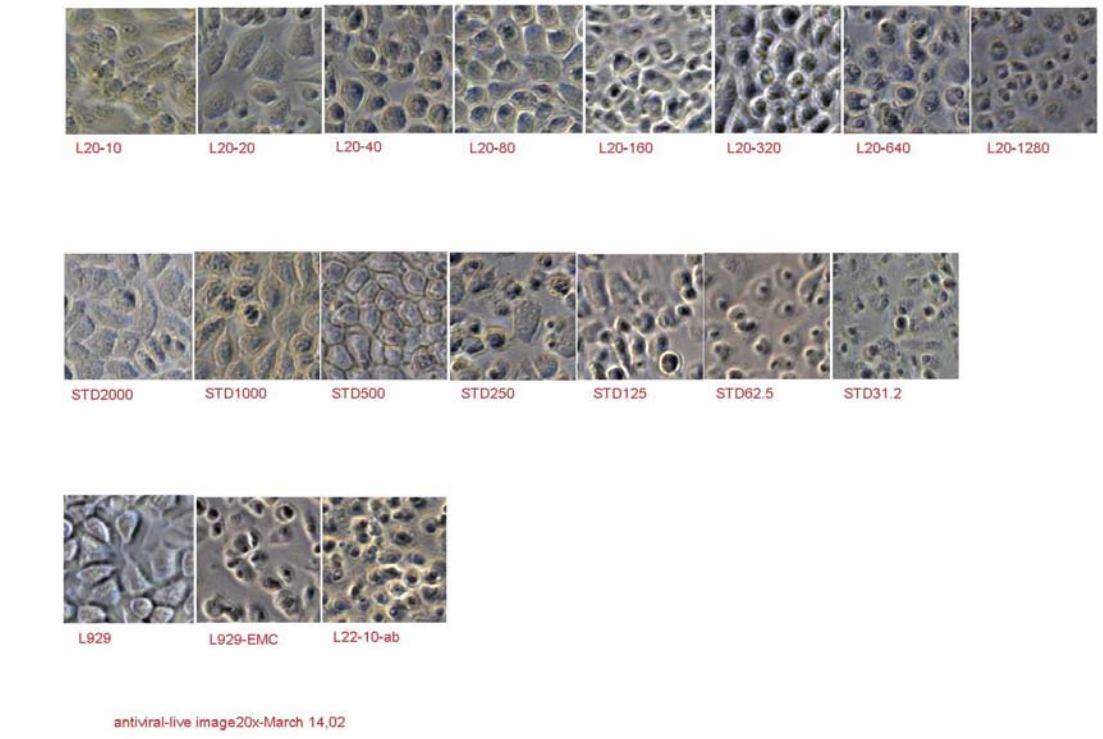

Figure VII.3. Phase contrast micrographs of L929 cells infected with EMC virus and protected by IFN-γ.

Top row: supernatants from cells transfected with pGTmCMV.IFN-GFP in two-fold serial dilutions from left to right, starting at 1/10 dilution (L20-10) to 1/1280 dilution (L20-1280). Cell viability decreases with increasing dilution.
Middle row: IFN-γ standard two-fold dilution from 2000 pg/mL (STD2000) to 31.2 pg/mL (STD31.2)
Bottom row: untreated cells (L929), cells infected with EMC virus (L929-EMC), and cells treated with supernatant from cells transfected with pGTmCMV.IFN-GFP in 1/10 dilution, blocked with XMG1.2 antibody (L22-10-ab).

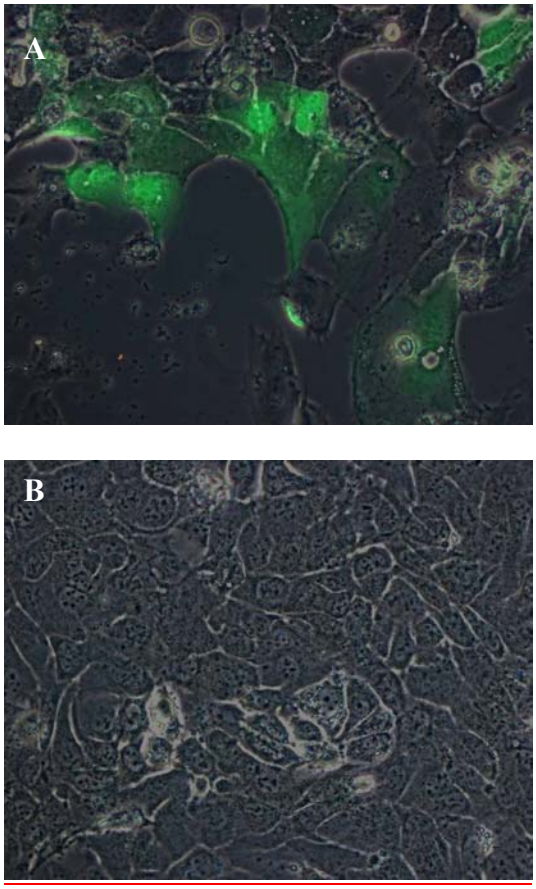

Figure VII.4. Fluorescence microscopic evaluation of the GFP expression in PAM 212 cells.

Cells were transfected with 0.2 µg pGTmCMV.IFN-GFP plasmid (A) or 0.2 µg pGTmCMV plasmid (B) using Lipofectamine Plus Reagent. Phase contrast micrographs were overlaid on fluorescent micrographs. GFP expression can be seen only in the cells transfected with the plasmid containing the *GFP*-gene (Panel A).

VII.1.3 Conclusions

Murine PAM 212 keratinocytes were used as an *in vitro* model for cutaneous gene delivery in mice. Both genes, IFN-γ and GFP, inserted into the pGTmCMV plasmid are expressed in PAM 212 cells, using Lipofectamine Plus reagent. Quantitative measurement and biological activity of the generated IFN-γ were demonstrated by ELISA and antiviral assay. The extent of expression was dependent on the nature of the backbone. The pSLRSV and pIRES backbones were less efficient than the pGT backbone. The highest IFN-γ expression was observed with the pGT and pGTmCMV vectors. Replacement of the human CMV (hMCMV) promoter with murine CMV (mMCMV) promoter was also beneficial in the case of the bicistronic systems. The pGTmCMV.IFN-GFP plasmid was selected for further experiments.

VII.2 Formulation development and physicochemical characterization of the in vitro *and* in vivo *delivery systems*

A series of gemini surfactants (Figure VI.1) with different alkyl chain (m=12, 16 or 18:1C) and spacer lengths (n=3-16) (Table VI.1) were synthesized and characterized in collaboration with Dr. Verrall's group (Department of Chemistry, University of Saskatchewan), and were tested for transfection efficiency using the pGTmVMV.IFN-GFP plasmid coding for IFN-γ and GFP.

VII.2.1 Physicochemical characterization of the PG complexes and PGL systems used for the in vitro *transfection*

In order to characterize the in vitro delivery systems, three aspects were explored: (1) the morphology, size distribution and ζ-potential of the PG complexes and

PGL systems, (2) structural modifications of the plasmid DNA caused by the delivery systems, and the effect of the gemini surfactant alone or in the presence of helper lipid and (3) structural phase behaviour of gemini surfactants and helper lipid and modifications induced by the DNA in the lipid packing. The first characteristic can provide information on the overall structure of the delivery systems, differences or similarities among formulations containing various surfactants and comparison of the structure of the PG complexes to the PGL systems, while the second and third characteristics can evaluate the interaction between the DNA and delivery system and indicate what features are important for efficient gene delivery.

VII.2.1.a. Characterization of the PG complexes and the PGL systems: morphology, size and charge

Selected PGL systems at a +/- charge ratio of 10 were viewed with TEM (Figure VII.5). In all three formulations, the particle size is heterogeneous. Most of the particles (probably single vesicles) had a maximum dimension of 100-200 nm, indicated by solid arrows. Aggregated particles of 300-600 nm could be seen in all formulations (open arrows). No free DNA strands were visualized by the negative staining. The aggregates are smaller for the P–12-3-12–L systems (Figure VII.5A) and larger for the P–18:1-3-18:1–L systems (Figure VII.5C). The pattern and distribution of the P–16-3-16–L systems visualized by TEM (Figure VII.5B) was similar to that obtained by AFM (Figure VII.7D). The AFM image shows small (~100nm) uniform particle-like structures and larger (400-600nm) vesicle-like features.

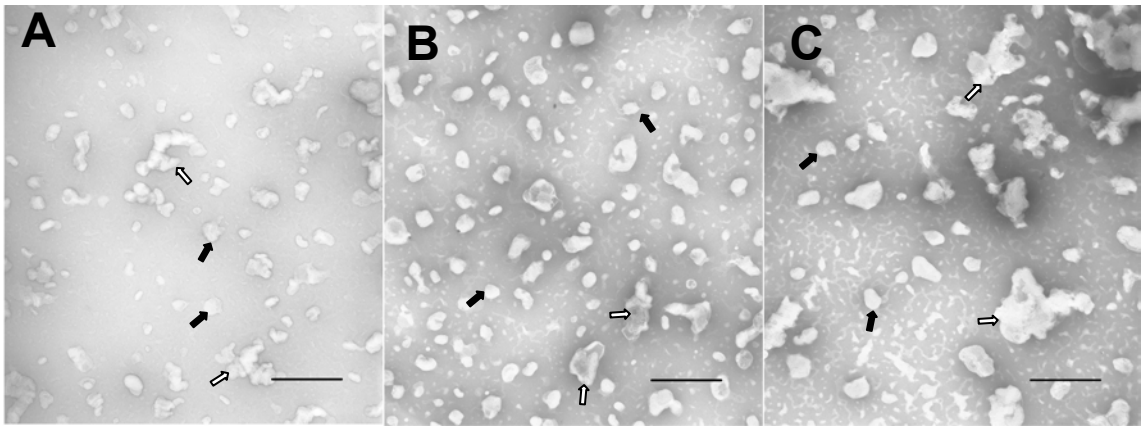

Figure VII.5. Transmission electron micrograph of PGL systems negatively stained with 1% phosphotungstic acid.

A— Vesicles prepared with the 12-3-12 gemini surfactant
B— Vesicles prepared with the 16-3-16 gemini surfactant
C— Vesicles prepared with the 18:1-3-18:1 surfactant
Solid arrows indicate single vesicles, while open arrows point to larger aggregates.
Bar represents 500 nm.

Morphological heterogeneity of transfection agents was addressed by Zabner et al. [39]. Electron micrographs of DNA–DMRIE–DOPE lipoplexes (weight ratio of 1:5 DNA/DMRIE) show that highly compacted dense particles of ~100 nm were present together with free DNA, partially complexed DNA and large aggregates of >500 nm. These lipoplexes were able to transfect cells *in vitro*, thus homogeneous structural make-up of the transfection agent is not necessary. Moreover, it has been shown that heterogeneous MLVs formed with cationic DOTAP induced higher transgene expression compared to large unilamellar vesicles (LUVs) [142]. Size measurements were carried out by using dynamic light scattering (Table VII.2). The measured average sizes of the PG complexes and PGL systems were approximately 100 nm and 150-200 nm, respectively, consistent with the size of individual particles visualized using TEM. The size of the PG complexes was smaller for all surfactants compared to PGL systems. The distribution was monomodal (average polydispersity index of 0.173±0.06), thus no large aggregates were present in the formulations. The absence of the 400-600 nm particles could be the result of the repulsion of the similarly charged particles and uniform spatial distribution in the liquid environment. To obtain a realistic image of both size and morphology of the particles, the three methods, TEM, AFM and DLS, have to be interpreted together. While the TEM and AFM imaging reveal the morphology of the particles, they also indicate that the particles aggregate on the substrate surfaces. On the other hand, DLS provides accurate information on the hydrodynamic diameter of a sphere that has the same translational diffusion coefficient as the particle, but the shape and morphology are not revealed by this method. High efficiency cationic lipid-based delivery agents of various sizes have been described in the literature. The particle sizes have ranged from 50-70 nm for DODAC containing self-assembling lipid-DNA particles

[298] to over 4 μm aggregates for a monocationic lipid (YKS-220)–DOPE system [299]. The particle sizes of the PGL systems reported here,150-200 nm, fall in the middle of this range. It has been shown that small particle size is not a crucial criterion for high efficiency cellular uptake and heterogeneous morphology and the ability of the particles to form larger aggregates does not seem to hinder their transfection efficiency [39, 300]. Based on the observed morphology and particle sizes, the mechanism of uptake for the PGL systems could be a mixture of endocytosis [39, 138] (favouring the 100-200 nm particles) and fusion with the cell membrane [44, 137] (due to the presence of the fusogenic DOPE, heterogeneous morphology and the ability of the particles to aggregate). In conclusion, heterogeneous morphology including particle-like and vesicular structures was observed, with a size distribution of 100-200 nm.

ζ-potential measurements indicated electrostatic interactions between the gemini surfactants and plasmid DNA since the negative potential of the DNA (-47 mV) shifted to positive values of +30-50 mV. Generally, the ζ-potential of the PGL systems is higher compared to the PG complexes with the exception of the 12-16-12 and 16-3-16 surfactants. The 35-45mV values for the PGL systems indicate the presence of high repulsive forces among the particles that icreases the stability of the system. It has been indicated that the coagulation of particles in colloidal systems occur when the ζ-potential is reduced below a critical value (20-50 mV) [301]. The generally higher ζ-potential of the PGL systems compared to the PG complexes is due to the microenvironment created around PG particles upon addition of the amphipatic DOPE [302]. Measurements of the ζ-potential at various +/- charge ratios indicated that neutralization of the particles occurred at +/- charge ratios <1 (Figure VII.6).

Table VII.2. Size and ζ-potential measurement of PG complexes and PGL systems.

Gemini Surfactant	Size (nm)		ζ-potential (mV)	
	PG	PGL	PG	PGL
12-n-12 series				
12-3-12	137±31	143±21	15±1.6	40.6±4.8
12-4-12	146±44	154±15	16.4±1.7	42.5±3.4
12-6-12	153±49	155±16	23.2±6.5	39.21±6.75
12-8-12	125±27	153±15	20.7±3.2	37.55±3.18
12-10-12	85±7	158±14	26.5±3	43.19±6.68
12-12-12	103±17	158±13	29.8±7.7	42.23±0.93
12-16-12	119±16	161±11	54.8±5.4	37.13±9.39
m-3-m series				
12-3-12	137±31	143±21	15±1.6	40.6±4.8
16-3-16	219±75	210±29	58.3±1.5	44.2±4.4
18:1-3-18:1	161±45	214±59	19.3±0.2	45.2±3.6
DNA	N/A	111±4	-47.1±15.1	-26.4±2.7

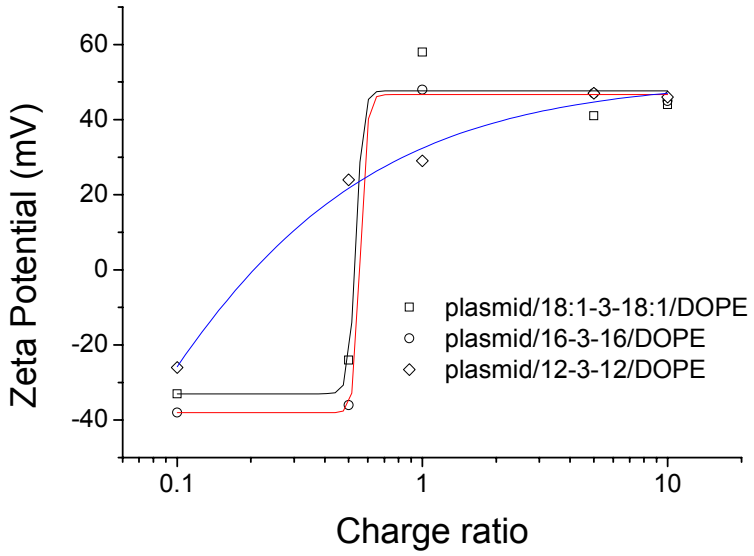

Figure VII.6. ζ-potential measurement of selected PGL systems at various +/- charge ratios.

The difference in the neutralization pattern of the 12-3-12 vs. the 16-3-16 and 18:1-3-18:1 surfactants might be due to its higher CMC. Comparison of the ζ-potential of several cationic lipids, having double C12 to C18 tails and single head groups having 1, 2, 3 or 5 net positive charges, revealed that transition from overall negative to positive charges occurred at charge ratios of 1.25 to 1.75 for all compounds [303].

Gemini surfactants, on the other hand, are able to neutralize particles at charge ratios < 1, indicating a better "utilization" of charges because of the fixed distance between the two nitrogen centers, leading to more efficient ionic interaction.

VII.2.1.b. Characterization of the interactions between the plasmid and gemini surfactants and the influence of the helper lipid DOPE on the nature of complexes. AFM, CD and dye binding evaluation

Gemini surfactants rapidly bind plasmid DNA as demonstrated here using naked DNA and 16-3-16 surfactant on a mica surface (Figure VII.7). The DNA is represented as open circular or loosely coiled strands (Figure VII.7A). Within 30 seconds, a bead-on-string-like structure formed (Figure VII.7B) followed by formation of more compact structures of ~100 nm within 15 minutes (Figure VII.7C). Recent AFM studies by Miyazawa et al. revealed that gemini surfactants, namely the 12-3-12 surfactant, induced rings-on-a-string chain formation in the linear DNA macromolecule, alternating the ordered "rings" with disordered "strings" in a concentration-dependent manner. The number of formed rings and the size of the rings were determined by the balance between the entropy associated with the formation of the rings and the bending energy. High concentration of surfactants (above 10 μM) caused fusion of the rings collapsing the DNA into a compact structure [304].

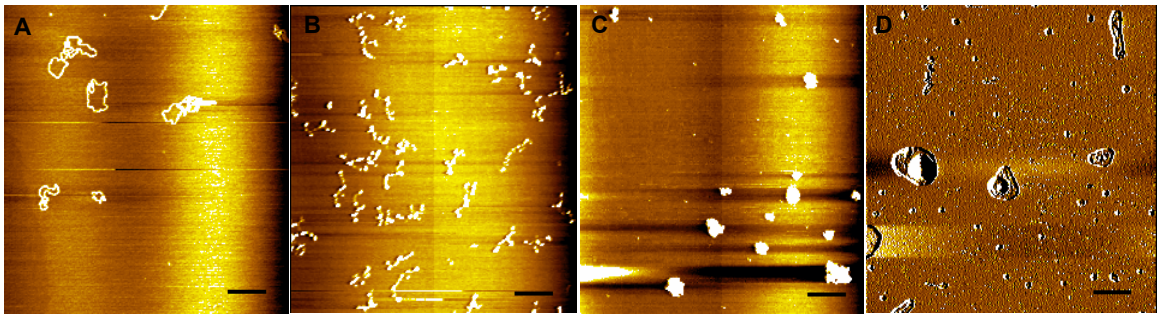

Figure VII.7. Atomic force microscopy images showing plasmid DNA compaction by the gemini surfactant 16-3-16 on freshly cleaved mica surface.

A – Naked DNA. A 20 μg/mL plasmid solution applied on the mica surface was incubated for 2 minutes before imaging;
B – PG complex formation. A 20 μg/mL plasmid solution applied on the mica surface was incubated for 2 minutes. The 16-3-16 gemini surfactant solution was added to the DNA *in situ* and incubated for 30 seconds before imaging;
C – PG complex formation. A 20 μg/mL plasmid solution applied on the mica surface was incubated for 2 minutes. The 16-3-16 gemini surfactant solution was added to the DNA *in situ* and incubated for 15 minutes before imaging;
D – P–16-3-16–L system.
Bar represents 400 nm.

We observed similar behaviour of the plasmid DNA in a time-dependent manner. In our case, the 30-second incubation time probably enabled only limited DNA-gemini surfactant interaction, corresponding to low local concentrations of the surfactant, whereas the longer incubation permitted accumulation of the 16-3-16 surfactant on the surface of the DNA and compaction into small particles. Addition of DOPE to the system further modified the morphology (Figure VII.7D), yielding a more heterogeneous composition of small complexes and larger (2-3 μm) vesicles.

Circular dichroism provides information on the helical conformation of the double-stranded DNA. Cationic lipids bind the native B-form of the DNA and induce secondary structure formation, which reduces the number of basepairs/turn from 10 to 9.33, characteristic for C-form DNA [305]. Increase in the +/- charge ratio causes condensation of the DNA into Ψ^- DNA, a left handed highly organized tertiary structure, characterized by an increase of the negative signal of the CD spectra [306]. The spectrum of the plasmid DNA in water presented two positive peaks at 260 and 290 nm (Figure VII.8A and B). The gemini surfactants, upon interaction with the native DNA induced changes in the CD spectrum, causing a blue shift in the 290 nm peak, and depression of the 260 nm peak into the negative region (Figure VII.8A), indicating the appearance of C-form DNA. The degree of depression was dependent on the spacer and tail length. Short and long spacers, n=3 and 16, caused deeper shifts of the 260nm peak compared to the intermediate spacer, n=8. The 16-3-16 surfactant (m=16 tail) induced a higher degree of depression compared to the 12-3-12 surfactant (m=12 tail). Addition of DOPE to the PG complexes further increased the interhelical interactions inducing Ψ^- DNA formation (Figure VII.8B), indicated by an increase of the overall negative signal due to the flattening of the 290 nm peak, in addition to the shift of the 260 nm positive

peak into the negative region in a structure-dependent manner. DOPE alone in the absence of the gemini surfactants could not cause disappearance of the 290-nm peak, but caused a shift of the 260 nm peak into the negative region. This shift might be the result of enhancement of the counterion release by DOPE on the DNA surface [307]. Figure VII.8C illustrates the degree of depression caused by PGL systems containing 12-n-12 series gemini surfactants. Generally, the depression was more pronounced for surfactants with short and long spacers compared to intermediate spacers. Monocationic lipids such as DDAB, DOTAP and DMRIE and polyvalent DOSPA could also induce formation of Ψ⁻ DNA in the presence of DOPE [131, 306]. Simberg et al. demonstrated that formation of the compact Ψ⁻ DNA is necessary for efficient gene delivery [131].

DNA gemini surfactant interaction and compaction of the polynucleotide was evaluated by fluorescent dye exclusion. Ethidium bromide can freely intercalate between the DNA base-pairs, resulting in a marked increase in fluorescence due to the hydrophobic environment that slows down the excited-state proton transfer rate. Dye binding can occur due to the flexibility of the native DNA and causes helical dislocation of ~1 Å [308]. The double-stranded DNA is considered saturated at a 1:4 dye to basepair ratio. Cationic lipids compact DNA and reduce its flexibility, thus preventing intercalation of the ethidium bromide between the base-pairs [309]. This causes a reduction in fluorescence intensity compared to naked DNA.

A

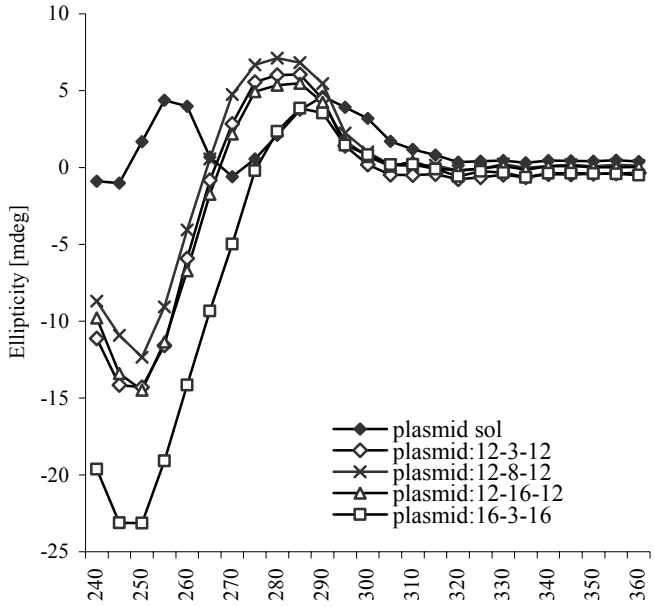
10
5
0
-5
-10
-15
-20
-25
Ellipticity [mdeg]
240
250
260
270
280
290
300
310
320
330
340
350
360
plasmid sol
plasmid:12-3-12
plasmid:12-8-12
plasmid:12-16-12
plasmid:16-3-16

B

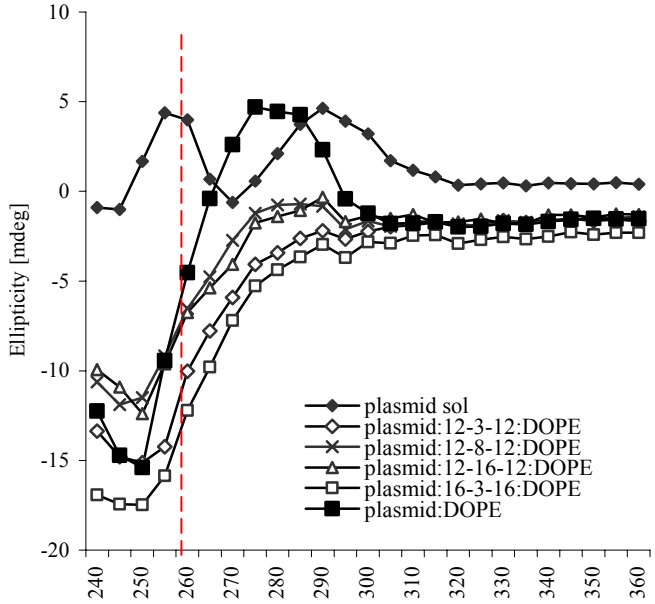
10
5
0
-5
-10
-15
-20
Ellipticity [mdeg]
240
250
260
270
280
290
300
310
320
330
340
350
360
plasmid sol
plasmid:12-3-12:DOPE
plasmid:12-8-12:DOPE
plasmid:12-16-12:DOPE
plasmid:16-3-16:DOPE
plasmid:DOPE

C

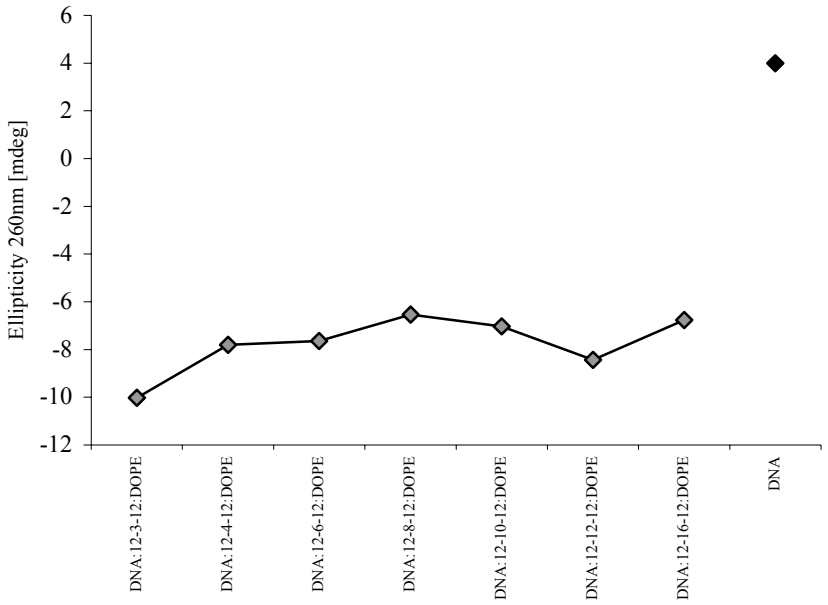

Figure VII.8. Circular dichroism spectra of the pGTmCMV.IFN-GFP plasmid in water and selected PG complexes and PGL systems.

A – CD spectra of pGTmCMV.IFN-GFP plasmid 20 μg/mL in water (solid diamond), and selected PG complexes
B – CD spectra of pGTmCMV.IFN-GFP plasmid 20 μg/mL in water (solid diamond), PG (solid rectangles) and PGL systems
C – Degree of depression of the 260 nm peak of the pGTmCMV.IFN-GFP plasmid (20 μg/mL in water) by the PGL systems of the 12-n-12 gemini surfactants

Gemini surfactants electrostatically bind the plasmid DNA causing a collapse of the helical structure into a compact particle. Upon addition of ethidium bromide, fluorescence is quenched due to the inability of the dye to penetrate between the nucleotides. The better the shielding of the DNA by the cationic gemini surfactant, the more pronounced the fluorescence quenching.

Titration of the plasmid DNA with selected gemini surfactants in the presence of DOPE (Figure VII.9A) indicated that the fluorescence quenching is concentration-dependent. At low +/- charge ratios of 0.1-1, fluorescence quenching is minimal for all surfactants. At a +/- charge ratio of 1.25, the fluorescence increases abruptly, due to the increase in the turbidity of the system. The fluorescence reached the lowest point at a +/- charge ratio of 10, and remained unchanged at ratios of 20 and 40. The fluorescence intensity at a +/- charge ratio of 10 was reduced by 75-90%, indicating a strong shielding of the DNA by the gemini surfactants. In similar conditions, DOTAP-DOPE and DOTAP-cholesterol complexes reduced the fluorescence by only 55-65%, albeit at a +/- charge ratio of 4 [309]. The better shielding of the DNA by the gemini surfactants compared to the monovalent DOTAP could provide better protection against endonucleases, increasing the transfection efficiency of these compounds.

For the 12-n-12 series at a +/- ratio of 10, the fluorescence increases as the intermediate spacer lengths increase (FigureVII.9B), indicating that molecules with 4, 6 and 8 carbons are less able to prevent dye penetration into the DNA. Fluorescence values were higher for the PGL systems, probably due to slight turbidity of the samples. Fluorescence quenching of the 12-n-12 series surfactants was dependent on the CMC (Pearson correlation of 0.901 at p=0.006 level of significance). For the PG complexes of the m-3-m series, increasing tail length induced higher levels of fluorescence quenching

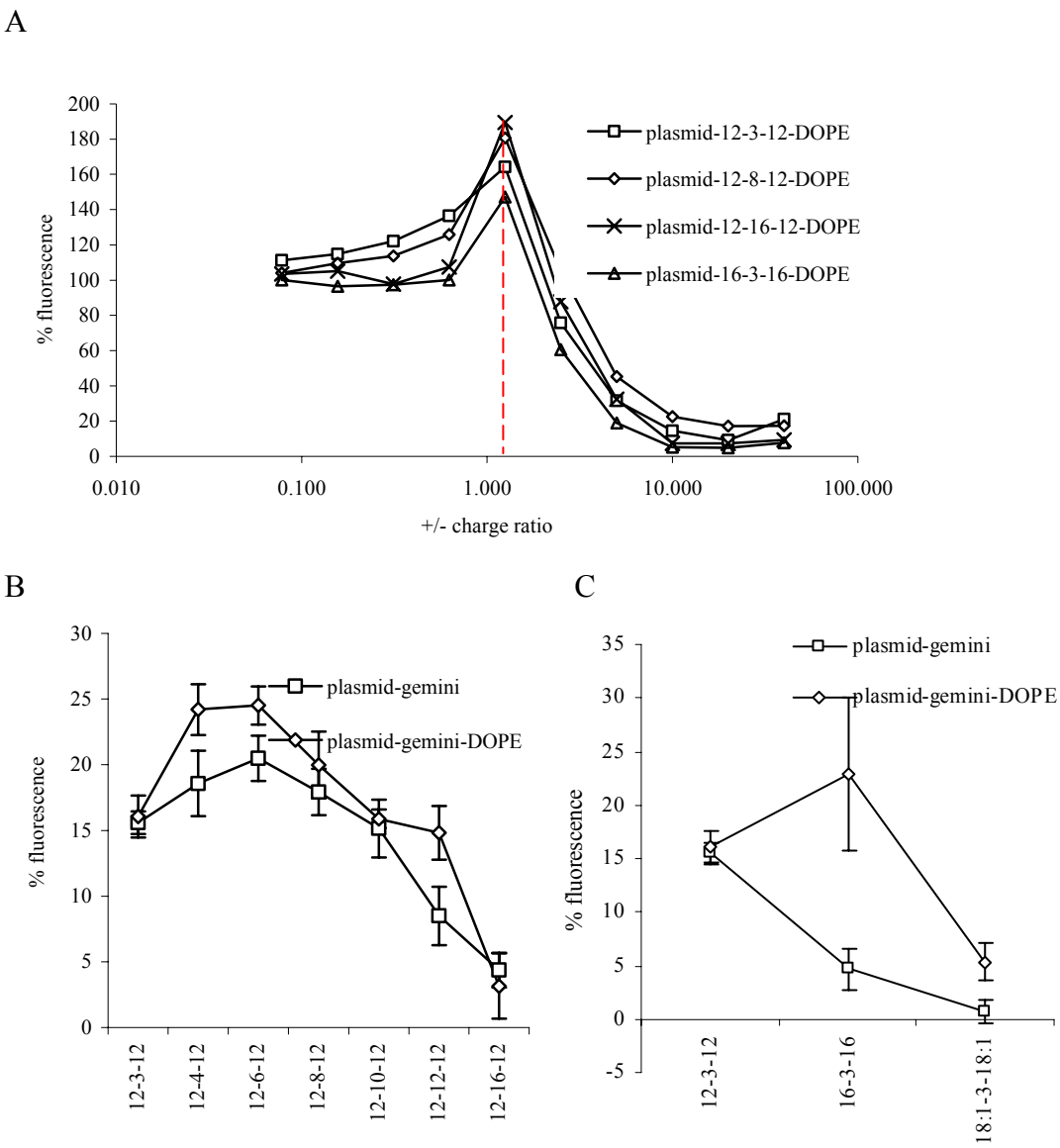

Figure VII.9. Fluorescent dye binding assay.

pGTmCMV.IFN-GFP plasmid was complexed with gemini surfactants at various charge ratios and mixed with DOPE. Fluorescent marker, ethidium bromide was added to the system and the fluorescence intensity was measured.

A – Fluorescence intensity measurements of PGL systems prepared with selected gemini surfactants at +/- charge ratios of 0.1 to 40

B – Fluorescence intensity measurements of PG complexes (rectangles) and PGL systems (diamonds) prepared with the 12-n-12 gemini surfactants

C – Fluorescence intensity measurements of PG complexes (rectangles) and PGL systems (diamonds) prepared with the m-3-m gemini surfactants

(Figure VII.9C). The variable value for the P–16-3-16–L system was due to the turbidity of the sample (Figure VII.9C).

VII.2.1.c. Characterization of the lipid organization in PG complexes and PGL systems from SAXS studies

SAXS is a technique that provides structural information (size, shape and interaction of the particles) on poorly organized materials such as polymers, proteins, lipids, and biological tissues (e.g., muscles, skin) at a 1-15 nm scale (d). These materials broadly scatter the incident beam at small angles (usually less than 3-5° for standard wavelengths). The requirements for the x-ray beam are low divergence to compensate for weak scattering, small cross-sections to reduce distortions, high flux to facilitate isolation of scattering at small angles from the direct beam, and tunability of the energy level. Contrary to x-ray crystallography of organized materials where the scattering planes are parallel and the scattering vector (q) is perpendicular to those planes, in SAXS measurements averages of amplitudes are calculated for all secondary waves of partially ordered systems. The Bragg peaks indicate the diffuse scattering of these various planes. Their positions in q-space reveal the structural organization of the material, and the intensity of the peaks (I) is a quantitative measure of the degree of organization of the system. Lipid dispersions in aqueous media are characterized by structural heterogeneity and are suitable for SAXS analysis. Bragg reflections of these systems indicate nanostructural organization into micellar, lamellar, hexagonal or various cubic phases. Micellar microemulsions are characterized by a single broad peak whose position depends on the water content of the system. Higher water content shifts the peak position to lower angles, indicating increasing distances [310]. Inverted

hexagonal phase structure ratios are 1: √3: √4: √7, reflecting the peak positions, while lamellar structures show linear ratios of 1:2:3:4 [154]. Cubic lattices show characteristic ratios of Bragg reflections depending on the polymorphs (e.g., √2: √3: √4:√6 for *Pn3m*) [311]. The Bragg peak intensities reveal the degree of the lipid organization, i.e., the fraction of lipids organized into vesicles, micelles or other structures. The higher the degree of organization, the more rigid the systems are, approaching the crystalline form of highly organized materials.

SAXS measurements of the PG complexes and PGL systems demonstrated measurable structural organization. The scattering profile for DNA was virtually featureless. Gemini surfactants alone showed very weak scattering, indicating micellar organization, and the gemini surfactant–DOPE mixtures in the absence of the DNA indicated a high degree of disorganization (results not shown). For the PG complexes, a single sharp peak was observed at q-values of 0.12-0.176, corresponding to a d-spacing of 35-52 Å (Figure VII.10A). The addition of the neutral lipid DOPE to the system (PGLs) resulted in an increase of structural organization (FigVII.10B). The intensities of the main peaks (red arrows) were 2-3 orders of magnitude higher compared to the PG complexes. The DNA–DOPE mixtures without the gemini surfactants show hexagonal structure, with peak positions at q=0.109, 0.188 and 0.218 (Figure VII.10B). Addition of the gemini surfactants caused lamellar phase organization with q-values of 0.105 and 0.210 for the P–12-3-12–L system and q= 0.098 and 0.194 for the P–16-3-16–L system (Figure VII.10B). The position of the main scattering peak corresponds to a d-spacing of 50-65 Å, consistent with the results presented in literature for lamellar organization [141, 160]. However, for short spacers of the 12-s-12 series, multiple structural phases appear to be present (Table VII.3). Additional to the lamellar structure, a *Pn3m* cubic

phase appears in the P–12-3-12–L and P–12-6-12–L systems, characterized by √2: √3:√4:√6 periodicity.

Scattering studies of DNA–cationic gemini surfactant–helper lipid complexes demonstrate that both DNA and lipid undergo major conformational changes [133]. Tarahovsky et al.[159] demonstrated that complexes assuming lamellar lipid organization are able to transfect more efficiently compared to thermolable complexes. Conversely, Zuhorn et al. [160] indicate that the presence of hexagonal phase is crucial for efficient cellular delivery and endosomal escape of the DNA. Since both lamellar and hexagonal structures can facilitate DNA delivery in specific conditions, the ability of the system to adopt various phases according to their milieu can promote efficient gene delivery. Moreover, addition of DNA to a mixture of two nanoparticle formulations induces fusion and lipid reorganization [141]. This indicates that not only the delivery system influences the structure of the DNA (e.g., compaction), but also the DNA imposes a certain organization of the lipid systems (e.g., polymorphic phases and lipid mixing).

Foldvari et al. [161] have shown that efficient cell transfection can be achieved due to the ability of the gemini cationic surfactant/DOPE/DNA systems to adopt polymorphic structures coexisting with lamellar phases, like the 12-3-12 and 12-4-12 surfactants demonstrated here (Table VII.3).

A

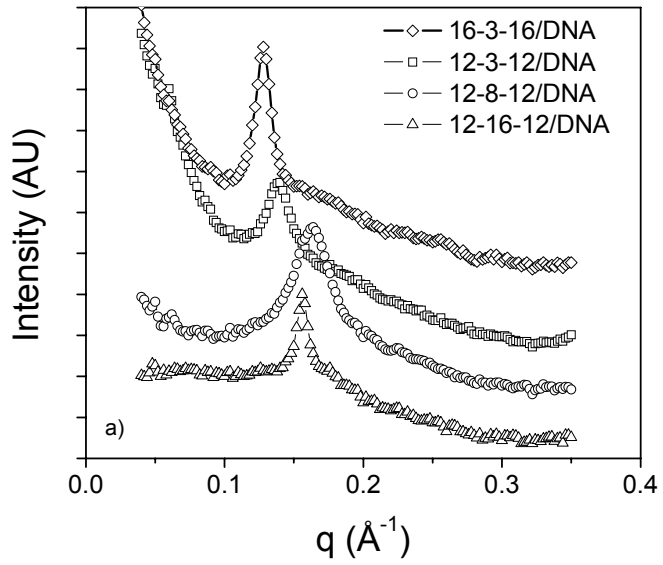

B

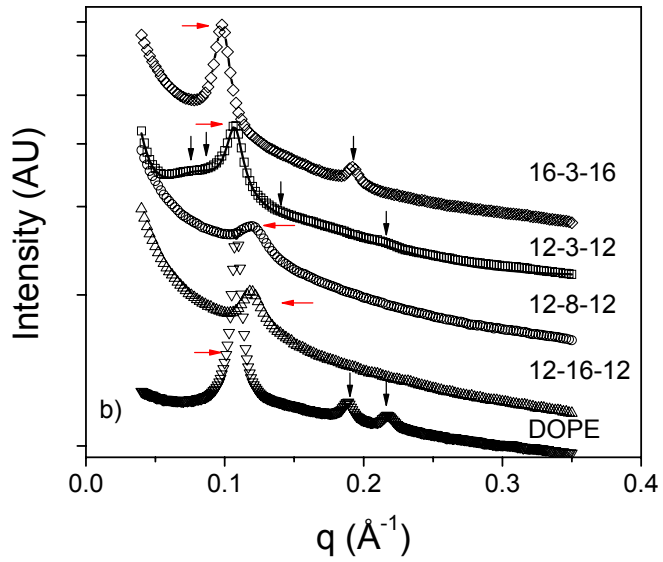

Figure VII.10. Small angle X-ray scattering (SAXS) indicated structural differences among PG complexes and PGL system.

A – Scattering curves of selected PG complexes (12-3-12, 12-8-12 and 12-16-12 and 16-3-16) show a shift in the position of the main scattering peak, depending on the spacer and tail length – intensities are measured on a linear scale.
B – Scattering profiles of the selected PGL systems (12-3-12, 12-8-12 and 12-16-12 and 16-3-16) are complex, showing polymorphic structure. Intensities are measured on a logarithmic scale.

Table VII.3. Scattering peak positions and d-spacings for transfection mixtures containing DNA (d-values were calculated from single-point measurements).

Gemini surfactant	PG		PGL		
	q ($Å^{-1}$)	d (Å)	q ($Å^{-1}$)	Structure	d (Å)
12-n-12 series					
12-3-12	0.142	44.2	0.105, 0.210 0.074, 0.092, 0.133	Lamellar *Pn3m*	59.8
12-4-12	0.154	40.7	0.107, 0.214 0.105, 0.139	Lamellar	58.5
12-6-12	0.162	38.8	0.112 0.086, 0.106, 0.123	 *Pn3m*	56.2
12-8-12	0.166	37.8	0.121		51.9
12-10-12	0.174	36.1	0.113		55.6
12-12-12	0.176	35.7	0.113		55.6
12-16-12	0.158	39.8	0.116		54.2
m-3-m series					
12-3-12	0.142	44.2	0.105, 0.210 0.074, 0.092, 0.133	Lamellar *Pn3m*	59.8
16-3-16	0.130	48.3	0.098, 0.194		64.1
18:1-3-18:1	0.120	52.4	0.106		59.3
DNA	Featureless	-	0.109, 0.188, 0.218		66.9

VII.2.2 Physicochemical characterization of the topical formulations

VII.2.2.a. Size and morphology

The *in vivo* formulations were based on the results obtained for cell culture experiments and optimized for topical application. Surfactants of the m-3-m series were selected for the topical formulations, due to their higher transfection efficiency *in vitro* compared to longer spacers. As a control, the gemini surfactants were replaced with Dc-chol, a cationic cholesterol-derivative that was used for topical gene delivery into nasal epithelia in animal studies [312] and cystic fibrosis patients [313]. The +/- charge ratio was increased from 10 to 20 in order to facilitate protection of the DNA in the skin penetration process. In the nanoparticle formulations, the DOPE content was increased 10 fold (from 1 mM for the *in vitro* transfection agents to about 10 mM in the topical nanoparticles) and additional lipids, DPPC or soybean PC were added. The neutral lipids, due to their amphiphilic character, can facilitate partitioning of the polynucleotide into the skin. Cutaneous permeation enhancers (diethylene glycol monoethyl ether, propylene glycol and PDM 27) were incorporated into the formulations. The diethylene glycol monoethyl ether is a hygroscopic liquid, miscible with both polar and apolar solvents. It is a permeation enhancer shown to work with small molecules by causing a swelling of the stratum corneum lipids [314]. PDM 27 is an acylated amino acid derivative that facilitates DNA delivery into intact skin [315]. Although it has been recognized that liposomal vesicles were present in these delivery systems and lammelar phase was the dominant nanostructural feature, the addition of permeation enhancers induced formation of polymorphic structure and morphological heterogeneity. Thus, the "nanoparticle" term is more appropriate than "liposomal system". A cationic

nanoemulsion system with the gemini surfactants was also included in the evaluation. Nanoemulsions are optically clear, thermodynamically stable disperse systems, used successfully as delivery systems for pharmaceutical agents [316]. Depending on oil/water/surfactant ratios, they can be oil-in-water, water-in-oil or bicontinuous (water and oil domains separated by the emulsifying agents) systems. The PEG-8 caprylic/capric glycerides were used as primary surfactant and permeation enhancer to facilitate drug transport, polyglyceryl-3-isostearate is the co-surfactant, and octyldodecyl myristate as the oil component of the system with emollient properties. The DNA to cationic lipid ratio was the same as in the nanoparticles.

Physicochemical characterization of the nanoparticle and nanoemulsion formulations was carried out using atomic force microscopy (AFM), particle-size measurement and SAXS.

AFM and size measurements indicated the presence of two populations of particles (100-200 nm and larger 2-5 μm particles) in the topical nanoparticle formulation prepared with the 16-3-16 surfactant (Figure VII.11A). The larger particles presented a rough surface morphology and the population of the smaller particles distributed evenly in the field were relatively uniform with smooth surfaces. TEM images of the same formulation showed particles ranging between 100-300 nm in diameter (Figure VII.11B). The smaller particles (indicated by the white arrows) are individual vesicles, while the larger particles (black arrows) are aggregates of the small vesicles. AFM imaging of the nanoemulsion system indicates the presence of particles of 5-10 nm (Figure VII.11C), based on the amplitude of cantilever deflection. Since the removal of excess formulation from the mica with absorbent tissue removed the water phase, these particles represent the oil domain of the formulation.

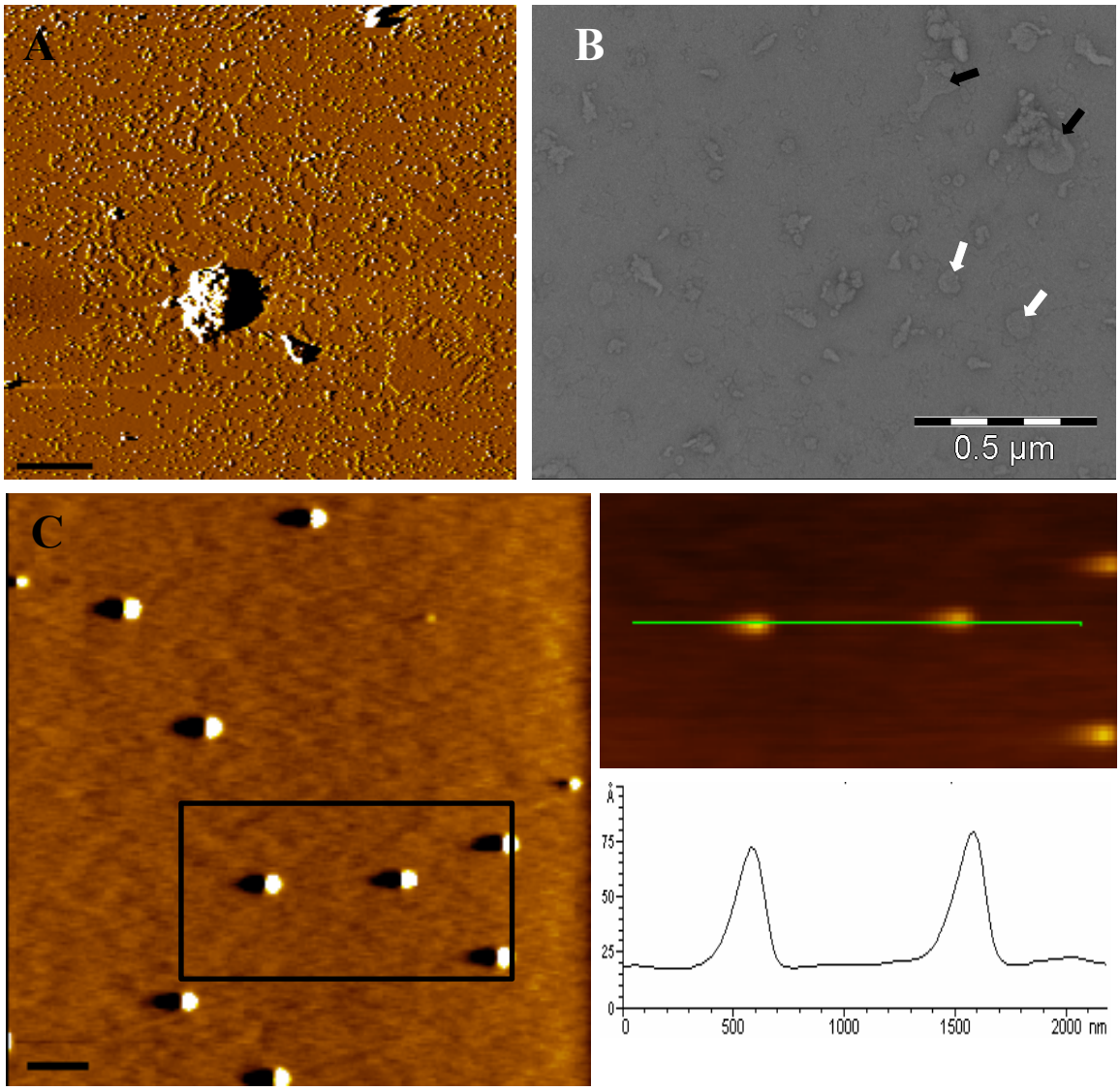

Figure VII.11. Structural characterization of the topical delivery systems.

A – Atomic force microscopic evaluation of the structure of the topical gemini nanoparticle DNA formulation. Bar = 2 µm.
B – TEM image of the NP16-DNA formulation.
C – Atomic force microscopic evaluation of the structure of the topical gemini nanoemulsion DNA formulation. Bar = 400 nm. Inset: size measurement based on cantilever deflection.

Light scattering size measurement of all topical nanoparticle formulations prepared with the gemini surfactants or Dc-chol indicated bimodal size distribution (Figure VII.12A1-D1). The three peaks of the DNA solution correspond to different topological forms (supercoiled, open circular and small amount of linear DNA) [317]. In the blank formulations prepared with the gemini surfactants, the largest percentage of particles (8-10%) were in the 100-200 nm range. The addition of the plasmid to the formulations shifted the size towards 500-1000 nm diameter. In the blank Dc-chol formulation, the bimodal distribution is present, but a larger portion of the particles is in the 1-2 μm range. By adding DNA to the formulation, the size of both populations (the 100-200 nm and 1-2 μm particles) is reduced. Compared to the *in vitro* PGL system, a subpopulation of larger aggregates is present in the topical formulation due to the higher lipid content and more complex composition. Light microscopy images complement the light scattering measurements (Figure VII.12 A2-D2). While light scattering could detect particles in the 1 nm-10 μm range, larger particles of 1-100 μm could be visualized by light microscopy. Mixed population of lipid-like particles and vesicles (white arrows) of 2-10 μm are present in the blank formulations (Figure VII.12 A2-D2 insets). Addition of DNA causes aggregation (black arrows), and fewer vesicles of small sizes (red arrows) are visible. In the DNA formulation prepared with Dc-chol (Figure VII.12 D2), larger numbers of small particles are visible compared to other DNA formulations.

A1

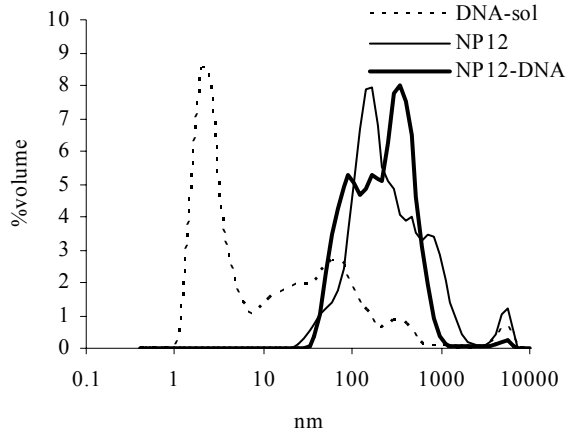

A2

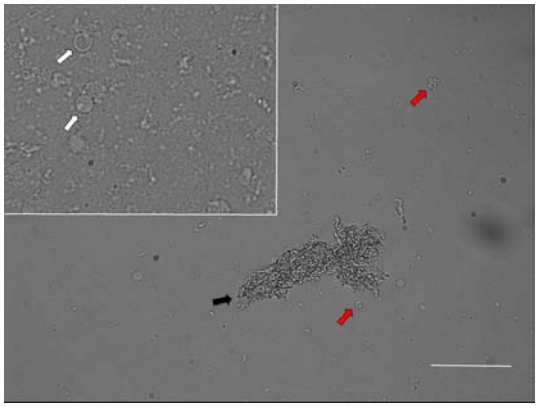

B1

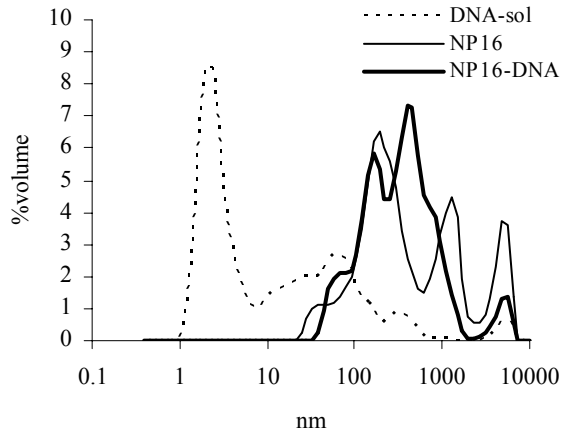

B2

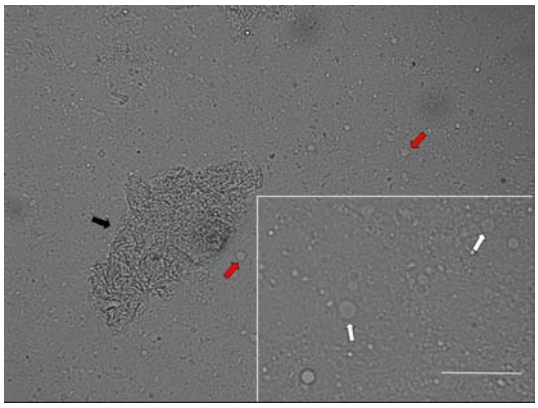

C1

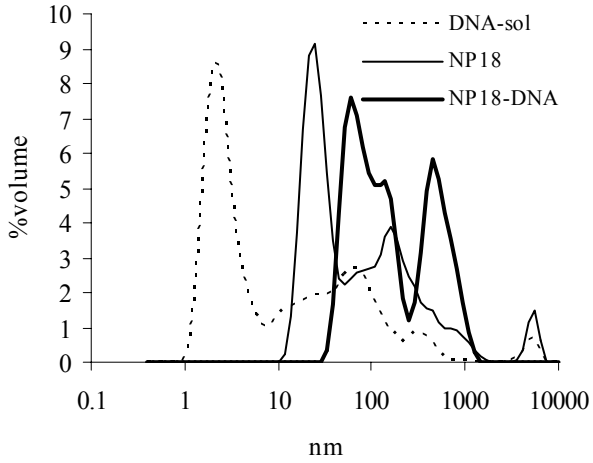

C2

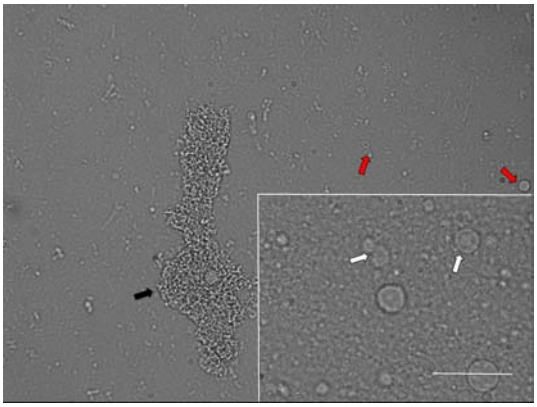

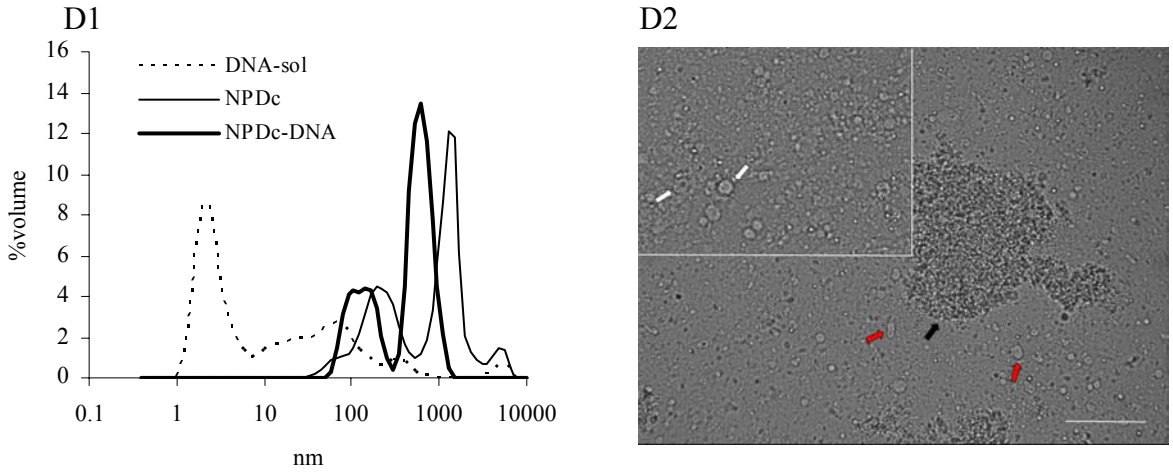

Figure VII.12. DLS size measurements and light microscopy of the topical nanoparticle formulations.

The heterogeneous nature of the formulations is indicated by the bimodal size distribution.
A1 – Size measurement of the nanoparticle blank and DNA formulations prepared using the 12-3-12 gemini surfactant.
A2 – Light micrograph of the nanoparticle DNA formulations prepared using the 12-3-12 gemini surfactant. Inset: blank formulation. Bar represents 50 μm.
B1 – Size measurement of the nanoparticle blank and DNA formulations prepared using the 16-3-16 gemini surfactant. Bar represents 50 μm.
B2 – Light micrograph of the nanoparticle DNA formulations prepared using the 16-3-16 gemini surfactant. Inset: blank formulation. Bar represents 50 μm.
C1 – Size measurement of the nanoparticle blank and DNA formulations prepared using the 18:1-3-18:1 gemini surfactant.
C2 – Light micrograph of the nanoparticle DNA formulations prepared using the 18:1-3-18:1 gemini surfactant. Inset: blank formulation. Bar represents 50 μm.
D1 – Size measurement of the nanoparticle blank and DNA formulations prepared using Dc-Chol.
D2 – Light micrograph of the nanoparticle DNA formulations prepared using Dc-chol surfactant. Inset: blank formulation. Bar represents 50 μm.

The same formulations were used for ζ-potential measurements (Table VII.4). The plasmid solution showed a negative ζ-potential of -75 mV. The blank formulations had positive ζ-potentials, due to the cationic component. As expected, the addition of the negatively charged plasmid DNA reduced the ζ-potential by 20-30%, compared to the blank formulations, but remained positive due to the high +/- charge ratio.

VII.2.2.b SAXS analysis of the topical formulations

The SAXS profiles of the nanoparticle and nanoemulsion formulations (Figure VII.13) showed differences in both scattering peak positions and intensities. Topical nanoparticle and nanoemulsion formulations with the 12-3-12, 16-3-16 and 18:1-3-18:1 gemini surfactants were prepared as described in the "Materials and methods" section. The scattering profiles obtained for the topical nanoparticle formulations do not fit into a hexagonal or lamellar structure typically observed for cationic lipid–DNA complexes. Instead, in consideration of both the peak positions and the relative intensities (Table VII.5), there appears to be a coexistence of two structural phases: a lamellar phase, indicated by peaks 4 and 5 (q=0.104 $Å^{-1}$ and 0.207 $Å^{-1}$) for the NP12-DNA formulation, and a second unknown phase, peaks 1, 2 and 3 (q= 0.046 $Å^{-1}$, 0.069 $Å^{-1}$ and 0.092 $Å^{-1}$), that might indicate the presence of one of the cubic polymorphs [311]. An emulsion phase is present in all nanoparticle formulations, indicated by the broad peak [310] underlying the Bragg peaks of these heterogeneous systems. Interestingly, the main scattering peak in the DNA gemini nanoparticles (indicated by arrow) was sharp above the broad scattering peak, indicating lipid-DNA interaction.

Table VII.4. ζ-potential measurements of the topical nanoparticles.

Formulation	**ζ-potential**
DNA solution	-75±13
NP-12	61±1.2
NP12-DNA	46±1.5
NP-16	64±5.3
NP16-DNA	51±2.4
NP18	64±3.9
NP18-DNA	46±2.1
NPDc	62±4.5
NPDc-DNA	44±7

This peak was less evident in the Dc-chol formulation. Since light microscopy of this formulation showed a significant number of lipid-like and vesicular particles (Figure VII.12 D2), the broad peak in the scattering pattern might overlap the peak indicating interaction between the lipid and the DNA. It is difficult to interpret Bragg reflections of the gemini cationic nanoparticles due to the complexity of the system.

Generally, SAXS profiles of simple DNA delivery systems are described in the literature as containing only complexes of the cationic lipid with the polynucleotides alone or in the presence of one helper lipid [141, 154, 318]. In topical nanoparticle delivery systems, co-existence of various phases such as micellar, lamellar or hexagonal might cause overlap of the Bragg reflections of the polymorphs. The scattering curves obtained for the nanoemulsion formulation (Figure VII.13E) are characteristic of those obtained in other emulsion systems, exhibiting a single broad feature characteristic of strong interparticle correlations. In all cases the scattering peak is observed at q = 0.030 $Å^{-1}$, corresponding to a d-spacing of 20.9 nm. It has been shown [319] that the scattering profiles of microemulsion system depend on the oil/water/surfactant ratios. High oil content present in the oil-in-water type of microemulsions induce weak scattering. Addition of water increases the scattering intensity and shifts the peak position to smaller q-values, corresponding to the presence of globular particles of 13 nm at 15% water content. At water concentrations of 25-50%, a bicontinuos system forms, characterized by a broad high intensity peak.

A

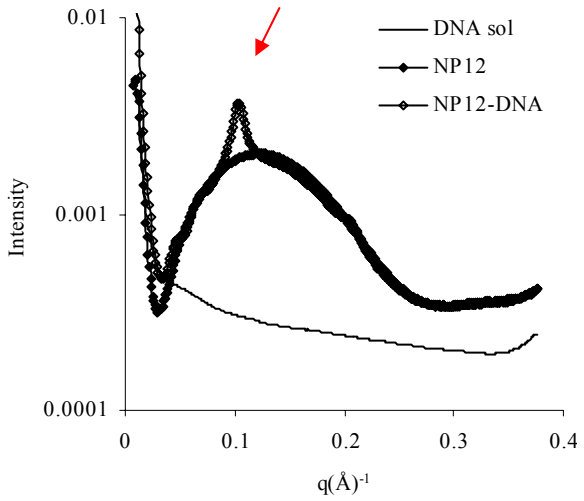
0.01
0.001
0.0001
Intensity
0
0.1
0.2
0.3
0.4
q(Å)-1
DNA sol
NP12
NP12-DNA

B

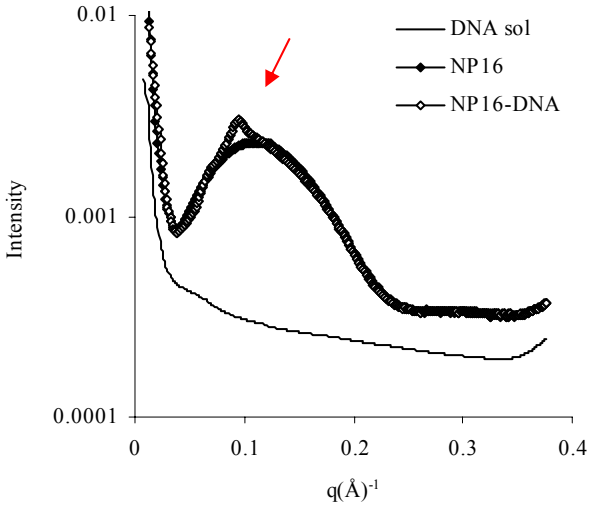
0.01
0.001
0.0001
Intensity
0
0.1
0.2
0.3
0.4
q(Å)-1
DNA sol
NP16
NP16-DNA

C

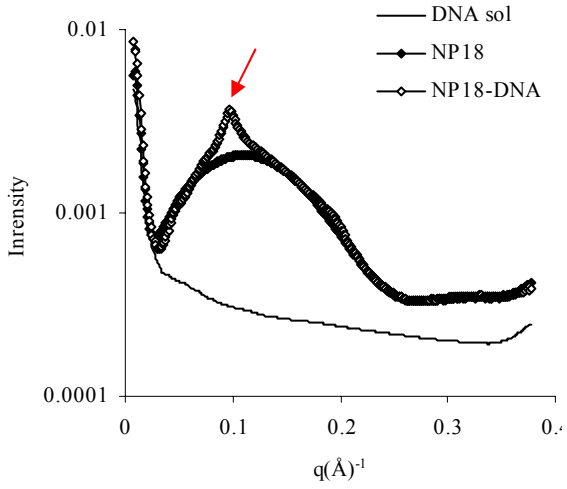
0.01
0.001
0.0001
Inrensity
0
0.1
0.2
0.3
q(Å)-1
DNA sol
NP18
NP18-DNA

D

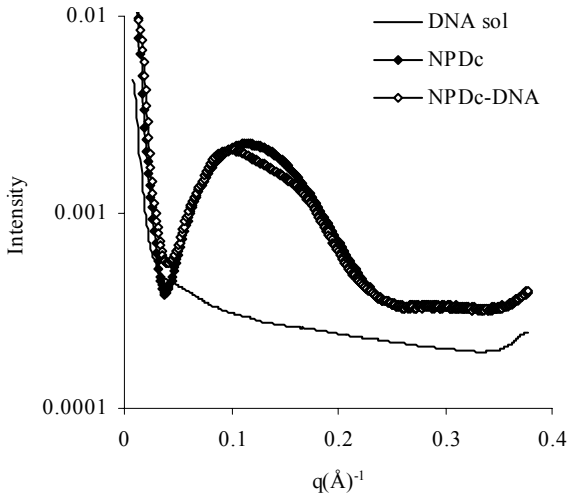
0.01
0.001
0.0001
Intensity
0
0.1
0.2
0.3
0.4
q(Å)-1
DNA sol
NPDc
NPDc-DNA

E

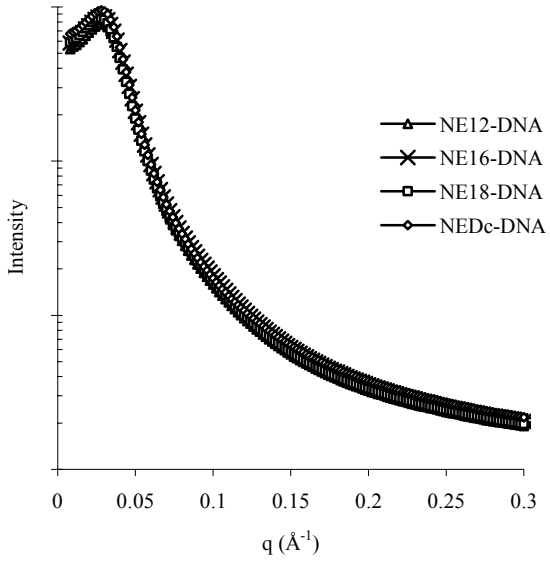

Figure VII.13. Scattering curves of the topical nanoparticle and nanoemulsion formulations.

A – Nanoparticle blank and DNA formulations prepared using the 12-3-12 gemini surfactant.
B – Nanoparticle blank and DNA formulations prepared using the 16-3-16 gemini surfactant.
C – Nanoparticle blank and DNA formulations prepared using the 18:1-3-18:1 gemini surfactant
D – Nanoparticle blank and DNA formulations prepared using the Dc-Chol.
E – Nanoemulsion DNA formulations prepared with 12-3-12, 16-3-16 and 18:1-3-18:1 gemini surfactant or Dc-chol .

Table VII.5. SAXS peaks of the topical nanoparticle formulations (values of d and Δ/d were calculated from single-point measurements).

Formulation	q ($Å^{-1}$)	Structure	d	Δ/d
NP12	**0.101**		62.4	0.127
NP12-DNA	0.046, 0.069, 0.092, **0.104**, 0.207	lamellar + other	60.4	0.031
NP16	**0.093**, 0.134		67.7	0.074
NP16- DNA[a]	0.07, **0.094**, 0.116, 0.143	lamellar + other	67.2	0.052
NP18	0.064, **0.098**, 0.143		64	0.075
NP18- DNA	0.047, 0.067, 0.093, **0.098**, 0.145, 0.193	lamellar + other	64	0.036
NPDc	0.075, **0.105,** 0.145		59.7	0.069
NPDc- DNA	0.088, **0.089**, 0.153, 0.176	lamellar	70.4	0.083

Bold numbers indicate the main scatteing peak
[a] – lamellar structure is hypothesized

Formation of oil-in-water microemulsion at >52% water content is indicated by the appearance of a sharp peak [319]. Djordjevic et al. [316] demonstrated that formulations having 20-40% water content and 48-60% surfactants (PEG-8 caprylic/capric glycerides and polyglyceryl-6 oleate mixture) formed optically clear bicontinuous microemulsion system. In the topical nanoemulsion DNA formulations, water content of 20% and the presence of intense scattering peaks at small q-values might also indicate the formation of a bicontinuous system (oil and water phases separated by surfactant layer). Although AFM images (Figure VII.11) show structures of 5-10 nm, particle-formation might be due to the removal of the water phase before imaging.

VII.2.3 Effect of the gemini surfactants on the SC lipids

Interaction between the gemini surfactant-based delivery systems (Figure VII.14) and the lipids in the stratum corneum could lead to better understanding of the mechanism of penetration of the DNA macromolecule into the skin. Peak positions of the bare stratum corneum before and after treatment with topical nanoparticle formulations are similar with q-values of the main peak of 0.098-0.101 $Å^{-1}$. On the other hand, scattering intensies of the formulation-treated stratum corneum samples (with the exception of the NP12) are lower compared to the untreated stratum corneum, indicating a higher degree of disorder. Calculation of the d-spacing (Table VII.6) for the nanoparticle-treated stratum corneum showed that the values are consistently between 62 and 65 Å (average = 63.3 ± 0.7 Å) with the exception of the stratum corneum treated with blank NP16 formulations. This indicates that the formulations do not induce significant changes in the repeat spacing of the stratum corneum, or that the d-spacing of

the formulations alone (Table VII.5) and the lipids in the stratum corneum have similar values, and the scattering patterns overlap. This, however, does not imply that the formulations have no effect on the stratum corneum lipids, but rather that the bilayer thicknesses remain essentially unchanged. A better measure of the effect of the formulations on the stratum corneum lipids is the intensity of the scattering peak related to the degree of disorder in a partially ordered system (Δ/d). When the plasmid DNA is added to the formulations, it induces organization of the formulation, reflected in the generally lower Δ/d values of the stratum corneum treated with the NP-DNA formulations compared to the blank formulations. From the Δ/d values (Table VII.6), we can conclude that the blank formulations have a pronounced effect on the organization of the stratum corneum lipids with the NP16 formulation inducing the highest degree of disorder (0.117) compared to the other formulations (generally $\Delta/d<0.1$). Based on the d-spacing of the stratum corneum lipids and the degree of disorder, we can conclude that the nanoparticle formulations had minimal influence on the distance between the lipid bilayers, while increase in the degree of disorder indicated that the continuity of these bilayers was interrupted by the delivery system, increasing lipid fluidity similar to laurocapram-type permeation enhancers [320].

The nanoparticle formulation prepared with the 16-3-16 gemini surfactant (NP16) was the most efficient for *in vivo* DNA delivery, indicating that one of the important features of the formulation is to perturb the lipid organization in order to facilitate the penetration of the macromolecule.

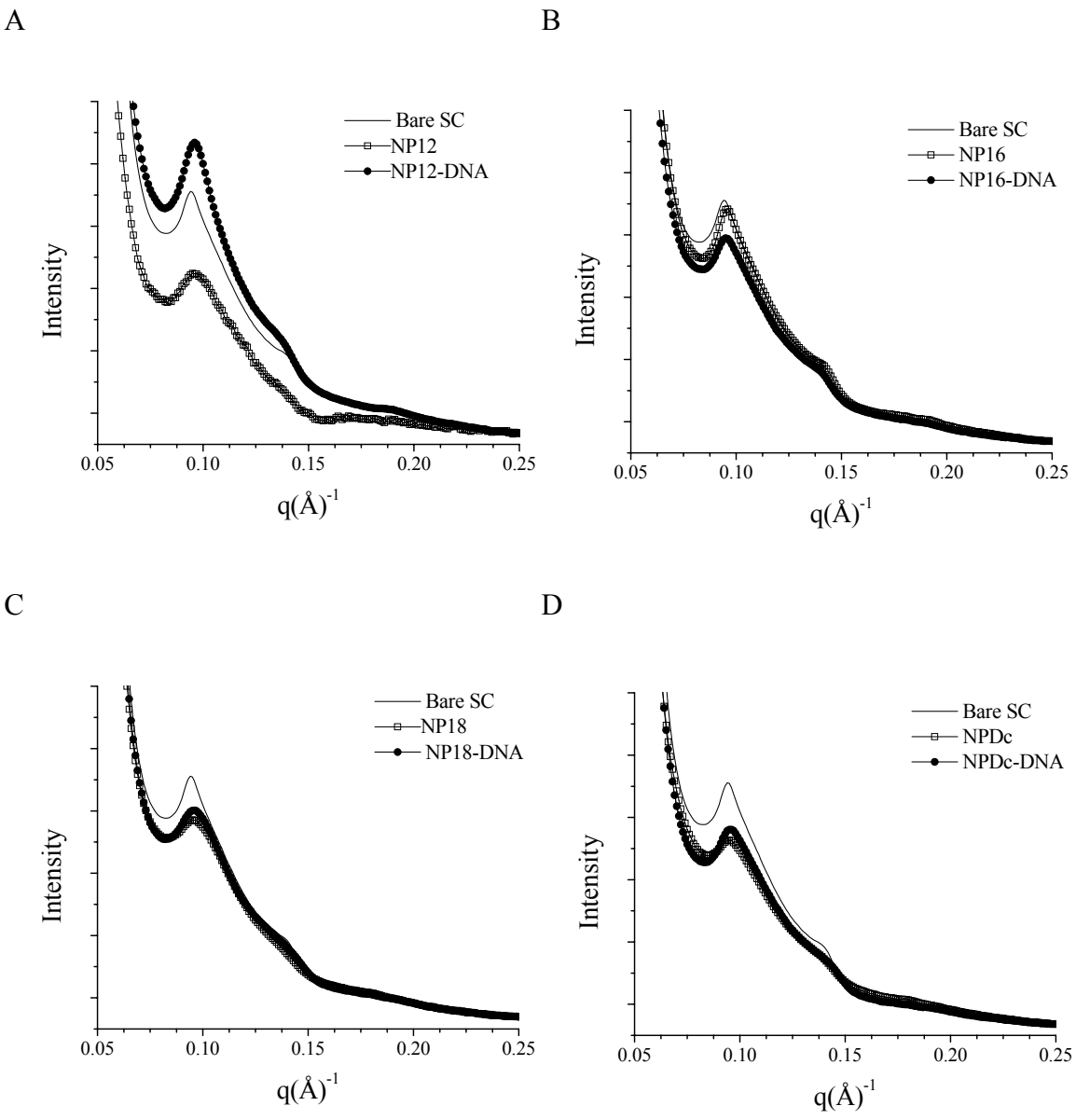

Figure VII.14. Scattering curves of the topical nanoparticle-treated stratum corneum

A – Stratum corneum samples treated with NP12 and NP12-DNA formulations.
B – Stratum corneum samples treated with NP16 and NP16-DNA formulations.
C – Stratum corneum samples treated with NP18 and NP18-DNA formulations.
D – Stratum corneum samples treated with NPDc and NPDc-DNA formulations.

Table VII.6. Calculation of d-spacing and degree of disorder (Δ/d) for the topical nanoparticle-treated stratum corneum (values of d and Δ/d were calculated from single-point measurements).

Formulation	**d**	**Δ/d**
Bare stratum corneum	64.5	0.090
NP12	63.2	0.109
NP12- DNA	64.3	0.090
NP16	79.1	0.117
NP16- DNA	62.4	0.089
NP18	63.4	0.093
NP18- DNA	63.3	0.102
NPDc	62.7	0.097
NPDc-DNA	63.2	0.095

VII.2.4 Conclusions

Physicochemical characterization of the transfection agents has provided a better understanding of the interaction between the plasmid DNA and gemini surfactants and between PG complexes and helper lipid. The gemini surfactants are able to compact the plasmid. The multimodal size distribution characteristic of plasmid DNA, corresponding to linear, open circular and supercoiled species, becomes unimodal with the size of the PG complexes being around 100 nm. Gemini surfactants in the absence and presence of the helper lipid were able to induce changes in the structure of the DNA, confirmed by CD spectra. These changes depended on the distance between the two positively charged nitrogens, the length and nature of the hydrophobic tail, and the presence or absence of the helper lipid.

Fluorescence intensity of an intercalating dye depended also on the structural features of the gemini surfactants influencing the ability of the dye to penetrate between the base-pairs. Scattering profiles of the PG complexes presented a single peak, whose position shifted depending on the spacer and tail length. The presence of DOPE increased the complexity of the system, as the scattering curves contained multiple peaks indicating polymorphic structure. Based on the physicochemical properties, *in vitro* delivery systems can be optimized in order to increase transfection efficiency. Additional issues such as the nature of the DNA complexation, localization of the plasmid in the complexes and vesicles, and influence of changes in environmental pH can be addressed.

Delivery of plasmid into intact skin poses additional challenges compared to *in vitro* transfection. The stratum corneum represents a formidable barrier, thus the delivery

system should be able to temporarily perturb the integrity of this layer and facilitate the diffusion of macromolecules. The delivery system should be non-toxic to avoid destruction of the delivered genetic materials by scavenger cells. Within the skin, the delivery system has to protect the DNA against lysosomal degradation by the endonucleases. The excipients included in the nanoparticle formulations to increase intradermal DNA delivery were penetration enhancers such as diethylene glycol monoethyl ether, propylene glycol and PDM 27. The increased complexity of the delivery system was reflected in various parameters. The size measurement of the nanoparticle formulation revealed polymodal particle distribution, confirmed by AFM and TEM images. The SAXS profiles of the topical nanoparticle formulations show multiple peaks, indicating polymorphic structure. The nanoemulsion systems haveuniform size distribution and SAXS profiles characteristic of emulsion systems. SAXS curves of the stratum corneum treated with topical formulations indicated that the distance between lipid layers is constant at 62-65 Å, but the degree of disorder was dependent on the nature of the gemini surfactant and the presence or absence of the plasmid in the formulations.

Characterization of the nanoparticle and nanoemulsion formulations provided information about the interaction of the components with the plasmid DNA. The effect of the delivery system on the stratum corneum is important, since increased penetration is a major requirement in cutaneous gene delivery. The formulation selection for topical application was based on the following criteria: (1) induction of structural changes, i.e., compaction of the DNA achieved by the presence of the gemini surfactants, (2) structural polymorphism, contributing to the efficient cellular transduction, and (3)

effect on the stratum corneum lipids, indicated by the increased degree of disorder induced by the topical formulations.

VII.3 Transfection of PAM 212 cells with pGTmCMV.IFN-GFP plasmid using gemini surfactants as novel agents for the delivery of plasmid DNA

The purpose of the study was to evaluate a series of novel gemini cationic surfactants as delivery systems for plasmid delivery *in vitro*.

The expressed proteins were detected by ELISA (IFN-γ) and fluorescence microscopy (GFP). In order to establish a relationship between the structure of the gemini surfactants and their potency to transfect cells *in vitro*, correlations of physical characteristics of the compounds such as critical micelle concentration (CMC), the degree of micelle ionization at the CMC (α) and surface area (a) occupied by one molecule at the air-water interface with the transfection efficiency were evaluated.

VII.3.1 IFN-γ expression in cells measured by ELISA

A +/- charge ratio of 10 in PGL vesicles was selected based on the optimization studies with the 12-n-12 series and 16-3-16 surfactant. The transfection efficiency was found to be dependent on the length of the spacer between the two positively charged head groups, with the n=3 spacer showing the highest activity (12-3-12, 16-3-16 and 18:1-3-18:1; Figure VII.15). In the 12-n-12 series of gemini surfactants, a hyperbolic pattern is noticeable with a minimum of protein expression occurring at spacer n=8 (Figure VII.15A). Significantly higher IFN-γ levels were found when the cells were transfected with 12-3-12 and 12-4-12 versus the other compounds with longer linkers ($p<0.05$). No IFN-γ was detected when the cells were transfected without DOPE in the

A

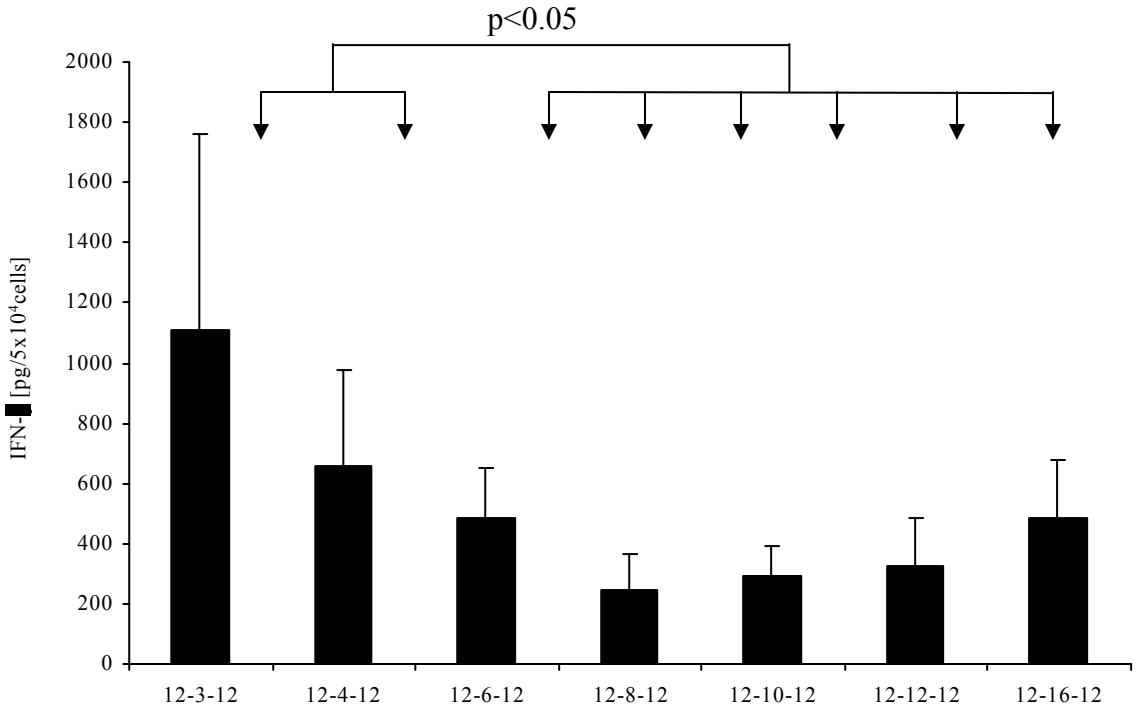
p<0.05
2000
1800
1600
1400
1200
1000
800
600
400
200
0
IFN-■ [pg/5x10⁴cells]
12-3-12
12-4-12
12-6-12
12-8-12
12-10-12
12-12-12
12-16-12

B

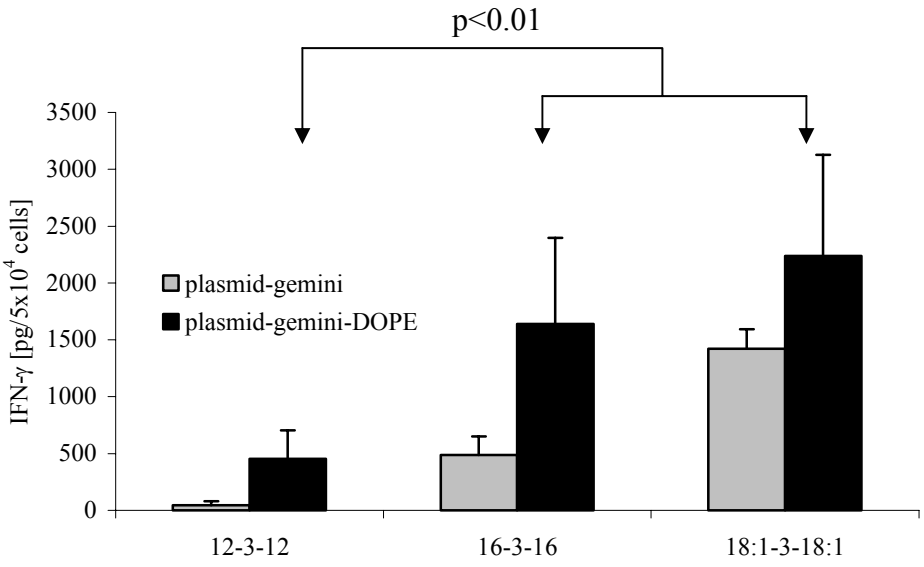
p<0.01
3500
3000
2500
2000
1500
1000
500
0
IFN-γ [pg/5x10⁴ cells]
plasmid-gemini
plasmid-gemini-DOPE
12-3-12
16-3-16
18:1-3-18:1

C

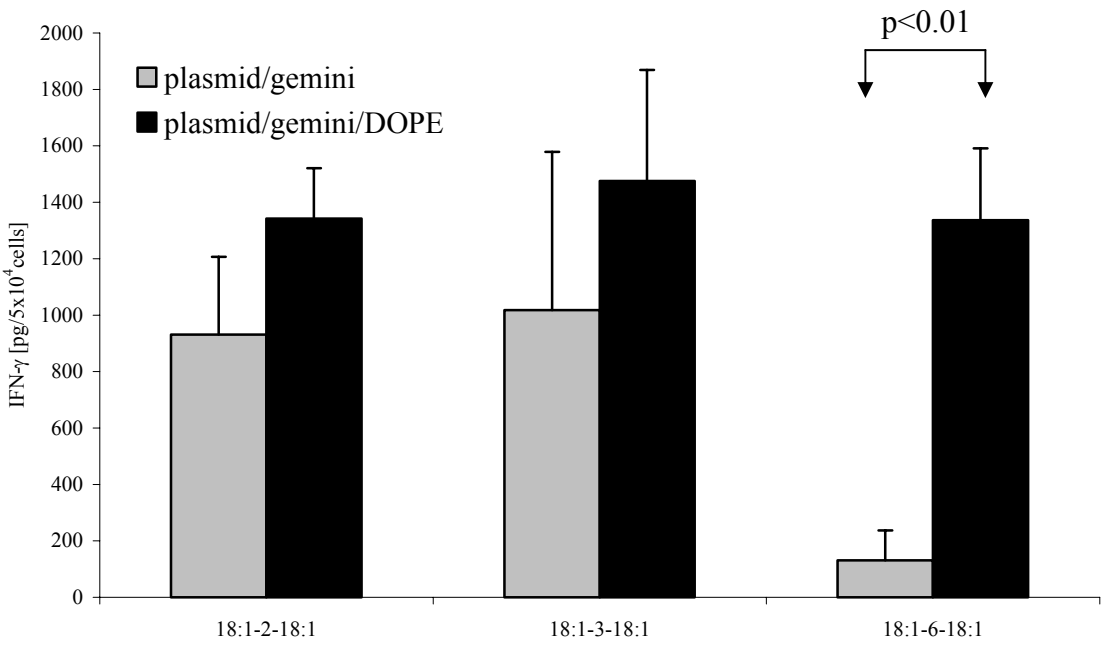

Figure VII.15. IFN-γ expression in PAM 212 cells transfected with 0.2 µg pGTmCMV.IFN-GFP and gemini surfactants in the presence or absence of the helper lipid DOPE.

A – 12-n-12 gemini surfactant series at a +/- charge ratio of 10 in the presence of DOPE. The length of the spacer influences the transfection efficiency of the gemini surfactants.
B – m-3-m gemini surfactant series at a +/- charge ratio of 10 with or without DOPE as helper lipid. The length and nature of tail influence the transfection efficiency of the gemini surfactants.
C – 18:1-n-18:1 gemini surfactant at a +/- charge ratio of 10 with or without DOPE as helper lipid. The lengthof spacer influences the transfection efficiency of the gemini surfactants.
Significant differences were observed at the $p<0.05$ level (ANOVA).

12-n-12 series. The effect of the tail length influenced the transfection efficiency, with longer tails being associated with higher protein expression (Figure VII.15B). Transfections with the PGL systems of the 16-3-16 and 18:1-3-18:1 surfactants resulted in significantly higher IFN-γ levels compared to the P – 12-3–12–L system ($p<0.01$). The PG complexes of the 16-3-16 and 18:1-3-18 surfactants were able to transfect cells, albeit at lower efficiency than the corresponding PGL systems. Generally, the n=3 spacer surfactants showed the highest transfection efficiency in both m=12 and 18:1 series (Figures VII.15A and C). No IFN-γ was detected when the cells were transfected with DOPE alone, or with plasmid without transfection agents.

The transfection efficiency was found to be dependent on the length of both spacer and tail. The highest *in vitro* transfection efficiency was recorded with the 18:1-3-18:1 surfactant (1475±393 pg/5x10^4cells) in the presence of helper lipid, DOPE. The transfection efficiency reached a minimum value with the 12-8-12 compound.

VII.3.2 Optimization of the transfection: effect of transfection time and charge ratio

As part of the optimization process, we tested the influence of the transfection time on gene expression (Figure VII.16). Although increased contact of the cells with the transfection agent (24 hours versus 6 hours) increased protein levels, microscopic evaluation of the cell viability showed many dead cells after 24 hours, due to nutrient depletion of the media (not shown). The higher IFN-γ levels might be due to the increased number of cells at 24 hour compared to 6 hours.For the 12-3-12 compound, 8-24-hour incubation did not significantly improve the transfection efficiency, where as for the 16-3-16 surfactant the protein expression was the highest after a 24-hour

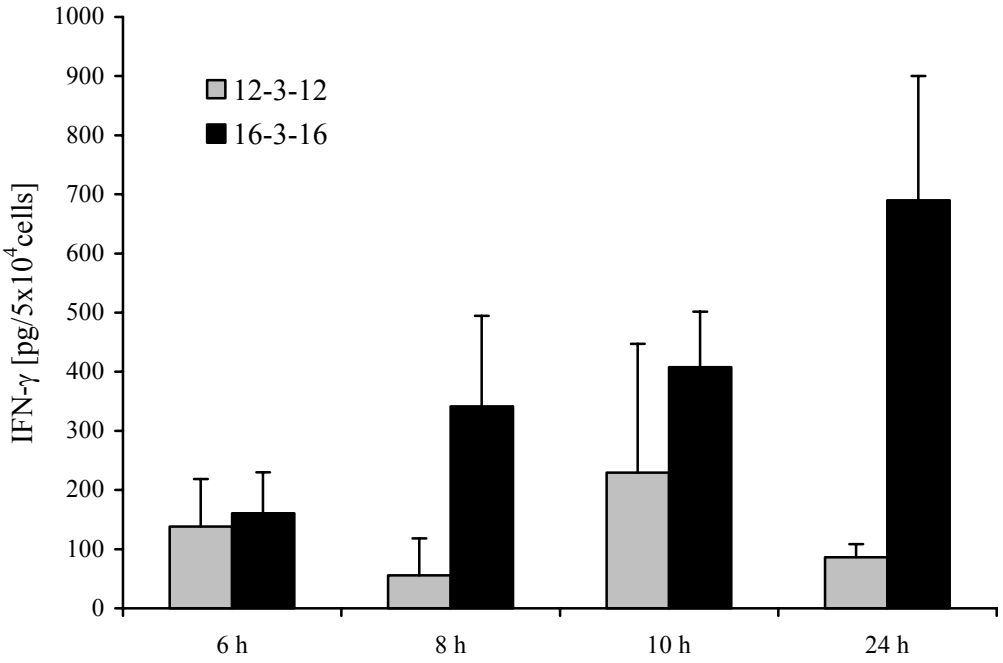

Figure VII.16. Influence of transfection time on the efficiency of the transfection.

PAM 212 cells were transfected with 0.2 μg pGTmCMV.IFN-GFP using the 12-3-12 and 16-3-16 gemini lipids at a +/- ratio of 10. The mixtures were in contact with the cells for 6, 8, 10 or 24 hours. Protein levels were measured 24 hours after the transfection agent was removed from the cells. The longer transfection time yields higher transfection, but a high percentage of cells died due to chemical toxicity and depletion of nutrients.

transfection period. However, due to the greater variability and the visually observable cell toxicity at longer incubation periods, a 6-hour incubation time was selected in further experiments.

The formulations using the 16-3-16 surfactant were optimized for the gemini surfactant/ plasmid DNA charge ratio by correlating with cell toxicity (Figure VII.17). The optimal +/- charge ratio was determined by comparing the percentage of fluorescent cells with cell viability. A high percentage (2.36%) of fluorescent cells were observed at a charge ratio of 10, with 74% cell viability. It is estimated that at $1x10^6$-cell density, 23,000 cells were producing the GFP protein. Since the two proteins (GFP and IFN-γ) coexpress, the same number of cells produced 10.8±0.3ng IFN-γ, hence each cell produced approximately 0.5 pg of IFN-γ.

Overall, an increase in the cationic charge ratio with gemini surfactants resulted in increasing transfection efficiency but lower cell viability. At a charge ratio of 40 the transfection efficiency was 3.13%, however, cell viability fell to 20%. The commercially available Lipofectamine Plus™ Reagent (DOSPA:DOPE 3:1; at the concentration recommended by the manufacturer), used as positive control yielded a slightly higher fluorescent cell count (5.87%), but cell viability was only 32%.

No fluorescence was detected in the non-transfected cells.

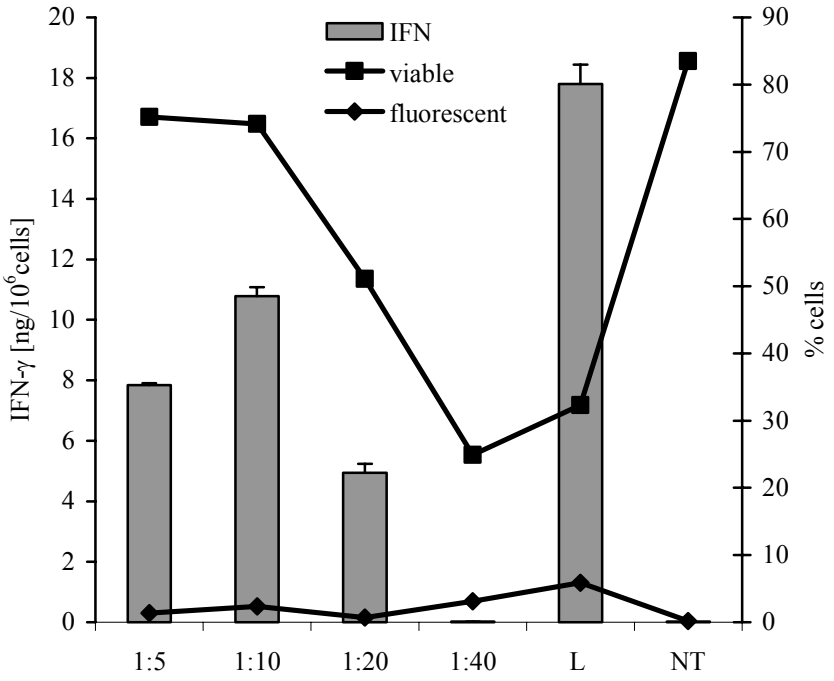

Figure VII.17. IFN-γ expression in PAM 212 keratinocytes assessed by ELISA and GFP expression and cell viability by FACS.

The cells were transfected with either PGL systems, using the 16-3-16 gemini surfactant at +/- charge ratios of 5, 10, 20 and 40, or Lipofectamine PLUS Reagent, using 0.2 μg pGTmCMV.IFN-GFP. The primary y-axis represents the IFN-γ expression (bars); the secondary y-axis represents the percentage of fluorescent cells and viable cells.

VII.3.3 Correlation of the physicochemical characteristics of the gemini surfactants and their transfection efficiency

In order to correlate the structure of the gemini compounds with the transfection efficiency, we compared the extent of IFN-γ expression (Figure VII.15) with the measured physical properties of the surfactants (Table VII.7).

A correlation at significant levels was found between the transfection efficiency and surface area occupied by one molecule (a) (Pearson correlation of 0.836 at p=0.019 level of significance).

The size of the PGL system of the 12-n-12 series correlated with the binding properties (Pearson correlation of 0.943 at p=0.001 level of significance) and CMC (Pearson correlation of 0.778 at p=0.04 level of significance), with smaller particle size leading to lower dye binding and hence lower fluorescence. Size and ζ-potential measurements of both PG complexes and PGL system did not show marked differences among the formulations, yet transfection efficiency between the two systems and within the system was significantly different. The PG complexes showed particulate nature, whereas the PGL systems were vesiculate. The PGL systems with short spacers (n=3-4) and high transfection efficiency exhibited polymorphic structure, predominantly lamellar, with additional polymorphic phases.

The plasmid–DOPE system, showing typical hexagonal phase (Table VII.3), in the absence of the cationic gemini surfactant was not able to transfect the PAM 212 cells due to the negative ζ-potential.

Table VII.7. Measured physicochemical parameters of gemini surfactants.

Gemini surfactant	**CMC [mM]**	**a** [321] **[nm^2/molecule]**	**α** [322]
12-n-12 series			
12-3-12	0.98±0.04	0.98	0.23±0.02
12-4-12	1.17±0.04	1.10	0.26±0.02
12-6-12	1.09±0.04	1.40	0.34±0.02
12-8-12	0.84±0.03	1.78	0.46±0.04
12-10-12	0.62±0.03	2.16	0.51±0.06
12-12-12	0.36±0.03	2.14	0.56±0.08
12-16-12	0.12±0.01	1.44	0.59±0.08
m-3-m series			
12-3-12	0.98±0.04	0.98	0.23±0.02
16-3-16	0.026±0.001	1.21	0.35±0.02
18:1-3-18:1	0.023±0.001	0.72	0.42±0.06

CMC – critical micellar concentration
a – surface area occupied by one molecule at air-water interface
α – degree of micelle ionization at CMC

Conversely, lamellar systems were shown to transfect cells with high efficiency if the average membrane charge density (σ_M) of the cationic component exceeded a threshold value ($1.04x10^{-2}e/Å^2$) [152]. The PGL systems with the 12-3-12 and 16-3-16 surfactants meet and exceed this value [161]. Thus, although the PGL sytems show lamellar structure, they can transfect cells *in vitro* due to the high membrane charge density.

In vitro transfection efficiency was significantly dependent on the spacer lengths and the nature of the hydrophobic tail of the surfactants. A larger Gibbs area (a) per molecule (lower surface excess concentration, Γ, at the air/water interface) [321] correlated with a lower transfection efficiency (Table VII.7). These parameters reflect the importance of the spacer length in binding of the gemini surfactant to DNA. The distance between two phosphate groups in a DNA molecule is 0.34 nm, whereas the distance between the cationic head groups in gemini surfactants 12-3-12 and 12-6-12 are estimated to be 0.49 and 0.91 nm, respectively at the air-water interphase [323]. Thus, when the distance between head groups in gemini surfactants approaches that between phosphate groups in DNA, stronger complexation can occur. There is also evidence that longer spacers will bend into a U shape and preferentially locate in the more hydrophobic environment of the hydrocarbon tails. This U shape formation and the resulting decrease in distance between the two cationic head groups are apparent at spacer lengths greater than twelve carbon atoms, and can be facilitated by the vicinity of the phosphate groups of the DNA [323]. Our results indicate that transfection efficiency begins to increase again at spacer C12 (Figure VII.15), consistent with a decrease in the head group distance and possibly an increase in DNA binding of the gemini surfactants with spacers n=12–16.

Compaction studies of DNA with the 12-n-12 series of compounds also indicate that gemini surfactants with small spacer lengths of 2-3 carbon atoms, i.e., smaller head group area, have the highest capacity to compact DNA [127]. The charge concentration ratio, α_C of gemini surfactant/DNA expressed in relative concentrations of equivalent charges, $C_{s,\,eq}$ and $C_{DNA,\,eq}$ is given as

$$\alpha_c = \frac{c_{s,eq}}{c_{DNA,eq}} = \frac{c_s \nu_s}{c_{DNA} \nu_{DNA}} \qquad \text{(VII.1)}$$

where ν is the valency and c_s and c_{DNA} are the concentration of gemini surfactant and DNA, respectively [127]. At α_c = 1, a neutral complex is expected to form when sufficient numbers of gemini surfactants are present to bind all charges on the DNA. However, this may not be true if some gemini molecules self-associate instead of binding to DNA. The actual concentration of gemini surfactants that bind DNA can be calculated as

$$c_{local} = \frac{c_s}{c_{DNA}} \frac{1}{\pi h N_A (2Rd + d^2)} \qquad \text{(VII.2)}$$

where h is the helical rise per DNA base pair (0.34 nm), C_{DNA} is the DNA basepair concentration, N_A is the Avogadro number, R is the DNA helix radius (1 nm) and d is the length of the gemini surfactant [127]. Higher ratios of α_c /c_{local} indicate lower binding efficiency and DNA compaction by the gemini surfactant, with the excess surfactant present in the formulation self-associating instead of binding to DNA. Of the 12-n-12 and 16-n-16 series, the gemini surfactants with low α_c /c_{local} ratios, but α_c >1, could be considered more advantageous for increased transfection efficiency. However, the reverse may be true for transdermally effective formulations. Formulations with considerable excess gemini surfactant, i.e. concentration above the CMC, especially

containing gemini compounds with short spacers that can form "worm-like" micelles [115], could create high α_c /c_{local} ratios and provide greater interaction with skin lipids due to their better solubilizing ability.

Another important element, besides the electrostatically favorable interactions, leading to complexation of the gemini surfactant and DNA is the structural element. At the air/water interphase, the spacer of surfactants with n>8 folds into the hydrophobic domain, causing shortening of the distance between the two positively charged nitrogen [322]. Similar structural organization of the PGL systems with higher spacers (10-16 carbons) might explain the increase of transfection efficiency in the 12-n-12 series. Rosenzweig et al. [116] found certain 16-n-16 series of diquaternary ammonium compounds were capable of transfecting BHK-21 hamster kidney cells *in vitro* in the absence of DOPE. Transfection efficiency was highest for an intermediate spacer length 16-6-16; shorter spacers (2 or 3) were 5-10 fold less effective. DOPE inhibited transfection by the 16-2-16 gemini surfactant even at low amounts (2:1 gemini-DOPE ratio) [116]. In our study, it was observed that DOPE increased the transfection efficiency of the gemini surfactants regardless of the nature of head-group or tail-length. MacDonald's group [116] used a low DNA/gemini ratio (1:1 mole ratio) and low amounts of DOPE (up to twice the amount of gemini surfactant) for transfection, while we found that the best basepair/gemini surfactant mole ratio was approximately 1:10 (corresponding to a +/- charge ratio of 10) with the amount of DOPE eight fold compared to the gemini surfactant. Using the n=3 spacer with m=12, 16 and 18:1 tails, we detected increased transfection efficiency for the PGL systems with increasing tail length, and interestingly, the systems with the 16-3-16 and 18:1-3-18:1 surfactants were able to deliver the plasmid into the cells even in the absence of the helper lipid, albeit at

much lower efficiency. Fisicaro et al.'s [119] recent results show that DOPE increases the transfection efficiency of C2 spacer alkyl-tail gemini surfactants. Although longer-tail compounds (C14-18) are able to transfect cells even in the absence of helper lipid, their efficiency is low. These findings are consistent with results obtained in our laboratory [153]. Dauty et al. [324] suggest the CMC of certain gemini cationic surfactants (specifically C12-16 chain length ornithine based dimerizable surfactants) could be very important for transfection. A high CMC would be essential for having a high concentration of monomers for DNA complexation; however, a low CMC may increase the stability of the complex due to micellar aggregation that could keep the complex together during the delivery process. In our studies with gemini compounds in the 12-n-12 series having short spacers (n=3-10), lower CMCs were associated with lower transfection rates (Table VII.7). However, at n=12-16 transfection efficiency gradually increased with decreasing CMC. The highest transfection efficiency was observed with the 18:1-3-18:1, which has the lowest CMC among all gemini compounds investigated in this study (0.023 mM). Since a lower CMC is advantageous for maintaining DNA complex stability, controlling the formation of the complex by the formulation procedure is important. We found that DNA complex formation was dependent upon the order of addition of complex forming excipients, such as the gemini compounds and DOPE. The addition of gemini surfactant first to the plasmid (to create high c_{local} / α_c) followed by addition of preformed DOPE vesicles was crucial to form the complex. Adding the gemini surfactants to DOPE first, and then combining with the plasmid did not form suitable complexes for transfection (results not shown).

Analysis of the CD spectra, namely the decrease in the positive peak at 290 nm (Figure VII.8B), correlated with transfection efficiency. The PG complexes and the

plasmid–DOPE mixtures exhibited a blue shift, but neither the gemini surfactant nor the DOPE alone, were able to depress the peak. They were able to induce only very low or no cell transfection in PAM 212 cells. In the PG complexes of the 12-n-12 series, the changes induced in the DNA structure (degree of depression at 260 nm) indicated significant correlation with the fluorescence quenching properties (Pearson correlation 0.838, with a p=0.019 level of significance). The PGL systems showed correlation with the *in vitro* transfection efficiency (Pearson correlation of 0.814 at p=0.026 level of significance). A higher degree of depression of the 260 nm peak correlated with higher transfection efficiency in the murine kerationocytes. CD measurements showed that the gemini surfactants and DOPE induced changes similar to those described in the literature, namely the formation of Ψ^- DNA, a left handed highly organized structure [131], as evidenced by the decreased positive peak at 290 nm and shift of the 260 nm peak to negative values.

SAXS spectra of the PG complexes showed a single sharp peak, and lacked any indication of polymorphic arrangements. The relative position of the peak in the 12-n-12 series correlated with the transfection efficiency (Pearson correlation 0.937 at $p<0.002$ level of significance), a shift of the main peak to smaller values of q being associated with higher transfection efficiency. The PGL systems showed increased structural complexity, with lamellar and other possible phases present.

In summary, in this work it has been demonstrated that no single characteristic of the gemini surfactants is responsible for *in vitro* transfection efficiency. Although it has been recognized in the literature that size, ζ-potential, electrostatic interactions and phase behaviour are important properties in determination of transfection efficiency of cationic lipid-based delivery systems, a combined evaluation of these factors is

necessary to select optimal delivery systems. Factors that play an important role in the ability of the gemini cationic surfactants to deliver genetic material are: (1) size of complexes of 100-200 nm, (2) positive ζ-potential, (3) ability to compact DNA, (4) presence of helper lipid, (5) polymorphic structure that increases the delivery of the DNA into the cell and facilitates the release in the cytoplasm, and (6) charge density that exceeds a critical value. An optimal combination of these features contributes to the high transfection efficiency of these delivery systems.

VII.3.4 Conclusion

Our results demonstrate that novel cationic gemini surfactants are able to transfect PAM 212 keratinocytes *in vitro*. The transfection efficiency is dependent on both spacer and tail length; however, the transfection efficiency of these compounds was generally lower than that of the commercial agent, but was better tolerated by the cells, i.e., lower cytotoxicity. We have evaluated the physicochemical characteristics of PG surfactant complexes and PGL systems and evaluated the possibility of predicting the *in vitro* transfection efficiency of gemini cationic surfactants. Considering the transfection efficiency of the PG and PGL systems and the physicochemical properties of the gemini surfactants, we can draw the following conclusions:

1. The DNA must be compacted through neutralization of the negative charges by the cationic gemini surfactants. This is evident from AFM images. The 12-3-12 and 12-4-12 surfactants yield somewhat smaller particles of 145-155 nm compared to the other formulations (average about 175 nm), but there was no significant difference among the PGL systems. The gemini surfactants with short (C3) or long (C16) spacers protect the DNA from dye intercalation causing 10-20% more fluorescent quenching

than species with intermediate spacers (C4-C10). Comparing the helical pitch of the B-DNA (3.4 Å) with the calculated distance between the two positively charged atoms in the headgroup of the surfactant (5.1 Å for the 12-3-12, 6.5 Å for the 12-4-12 and average of 6.55 Å for all other spacers obtained from the energy-minimized structures calculated (using Chem 3D Pro v. 8.0), we might expect no significant differences in the ionic interactions. Yet, fluorescence-quenching measurements show differently, indicating that other conformational criteria might be more important than a perfect electrostatic fit.

2. Structural alteration of the DNA, shown in the CD spectra, is crucial for delivery of plasmid into cells. The structure of the native DNA is altered by the gemini surfactants causing a shift of the 260 nm peak into the negative region, indicating an increase in the interhelical interactions. Since the transfection efficiency of the PG complexes was very low or nil, additional structural changes are necessary. The presence of the helper lipid in the PGL systems causes a shift of the positive 260 nm peak into the negative region and flattening of the 290 nm peak. For efficient transfection, both flattening the 290nm peak and depression of the 260nm peak may be required. The degree of depression of the 260 nm peak correlates with the transfection efficiency, a deeper depression being associated with higher transgene expression.

3. SAXS analysis of the PG complexes and PGL systems demonstrated correlation of the structure of the PG complexes with the transfection efficiency. Analysis of scattering vector (q) positions showed that a shift of the main scattering peak relates to the size of the headgroup, and reflects differences associated with the packing of the PG complex. The complexity of the structural elements increases by introducing a helper lipid in the system. Lamellar and possibly cubic *Pn3m* phases appear in the system, characterized by 1:2:3:4 and √2: √3:√4:√6 periodicity. This heterogeneity

influences the transfection efficiency of the delivery systems. The size of the headgroup is a determining factor in the overall structure of the complex, and is directly implicated in the *in vitro* transfection ability. The helper lipid contributes to the stabilization of the DNA–lipid complexes. Felgner et al. [186] indicate that the phosphate group of the DOPE interacts with the cationic lipid, forming a heterodimer, a unit responsible for the high transfection efficiency. Compared to other phospholipids having two C14, C16 or C18 saturated acyl chains or one saturated and one unsaturated chain, DOPE was a better helper lipid, transfecting cells more efficiently. A high degree of chain saturation conferes rigidity to the molecule and stiffness to the lipid bilayer, influencing negatively the transfection efficiency [186]. Due to its fusogenic properties, DOPE also helps DNA escape from the endosomes [62]. In a study of DNA–cationic lipid–phospholipid systems both DOPE and DOPC mixed equally with plasma membranes; however, only DOPE was able to transfect cells efficiently. Of the two lipids, only DOPE caused hemolysis of red blood cells, by membrane disruption. The authors concluded that important feature of the helper lipid DOPE is not its ability to intermix with biological membranes, but the ability to perturb the structure of the membrane [325].

It has been demonstrated that gemini surfactants are capable of compacting the plasmid DNA. We found that the transfection efficiency correlated with changes induced by the gemini surfactants in the CD spectrum of the DNA, the scattering patterns of the complexes and the surface area occupied by a molecule at the air/water interface (a). The correlations indicate that predictions on the transfection efficiency of new compounds can be made by analyzing the PG complexes and measuring their physicochemical properties, such as surface area and CMC.

Hydration behaviour of the gemini surfactants might also play an important role in their ability to interact with biological membranes and consequently deliver DNA. A study of 16-n-16 and 18:1-n-18:1 surfactants (n=2, 3 and 6) [116] demonstrated that all cetyl derivatives and the 18:1-2-18:1 showed lamellar structure and the 18:1-6-16:1 was of micellar conformation. These compounds in our case showed lower transfection efficiency compared to the 18:1-3-18:1, the most efficient agent. This surfactant presents lamellar structure in water and micellar conformation in high ionic strength medium [116]. We can speculate that the ability of polymorphic transition of the gemini surfactants and increased structural complexity conferred by the helper lipid are key requirements for efficient gene delivery. In a recent publication by Fisicaro et al. [119], the importance of the interaction of alkyl-cationic gemini surfactants with DNA was also described. The biological activity of these compounds increases with increasing chain length, similar to our observations (12-3-12 < 16-3-16 < 18:1-3-18:1).

*VII.*4 In vivo *evaluation of various topical DNA delivery systems containing gemini surfactants*

VII.4.1 Topical application of nanoparticle (NP) and nanoemulsion (NE) formulations using novel gemini surfactants: optimization of formulations and treatment regimen in normal CD1 mice

VII.4.1.a Formulation selection for topical application

In order to evaluate topical delivery of plasmid DNA, nanoparticle and nanoemulsion DNA formulations were compared to the blank formulations. The level of expressed protein was measured in the treated skin. Additionally IFN-γ levels were

measured in both lymph nodes and blood in order to evaluate possible cytokine trafficking pathways. The 18:1-3-18:1 gemini surfactant, which showed the highest *in vitro* transfection efficiency, was incorporated in all formulations. Protein expression was higher in the skin of animals treated with the nanoparticle formulation (178±220 pg/cm^2) compared to the nanoemulsion formulation (80±56 pg/cm^2) (Figure VII.18A). The blank formulations also showed relatively high background IFN-γ levels. IFN-γ levels in the lymph nodes of the formulation-treated animals were low, with the exception of the NP18-DNA formulation (44±30 pg/animal) almost undetectable (Figure VII.18B). No significant differences were observed among treatment groups.

The nanoparticle formulation was selected from the previous experiment, and the 18:1-3-18:1 gemini surfactant was replaced with either the 12-3-12 or the 16-3-16 surfactant. The purpose of this experiment was to correlate the *in vitro* transfection efficiency to the *in vivo* delivery. Contrary to the *in vitro* findings, where the 18:1-3-18:1 surfactant showed the best efficiency (see Figure VII.15B), the highest IFN-γ levels in the skin (359±239 pg/cm^2) were generated by the nanoparticle formulation prepared with the 16-3-16 surfactant ($p<0.05$ compared to the blank formulation) (Figure VII.19A). Formulation prepared with the cationic cholesterol derivative, Dc-chol, was used as a comparison, and showed lower efficiency than the gemini 16-3-16 surfactant (82±74 pg IFN-γ /cm^2). As in the previous experiment, the IFN-γ in the lymph nodes was generally lower than in the skin, with the exception of the animals treated with the nanoparticle 16-3-16 formulation (443±456 pg/animal) (Figure VII.19B).

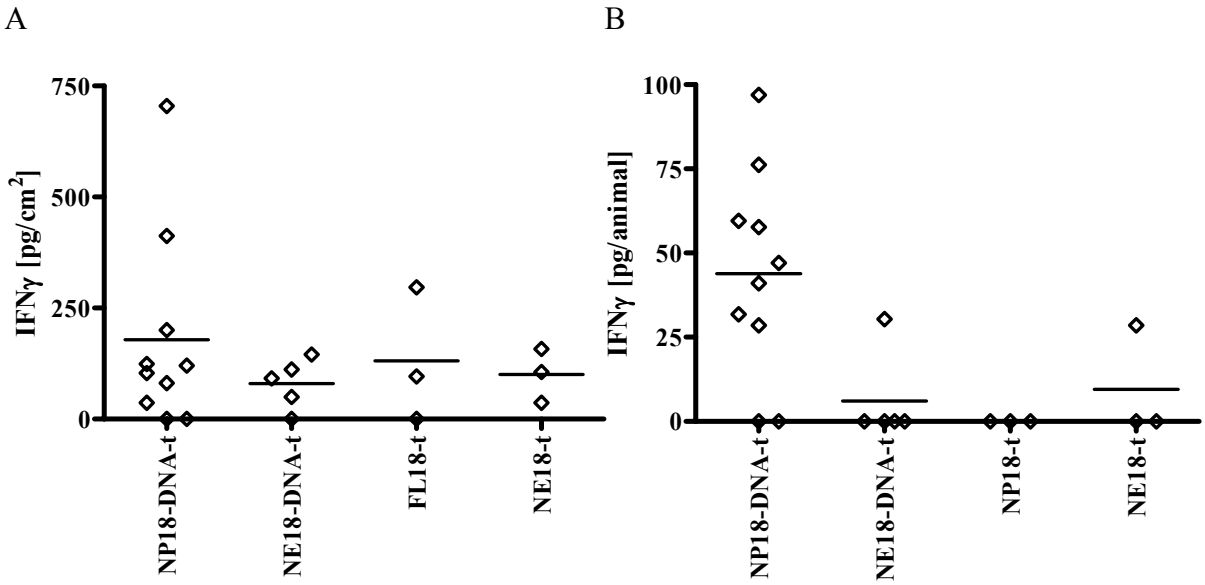

Figure VII.18. IFN-γ expression measured by ELISA in the skin and lymph nodes of CD1 mice.

A – IFN-γ expression in skin in the CD1 mice treated with the pGTmCMV.IFN-GFP plasmid and the 18:1-3-18:1 gemini surfactant in various formulations.
B – IFN-γ expression in lymph nodes in the CD1 mice treated with the pGTmCMV.IFN-GFP plasmid and the 18:1-3-18:1 gemini surfactant in various formulations.
Results were standardized by subtracting the average IFN-γ levels measured in skin and lymph nodes of the control animals (Background values were 683±61 pg/cm^2 for the skin and 208±37 pg/animal for the lymph nodes, n=5).

- **NP18-DNA-t** (n=10) – topically treated with pGTmCMV.IFN-GFP in gemini 18:1-3-18:1 nanoparticle formulation 25 μg in 50 μL for three days (total dose 75 μg);
- **NE18-DNA-t** (n=5) – topically treated with pGTmCMV.IFN-GFP in gemini 18:1-3-18:1 nanoemulsion formulation 25 μg in 50 μL for three days (total dose 75 μg);
- **NP18-t** (n=3) – topically treated with blank gemini 18:1-3-18:1 nanoparticle formulation for three days;
- **NE18-t** (n=3) – topically treated with blank gemini 18:1-3-18:1 nanoemulsion formulation for three days.

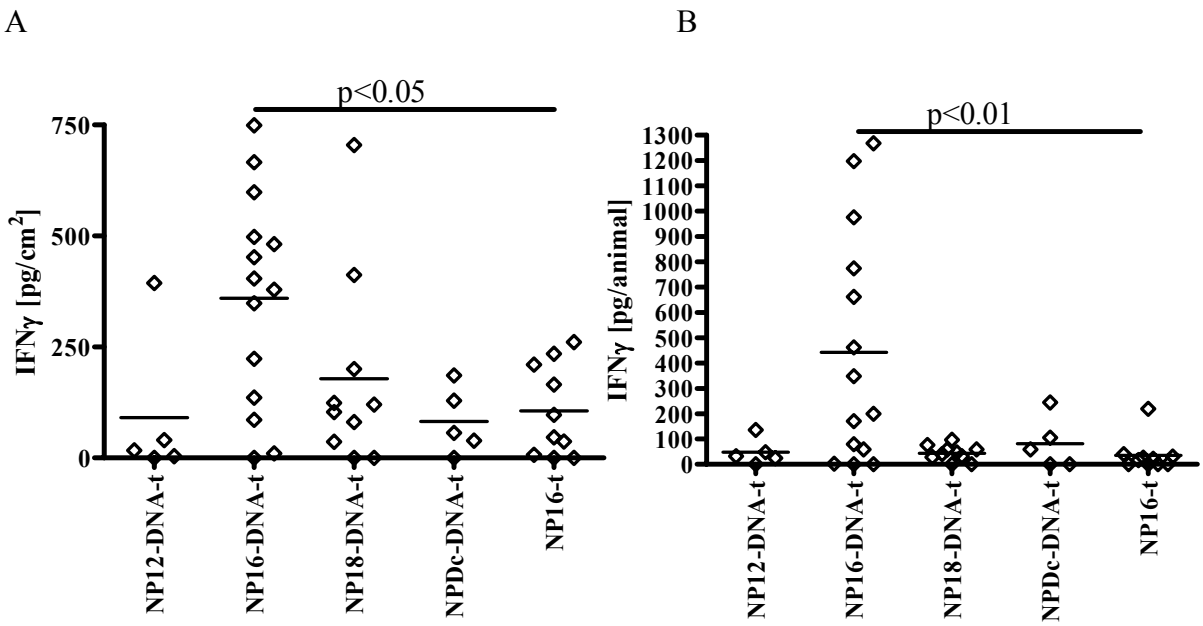

Figure VII.19. IFN-γ expression in CD1 mice treated with the pGTmCMV.IFN-GFP plasmid and various gemini surfactants in nanoparticle formulations.

A – IFN-γ expression in skin.
B – IFN-γ expression in lymph nodes.
Results were standardized by subtracting the background values obtained in the control animals. (Background values were 152±50 pg/cm^2 for the skin and 233±89 pg/animal for the lymph nodes, n=5)
Significant differences were observed at the $p<0.05$ level (ANOVA).

- **NP12-DNA-t** (n=5) – topically treated with pGTmCMV.IFN-GFP in gemini 12-3-12 nanoparticle formulation 25 μg in 50 μL for three days (total dose 75 μg);
- **NP16-DNA-t** (n=14) – topically treated with pGTmCMV.IFN-GFP in gemini 16-3-16 nanoparticle formulation 25 μg in 50 μL for three days (total dose 75 μg);
- **NP18-DNA-t** (n=10) – topically treated with pGTmCMV.IFN-GFP in gemini 18:1-3-18:1 liposomalnanoparticle formulation 25 μg in 50 μL for three days (total dose 75 μg);
- **NPDc-DNA-t** (n=5) – topically treated with pGTmCMV.IFN-GFP in Dc-Chol nanoparticle formulation 25 μg in 50 μL for three days (total dose 75 μg);
- **NP16-t** (n=10) – topically treated with blank gemini 16-3-16 liposomalnanoparticle formulation for three days.

VII.4.1.b Topical treatment of CD1 mice with various selected formulations

Four experiments were carried out using 25-40 CD1 mice/ experiment to optimize formulations and treatment regimen. Generally, topical treatment of mice with pGTmCMV.IFN-GFP plasmid in nanoparticle or nanoemulsion lipid formulations resulted in high levels of IFN-γ expression in the skin (Figure VII.20A) and lymph nodes (Figure VII.20B). The highest levels of gene expression were detected in the skin of the animals treated topically with nanoparticle and nanoemulsion formulation (359±239 and 607±411 pg/cm^2). Both formulations lead to significantly higher IFN-γ expression in the skin than topical naked DNA and blank nanoparticle formulation (359±239 and 607±411, respectively, compared to 136±125 and 106±103 pg/cm^2). Interestingly, IFN-γ levels in the skin after topical application of DNA-NE16 nanoemulsion formulations were higher compared to the NP16-DNA (607±411 vs. 359±239 pg/cm^2), whereas in formulations prepared with the 18:1-3-18:1 gemini surfactant the nanoparticle formulation led to higher gene expression (Figure VII.18A). The IFN-γ levels in the skin of animals treated topically with naked DNA (136±125 pg /cm^2) or Dc-chol formulation (82±74 pg/cm^2) were not statistically different from the control group treated with placebo nanoparticles (106±103 pg/cm^2). Based on the number of cells transfected *in vitro* and the amount of protein generated in 24h, we estimate that approximately 1x10^3 cells/cm^2 were expressing IFN-γ after topical administration. We selected Dc-chol as a comparison for the *in vivo* studies because laboratory [326, 327] and clinical trials [328] showed its ability to deliver plasmid DNA *in vivo* in various tissues, although this is the first time it was used on the skin. The use of Lipofectamine Plus for the animal experiments was not feasible due to the high

plasmid concentration in the topical formulations. IFN-γ expression in the lymph nodes was the highest in the animals treated topically with gemini nanoparticles, at significantly higher levels compared to the control gemini nanoparticles (443± 456 vs. 36±66 pg/animal) ($p<0.05$). Application of the 16-3-16 gemini nanoparticle formulation induced four fold higher levels of IFN-γ than the Dc-chol formulation in the lymph nodes. The IFN-γ expression after intradermal injection of nanoparticle formulation of the plasmid in gemini nanoparticles (2.5 μg/10μL) was approximately three times higher than intradermal injection of naked DNA solution (same dose) in both skin and lymph nodes. In the animals injected intradermally with naked DNA at a dose of 5 μg/10μL and 2.5 μg/10 μL, respectively, protein expression was proportional with the dose, both in the skin (256±130 pg/cm^2 vs. 127±100 pg/cm^2) and the lymph nodes (281±173 pg/animal vs. 115±124 pg/animal). No IFN-γ could be detected in the sera obtained from animals in any of the groups.

In addition to IFN-γ quantification, GFP expression was detected in the skin treated with nanoparticle formulation in the epidermis (Figure VII.21, Panels A1-D1) and around the injection site in skin injected with 2.5 μg DNA/site (Figure VII.21, Panel E1). No GFP fluorescence was observed in the skin of animals treated with control (no DNA) nanoparticle formulation (Figure VII.21, Panel F1 shows the autofluorescence of a hair shaft in the GFP band and Panel 2 in Rhodamine band).

Autofluorescence was ruled out by comparing the images to those taken in the rhodamine emission band (Figure VII.21 Panels A2-F2).

A

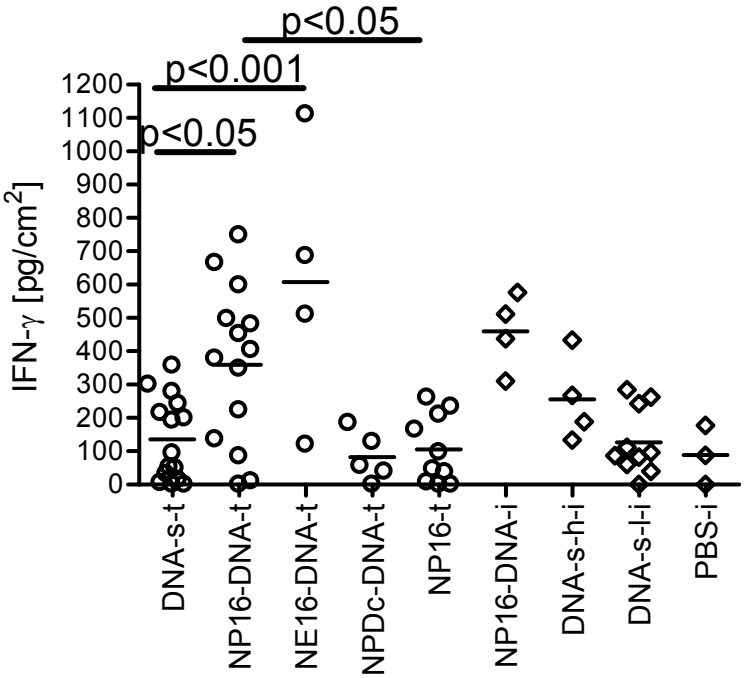
p<0.05
p<0.001
p<0.05
IFN-γ [pg/cm2]
1200
1100
1000
900
800
700
600
500
400
300
200
100
0
DNA-s-t
NP16-DNA-t
NE16-DNA-t
NPDc-DNA-t
NP16-t
NP16-DNA-i
DNA-s-h-i
DNA-s-l-i
PBS-i

B

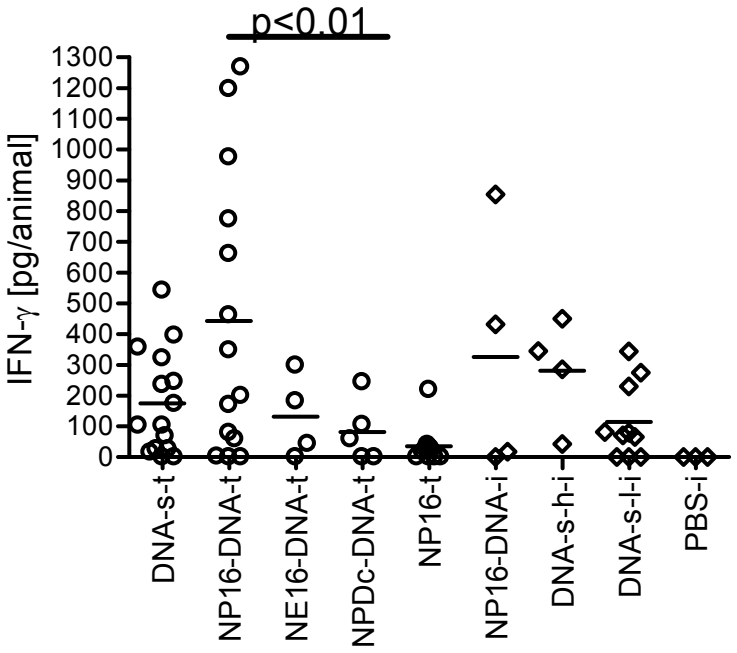
p<0.01
IFN-γ [pg/animal]
1300
1200
1100
1000
900
800
700
600
500
400
300
200
100
0
DNA-s-t
NP16-DNA-t
NE16-DNA-t
NPDc-DNA-t
NP16-t
NP16-DNA-i
DNA-s-h-i
DNA-s-l-i
PBS-i

Figure VII.20. IFN-γ expression in CD1 mice treated with the pGTmCMV.IFN-GFP plasmid and gemini lipid 16-3-16 in various formulations.

A – IFN-γ expression in skin. Results are expressed as amount of IFN-γ/cm^2 treated skin for the topical treatment (circles) and as amount of IFN-γ/animal for the injected groups (diamonds).
B – IFN-γ expression in lymph nodes. Results are expressed as amount of IFN-γ/animal for all groups.
Results were combined from four experiments and standardized by subtracting the background values obtained in the naïve animals in each experiment from the other groups. (Background values ranged 100-300 pg/cm^2 with an average of 239±127 pg/cm^2 for the skin and 150-800 pg/animal with an average of 490±289 pg/animal for the lymph nodes).
Circles – topical treatment; diamonds – intradermal injection
Significant differences were observed at the $p<0.05$ level (ANOVA).

- **DNA-s-t** (n=15) – topically treated with pGTmCMV.IFN-GFP 25 μg in 50 μL in aqueous solution for three days (total dose 75 μg);
- **NP16-DNA-t** (n=14) – topically treated with pGTmCMV.IFN-GFP in cationic gemini nanoparticle formulation 25 μg in 50 μL for three days (total dose 75 μg);
- **NE16-DNA-t** (n=4) – topically treated with pGTmCMV.IFN-GFP in cationic gemini nanoemulsion formulation 25 μg in 50 μL for three days (total dose 75 μg);
- **NPDc-DNA-t** (n=5) – topically treated with pGTmCMV.IFN-GFP in Dc-chol nanoparticle formulation 25 μg in 50 μL for three days (total dose 75 μg);
- **NP16-t** (n=10) – topically treated with 50 μL blank cationic gemini nanoparticle formulation for three days;
- **NP16-DNA-i** (n=4) – intradermally injected with pGTmCMV.IFN-GFP in cationic gemini nanoparticle formulation 5 μg in 10 μL (total dose 15 μg) for one day;
- **DNA-s-h-i** (n=4) – intradermally injected with pGTmCMV.IFN-GFP in aqueous solution (5 μg in 10 μL, total dose 15 μg) for one day;
- **DNA-s-l-i** (n=10) – intradermally injected with pGTmCMV.IFN-GFP in aqueous solution (2.5 μg in 10 μL, total dose 7.5 μg) for one day;
- **PBS-i** (n=3) – intradermally injected with 10 μL PBS for one day.

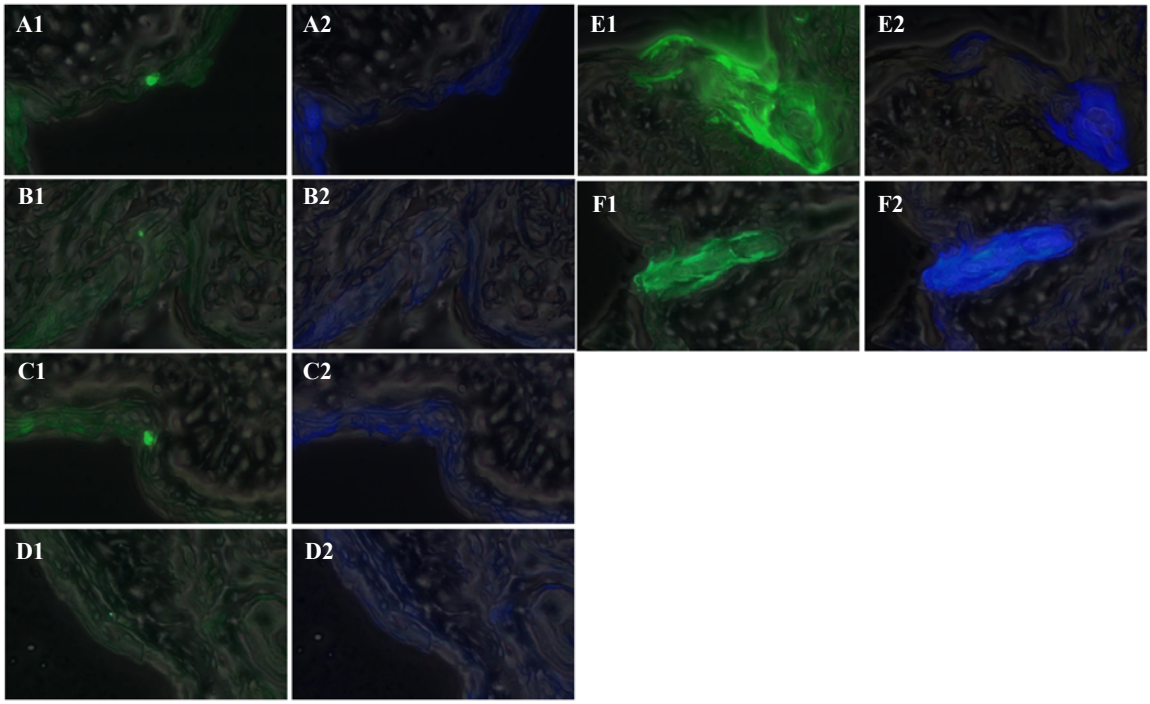

Figure VII.21. Fluorescence microscopic evaluation of the GFP expression in skin of mice treated with the pGTmCMV.IFN-GFP plasmid and gemini lipid 16-3-16 in various formulations.

Phase contrast micrographs were overlaid on fluorescent micrographs of 7 μm thick skin sections. Panels A1-F1 represent the GFP fluorescence and Panels A2-F2 are taken in the rhodamine emission band.

- Panels A-D – **NP16-DNA-t** (n=14) – animals topically treated with pGTmCMV.IFN-GFP in cationic gemini nanoparticle formulation 25 μg in 50 μL for three days (total dose 75 μg);
- Panel E – **DNA-s-l-i** (n=10) – animals intradermally injected with pGTmCMV.IFN-GFP in aqueous solution (2.5 μg in 10 μL, total dose 7.5 μg) for one day;
- Panel F – **NP16-t** (n=10) – animals topically treated with 50 μL blank cationic gemini nanoparticle formulation for three days. Autofluorescence of a hair shaft is shown.

Quantification of plasmid delivery was carried out by nested PCR in the skin of the animals treated intradermally and topically with the gemini cationic nanoparticle formulation (Table VII.8). Approximately 20 $x10^6$ copies/cm^2 skin were detected after topical treatment with 3x25 μg DNA in gemini nanoparticles (NP16-DNA-t) (a single treatment resulted in $15x10^6$ copies/cm^2 skin; results not shown). When gemini cationic nanoparticle formulation of 5 μg DNA/site was injected intradermally (NP16-DNA-i), about 130 $x10^6$ copies of DNA/cm^2 skin were detected. Low plasmid levels were detected in the skin of the gemini nanoemulsion treated group ($2.5x10^6$ copies/cm^2). Plasmid was not present in either the skin of animals injected with 5 μg DNA solution/site (DNA-s-h-i) or in the control group (PBS-i).

VII.4.2 Conclusion

Two different types of formulations were selected for *in vivo* screening in CD1 mice: nanoparticles and nanoemulsion. Initially, the 18:1-3-18:1 surfactant, showing the highest *in vitro* transfection efficiency of all eleven tested surfactants, was incorporated in the formulations. The results show that in the skin, the IFN-γ levels were higher after topical application of the nanoparticle DNA formulation (178 pg/cm^2) compared to the nanoemulsion (80 pg/cm^2). Both blank formulations showed relatively high background, a normal response to physical manipulation of the skin. Protein levels in the lymph nodes were low, with the exception of the NP18-DNA formulation.

Table VII.8. Nested PCR for pGTmCMV.IFN-GFP plasmid detection in the skin.

Treatment	Number of copies of pGTmCMV.IFN-GFP/cm^2 skin
NP16-DNA-t (n=4)	20 million 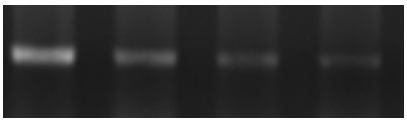
NE16-DNA-t (n=4)	2 million 
NP16-DNA-i (n=3)	130 million 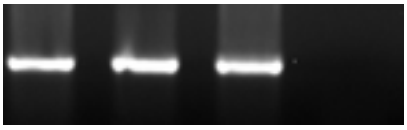
DNA-s-h-i (n=4)	0 
PBS-i (n=3)	0 

The ethidium bromide-stained bands were quantified based on standard dilutions of the same plasmid.

In order to correlate the *in vitro* transfection efficiency and *in vivo* cutaneous delivery, the nanoparticle formulation was prepared with the three gemini surfactants of the m-3-m series (showing better overall transfection efficiency than the 12-n-12 compounds). All three formulations demonstrated transgene expression, but only the NP16-DNA formulation yielded significantly higher IFN-γ levels than background (the blank NP16 formulation).

For further experiments, the highest transfection efficiency nanoparticle 16-3-16 formulation (NP16-DNA-t) was compared to topically applied nanoemulsion formulation (DNA-NE16-t) and naked DNA solution (DNA-s-t). Positive control groups included intradermally injected plasmid solution (2.5 and 5 μg doses) and topical formulation (5 μg doses). The topical blank formulation and intradermally injected PBS represented negative controls. Protein quantification indicated that topical application of nanoparticle DNA formulation generated 359 pg IFN-γ/cm^2, whereas the nanoemulsion formulation produced 607 pg/cm^2. These levels were 2.6-fold and 4.5-fold higher than for the naked DNA treatment. Furthermore, IFN-γ levels in the skin of animals treated with gemini nanoparticle formulation were approximately 3.5-fold higher than in the skin treated with the Dc-chol-based formulation. From this level of expression, one could assume potential for using the topical non-invasive gemini surfactant based delivery systems to generate IFN-γ levels within the skin, sufficient to induce biological changes leading to reduction of excessive collagen synthesis. In the lymph nodes, topical gemini nanoparticle formulations induced a 12-fold increase of protein compared to blank formulation and a 3.6-fold increase in the gemini nanoemulsion treated animals. The nanoemulsion formulation leads to higher levels of IFN-γ in the skin and lower levels in the lymph nodes compared to the nanoparticle formulation with 16-3-16 and

18:1-3-18:1 gemini surfactants. The difference in the expression pattern could be further evaluated in the context of penetration pathways. Evaluation of the distribution of IFN-γ and its involvement in immunological processes such as cellular trafficking (e.g. drainage into lymp nodes) and Th1/Th2 balance are worth pursuing in further studies. Correlating the expression of the two genes, IFN-γ and GFP, with the detection of the plasmid in the skin, one could conclude at the time of sample collection, 24 hours post-treatment, that high levels of IFN-γ detected in the skin of the animals treated with nanoparticle DNA formulation were associated with the presence of GFP and plasmid DNA. In the skin of the animals treated with the nanoemulsion formulation, the IFN-γ levels were higher, compared to the nanoparticle formulation, but 10-fold less plasmid was present. The rate of DNA-penetration into the skin, uptake and transgene expression are different for the two types of delivery systems. In the animals injected with DNA solution, the IFN-γ levels were lower (short half-life) compared to the topical application, but the GFP fluorescence was strong. All the naked plasmid injected into the skin was destroyed in the 24-hour interval, while the nanoparticle formulation conferred protection against degradation, reflected in the highest amount of DNA in the skin.

It is difficult to compare different gene delivery systems presented in the literature. The differences in carrier vectors, inserted genes, delivery mechanisms, and pretreatments are factors contributing to the diversity of results. We compared the extent of expression of IFN-γ gene to cytokines described in the literature and found them to have comparable half-lives. For example, application of 10 μg plasmid coding for human IFNα2 in a nanoemulsion formulation in mice for four days generated approximately 100 pg protein/cm^2 skin [211] while topical application of 2x350 μg plasmid DNA (coding for human IL-1ra) for three days resulted in approximately 165

pg/cm^2 protein in hamster ears [213]. IL-12 levels of 266±27.8 pg in the epidermal layer were measured in mouse skin after introduction of plasmid DNA coding for IL-12 into the skin with the aid of a gene gun. This protein level was sufficient to exert a biological effect, causing tumour regression in mice [214]. We could detect comparable, even higher levels of protein in the CD1 mice treated with nanoparticle formulation (359.9 pg/cm^2). The present data suggest that topical application of IFN-γ coding plasmid DNA using gemini cationic delivery vehicles significantly enhances cutaneous IFN-γ levels after application to intact skin and appears to be several-fold more efficient than other delivery systems tested *in vivo*. PCR results confirmed the successful delivery of the plasmid into the skin.

Although the IFN-γ levels in the skin of NP16-DNA formulation-treated animals was lower compared to the DNA-NE16 nanoemulsion formulation, the nanoparticle formulation was selected for further experiments due to the high variability in transgene expression in the nanoemulsion formulation.

VII.5 Study of the extent of gene expression in IFN-γ-deficient mice

From the results of studies of CD1 mice, the topical nanoparticle formulation with the 16-3-16 surfactant was selected for gene delivery in IFN-γ-deficient mice [329]. This strain was created by homozygous targeted mutation. These animals are unable to synthesize IFN-γ, appear normal in a clean environment, but cannot mount immune response to external stimuli. This model was selected for evaluation of *in vivo* gene delivery in order to distinguish between the exogenous IFN-γ and transgene expression. In normal CD1 mice, IFN-γ secretion can be triggered by physical injury (scratching, shaving or injection) or chemical irritation. The "background" IFN-γ levels of the IFN-γ-

deficient strain are minimal (30 pg/cm^2), thus the measured protein levels are a reflection solely of transgene expression. In the IFN-γ-deficient mice, topical treatment with the pGTmCMV.IFN-GFP in 16-3-16 nanoparticle formulations resulted in the highest levels of IFN-γ expression in the skin (278 pg/cm^2) (Figure VII.22). These levels were only about 30% lower than in the CD1 mice, indicating that topical application of the plasmid in nanoparticle 16-3-16 formulation induces minimal endogenous IFN-γ secretion in normal mice. The protein expression in animals treated topically with both nanoparticle formulations (NP16-DNA and NPDc-DNA) was significantly higher compared to the untreated animals ($p<0.001$). IFN-γ levels in the skin of DNA solution-treated animals were significantly lower ($p<0.05$) than in the 16-3-16 formulation-treated animals (157 pg/cm^2 vs. 278 pg/cm^2). Interestingly, the nanoparticle Dc-chol formulation led to protein expression levels similar to the nanoparticle 16-3-16 formulation in the IFN-γ-deficient strain, but significantly lower levels in the CD1 animals. This difference might be due to differences between the two strains. No IFN-γ was detected in the sera of the mice.

In conclusion, the pattern of protein expression in the IFN-γ-deficient mice was similar to the normal CD1 animals, with generally lower levels (due to complete lack of endogeneous IFN-γ). By using an IFN-γ-deficient strain, the transgene expression could be measured without the interference of endogenous IFN-γ. However, due to obtainability of very similar data, we conclude that the normal CD1 mice are appropriate for formulation screening, due to their ready availability and lower cost (US$5 vs. US$60/animal).

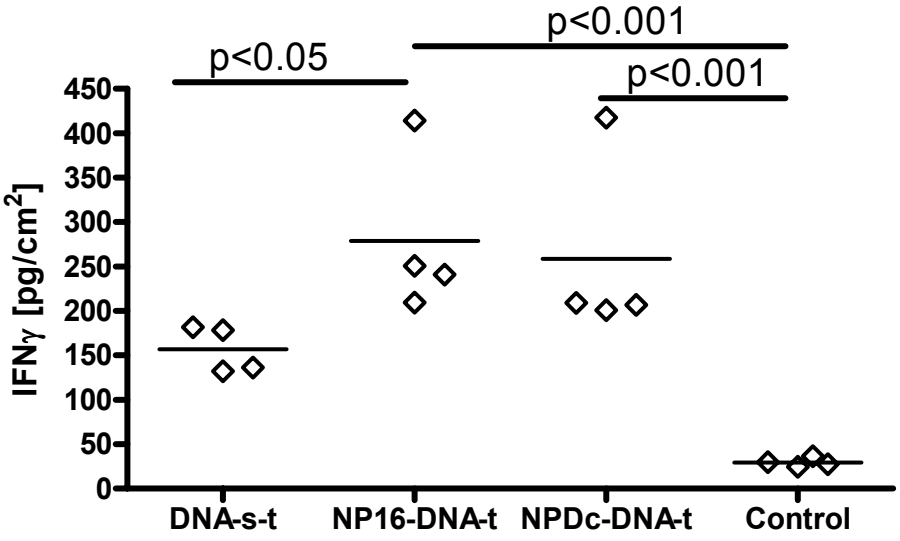

Figure VII.22. IFN-γ expression in the skin of IFN-γ-deficient mice treated with the pGTmCMV.IFN-GFP in solution and nanoparticle formulations.

Significant differences were observed at the $p<0.05$ level (ANOVA).

- **DNA-s-t** (n=4) – topically treated with pGTmCMV.IFN-GFP 25 μg in 50 μL in aqueous solution for four days (total dose 100 μg);
- **NP16-DNA-t** (n=4) – topically treated with pGTmCMV.IFN-GFP in cationic gemini 16-3-16 nanoparticle formulation 25 μg in 50 μL for four days (total dose 100 μg);
- **NPDc-DNA-t** (n=4) – topically treated with pGTmCMV.IFN-GFP in Dc-chol nanoparticle formulation 25 μg in 50 μL for four days (total dose 100 μg).
- **Control** (n=4) – no treatment.

VII.6. Topical application of gemini nanoparticle formulation in Tsk mice: study of the biological effect

The Tsk strain was generated by a spontaneous mutation of the fibrillin-1 gene causing excessive collagen synthesis and deposition in the skin [236]. The mice present tight skin, similar to patients suffering from localized scleroderma. The Tsk mice were chosen for *in vivo* evaluation of the effect of the transgene IFN-γ on collagen synthesis. Gene delivery into the tight skin, IFN-γ expression and biological effect was used as a model for gene delivery into scleroderma patients. Since significant differences between topical DNA solution and nanoparticle formulations were demonstrated in CD1 and IFN-γ-deficient mice, the treatment of the Tsk mice with topical nanoparticle formulations was compared to intradermal injection (used as a positive control). Two different treatment regimens were tested: a 4-day and 20-day application. The 4-day regimen consisted of four topical applications of 50 μg plasmid in NP16 nanoparticle formulation at 24-hour intervals and a single injection. The 20-day treatment consisted of five topical applications of 100 μg plasmid in NP16-PDM formulation per week at 24-hour intervals (no treatment on weekends), and two intradermal injections weekly for four weeks.

VII.6.1 Protein expression measured by ELISA and confocal microscopy

Protein levels (IFN-γ and GFP) as well as biological effect (mRNA levels of procollagen and ICAM-1) were measured. Both topical and intradermal treatments increased IFN-γ expression in the skin of Tsk mice (Figure VII.23). Short term, topical treatment was equivalent to intradermal injection (472±171 and 559 pg/cm^2). These

protein levels were similar to those measured in the skin of CD1 animals treated topically with NP16-DNA formulation (359±239 pg/cm^2) and intradermal injection (256±130 pg/cm^2) (Figure VII.20). After a month of treatment, intradermal injections appeared to produce higher transgene expression (1069±612 pg/cm^2), although, statistically it was not different from topical treatment (345±275 pg/cm^2).

In addition to IFN-γ expression, the GFP was also monitored by confocal microscopy in the DNA nanoparticle formulation-treated Tsk mice (Figure VII.24, Panels A to D), intradermally injected Tsk animals (Figure VII.24, Panels E and F) and non-treated Tsk animals (Figure VII.24, Panels G and H). In the intradermally injected animals, the fluorescence was strong around the injection site but was confined to a smaller area. In the skin of animals treated topically, the fluorescence was weaker, but distributed across the entire examined area. No GFP fluorescence was detected in the skin of control animals.

In conclusion, IFN-γ expression was at high levels in the skin of Tsk mice after 4-day and 20-day treatments. Topical application led to protein levels similar to intradermal injection, thus the topical non-invasive delivery route using the gemini cationic surfactant delivery system is a feasible alternative for gene delivery.

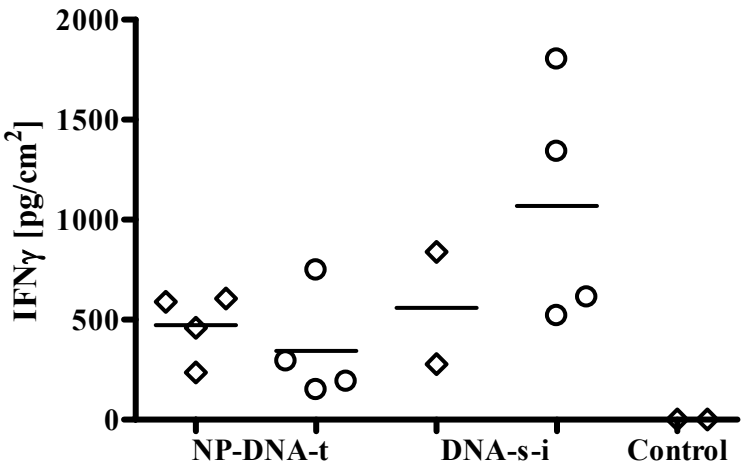

Figure VII.23. IFN-γ levels in the skin of Tsk mice treated topically with pGTmCMV.IFN-GFP in nanoparticle formulations or injected intradermally with DNA solution.

The 4-day regimen (diamonds) consisted of four topical applications of 50 μg plasmid in NP16 nanoparticle formulation at 24-hour intervals and a single injection. The 20-day treatment (circles) consisted of five topical applications of 100 μg plasmid in NP16-PDM formulation per week at 24-hour intervals (no treatment on weekends), and two intradermal injections weekly for four weeks.

- **NP-DNA-t** – Tsk mice topically treated with pGTmCMV.IFN-GFP in cationic gemini 16-3-16 nanoparticle formulations.
- **DNA-s-i** – Tsk mice intradermally injected with pGTmCMV.IFN-GFP 2.5 μg in 10 μL in aqueous solution;
- **Control** – untreated animals.

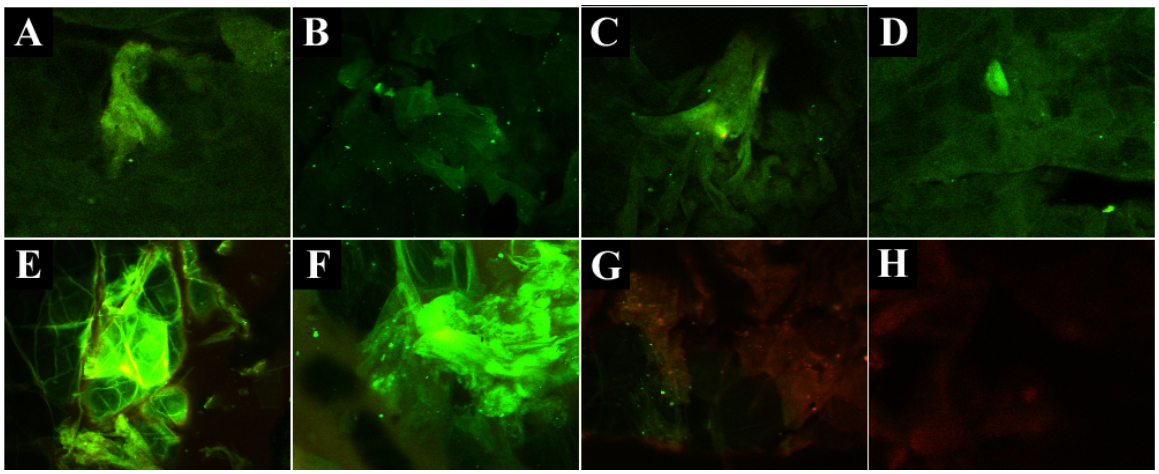

Figure VII.24. Confocal one-photon images of GFP expression in the skin of the Tsk mice.

Panels A-D: treated topically with plasmid nanoparticle formulation.
Panels E-F: injected intradermally with DNA solution.
Panels G-H: untreated.
The images were recorded 15-30 μm deep in the skin.

VII.6.2 Biological effect of the transgene IFN-γ on molecular and cellular markers of scleroderma: collagen and ICAM-1 mRNA measurements

Keratinocytes in the skin can act as a "bioreactor" and participate in immune processes [177], hence secreted IFN-γ can upregulate surface expression of ICAM-1 on keratinocytes (Figure I.4). Diffusion of the IFN-γ secreted by the keratinocytes in the epidermis into the dermis can reduce collagen synthesis by the fibroblasts directly, by interfering with the YB1 pathway, and indirectly by the Jak/STAT1 signaling pathway (Figure I.7). In order to evaluate the biological effect of the *in situ* generated IFN-γ, markers of the gene expression such as the murine procollagen type Iα1 mRNA and ICAM-1 mRNA were determined quantitatively by real-time PCR (Table VII.9). Both 4-day and 20-day treatments reduced the procollagen type I α1 mRNA levels for the topical and injected treatments. The 20-day treatment was about 6% more efficient compared to the 4-day treatment in the topically treated animals and 14% more efficient in the intradermally injected groups. Both treatments (topical and intradermal) induced a significant decrease in the collagen level compared to the untreated animals ($p<0.01$). The highest degree of reduction of approximately 70% was caused by the IFN-γ generated by 20-day injection regimen of pGTmCMV.IFN-GFP solution, correlating with the highest level of transgene expression (1069 pg/cm^2; Figure VII.23). ICAM-1 was upregulated by 50% in both topically treated and injected animals after 20-day treatment, but no effect of the IFN-γ was observed after 4-day treatment in the nanoparticle formulation-treated animals.

Table VII.9. Procollagen and ICAM-1 mRNA levels quantified by real-time PCR in Tsk mice treated with topical and injected nanoparticle formulations.

Treatment	Procollagen type Iα1		ICAM-1	
	4-day	20-day	4-day	20-day
Control	100%	100%	100%	100%
NP-DNA-t	36±29%↓	30±19%↓*	103±40%	154±65%↑
DNA-s-i	42↓	28±10%↓*	N/D	142±81%↑

Arrows indicate increase (↑) or decrease (↓) compared to the control animals (n=4 for all groups except DNA-s-i for 4-day regimen n=2).
*Indicates significant differences compared to the control animals (ANOVA, $p<0.01$)
N/D – not determined
Mean value for four samples ± standard deviation.

Evidence for reduced collagen synthesis in the skin was also obtained by evaluating the dermal thickness in histologic sections (Figure VII.25). Tsk mice develop hypertrophy of the connective tissue, bone and cartilage. The structure of the skin is different from the homozygous siblings in regards to tensile properties and histology. Normal skin presents differences in the longitudinal and transversal tensile properties due to the organization of collagen fibres, thus puncure wounds show eliptical pattern. Tsk skin, on the other hand, presents nearly round puncture wounds, indication of disorganized and densely packed collagen, also evidenced by histological staining [237]. Histologic examination of skin sections stained with hematoxylin-eosine reveals a thicker dermis of the Tsk mice compared to the normal animals, with excessive deposition of collagen fibers extending into the underlaying adipose tissue [244]. In the skin of animals treated topically with NP-PDM-DNA formulation (Figure VII.25, Panel A), or injected with DNA solution (Figure VII.25, Panel B), the thickness of the dermal layer (indicated by arrows) is reduced compared to the untreated animals (Figure VII.25, Panel C). The homozygous littermates of the Tsk animals, without the tight-skin mutation (Figure VII.25, Panel D), showed similar dermal thickness to the Tsk animals treated with nanoparticle formulation and intradermal injection, indicating that in addition to the collagen reduction, the clinical manifestation of the disease could also be reduced. McGaha et al. indicated that a two-fold decrease in the skin thickness after intraperitoneal injection of halofuginone for 60 days was associated with reduced collagen synthesis, evidenced in fibroblast cell culture exposed to halofuginone. Collagen α2I mRNA levels were significantly reduced 8 hours after treatment and completely inhibited after 12 h. Additionally, collagen levels were also reduced in fibroblast cultures derived from Tsk animals [330].

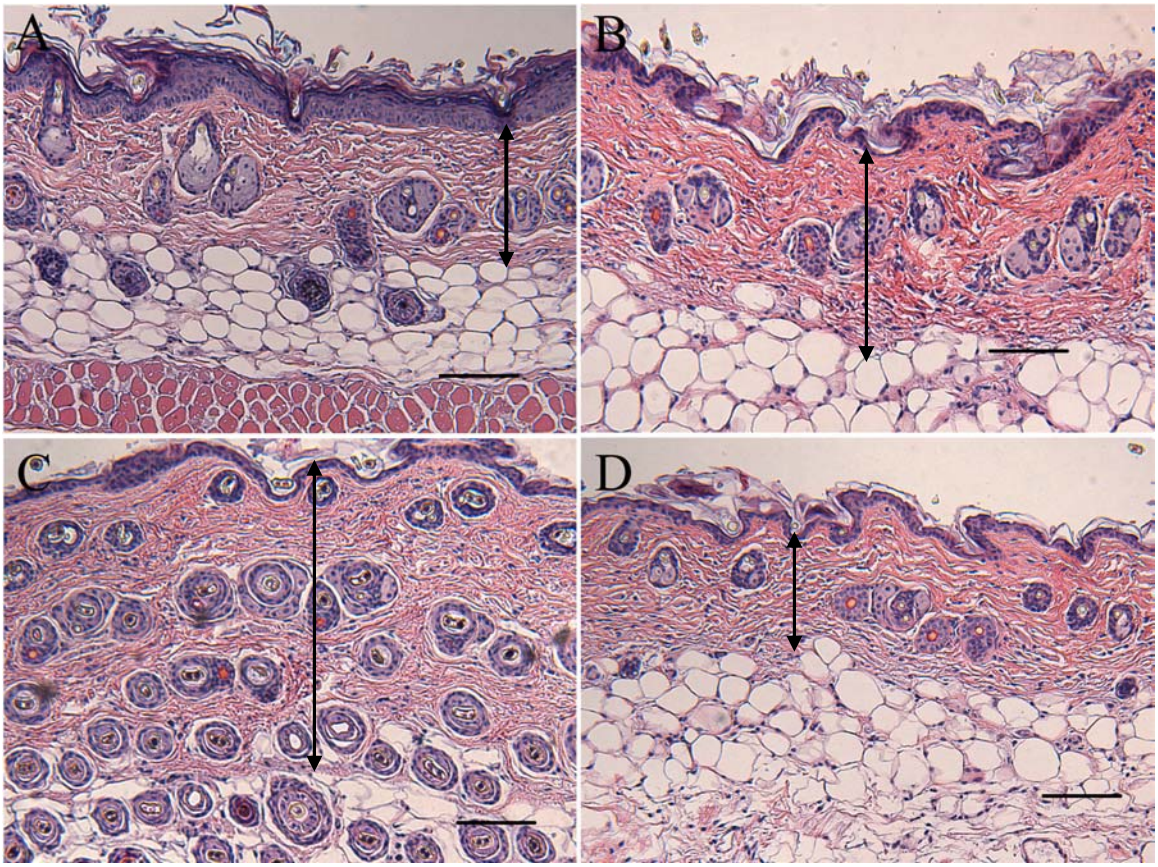

Figure VII.25. Light microscopy images of the skin of the Tsk mice, treated topically with plasmid nanoparticle formulation (A), injected intradermally with DNA solution (B) and untreated (C), compared to homozygous littermates without the tight-skin mutation (D) and images of Tsk mice (E) and homozygous siblings (F).

Paraffin-embedded sections (7 μm) were stained with hematoxylin-eosin. Arrows indicate the thickness of the dermis. Two sections of 1cm x 1cm biopsies were evaluated from each animal. The images are representative for each treatment (n=4 for Tsk animals and n=3 for the homozygous siblings). Bar represents 100 μm.

VII.6.3. Conclusions

Early clinical studies demonstrated that intramuscular injections of increasing doses of IFN-γ (10-100 μg) could improve the clinical signs of the scleroderma, such as skin score, range of motion, oral opening and dysphagia [331]. Similarly, subcutaneously injected IFN-γ (50 μg dose three times per week) caused significant improvement of skin score and lung function in scleroderma patients with pulmonary and skin involvement [332]. Later clinical trials using subcutaneously injected IFN-γ described modest results and common flu-like side effects [333, 334]. Here, we have demonstrated that *in situ* generated IFN-γ from injected plasmid DNA can significantly reduce collagen levels in a Tsk mouse model and cause decrease of the dermal thickness in the Tsk mice.

Moreover, topical application of the plasmid DNA coding for the IFN-γ in cationic gemini nanoparticle formulations can induce similar changes in the collagen synthesis and skin thickness. The absence of IFN-γ in the serum might suggest minimal systemic exposure to the protein, hence side effects observed in the clinical trials can be avoided by the topical administration of plasmid DNA in nanoparticle delivery systems. The present data suggest that topical application of IFN-γ coding plasmid DNA using gemini cationic delivery vehicles significantly enhances cutaneous IFN-γ levels after application to intact skin and appears to be comparable or more efficient than other non-viral delivery systems tested *in vivo* [211, 213, 214]. In addition, its effect on collagen synthesis and reduction of dermal thickness indicate the feasibility of this application in the treatment of cutaneous involvement of scleroderma.

VIII. OVERALL CONCLUSIONS

In the present study, two dimensions of research into improved therapy of localized scleroderma were probed. The first was the design, construction and characterization of a cationic, non-viral gemini surfactant-based delivery system for an IFN-γ coding plasmid suitable for cutaneous gene therapy. The second was the evaluation of this novel therapeutic approach in a Tsk (tight-skin scleroderma) mouse model to determine its clinical feasibility.

VIII.1 Plasmid vectors and in vitro *delivery*

The first key element in efficient transgene expression is the design of a plasmid carrier of the targeted gene, suitable for gene therapy. The ability of the plasmid to express the reporter gene at high levels in mammalian cells is the foremost requirement in gene delivery. An important feature of the plasmid should be transient gene expression, since continuous generation of a foreign protein after alleviation of clinical signs of the disease could cause imbalance in the body. Important features of the pGTmCMV carrier vector, specifically designed for gene therapy were: absence of CpG motifs, lack of ability to induce an immune response, presence of a murine CMV promoter, and the *GFP* gene for easy qualitative evaluation of protein expression (Figure VII.1). The therapeutic gene of *IFN-γ* was inserted into the multiple-cloning site with the *GFP* in a bicistronic format. It was demonstrated that these considerations were important, since the level of IFN-γ expression was 20 times higher using the pGTmCMV.IFN-GFP compared to the pIRES.IFN-GFP plasmid. Replacement of the human CMV promoter with murine CMV promoter increased gene expression; the IFN-

γ levels in the supernatant of cells transfected with the pGTmCMV.IFN-GFP plasmid were 20% higher compared to the pGT.IFN-GFP (Figure VII.2).

VIII.2 Cationic gemini surfactant based formulation development and in vitro *assessment of the delivery efficiency*

Physicochemical characterization of the gemini surfactant-based transfection agents revealed that these compounds in conjunction with DOPE can induce changes in the structure of the plasmid DNA and assume morphological conformations suitable to efficient gene delivery in PAM 212 kerationocytes. All gemini surfactants studied were found to bind the DNA and induce changes of the B-DNA into a highly compacted Ψ^{-} DNA, and the degree of this change was dependent on the spacer length and nature of the tails. Addition of the helper lipid, DOPE to the PG complexes caused additional structural changes (Figure VII.8).

The ability of the gemini surfactants to bind the DNA by electrostatic interaction was demonstrated by dye exclusion measurements (Figure VII.9). Study of the lipid organization in the PG complexes and PGL systems indicated increasing structural complexity caused by the addition of the helper lipid. In the PGL systems, the presence of lamellar structure was detected by SAXS measurements, with additional, probably cubic phases, being present (Figure VII.10). Generally, the PG complexes exhibited low or no transfection in the PAM 212 keratinocytes. The presence of DOPE significantly increased transgene expression. The efficiency of the PGL systems was dependent on the spacer-length, showing a hyperbolic profile (Figure VII.15). Gene expression was the highest for the n=3 spacers, lowest for n=8, after which it gradually increased to n=16. The transfection efficiency correlated with changes induced in DNA structure,

with a higher degree of compaction leading to higher transgene expression. Morphological requirements for successful transfection included the presence of polymorphic phases, present in the PGL systems, but absent in the PG complexes. Physicochemical properties of the gemini surfactants such as surface area of the head-group and CMC also influenced cell transfection.

One of the limitations of the non-viral delivery systems is that it is still less efficient compared to viral vectors. In an attempt to increase transfection efficiency of the non-viral vectors at the cellular level, modifications in the map of the plasmid and improvements in the delivery system have been pursued by several research groups. Several approaches such as use of cationic lipids, neutral fusogenic lipids, pH sensitive polymers, targeting peptides, and nuclear localization signals have been tested. These agents have been used individually or in combination. Combination of various delivery agents increased transgene expression to levels high enough to trigger immune reactions, but to date the therapeutic success has been minimal, as demonstrated by the reduced number of current clinical trials involving gene delivery for therapeutic purposes. In order to achieve higher levels of gene expression, more complex systems need to be built by a stepwise combination of several components. In this project, a gemini surfactant-based delivery system was developed as shown in Figure VIII.1A. The DNA is complexed by a mixture of lipids; cationic lipids causing neutralization and compaction of DNA, which is necessary to penetrate into the cell and fusogenic lipids that perturb the cellular membrane, temporarily increasing its permeability. Further possibilities for improvement may include the addition of pH-sensitive polymers to facilitate endosomal escape of the DNA. The targeting peptides attached to the surface of particles to specifically anchor the DNA onto the surface of target cells, thus directing

gene expression to the affected tissue. This multicomponent modular design might increase cellular delivery and gene expression at therapeutic levels (Figure VIII.1B and C).

VIII.3 In vivo *evaluation of gene delivery and potential for gene therapy*

The delivery of plasmids through intact skin has been a challenging task. Typically, many of the studies have demonstrated delivery after the skin was damaged in some way with depilatory lotion, scraping, stripping or micromechanical disruption [166, 202-204]. Topical delivery of the DNA molecules through intact skin of mice was demonstrated using novel lipid-based delivery systems such as liposomes [107], biphasic vesicles [209], cationic nanoparticles [104], ethanol-in-fluorocarbon microemulsion [208] or water-in-oil nanoemulsion [211].

Using gemini cationic surfactant based topical delivery systems, we have demonstrated the feasibility of delivery of plasmid DNA into the skin through intact stratum corneum, gene expression and its biological effect. The choice of the topical delivery system was based on several criteria: (1) the ability of the cationic component to bind and compact DNA, (2) presence of structural polymorphism that contributes to efficient cellular transfection, and (3) ability of the delivery system to perturb the lipid organization of the stratum corneum and facilitate partitioning of the DNA into the viable layers of the epidermis.

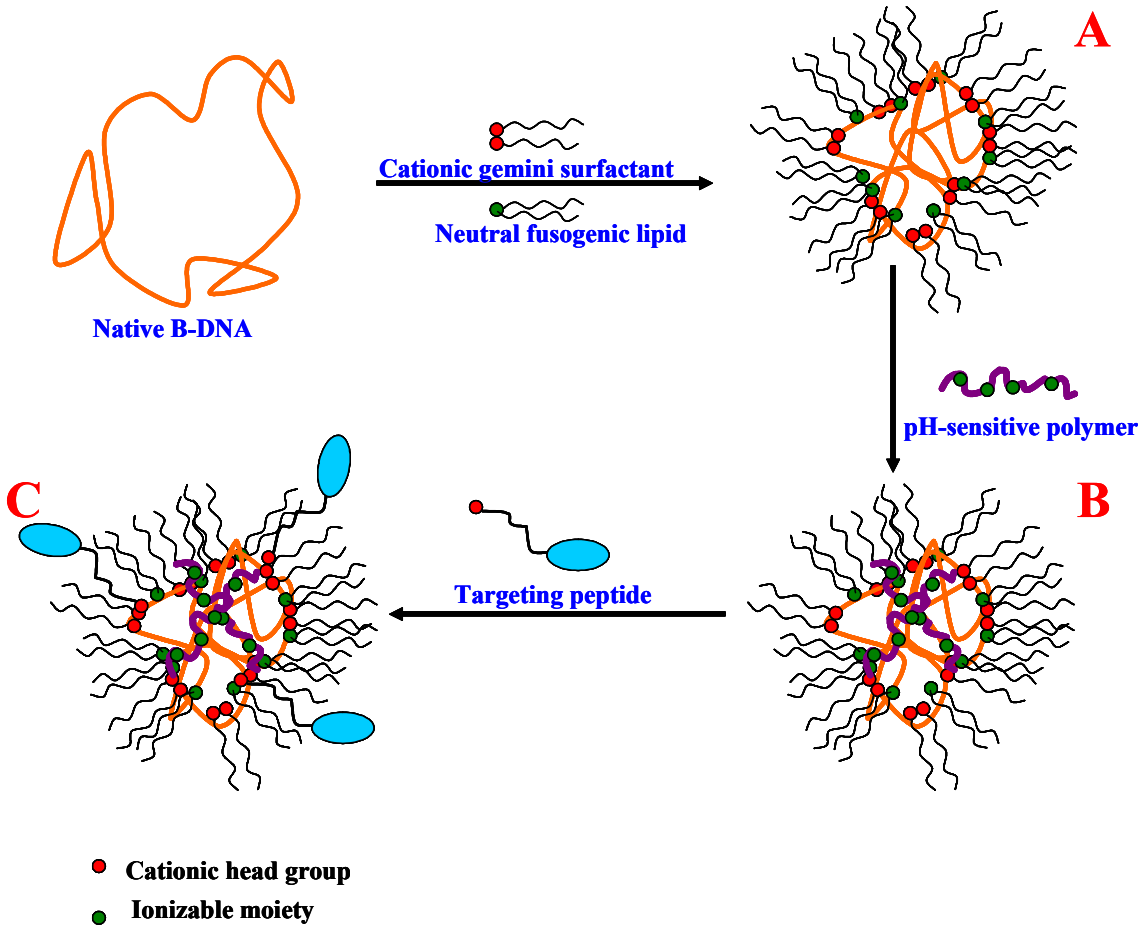

Figure VIII.1. Future possibilities: schematic representation of the building of an improved delivery system.

A multicomponent modular design could include cationic lipids (to neutralize and compact DNA), neutral fusogenic lipids (to perturb the cellular membrane and increase penetration of the DNA into the cell), pH-sensitive polymers (to facilitate endosomal escape of the DNA), cellular targeting peptides (to direct gene expression to the affected tissue) and nuclear targeting peptides (to increase gene expression).
A – Gemini surfactant-based gene delivery system presented in this study;
B – Addition of pH-sensitive polymers to form a more complex delivery system with increased transfection efficiency
C – Cellular targeting peptides anchor DNA to the surface of cells in the affected tissue and nuclear targeting peptides facilitate penetration of the DNA into the nucleus.

In normal CD1 mice, three topical applications of nanoparticle DNA formulation (3 x 25 μg total dose) generated 359.4 ± 238.9 pg IFN-γ/cm^2, whereas the nanoemulsion formulation produced 607.24 ± 411.34 pg IFN-γ/cm^2 (Figure VII.20). These levels are 2.6-fold and 4.5-fold higher than for the naked DNA treatment. Interestingly, plasmid DNA was detected in the nanoparticle formulation-treated skin at 10-fold higher levels compared to the nanoemulsion. This difference might be due to differences in partitioning of the DNA into the skin from the two delivery systems. Furthermore, IFN-γ levels in the skin of CD1 animals treated with gemini nanoparticle formulation were approximately 3.5-fold higher than in the skin treated with the Dc-chol-based formulation. Topical treatment with both gemini nanoparticle and gemini nanoemulsion formulation generated higher levels of protein in the skin than a single intradermal injection of 15 μg DNA (359.4 ± 238.9 and 607.24 ± 411.34 vs. 255.68 ± 130.3 pg, respectively) (Figure VII.20). These levels of protein are 3.5-6 fold higher compared to results reported in the literature for huIFN α2 [211], and 3-5 times higher than levels reported for IL-12, calculated per cm^2 [213]. From this level of expression, it can be assumed that there is a potential for using the topical non-invasive gemini surfactant based delivery systems to generate IFN-γ levels within the skin, sufficient to induce biological changes leading to blockage of excessive collagen synthesis. In the lymph nodes, topical gemini nanoparticle formulations induced a 12-fold increase of protein compared to blank formulation and a 3.6-fold increase in animals treated by the gemini nanoemulsion (Figure VII.20). The present data suggest that topical application of IFN-γ coding plasmid DNA using gemini cationic delivery systems significantly enhances cutaneous IFN-γ levels after application to intact skin and appear to be several-fold more efficient than other delivery systems tested *in vivo*. The nanoemulsion formulation leads

to higher levels of IFN-γ in the skin and lower levels in the lymph nodes compared to the nanoparticle formulation, suggesting that the two delivery systems may have different penetration pathways (Figure VII.20). Additionally, the presence of plasmid DNA in the skin of animals treated topically with nanoparticle and nanoemulsion formulations has been detected (Table VII.8).

Studies of the delivery of genetic material into the skin performed by Khavari et al. [9] demonstrated that immune response could be elicited by applying naked DNA on the skin. However, the same group recognized that for treatment of skin diseases higher transfection efficiency would be necessary [200]. Although some success was demonstrated after delivery of plasmid DNA into the skin by semi-invasive methods such as gene gun, electroporation or microneedles [204, 207, 219, 335-337], ultimately improved non-invasive, topically applied non-viral delivery systems could be the most appropriate therapeutic products.

Here, we have demonstrated significant improvements in topical delivery of plasmid DNA using gemini cationic nanoparticle formulations. Significant increases in pGTmCMV.IFN-GFP plasmid delivery and IFN-γ expression in the skin and lymph nodes compared to naked DNA and Dc-chol based complex are evident. These systems show potential for use in the treatment of localized scleroderma.

Evaluation of the gene delivery into the skin of IFN-γ-deficient animals treated with nanoparticle formulation showed a significantly higher level of gene expression compared to naked DNA (Figure VII.22). The protein levels were about 20% lower compared to the CD1 mice, indicating higher endogenous IFN-γ levels in CD1 mice, caused by the manipulation of the animals preceding and during the treatment (clipping, shaving and cleaning of the skin).

The therapeutic effect of the transgene IFN-γ was evaluated *in vivo* in Tsk mice, an animal model for scleroderma. It was shown that skin collagen levels were slightly decreased after a 3-day treatment in both intradermally injected and topically treated animals, and showed significant decrease after a 20-day treatment regimen, compared to the untreated animals (Table VII.9). Skin thickness was also visibly reduced by day 20 of the treatment (Figure VII.25). The 4-day treatment had no effect on the ICAM-1 expression on the surface of keratinocytes in the skin, but was upregulated 50% after the 20-day treatment. This indicated that skin lesions in scleroderma patients would require a 20-day or longer treatment regimen, which would not be unreasonable. Current treatment options also involve drug administration for several weeks to months. A case study of topical treatment of localized scleroderma with imiquimod (a cytokine inducer compound) cream showed that skin lesions were significantly improved at the 6-week follow-up visit, and some cleared completely by 8 months [262]. To date, no topical IFN-γ gene applications have been described in the literature. Injectable treatment varied from intramuscular injections for 18 weeks [270, 333] or subcutaneous injections for 1 year [334]. The modest improvements observed in these treatments could be due to the short half-life of the IFN-γ and the relatively low local concentrations in the skin lesions that are achieved by the subcutaneous and intramuscular injections. At the same time, the presence of side effects could be attributed to the systemic exposure to the drug.

By using a genetic approach, namely generating IFN-γ *in situ* by the cells in the epidermis (mostly keratinocytes), the half-life of the protein can be extended. The topical transfection could create high local concentrations of therapeutic protein with minimal systemic exposure. The length of the treatment could be evaluated based on the clinical improvement, since overexposure to IFN-γ in the skin could cause undesired

reactions in the skin. Such symptoms could include redness, flaky skin, hair loss and depigmentation, and growth retardation described in transgenic (but otherwise normal) mice overexpressing IFN-γ by keratinocytes in the skin [338].

Here, it has been demonstrated that cationic gemini surfactant-based delivery systems are able to transfect epidermal cells *in vivo*, and the transgene IFN-γ expression is sufficient to cause significant reduction of collagen in the animal model of scleroderma. It has been shown for the first time that topical IFN-γ gene therapy could be a feasible approach for the modulation of excessive collagen synthesis in scleroderma-affected skin.

The debate whether viral or non-viral approaches are the future of gene delivery still continues to be vigorous. After an initial success, the use of viral vectors for genetic diseases (ornitine transcarbamylase deficiency and X-linked severe combined immunodeficiency), has declined due to the severe toxicity caused by the viral carriers. Yet, the role of the viral vectors in cancer treatment (67% worldwide) and vaccine delivery (6.7%) is significant, as demonstrated by the fact that the majority of clinical trials worldwide [http://www.wiley.co.uk/genmed/clinical/] implicate viral vectors (over 70%). Due to the high toxicity of viral vectors, their role in genetic reconstitution is limited. In my opinion, non-viral gene delivery will gain more and more importance in this area, focusing on monogenetic, cutaneous and cardiovascular diseases. By combination of appropriate carrier vectors and delivery systems, high levels of transgene expression could be achieved.

VIII.4 Future research directions

The next steps for the development of the gemini-based gene delivery system could be in the following areas:

VIII.4.1 Testing in human skin

Experiments should include testing in human skin, which could be done *in vitro* using a viable skin model. Such system was developed in our laboratory by a previous graduate student (P. Asavapichayont). Alternatively, a miniature swine (Hanford minipig) could be used, which is a particularly suitable model for human skin. These experiments will contribute to the characterization of delivery and expression of the IFN-γ gene in human or a close model skin.

VIII.4.2 Optimization of the plasmid vector and formulation

Further optimization of the plasmid could improve transgene expression. It has been shown that murine skin transfected via gene gun with plasmid DNA containing the CMV promoter induced gene expression in the epidermis and dermis, while keratin14 promoter allowed protein expression only in the epidermis [339]. By using keratin14 promoter, gene expression could be targeted to the epidermis and exposure to the transgene limited to the skin. Insertion of an episomal replication sequence, such as a scaffold/matrix attachment region (S/MAR) in the plasmid can allow extrachromosomal replication of the plasmid and perpetuate gene expression in the cell proliferation process [340]. It has been shown that this system facilitated episomal plasmid replication in a once-per-cell cycle manner, preserving the gene expression without overpowering the cells. It is especially important to perpetuate the plasmid in epidermal transfection by cellular division, since skin renewal can lead to loss of plasmid in the tissue.

The formulation improvement could include evaluation of cationic gemini surfactants with substituted head groups that increase the *in vitro* and *in vivo* transfection efficiency. Parameters such as DNA compaction, interaction with biological membranes, and release of the genetic material in the cell could be addressed. New helper lipids could be added to the formulations, and their ability to induce polymorphic phase behaviour could be evaluated. The multicomponent modular approach including permeation enhancers, targeting moieties and polymers could also be evaluated. Addition of pH-sensitive polymers to facilitate endosomal escape of the DNA, targeting peptides attached to the surface of particles to specifically anchor the DNA onto the surface of target cells, and nuclear targeting moieties to increase nuclar uptake could be explored.

VIII.4.3 Study of the mechanism

The understanding of the mechanism of topical delivery and interaction of the topical formulations with stratum corneum lipids, uptake of the DNA by various cells in the skin (keratinocytes, dendritic cells and fibroblasts), and trafficking of the generated IFN-γ will be important.

VIII.4.4 Toxicology studies

Animal experiments should focus on the optimization of the treatment regimen: the dose, dosage frequency and length of the treatment. Kinetic studies are necessary to establish the pharmacological profile of the DNA drug. Prior to any clinical trials, evaluation of safety and efficacy must be performed.

IX. LITERATURE

1. **T. Tüting, J. Austyn, W. Stokus and L. D. Falo**. (2000) The immunology of the DNA vaccines. In *DNA Vaccines; Methods and Protocols*, D. Lowrie and R. Whalen (eds), Humana Press, Totowa, NJ; p 37-64.
2. **A. T. Larregina and L. D. Falo, Jr.** (2000) Generating and regulating immune responses through cutaneous gene delivery. *Hum Gene Ther* **11**: 2301-2305.
3. **M. J. Cline**. (1985) Perspectives for gene therapy: inserting new genetic information into mammalian cells by physical techniques and viral vectors. *Pharmacol Ther* **29**: 69-92.
4. **S. C. Hyde, D. R. Gill, C. F. Higgins, A. E. Trezise, L. J. MacVinish, A. W. Cuthbert, R. Ratcliff, M. J. Evans and W. H. Colledge**. (1993) Correction of the ion transport defect in cystic fibrosis transgenic mice by gene therapy. *Nature* **362**: 250-255.
5. **K. H. Choo, K. Raphael, W. McAdam and M. G. Peterson**. (1987) Expression of active human blood clotting factor IX in transgenic mice: use of a cDNA with complete mRNA sequence. *Nucleic Acids Res* **15**: 871-884.
6. **M. Baru, J. H. Axelrod and I. Nur**. (1995) Liposome-encapsulated DNA-mediated gene transfer and synthesis of human factor IX in mice. *Gene* **161**: 143-150.
7. **N. Wivel**. (1995) Human gene transfer trials. *Advanced Drug Delivery Reviews* **17**: 211-212.
8. **J. Uitto and L. Pulkkinen**. (2000) The genodermatoses: candidate diseases for gene therapy. *Hum Gene Ther* **11**: 2267-2275.
9. **P. A. Khavari**. (2000) Genetic correction of inherited epidermal disorders. *Hum Gene Ther* **11**: 2277-2282.
10. **C. R. Middaugh, R. K. Evans, D. L. Montgomery and D. R. Casimiro**. (1998) Analysis of plasmid DNA from a pharmaceutical perspective. *J Pharm Sci* **87**: 130-146.
11. **S. M. Short, W. Rubas, B. D. Paasch and R. J. Mrsny**. (1995) Transport of biologically active interferon-gamma across human skin in vitro. *Pharm Res* **12**: 1140-1145.
12. **M. A. Israel, H. W. Chan, W. P. Rowe and M. A. Martin**. (1979) Molecular cloning of polyoma virus DNA in Escherichia coli: plasmid vector system. *Science* **203**: 883-887.
13. **N. C. Jones, J. D. Richter, D. L. Weeks and L. D. Smith**. (1983) Regulation of adenovirus transcription by an E1a gene in microinjected Xenopus laevis oocytes. *Mol Cell Biol* **3**: 2131-2142.
14. **M. R. Green, T. Maniatis and D. A. Melton**. (1983) Human beta-globin pre-mRNA synthesized in vitro is accurately spliced in Xenopus oocyte nuclei. *Cell* **32**: 681-694.

15. **R. J. Watson, A. M. Colberg-Poley, C. J. Marcus-Sekura, B. J. Carter and L. W. Enquist**. (1983) Characterization of the herpes simplex virus type 1 glycoprotein D mRNA and expression of this protein in Xenopus oocytes. *Nucleic Acids Res* **11**: 1507-1522.
16. **R. L. Brinster, H. Y. Chen, M. Trumbauer, A. W. Senear, R. Warren and R. D. Palmiter**. (1981) Somatic expression of herpes thymidine kinase in mice following injection of a fusion gene into eggs. *Cell* **27**: 223-231.
17. **K. R. Folger, E. A. Wong, G. Wahl and M. R. Capecchi**. (1982) Patterns of integration of DNA microinjected into cultured mammalian cells: evidence for homologous recombination between injected plasmid DNA molecules. *Mol Cell Biol* **2**: 1372-1387.
18. **A. Kudo, F. Yamamoto, M. Furusawa, A. Kuroiwa, S. Natori and M. Obinata**. (1982) Structure of thymidine kinase gene introduced into mouse Ltk- cells by a new injection method. *Gene* **19**: 11-19.
19. **M. R. Capecchi**. (1980) High efficiency transformation by direct microinjection of DNA into cultured mammalian cells. *Cell* **22**: 479-488.
20. **C. Winkler, J. R. Vielkind and M. Schartl**. (1991) Transient expression of foreign DNA during embryonic and larval development of the medaka fish (Oryzias latipes). *Mol Gen Genet* **226**: 129-140.
21. **C. H. Wu, J. M. Wilson and G. Y. Wu**. (1989) Targeting genes: delivery and persistent expression of a foreign gene driven by mammalian regulatory elements in vivo. *J Biol Chem* **264**: 16985-16987.
22. **C. Nicolau, A. Le Pape, P. Soriano, F. Fargette and M. F. Juhel**. (1983) In vivo expression of rat insulin after intravenous administration of the liposome-entrapped gene for rat insulin I. *Proc Natl Acad Sci U S A* **80**: 1068-1072.
23. **U. Wienhues, K. Hosokawa, A. Hoveler, B. Siegmann and W. Doerfler**. (1987) A novel method for transfection and expression of reconstituted DNA-protein complexes in eukaryotic cells. *DNA* **6**: 81-89.
24. **T. von Ruden, L. Stingl, M. Cotten, E. Wagner and K. Zatloukal**. (1995) Generation of high-titer retroviral vectors following receptor-mediated, adenovirus-augmented transfection. *Biotechniques* **18**: 484-489.
25. **H. Nakai, E. Montini, S. Fuess, T. A. Storm, L. Meuse, M. Finegold, M. Grompe and M. A. Kay**. (2003) Helper-independent and AAV-ITR-independent chromosomal integration of double-stranded linear DNA vectors in mice. *Mol Ther* **7**: 101-111.
26. **M. Nishikawa and L. Huang**. (2001) Nonviral vectors in the new millennium: delivery barriers in gene transfer. *Hum Gene Ther* **12**: 861-870.
27. **J. C. Vogel**. (2000) Nonviral skin gene therapy. *Hum Gene Ther* **11**: 2253-2259.
28. **S. Ghazizadeh, R. S. Kalish and L. B. Taichman**. (2003) Immune-mediated loss of transgene expression in skin: implications for cutaneous gene therapy. *Mol Ther* **7**: 296-303.
29. **R. M. Hoffman**. (2003) Immune reactions in skin and hair follicle gene therapy. *Mol Ther* **7**: 294-295.
30. **C. M. Varga, K. Hong and D. A. Lauffenburger**. (2001) Quantitative analysis of synthetic gene delivery vector design properties. *Mol Ther* **4**: 438-446.

31. **R. E. Dickerson, H. R. Drew, B. N. Conner, R. M. Wing, A. V. Fratini and M. L. Kopka**. (1982) The anatomy of A-, B-, and Z-DNA. *Science* **216**: 475-485.
32. **K. Kawabata, Y. Takakura and M. Hashida**. (1995) The fate of plasmid DNA after intravenous injection in mice: involvement of scavenger receptors in its hepatic uptake. *Pharm Res* **12**: 825-830.
33. **X. Meng, D. Sawamura, S. Ina, K. Tamai, K. Hanada and I. Hashimoto**. (2002) Keratinocyte gene therapy: cytokine gene expression in local keratinocytes and in circulation by introducing cytokine genes into skin. *Exp Dermatol* **11**: 456-461.
34. **J. W. Tyrone, J. E. Mogford, L. A. Chandler, C. Ma, Y. Xia, G. F. Pierce and T. A. Mustoe**. (2000) Collagen-embedded platelet-derived growth factor DNA plasmid promotes wound healing in a dermal ulcer model. *J Surg Res* **93**: 230-236.
35. **H. Herweijer and J. A. Wolff**. (2003) Progress and prospects: naked DNA gene transfer and therapy. *Gene Ther* **10**: 453-458.
36. **G. O'Toole, D. MacKenzie, R. Lindeman, M. F. Buckley, D. Marucci, N. McCarthy and M. Poole**. (2002) Vascular endothelial growth factor gene therapy in ischaemic rat skin flaps. *Br J Plast Surg* **55**: 55-58.
37. **S. Chesnoy and L. Huang**. (2000) Structure and function of lipid-DNA complexes for gene delivery. *Annu Rev Biophys Biomol Struct* **29**: 27-47.
38. **M. G. Jeschke, G. Richter, D. N. Herndon, E. K. Geissler, M. Hartl, F. Hofstatter, K. W. Jauch and J. R. Perez-Polo**. (2001) Therapeutic success and efficacy of nonviral liposomal cDNA gene transfer to the skin in vivo is dose dependent. *Gene Ther* **8**: 1777-1784.
39. **J. Zabner, A. J. Fasbender, T. Moninger, K. A. Poellinger and M. J. Welsh**. (1995) Cellular and molecular barriers to gene transfer by a cationic lipid. *J Biol Chem* **270**: 18997-19007.
40. **A. D. Bangham, M. M. Standish and N. Miller**. (1965) Cation permeability of phospholipid model membranes: effect of narcotics. *Nature* **208**: 1295-1297.
41. **D. D. Lasic and D. Papahadjopoulos**. (1995) Liposomes revisited. *Science* **267**: 1275-1276.
42. **R. Fraley, S. Subramani, P. Berg and D. Papahadjopoulos**. (1980) Introduction of liposome-encapsulated SV40 DNA into cells. *J Biol Chem* **255**: 10431-10435.
43. **D. Papahadjopoulos, N. Lopez and A. Gabizon**. Liposomes in drug delivery: from serendipity to drug targeting. In G. Lopez-Berestein and I. Fidler (eds), *Liposomes in the therapy of infectious diseases and cancer* (G. Lopez-Berestein and I. Fidler, eds), Proceedings of a Ciba-Geigy-Squibb-UCLA Colloquium, Liss, Lake Tahoe, California, 1989, pp. 135-154.
44. **P. L. Felgner, T. R. Gadek, M. Holm, R. Roman, H. W. Chan, M. Wenz, J. P. Northrop, G. M. Ringold and M. Danielsen**. (1987) Lipofection: a highly efficient, lipid-mediated DNA-transfection procedure. *Proc Natl Acad Sci U S A* **84**: 7413-7417.
45. **M. Subramanian, J. M. Holopainen, T. Paukku, O. Eriksson, I. Huhtaniemi and P. K. Kinnunen**. (2000) Characterisation of three novel cationic lipids as liposomal complexes with DNA. *Biochim Biophys Acta* **1466**: 289-305.

46. **S. W. Yi, T. Y. Yune, T. W. Kim, H. Chung, Y. W. Choi, I. C. Kwon, E. B. Lee and S. Y. Jeong**. (2000) A cationic lipid emulsion/DNA complex as a physically stable and serum-resistant gene delivery system. *Pharm Res* **17**: 314-320.
47. **Y. Horiguchi, W. A. Larchian, R. Kaplinsky, W. R. Fair and W. D. Heston**. (2000) Intravesical liposome-mediated interleukin-2 gene therapy in orthotopic murine bladder cancer model. *Gene Ther* **7**: 844-851.
48. **L. Baccaglini, A. T. Shamsul Hoque, R. B. Wellner, C. M. Goldsmith, R. S. Redman, V. Sankar, A. Kingman, K. M. Barnhart, C. J. Wheeler and B. J. Baum**. (2001) Cationic liposome-mediated gene transfer to rat salivary epithelial cells in vitro and in vivo. *J Gene Med* **3**: 82-90.
49. **R. Zeisig, A. Ress, I. Fichtner and W. Walther**. (2003) Lipoplexes with alkylphospholipid as new helper lipid for efficient in vitro and in vivo gene transfer in tumor therapy. *Cancer Gene Ther* **10**: 302-311.
50. **A. Elouahabi, V. Flamand, S. Ozkan, F. Paulart, M. Vandenbranden, M. Goldman and J. M. Ruysschaert**. (2003) Free cationic liposomes inhibit the inflammatory response to cationic lipid-DNA complex injected intravenously and enhance its transfection efficiency. *Mol Ther* **7**: 81-88.
51. **B. Wetzer, G. Byk, M. Frederic, M. Airiau, F. Blanche, B. Pitard and D. Scherman**. (2001) Reducible cationic lipids for gene transfer. *Biochem J* **356**: 747-756.
52. **J. A. Boomer, D. H. Thompson and S. M. Sullivan**. (2002) Formation of plasmid-based transfection complexes with an acid-labile cationic lipid: characterization of in vitro and in vivo gene transfer. *Pharm Res* **19**: 1292-1301.
53. **W. J. Choi, J. K. Kim, S. H. Choi, J. S. Park, W. S. Ahn and C. K. Kim**. (2004) Low toxicity of cationic lipid-based emulsion for gene transfer. *Biomaterials* **25**: 5893-5903.
54. **J. A. Gruneich, A. Price, J. Zhu and S. L. Diamond**. (2004) Cationic corticosteroid for nonviral gene delivery. *Gene Ther* **11**: 668-674.
55. **A. Kim, E. H. Lee, S. H. Choi and C. K. Kim**. (2004) In vitro and in vivo transfection efficiency of a novel ultradeformable cationic liposome. *Biomaterials* **25**: 305-313.
56. **D. Gilot, M. L. Miramon, T. Benvegnu, V. Ferrieres, O. Loreal, C. Guguen-Guillouzo, D. Plusquellec and P. Loyer**. (2002) Cationic lipids derived from glycine betaine promote efficient and non-toxic gene transfection in cultured hepatocytes. *J Gene Med* **4**: 415-427.
57. **Y. Perrie, P. M. Frederik and G. Gregoriadis**. (2001) Liposome-mediated DNA vaccination: the effect of vesicle composition. *Vaccine* **19**: 3301-3310.
58. **K. Tabatt, M. Sameti, C. Olbrich, R. H. Muller and C. M. Lehr**. (2004) Effect of cationic lipid and matrix lipid composition on solid lipid nanoparticle-mediated gene transfer. *Eur J Pharm Biopharm* **57**: 155-162.
59. **M. Ouyang, J. S. Remy and F. C. Szoka, Jr.** (2000) Controlled template-assisted assembly of plasmid DNA into nanometric particles with high DNA concentration. *Bioconjug Chem* **11**: 104-112.
60. **M. E. Ferrari, D. Rusalov, J. Enas and C. J. Wheeler**. (2002) Synergy between cationic lipid and co-lipid determines the macroscopic structure and transfection activity of lipoplexes. *Nucleic Acids Res* **30**: 1808-1816.

61. **I. M. Hafez, N. Maurer and P. R. Cullis**. (2001) On the mechanism whereby cationic lipids promote intracellular delivery of polynucleic acids. *Gene Ther* **8**: 1188-1196.
62. **T. Hara, F. Liu, D. Liu and L. Huang**. (1997) Emulsion formulations as a vector for gene delivery in vitro and in vivo. *Adv. Drug Deliv. Rev.* **24**: 265-271.
63. **A. Kikuchi, Y. Aoki, S. Sugaya, T. Serikawa, K. Takakuwa, K. Tanaka, N. Suzuki and H. Kikuchi**. (1999) Development of novel cationic liposomes for efficient gene transfer into peritoneal disseminated tumor. *Hum Gene Ther* **10**: 947-955.
64. **L. A. DeBruyne, K. Li, S. Y. Chan, L. Qin, D. K. Bishop and J. S. Bromberg**. (1998) Lipid-mediated gene transfer of viral IL-10 prolongs vascularized cardiac allograft survival by inhibiting donor-specific cellular and humoral immune responses. *Gene Ther* **5**: 1079-1087.
65. **N. J. Zuidam and Y. Barenholz**. (1999) Characterization of DNA-lipid complexes commonly used for gene delivery. *Int J Pharm* **183**: 43-46.
66. **M. Kerner, O. Meyuhas, D. Hirsch-Lerner, L. J. Rosen, Z. Min and Y. Barenholz**. (2001) Interplay in lipoplexes between type of pDNA promoter and lipid composition determines transfection efficiency of human growth hormone in NIH3T3 cells in culture. *Biochim Biophys Acta* **1532**: 128-136.
67. **M. Sheikh, J. Feig, B. Gee, S. Li and M. Savva**. (2003) In vitro lipofection with novel series of symmetric 1,3-dialkoylamidopropane-based cationic surfactants containing single primary and tertiary amine polar head groups. *Chem Phys Lipids* **124**: 49-61.
68. **T. W. Kim, H. Chung, I. C. Kwon, H. C. Sung and S. Y. Jeong**. (2001) Optimization of lipid composition in cationic emulsion as in vitro and in vivo transfection agents. *Pharm Res* **18**: 54-60.
69. **S. Arpicco, S. Canevari, M. Ceruti, E. Galmozzi, F. Rocco and L. Cattel**. (2004) Synthesis, characterization and transfection activity of new saturated and unsaturated cationic lipids. *Farmaco* **59**: 869-878.
70. **M. Scarzello, V. Chupin, A. Wagenaar, M. C. Stuart, J. B. Engberts and R. Hulst**. (2005) Polymorphism of pyridinium amphiphiles for gene delivery: influence of ionic strength, helper lipid content, and plasmid DNA complexation. *Biophys J* **88**: 2104-2113.
71. **A. Aljaberi, P. Chen and M. Savva**. (2005) Synthesis, in vitro transfection activity and physicochemical characterization of novel N,N'-diacyl-1,2-diaminopropyl-3-carbamoyl-(dimethylaminoethane) amphiphilic derivatives. *Chem Phys Lipids* **133**: 135-149.
72. **L. H. Lindner, R. Brock, D. Arndt-Jovin and H. Eibl**. (2006) Structural variation of cationic lipids: Minimum requirement for improved oligonucleotide delivery into cells. *J Control Release* **110**: 444-456.
73. **H. Farhood, R. Bottega, R. M. Epand and L. Huang**. (1992) Effect of cationic cholesterol derivatives on gene transfer and protein kinase C activity. *Biochim Biophys Acta* **1111**: 239-246.
74. **D. Lesage, A. Cao, D. Briane, N. Lievre, R. Coudert, M. Raphael, J. Salzmann and E. Taillandier**. (2002) Evaluation and optimization of DNA delivery into gliosarcoma 9L cells by a cholesterol-based cationic liposome. *Biochim Biophys Acta* **1564**: 393-402.

75. **X. Zhou and L. Huang**. (1994) DNA transfection mediated by cationic liposomes containing lipopolylysine: characterization and mechanism of action. *Biochim Biophys Acta* **1189**: 195-203.
76. **A. M. Funhoff, C. F. van Nostrum, M. C. Lok, M. M. Fretz, D. J. Crommelin and W. E. Hennink**. (2004) Poly(3-guanidinopropyl methacrylate): A Novel Cationic Polymer for Gene Delivery. *Bioconjug Chem* **15**: 1212-1220.
77. **T. Shangguan, D. Cabral-Lilly, U. Purandare, N. Godin, P. Ahl, A. Janoff and P. Meers**. (2000) A novel N-acyl phosphatidylethanolamine-containing delivery vehicle for spermine-condensed plasmid DNA. *Gene Ther* **7**: 769-783.
78. **D. L. McKenzie, E. Smiley, K. Y. Kwok and K. G. Rice**. (2000) Low molecular weight disulfide cross-linking peptides as nonviral gene delivery carriers. *Bioconjug Chem* **11**: 901-909.
79. **D. L. McKenzie, K. Y. Kwok and K. G. Rice**. (2000) A potent new class of reductively activated peptide gene delivery agents. *J Biol Chem* **275**: 9970-9977.
80. **K. Y. Kwok, Y. Yang and K. G. Rice**. (2001) Evolution of cross-linked non-viral gene delivery systems. *Curr Opin Mol Ther* **3**: 142-146.
81. **L. Collins, K. Gustafsson and J. W. Fabre**. (2000) Tissue-binding properties of a synthetic peptide DNA vector targeted to cell membrane integrins: a possible universal nonviral vector for organ and tissue transplantation. *Transplantation* **69**: 1041-1050.
82. **J. M. Li, L. Collins, X. Zhang, K. Gustafsson and J. W. Fabre**. (2000) Efficient gene delivery to vascular smooth muscle cells using a nontoxic, synthetic peptide vector system targeted to membrane integrins: a first step toward the gene therapy of chronic rejection. *Transplantation* **70**: 1616-1624.
83. **D. G. Affleck, L. Yu, D. A. Bull, S. H. Bailey and S. W. Kim**. (2001) Augmentation of myocardial transfection using TerplexDNA: a novel gene delivery system. *Gene Ther* **8**: 349-353.
84. **L. Yu, H. Suh, J. J. Koh and S. W. Kim**. (2001) Systemic administration of TerplexDNA system: pharmacokinetics and gene expression. *Pharm Res* **18**: 1277-1283.
85. **M. Nishikawa, S. Takemura, F. Yamashita, Y. Takakura, D. K. Meijer, M. Hashida and P. J. Swart**. (2000) Pharmacokinetics and in vivo gene transfer of plasmid DNA complexed with mannosylated poly(L-lysine) in mice. *J Drug Target* **8**: 29-38.
86. **M. Nishikawa, M. Yamauchi, K. Morimoto, E. Ishida, Y. Takakura and M. Hashida**. (2000) Hepatocyte-targeted in vivo gene expression by intravenous injection of plasmid DNA complexed with synthetic multi-functional gene delivery system. *Gene Ther* **7**: 548-555.
87. **K. Anwer, G. Kao, A. Rolland, W. H. Driessen and S. M. Sullivan**. (2004) Peptide-mediated gene transfer of cationic lipid/plasmid DNA complexes to endothelial cells. *J Drug Target* **12**: 215-221.
88. **C. Pichon, C. Goncalves and P. Midoux**. (2001) Histidine-rich peptides and polymers for nucleic acids delivery. *Adv Drug Deliv Rev* **53**: 75-94.
89. **G. Quick, J. van Zyl, A. Hawtrey and M. Ariatti**. (2000) Effect of nicotinic acid conjugated to DNA-transfecting complexes targeted at the transferrin receptor of HeLa cells. *Drug Deliv* **7**: 231-236.

90. **M. Ohsaki, T. Okuda, A. Wada, T. Hirayama, T. Niidome and H. Aoyagi**. (2002) In vitro gene transfection using dendritic poly(L-lysine). *Bioconjug Chem* **13**: 510-517.
91. **C. G. Oster, N. Kim, L. Grode, L. Barbu-Tudoran, A. K. Schaper, S. H. Kaufmann and T. Kissel**. (2005) Cationic microparticles consisting of poly(lactide-co-glycolide) and polyethylenimine as carriers systems for parental DNA vaccination. *J Control Release* **104**: 359-377.
92. **O. Boussif, F. Lezoualc'h, M. A. Zanta, M. D. Mergny, D. Scherman, B. Demeneix and J. P. Behr**. (1995) A versatile vector for gene and oligonucleotide transfer into cells in culture and in vivo: polyethylenimine. *Proc Natl Acad Sci U S A* **92**: 7297-7301.
93. **K. Aoki, S. Furuhata, K. Hatanaka, M. Maeda, J. S. Remy, J. P. Behr, M. Terada and T. Yoshida**. (2001) Polyethylenimine-mediated gene transfer into pancreatic tumor dissemination in the murine peritoneal cavity. *Gene Ther* **8**: 508-514.
94. **L. Wightman, R. Kircheis, V. Rossler, S. Carotta, R. Ruzicka, M. Kursa and E. Wagner**. (2001) Different behavior of branched and linear polyethylenimine for gene delivery in vitro and in vivo. *J Gene Med* **3**: 362-372.
95. **S. Li, Y. Tan, E. Viroonchatapan, B. R. Pitt and L. Huang**. (2000) Targeted gene delivery to pulmonary endothelium by anti-PECAM antibody. *Am J Physiol Lung Cell Mol Physiol* **278**: L504-511.
96. **R. Kircheis, T. Blessing, S. Brunner, L. Wightman and E. Wagner**. (2001) Tumor targeting with surface-shielded ligand--polycation DNA complexes. *J Control Release* **72**: 165-170.
97. **A. R. Thierry, P. Rabinovich, B. Peng, L. C. Mahan, J. L. Bryant and R. C. Gallo**. (1997) Characterization of liposome-mediated gene delivery: expression, stability and pharmacokinetics of plasmid DNA. *Gene Ther* **4**: 226-237.
98. **X. Zhang, L. Collins and J. W. Fabre**. (2001) A powerful cooperative interaction between a fusogenic peptide and lipofectamine for the enhancement of receptor-targeted, non-viral gene delivery via integrin receptors. *J Gene Med* **3**: 560-568.
99. **S. Ina, D. Sawamura, X. Meng, K. Tamai, K. Hanada and I. Hashimoto**. (2000) In vivo gene transfer method in keratinocyte gene therapy: intradermal injection of DNA complexed with high mobility group-1 protein in rats. *Acta Derm Venereol* **80**: 10-13.
100. **L. D. Shea and T. L. Houchin**. (2004) Modular design of non-viral vectors with bioactive components. *Trends Biotechnol* **22**: 429-431.
101. **M. T. da Cruz, S. Simoes and M. C. de Lima**. (2004) Improving lipoplex-mediated gene transfer into C6 glioma cells and primary neurons. *Exp Neurol* **187**: 65-75.
102. **M. C. de Lima, S. Simoes, P. Pires, R. Gaspar, V. Slepushkin and N. Duzgunes**. (1999) Gene delivery mediated by cationic liposomes: from biophysical aspects to enhancement of transfection. *Mol Membr Biol* **16**: 103-109.
103. **X. Zhang, L. Collins, G. J. Sawyer, X. Dong, Y. Qiu and J. W. Fabre**. (2001) In vivo gene delivery via portal vein and bile duct to individual lobes of the rat

liver using a polylysine-based nonviral DNA vector in combination with chloroquine. *Hum Gene Ther* **12**: 2179-2190.

104. **Z. Cui and R. J. Mumper**. (2002) Topical immunization using nanoengineered genetic vaccines. *J Control Release* **81**: 173-184.
105. **S. Zhang, Y. Xu, B. Wang, W. Qiao, D. Liu and Z. Li**. (2004) Cationic compounds used in lipoplexes and polyplexes for gene delivery. *J Control Release* **100**: 165-180.
106. **I. M. Hafez, S. Ansell and P. R. Cullis**. (2000) Tunable pH-sensitive liposomes composed of mixtures of cationic and anionic lipids. *Biophysical Journal* **79**: 1438-1446.
107. **M. Y. Alexander and R. J. Akhurst**. (1995) Liposome-medicated gene transfer and expression via the skin. *Hum Mol Genet* **4**: 2279-2285.
108. **J. Sen and A. Chaudhuri**. (2005) Design, syntheses, and transfection biology of novel non-cholesterol-based guanidinylated cationic lipids. *J Med Chem* **48**: 812-820.
109. **X. Gao and L. Huang**. (1991) A novel cationic liposome reagent for efficient transfection of mammalian cells. *Biochem Biophys Res Commun* **179**: 280-285.
110. **D. Putnam, A. N. Zelikin, V. A. Izumrudov and R. Langer**. (2003) Polyhistidine-PEG:DNA nanocomposites for gene delivery. *Biomaterials* **24**: 4425-4433.
111. **Z. Cui and R. J. Mumper**. (2001) Chitosan-based nanoparticles for topical genetic immunization. *J Control Release* **75**: 409-419.
112. **Z. Yang, B. Song, Q. Li, H. Fan and F. Ouyang**. (2004) Effects of surfactant and acid type on preparation of chitosan microcapsules. *China Particuology* **2**: 70-75.
113. **Q. S. Zhang, B. N. Guo and H. M. Zhang**. (2004) Development and application of gemini surfactants. *Progress in Chemistry* **16**: 343-348.
114. **S. Li, M. A. Rizzo, S. Bhattacharya and L. Huang**. (1998) Characterization of cationic lipid-protamine-DNA (LPD) complexes for intravenous gene delivery. *Gene Ther* **5**: 930-937.
115. **F. M. Menger and J. S. Keiper**. (2000) Gemini Surfactants. *Angew Chem Int Ed Engl* **39**: 1906-1920.
116. **H. S. Rosenzweig, V. A. Rakhmanova and R. C. MacDonald**. (2001) Diquaternary ammonium compounds as transfection agents. *Bioconjug Chem* **12**: 258-263.
117. **R. Zana**. (2002) Dimeric (gemini) surfactants: Effect of the spacer group on the association behavior in aqueous solution. *Journal of Colloid and Interface Science* **248**: 203-220.
118. **S. J. Ryhanen, M. J. Saily, T. Paukku, S. Borocci, G. Mancini, J. M. Holopainen and P. K. J. Kinnunen**. (2003) Surface charge density determines the efficiency of cationic gemini surfactant based lipofection. *Biophysical Journal* **84**: 578-587.
119. **E. Fisicaro, C. Compari, E. Duce, G. Donofrio, B. Rozycka-Roszak and E. Wozniak**. (2005) Biologically active bisquaternary ammonium chlorides: physico-chemical properties of long chain amphiphiles and their evaluation as non-viral vectors for gene delivery. *Biochim Biophys Acta* **1722**: 224-233.

120. **J. Gaucheron, T. Wong, K. F. Wong, N. Maurer and P. R. Cullis**. (2002) Synthesis and properties of novel tetraalkyl cationic lipids. *Bioconjug Chem* **13**: 671-675.
121. **M. L. Fielden, C. Perrin, A. Kremer, M. Bergsma, M. C. Stuart, P. Camilleri and J. B. Engberts**. (2001) Sugar-based tertiary amino gemini surfactants with a vesicle-to-micelle transition in the endosomal pH range mediate efficient transfection in vitro. *Eur J Biochem* **268**: 1269-1279.
122. **P. C. Bell, M. Bergsma, I. P. Dolbnya, W. Bras, M. C. A. Stuart, A. E. Rowan, M. C. Feiters and J. B. F. N. Engberts**. (2003) Transfection mediated by gemini surfactants: Engineered escape from the endosomal compartment. *Journal of the American Chemical Society* **125**: 1551-1558.
123. **P. Camilleri, A. Kremer, A. J. Edwards, K. H. Jennings, O. Jenkins, I. Marshall, C. McGregor, W. Neville, S. Q. Rice, R. J. Smith, M. J. Wilkinson and A. J. Kirby**. (2000) A novel class of cationic gemini surfactants showing efficient in vitro gene transfection properties. *Chemical Communications* 1253-1254.
124. **C. McGregor, C. Perrin, M. Monck, P. Camilleri and A. J. Kirby**. (2001) Rational approaches to the design of cationic gemini surfactants for gene delivery. *J Am Chem Soc* **123**: 6215-6220.
125. **L. Karlsson, M. C. P. van Eijk and O. Soderman**. (2002) Compaction of DNA by gemini surfactants: Effects of surfactant architecture. *Journal of Colloid and Interface Science* **252**: 290-296.
126. **P. J. J. A. Buijnsters, C. L. G. Rodriguez, E. L. Willighagen, N. A. J. M. Sommerdijk, A. Kremer, P. Camilleri, M. C. Feiters, R. J. M. Nolte and B. Zwanenburg**. (2002) Cationic gemini Surfactants based on tartaric acid: Synthesis, aggregation, monolayer behaviour, and interaction with DNA. *European Journal of Organic Chemistry* 1397-1406.
127. **L. Karlsson, M. van Eijk and O. Soderman**. (2002) Compaction of DNA by gemini surfactants: Effects of surfactant architecture. *J Colloid Interface Sci* **252**: 290-296.
128. **P. A. Monnard, T. Oberholzer and P. Luisi**. (1997) Entrapment of nucleic acids in liposomes. *Biochim Biophys Acta* **1329**: 39-50.
129. **Y. Perrie and G. Gregoriadis**. (2000) Liposome-entrapped plasmid DNA: characterisation studies. *Biochim Biophys Acta* **1475**: 125-132.
130. **J. Gustafsson, G. Arvidson, G. Karlsson and M. Almgren**. (1995) Complexes between cationic liposomes and DNA visualized by cryo-TEM. *Biochim Biophys Acta* **1235**: 305-312.
131. **D. Simberg, D. Danino, Y. Talmon, A. Minsky, M. E. Ferrari, C. J. Wheeler and Y. Barenholz**. (2001) Phase behavior, DNA ordering, and size instability of cationic lipoplexes. Relevance to optimal transfection activity. *J Biol Chem* **276**: 47453-47459.
132. **F. Artzner, R. Zantl and J. O. Radler**. (2000) Lipid-DNA and lipid-polyelectrolyte mesophases: structure and exchange kinetics. *Cell Mol Biol (Noisy-le-grand)* **46**: 967-978.
133. **D. Uhrikova, M. Hanulova, S. S. Funari, I. Lacko, F. Devinsky and P. Balgavy**. (2004) The structure of DNA-DLPC-cationic gemini surfactant

aggregates: a small angle synchrotron X-ray diffraction study. *Biophys Chem* **111**: 197-204.

134. **D. Uhrikova, I. Zajac, M. Dubnickova, M. Pisarcik, S. S. Funari, G. Rapp and P. Balgavy**. (2005) Interaction of gemini surfactants butane-1,4-diyl-bis(alkyldimethylammonium bromide) with DNA. *Colloids Surf B Biointerfaces* **42**: 59-68.
135. **B. Sternberg, K. Hong, W. Zheng and D. Papahadjopoulos**. (1998) Ultrastructural characterization of cationic liposome-DNA complexes showing enhanced stability in serum and high transfection activity in vivo. *Biochim Biophys Acta* **1375**: 23-35.
136. **J. Gaucheron, C. Santaella and P. Vierling**. (2001) In vitro gene transfer with a novel galactosylated spermine bolaamphiphile. *Bioconjug Chem* **12**: 569-575.
137. **P. Pires, S. Simoes, S. Nir, R. Gaspar, N. Duzgunes and M. C. Pedroso de Lima**. (1999) Interaction of cationic liposomes and their DNA complexes with monocytic leukemia cells. *Biochim Biophys Acta* **1418**: 71-84.
138. **D. S. Friend, D. Papahadjopoulos and R. J. Debs**. (1996) Endocytosis and intracellular processing accompanying transfection mediated by cationic liposomes. *Biochim Biophys Acta* **1278**: 41-50.
139. **S. W. Hui, M. Langner, Y. L. Zhao, P. Ross, E. Hurley and K. Chan**. (1996) The role of helper lipids in cationic liposome-mediated gene transfer. *Biophys J* **71**: 590-599.
140. **M. R. Almofti, H. Harashima, Y. Shinohara, A. Almofti, Y. Baba and H. Kiwada**. (2003) Cationic liposome-mediated gene delivery: biophysical study and mechanism of internalization. *Arch Biochem Biophys* **410**: 246-253.
141. **G. Caracciolo, D. Pozzi, H. Amenitsch and R. Caminiti**. (2005) Multicomponent cationic lipid-DNA complex formation: role of lipid mixing. *Langmuir* **21**: 11582-11587.
142. **N. J. Zuidam, D. Hirsch-Lerner, S. Margulies and Y. Barenholz**. (1999) Lamellarity of cationic liposomes and mode of preparation of lipoplexes affect transfection efficiency. *Biochim Biophys Acta* **1419**: 207-220.
143. **P. C. Ross and S. W. Hui**. (1999) Lipoplex size is a major determinant of in vitro lipofection efficiency. *Gene Ther* **6**: 651-659.
144. **A. J. Fasbender, J. Zabner and M. J. Welsh**. (1995) Optimization of cationic lipid-mediated gene transfer to airway epithelia. *Am J Physiol* **269**: L45-51.
145. **M. Singh and M. Ariatti**. (2005) A cationic cytofectin with long spacer mediates favourable transfection in transformed human epithelial cells. *Int J Pharm*.
146. **Y. Xu, S. W. Hui, P. Frederik and F. C. Szoka, Jr.** (1999) Physicochemical characterization and purification of cationic lipoplexes. *Biophysical Journal* **77**: 341-353.
147. **R. J. Lee and L. Huang**. (1996) Folate-targeted, anionic liposome-entrapped polylysine-condensed DNA for tumor cell-specific gene transfer. *J Biol Chem* **271**: 8481-8487.
148. **W. Guo and R. L. Lee**. (1999) Receptor-targeted gene delivery via folate-conjugated polyethylenimine. *AAPS PharmSci* **1**: E19.

149. **E. Mastrobattista, R. H. Kapel, M. H. Eggenhuisen, P. J. Roholl, D. J. Crommelin, W. E. Hennink and G. Storm**. (2001) Lipid-coated polyplexes for targeted gene delivery to ovarian carcinoma cells. *Cancer Gene Ther* **8**: 405-413.
150. **B. Schwartz, C. Benoist, B. Abdallah, D. Scherman, J. P. Behr and B. A. Demeneix**. (1995) Lipospermine-based gene transfer into the newborn mouse brain is optimized by a low lipospermine/DNA charge ratio. *Hum Gene Ther* **6**: 1515-1524.
151. **K. Takeuchi, M. Ishihara, C. Kawaura, M. Noji, T. Furuno and M. Nakanishi**. (1996) Effect of zeta potential of cationic liposomes containing cationic cholesterol derivatives on gene transfection. *FEBS Lett* **397**: 207-209.
152. **A. J. Lin, N. L. Slack, A. Ahmad, C. X. George, C. E. Samuel and C. R. Safinya**. (2003) Three-dimensional imaging of lipid gene-carriers: membrane charge density controls universal transfection behavior in lamellar cationic liposome-DNA complexes. *Biophys J* **84**: 3307-3316.
153. **I. Badea, R. Verrall, M. Baca-Estrada, S. Tikoo, A. Rosenberg, P. Kumar and M. Foldvari**. (2005) In vivo cutaneous interferon-gamma gene delivery using novel dicationic (gemini) surfactant-plasmid complexes. *J Gene Med* **7**: 1200-1214.
154. **I. Koltover, T. Salditt, J. O. Radler and C. R. Safinya**. (1998) An inverted hexagonal phase of cationic liposome-DNA complexes related to DNA release and delivery. *Science* **281**: 78-81.
155. **J. O. Radler, I. Koltover, T. Salditt and C. R. Safinya**. (1997) Structure of DNA-cationic liposome complexes: DNA intercalation in multilamellar membranes in distinct interhelical packing regimes. *Science* **275**: 810-814.
156. **R. S. Dias, B. Lindman and M. G. Miguel**. (2002) DNA interaction with catanionic vesicles. *Journal of Physical Chemistry B* **106**: 12600-12607.
157. **S. Zhou, D. Liang, C. Burger, F. Yeh and B. Chu**. (2004) Nanostructures of complexes formed by calf thymus DNA interacting with cationic surfactants. *Biomacromolecules* **5**: 1256-1261.
158. **C. M. Wiethoff, M. L. Gill, G. S. Koe, J. G. Koe and C. R. Middaugh**. (2002) The structural organization of cationic lipid-DNA complexes. *J Biol Chem* **277**: 44980-44987.
159. **Y. S. Tarahovsky, V. A. Rakhmanova, R. M. Epand and R. C. MacDonald**. (2002) High temperature stabilization of DNA in complexes with cationic lipids. *Biophysical Journal* **82**: 264-273.
160. **I. S. Zuhorn, U. Bakowsky, E. Polushkin, W. H. Visser, M. C. Stuart, J. B. Engberts and D. Hoekstra**. (2005) Nonbilayer phase of lipoplex-membrane mixture determines endosomal escape of genetic cargo and transfection efficiency. *Mol Ther* **11**: 801-810.
161. **M. Foldvari, I. Badea, S. Wettig, R. Verrall and M. Bagonluri**. (2006) Structural characterization of novel micro- and nano-scale non-viral DNA delivery systems for cutaneous gene therapy. *Journal of Experimental Nanoscience* **Accepted for publication**.
162. **S. May and A. Ben-Shaul**. (2004) Modeling of cationic lipid-DNA complexes. *Curr Med Chem* **11**: 151-167.

163. **T. Fujiwara, S. Hasegawa, N. Hirashima, M. Nakanishi and T. Ohwada**. (2000) Gene transfection activities of amphiphilic steroid-polyamine conjugates. *Biochim Biophys Acta* **1468**: 396-402.
164. **D. Niculescu-Duvaz, J. Heyes and C. J. Springer**. (2003) Structure-activity relationship in cationic lipid mediated gene transfection. *Curr Med Chem* **10**: 1233-1261.
165. **J. C. Birchall, C. A. Waterworth, C. Luscombe, D. A. Parkins and M. Gumbleton**. (2001) Statistical modelling of the formulation variables in non-viral gene delivery systems. *J Drug Target* **9**: 169-184.
166. **Z. Shi, D. T. Curiel and D. C. Tang**. (1999) DNA-based non-invasive vaccination onto the skin. *Vaccine* **17**: 2136-2141.
167. **F. Spirito, G. Meneguzzi, O. Danos and M. Mezzina**. (2001) Cutaneous gene transfer and therapy: the present and the future. *J Gene Med* **3**: 21-31.
168. **N. Raghavachari and W. E. Fahl**. (2002) Targeted gene delivery to skin cells in vivo: a comparative study of liposomes and polymers as delivery vehicles. *J Pharm Sci* **91**: 615-622.
169. **J. Wepierre and J.-P. Marty**. (1979) Percutaneous absorption of drugs. *Trends in Pharmacological Sciences* 23-26.
170. **M. Heisig, R. Lieckfeldt, G. Wittum, G. Mazurkevich and G. Lee**. (1996) Non steady-state descriptions of drug permeation through stratum corneum. I. The biphasic brick-and-mortar model. *Pharm Res* **13**: 421-426.
171. **K. Tojo**. (1987) Random brick model for drug transport across stratum corneum. *J Pharm Sci* **76**: 889-891.
172. **W. R. Pfister and D. S. Hsieh**. (1990) Permeation enhancers compatible with transdermal drug delivery systems. Part I: selection and formulation considerations. *Med Device Technol* **1**: 48-55.
173. **R. C. Wester and H. I. Maibach**. (1992) Percutaneous absorption of drugs. *Clin Pharmacokinet* **23**: 253-266.
174. **D. Sawamura, M. Akiyama and H. Shimizu**. (2002) Direct injection of naked DNA and cytokine transgene expression: implications for keratinocyte gene therapy. *Clin Exp Dermatol* **27**: 480-484.
175. **J. C. Vogel**. (1999) A direct in vivo approach for skin gene therapy. *Proc Assoc Am Physicians* **111**: 190-197.
176. **D. Sawamura, K. Yasukawa, K. Kodama, K. Yokota, K. C. Sato-Matsumura, T. Toshihiro and H. Shimizu**. (2002) The majority of keratinocytes incorporate intradermally injected plasmid DNA regardless of size but only a small proportion of cells can express the gene product. *J Invest Dermatol* **118**: 967-971.
177. **A. C. Chu and J. F. Morris**. (2005) The keratinocyte. In *Skin Immune System (SIS)*, J. D. Boss (eds), CRC Press, Boca Raton; p 77-100.
178. **M. Hasegawa, M. Fujimoto, K. Takehara and S. Sato**. (2005) Pathogenesis of systemic sclerosis: altered B cell function is the key linking systemic autoimmunity and tissue fibrosis. *J Dermatol Sci* **39**: 1-7.
179. **A. Bouloc, P. Walker, J. C. Grivel, J. C. Vogel and S. I. Katz**. (1999) Immunization through dermal delivery of protein-encoding DNA: a role for migratory dendritic cells. *Eur J Immunol* **29**: 446-454.

180. **R. J. Mumper and H. C. Ledebur, Jr.** (2001) Dendritic cell delivery of plasmid DNA. Applications for controlled genetic immunization. *Mol Biotechnol* **19**: 79-95.
181. **A. T. Larregina, S. C. Watkins, G. Erdos, L. A. Spencer, W. J. Storkus, D. Beer Stolz and L. D. Falo, Jr.** (2001) Direct transfection and activation of human cutaneous dendritic cells. *Gene Ther* **8**: 608-617.
182. **Chu**. (1997). In *Skin Immune System (SIS)*, J. Bos (eds), CRC Press, Boca Raton; p.
183. **F. M. Watt**. (2000) Epidermal stem cells as targets for gene transfer. *Hum Gene Ther* **11**: 2261-2266.
184. **E. Dellambra, G. Pellegrini, L. Guerra, G. Ferrari, G. Zambruno, F. Mavilio and M. De Luca**. (2000) Toward epidermal stem cell-mediated ex vivo gene therapy of junctional epidermolysis bullosa. *Hum Gene Ther* **11**: 2283-2287.
185. **C. E. Thomas, A. Ehrhardt and M. A. Kay**. (2003) Progress and problems with the use of viral vectors for gene therapy. *Nat Rev Genet* **4**: 346-358.
186. **J. H. Felgner, R. Kumar, C. N. Sridhar, C. J. Wheeler, Y. J. Tsai, R. Border, P. Ramsey, M. Martin and P. L. Felgner**. (1994) Enhanced gene delivery and mechanism studies with a novel series of cationic lipid formulations. *J Biol Chem* **269**: 2550-2561.
187. **J. Y. Legendre and F. C. Szoka, Jr.** (1992) Delivery of plasmid DNA into mammalian cell lines using pH-sensitive liposomes: comparison with cationic liposomes. *Pharm Res* **9**: 1235-1242.
188. **C. Staedel, J. S. Remy, Z. Hua, T. R. Broker, L. T. Chow and J. P. Behr**. (1994) High-efficiency transfection of primary human keratinocytes with positively charged lipopolyamine:DNA complexes. *J Invest Dermatol* **102**: 768-772.
189. **S. Zellmer, F. Gaunitz, J. Salvetter, A. Surovoy, D. Reissig and R. Gebhardt**. (2001) Long-term expression of foreign genes in normal human epidermal keratinocytes after transfection with lipid/DNA complexes. *Histochem Cell Biol* **115**: 41-47.
190. **M. J. Bennett, M. H. Nantz, R. P. Balasubramaniam, D. C. Gruenert and R. W. Malone**. (1995) Cholesterol enhances cationic liposome-mediated DNA transfection of human respiratory epithelial cells. *Biosci Rep* **15**: 47-53.
191. **O. Freund, P. Mahy, J. Amedee, D. Roux and R. Laversanne**. (2000) Encapsulation of DNA in new multilamellar vesicles prepared by shearing a lyotropic lamellar phase. *J Microencapsul* **17**: 157-168.
192. **Y. Setoguchi, H. A. Jaffe, C. Danel and R. G. Crystal**. (1994) Ex vivo and in vivo gene transfer to the skin using replication-deficient recombinant adenovirus vectors. *J Invest Dermatol* **102**: 415-421.
193. **A. J. Gerrard, D. L. Hudson, G. G. Brownlee and F. M. Watt**. (1993) Towards gene therapy for haemophilia B using primary human keratinocytes. *Nat Genet* **3**: 180-183.
194. **J. C. Birchall, C. Marichal, L. Campbell, A. Alwan, J. Hadgraft and M. Gumbleton**. (2000) Gene expression in an intact ex-vivo skin tissue model following percutaneous delivery of cationic liposome-plasmid DNA complexes. *Int J Pharm* **197**: 233-238.

195. **E. Raz, D. A. Carson, S. E. Parker, T. B. Parr, A. M. Abai, G. Aichinger, S. H. Gromkowski, M. Singh, D. Lew, M. A. Yankauckas and et al.** (1994) Intradermal gene immunization: the possible role of DNA uptake in the induction of cellular immunity to viruses. *Proc Natl Acad Sci U S A* **91**: 9519-9523.
196. **Y. Sato, M. Roman, H. Tighe, D. Lee, M. Corr, M. D. Nguyen, G. J. Silverman, M. Lotz, D. A. Carson and E. Raz**. (1996) Immunostimulatory DNA sequences necessary for effective intradermal gene immunization. *Science* **273**: 352-354.
197. **U. R. Hengge, E. F. Chan, R. A. Foster, P. S. Walker and J. C. Vogel**. (1995) Cytokine gene expression in epidermis with biological effects following injection of naked DNA. *Nat Genet* **10**: 161-166.
198. **J. Haensler, C. Verdelet, V. Sanchez, Y. Girerd-Chambaz, A. Bonnin, E. Trannoy, S. Krishnan and P. Meulien**. (1999) Intradermal DNA immunization by using jet-injectors in mice and monkeys. *Vaccine* **17**: 628-638.
199. **D. Sawamura, S. Ina, K. Itai, X. Meng, A. Kon, K. Tamai, K. Hanada and I. Hashimoto**. (1999) In vivo gene introduction into keratinocytes using jet injection. *Gene Ther* **6**: 1785-1787.
200. **H. Fan, Q. Lin, G. R. Morrissey and P. A. Khavari**. (1999) Immunization via hair follicles by topical application of naked DNA to normal skin. *Nat Biotechnol* **17**: 870-872.
201. **L. Li and R. M. Hoffman**. (1995) The feasibility of targeted selective gene therapy of the hair follicle. *Nat Med* **1**: 705-706.
202. **S. Watabe, K. Q. Xin, A. Ihata, L. J. Liu, A. Honsho, I. Aoki, K. Hamajima, B. Wahren and K. Okuda**. (2001) Protection against influenza virus challenge by topical application of influenza DNA vaccine. *Vaccine* **19**: 4434-4444.
203. **W. H. Yu, M. Kashani-Sabet, D. Liggitt, D. Moore, T. D. Heath and R. J. Debs**. (1999) Topical gene delivery to murine skin. *J Invest Dermatol* **112**: 370-375.
204. **J. A. Mikszta, J. B. Alarcon, J. M. Brittingham, D. E. Sutter, R. J. Pettis and N. G. Harvey**. (2002) Improved genetic immunization via micromechanical disruption of skin-barrier function and targeted epidermal delivery. *Nat Med* **8**: 415-419.
205. **M. R. Prausnitz**. (2004) Microneedles for transdermal drug delivery. *Adv Drug Deliv Rev* **56**: 581-587.
206. **S. Kaushik, A. H. Hord, D. D. Denson, D. V. McAllister, S. Smitra, M. G. Allen and M. R. Prausnitz**. (2001) Lack of pain associated with microfabricated microneedles. *Anesth Analg* **92**: 502-504.
207. **Z. Cui, L. Baizer and R. J. Mumper**. (2003) Intradermal immunization with novel plasmid DNA-coated nanoparticles via a needle-free injection device. *J Biotechnol* **102**: 105-115.
208. **Z. Cui, W. Fountain, M. Clark, M. Jay and R. J. Mumper**. (2003) Novel ethanol-in-fluorocarbon microemulsions for topical genetic immunization. *Pharm Res* **20**: 16-23.
209. **S. Babiuk, M. E. Baca-Estrada, R. Pontarollo and M. Foldvari**. (2002) Topical delivery of plasmid DNA using biphasic lipid vesicles (Biphasix). *J Pharm Pharmacol* **54**: 1609-1614.

210. **S. M. Niemiec, J. M. Latta, C. Ramachandran, N. D. Weiner and B. J. Roessler**. (1997) Perifollicular transgenic expression of human interleukin-1 receptor antagonist protein following topical application of novel liposome-plasmid DNA formulations in vivo. *J Pharm Sci* **86**: 701-708.
211. **H. Wu, C. Ramachandran, A. U. Bielinska, K. Kingzett, R. Sun, N. D. Weiner and B. J. Roessler**. (2001) Topical transfection using plasmid DNA in a water-in-oil nanoemulsion. *Int J Pharm* **221**: 23-34.
212. **J. Glasspool-Malone, S. Somiari, J. J. Drabick and R. W. Malone**. (2000) Efficient nonviral cutaneous transfection. *Mol Ther* **2**: 140-146.
213. **S. N. Ciotti and N. Weiner**. (2002) Follicular liposomal delivery systems. *J Liposome Res* **12**: 143-148.
214. **A. L. Rakhmilevich, J. Turner, M. J. Ford, D. McCabe, W. H. Sun, P. M. Sondel, K. Grota and N. S. Yang**. (1996) Gene gun-mediated skin transfection with interleukin 12 gene results in regression of established primary and metastatic murine tumors. *Proc Natl Acad Sci U S A* **93**: 6291-6296.
215. **Z. Siprashvili and P. A. Khavari**. (2004) Lentivectors for regulated and reversible cutaneous gene delivery. *Mol Ther* **9**: 93-100.
216. **T. Sakamoto, E. Miyazaki, Y. Aramaki, H. Arima, M. Takahashi, Y. Kato, M. Koga and S. Tsuchiya**. (2004) Improvement of dermatitis by iontophoretically delivered antisense oligonucleotides for interleukin-10 in NC/Nga mice. *Gene Ther* **11**: 317-324.
217. **Y. N. Kalia, A. Naik, J. Garrison and R. H. Guy**. (2004) Iontophoretic drug delivery. *Adv Drug Deliv Rev* **56**: 619-658.
218. **J. Gehl**. (2003) Electroporation: theory and methods, perspectives for drug delivery, gene therapy and research. *Acta Physiol Scand* **177**: 437-447.
219. **S. Babiuk, M. E. Baca-Estrada, M. Foldvari, L. Baizer, R. Stout, M. Storms, D. Rabussay, G. Widera and L. Babiuk**. (2003) Needle-free topical electroporation improves gene expression from plasmids administered in porcine skin. *Mol Ther* **8**: 992-998.
220. **M. Foldvari, A. Gesztes and M. Mezei**. (1990) Dermal drug delivery by liposome encapsulation: clinical and electron microscopic studies. *J Microencapsul* **7**: 479-489.
221. **M. Foldvari, M. E. Baca-Estrada, Z. He, J. Hu, S. Attah-Poku and M. King**. (1999) Dermal and transdermal delivery of protein pharmaceuticals: lipid-based delivery systems for interferon alpha. *Biotechnol Appl Biochem* **30 (Pt 2)**: 129-137.
222. **M. E. Baca-Estrada, M. Foldvari, C. Ewen, I. Badea and L. A. Babiuk**. (2000) Effects of IL-12 on immune responses induced by transcutaneous immunization with antigens formulated in a novel lipid-based biphasic delivery system. *Vaccine* **18**: 1847-1854.
223. **M. E. Baca-Estrada, M. Foldvari, S. L. Babiuk and L. A. Babiuk**. (2000) Vaccine delivery: lipid-based delivery systems. *J Biotechnol* **83**: 91-104.
224. **A. Morita, K. Ariizumi, R. Ritter, 3rd, J. V. Jester, T. Kumamoto, S. A. Johnston and A. Takashima**. (2001) Development of a Langerhans cell-targeted gene therapy format using a dendritic cell-specific promoter. *Gene Ther* **8**: 1729-1737.

225. **A. Domashenko, S. Gupta and G. Cotsarelis**. (2000) Efficient delivery of transgenes to human hair follicle progenitor cells using topical lipoplex. *Nat Biotechnol* **18**: 420-423.
226. **T. L. Whiteside, J. G. Worrall, R. K. Prince, R. B. Buckingham and G. P. Rodnan**. (1985) Soluble mediators from mononuclear cells increase the synthesis of glycosaminoglycan by dermal fibroblast cultures derived from normal subjects and progressive systemic sclerosis patients. *Arthritis Rheum* **28**: 188-197.
227. **A. N. Sapadin, A. C. Esser and R. Fleischmajer**. (2001) Immunopathogenesis of scleroderma--evolving concepts. *Mt Sinai J Med* **68**: 233-242.
228. **S. Moschella and H. Hurley**. (1992) Connective tissue diseases. In *Dermatology*, 3rd ed, S. Moschella and H. Hurley (eds), W.B. Saunders Company, Philadelphia; p 1233-1245.
229. **D. Weedon**. (2002) Disorders of collagen. In *Skin Pathology*, Second, D. Weedon (eds), Churchill Livingstone, London; p 346-350.
230. **G. Lakos, S. Takagawa, S. J. Chen, A. M. Ferreira, G. Han, K. Masuda, X. J. Wang, L. A. DiPietro and J. Varga**. (2004) Targeted disruption of TGF-beta/Smad3 signaling modulates skin fibrosis in a mouse model of scleroderma. *Am J Pathol* **165**: 203-217.
231. **T. L. McGaha and C. A. Bona**. (2002) Role of profibrogenic cytokines secreted by T cells in fibrotic processes in scleroderma. *Autoimmun Rev* **1**: 174-181.
232. **A. K. Ghosh, W. Yuan, Y. Mori, S. Chen and J. Varga**. (2001) Antagonistic regulation of type I collagen gene expression by interferon-gamma and transforming growth factor-beta. Integration at the level of p300/CBP transcriptional coactivators. *J Biol Chem* **276**: 11041-11048.
233. **K. Higashi, Y. Inagaki, K. Fujimori, A. Nakao, H. Kaneko and I. Nakatsuka**. (2003) Interferon-gamma interferes with transforming growth factor-beta signaling through direct interaction of YB-1 with Smad3. *J Biol Chem* **278**: 43470-43479.
234. **T. Luger, S. Beisert and T. Schwarz**. (1997) The epidermal cytokine network. In *Skin Immune System (SIS)*, J. Bos (eds), CRC Press, Boca Raton; p 271-310.
235. **M. L. McCullough**. (2000) Primary cutaneous scleroses. In *Pathology of the Skin*, Second, E. R. Farmer and A. F. Hood (eds), McGraw-Hill, New York; p 426-430.
236. **L. D. Siracusa, R. McGrath, Q. Ma, J. J. Moskow, J. Manne, P. J. Christner, A. M. Buchberg and S. A. Jimenez**. (1996) A tandem duplication within the fibrillin 1 gene is associated with the mouse tight skin mutation. *Genome Res* **6**: 300-313.
237. **D. N. Menton, R. A. Hess, J. R. Lichtenstein and A. Eisen**. (1978) The structure and tensile properties of the skin of tight-skin (Tsk) mutant mice. *J Invest Dermatol* **70**: 4-10.
238. **T. G. Osborn, N. E. Bauer, S. C. Ross, T. L. Moore and J. Zuckner**. (1983) The tight-skin mouse: physical and biochemical properties of the skin. *J Rheumatol* **10**: 793-796.
239. **J. L. Pablos, E. T. Everett, R. Harley, E. C. LeRoy and J. S. Norris**. (1995) Transforming growth factor-beta 1 and collagen gene expression during postnatal skin development and fibrosis in the tight-skin mouse. *Lab Invest* **72**: 670-678.

240. **J. L. Pablos, E. T. Everett and J. S. Norris**. (2004) The tight skin mouse: an animal model of systemic sclerosis. *Clin Exp Rheumatol* **22**: S81-85.
241. **R. G. Phelps, C. Daian, S. Shibata, R. Fleischmajer and C. A. Bona**. (1993) Induction of skin fibrosis and autoantibodies by infusion of immunocompetent cells from tight skin mice into C57BL/6 Pa/Pa mice. *J Autoimmun* **6**: 701-718.
242. **D. A. Oble and H. S. Teh**. (2001) Tight skin mouse subcutaneous hypertrophy can occur in the absence of alphabeta T cell receptor-bearing lymphocytes. *J Rheumatol* **28**: 1852-1855.
243. **R. M. Baxter, T. P. Crowell, M. E. McCrann, E. M. Frew and H. Gardner**. (2005) Analysis of the tight skin (Tsk1/+) mouse as a model for testing antifibrotic agents. *Lab Invest* **85**: 1199-1209.
244. **P. J. Christner, J. Peters, D. Hawkins, L. D. Siracusa and S. A. Jimenez**. (1995) The tight skin 2 mouse. An animal model of scleroderma displaying cutaneous fibrosis and mononuclear cell infiltration. *Arthritis Rheum* **38**: 1791-1798.
245. **J. Gentiletti, L. J. McCloskey, C. M. Artlett, J. Peters, S. A. Jimenez and P. J. Christner**. (2005) Demonstration of autoimmunity in the tight skin-2 mouse: a model for scleroderma. *J Immunol* **175**: 2418-2426.
246. **T. Yamamoto and K. Nishioka**. (2005) Cellular and molecular mechanisms of bleomycin-induced murine scleroderma: current update and future perspective. *Exp Dermatol* **14**: 81-95.
247. **Y. Zhang, L. L. McCormick, S. R. Desai, C. Wu and A. C. Gilliam**. (2002) Murine sclerodermatous graft-versus-host disease, a model for human scleroderma: cutaneous cytokines, chemokines, and immune cell activation. *J Immunol* **168**: 3088-3098.
248. **C. S. Samuel, C. Zhao, Q. Yang, H. Wang, H. Tian, G. W. Tregear and E. P. Amento**. (2005) The relaxin gene knockout mouse: a model of progressive scleroderma. *J Invest Dermatol* **125**: 692-699.
249. **X. J. Wang, D. A. Greenhalgh, J. R. Bickenbach, A. Jiang, D. S. Bundman, T. Krieg, R. Derynck and D. R. Roop**. (1997) Expression of a dominant-negative type II transforming growth factor beta (TGF-beta) receptor in the epidermis of transgenic mice blocks TGF-beta-mediated growth inhibition. *Proc Natl Acad Sci U S A* **94**: 2386-2391.
250. **S. D. Sule and F. M. Wigley**. (2003) Treatment of scleroderma: an update. *Expert Opin Investig Drugs* **12**: 471-482.
251. **Y. Braun-Moscovici and D. E. Furst**. (2002) Stem cell therapy in scleroderma. *Curr Opin Rheumatol* **14**: 711-716.
252. **P. A. McSweeney, R. A. Nash, K. M. Sullivan, J. Storek, L. J. Crofford, R. Dansey, M. D. Mayes, K. T. McDonagh, J. L. Nelson, T. A. Gooley, L. A. Holmberg, C. S. Chen, M. H. Wener, K. Ryan, J. Sunderhaus, K. Russell, J. Rambharose, R. Storb and D. E. Furst**. (2002) High-dose immunosuppressive therapy for severe systemic sclerosis: initial outcomes. *Blood* **100**: 1602-1610.
253. **G. Giannelli, F. Iannone, F. Marinosci, G. Lapadula and S. Antonaci**. (2005) The effect of bosentan on matrix metalloproteinase-9 levels in patients with systemic sclerosis-induced pulmonary hypertension. *Curr Med Res Opin* **21**: 327-332.

254. **J. H. Korn, M. Mayes, M. Matucci Cerinic, M. Rainisio, J. Pope, E. Hachulla, E. Rich, P. Carpentier, J. Molitor, J. R. Seibold, V. Hsu, L. Guillevin, S. Chatterjee, H. H. Peter, J. Coppock, A. Herrick, P. A. Merkel, R. Simms, C. P. Denton, D. Furst, N. Nguyen, M. Gaitonde and C. Black**. (2004) Digital ulcers in systemic sclerosis: prevention by treatment with bosentan, an oral endothelin receptor antagonist. *Arthritis Rheum* **50**: 3985-3993.
255. **M. Ramos-Casals, P. Brito-Zeron, N. Nardi, G. Claver, G. Risco, F. D. Parraga, S. Fernandez, M. Julia and J. Font**. (2004) Successful treatment of severe Raynaud's phenomenon with bosentan in four patients with systemic sclerosis. *Rheumatology (Oxford)* **43**: 1454-1456.
256. **S. J. Oliver, A. Moreira and G. Kaplan**. (2000) Immune stimulation in scleroderma patients treated with thalidomide. *Clin Immunol* **97**: 109-120.
257. **T. McGaha, T. Kodera, R. Phelps, H. Spiera, M. Pines and C. Bona**. (2002) Effect of halofuginone on the development of tight skin (TSK) syndrome. *Autoimmunity* **35**: 277-282.
258. **G. J. Fisher and S. Kang**. (2002) Phototherapy for scleroderma: biologic rationale, results, and promise. *Curr Opin Rheumatol* **14**: 723-726.
259. **D. E. Furst**. (2000) Rational therapy in the treatment of systemic sclerosis. *Curr Opin Rheumatol* **12**: 540-544.
260. **A. N. Sapadin and R. Fleischmajer**. (2002) Treatment of scleroderma. *Arch Dermatol* **138**: 99-105.
261. **R. W. Simms and J. H. Korn**. (2002) Cytokine directed therapy in scleroderma: rationale, current status, and the future. *Curr Opin Rheumatol* **14**: 717-722.
262. **J. Man and M. T. Dytoc**. (2004) Use of imiquimod cream 5% in the treatment of localized morphea. *J Cutan Med Surg* **8**: 166-169.
263. **J. Tsuji-Yamada, M. Nakazawa, K. Takahashi, K. Iijima, S. Hattori, K. Okuda, M. Minami, Z. Ikezawa and T. Sasaki**. (2001) Effect of IL-12 encoding plasmid administration on tight-skin mouse. *Biochem Biophys Res Commun* **280**: 707-712.
264. **H. Ihn, K. Yamane, M. Kubo and K. Tamaki**. (2001) Blockade of endogenous transforming growth factor beta signaling prevents up-regulated collagen synthesis in scleroderma fibroblasts: association with increased expression of transforming growth factor beta receptors. *Arthritis Rheum* **44**: 474-480.
265. **X. Zhou, F. K. Tan, J. D. Reveille, D. Wallis, D. M. Milewicz, C. Ahn, A. Wang and F. C. Arnett**. (2002) Association of novel polymorphisms with the expression of SPARC in normal fibroblasts and with susceptibility to scleroderma. *Arthritis Rheum* **46**: 2990-2999.
266. **A. R. Harrop, A. Ghahary, P. G. Scott, N. Forsyth, A. Uji-Friedland and E. E. Tredget**. (1995) Regulation of collagen synthesis and mRNA expression in normal and hypertrophic scar fibroblasts in vitro by interferon-gamma. *J Surg Res* **58**: 471-477.
267. **R. L. Widom**. (2000) Regulation of matrix biosynthesis and degradation in systemic sclerosis. *Curr Opin Rheumatol* **12**: 534-539.
268. **W. Yuan, T. Yufit, L. Li, Y. Mori, S. J. Chen and J. Varga**. (1999) Negative modulation of alpha1(I) procollagen gene expression in human skin fibroblasts: transcriptional inhibition by interferon-gamma. *J Cell Physiol* **179**: 97-108.

269. **T. Yamamoto, S. Takagawa, M. Kuroda and K. Nishioka**. (2000) Effect of interferon-gamma on experimental scleroderma induced by bleomycin. *Arch Dermatol Res* **292**: 362-365.
270. **B. Freundlich, S. A. Jimenez, V. D. Steen, T. A. Medsger, Jr., M. Szkolnicki and H. S. Jaffe**. (1992) Treatment of systemic sclerosis with recombinant interferon-gamma. A phase I/II clinical trial. *Arthritis Rheum* **35**: 1134-1142.
271. **P. G. Vlachoyiannopoulos, N. Tsifetaki, I. Dimitriou, D. Galaris, S. A. Papiris and H. M. Moutsopoulos**. (1996) Safety and efficacy of recombinant gamma interferon in the treatment of systemic sclerosis. *Ann Rheum Dis* **55**: 761-768.
272. **H. Lortat-Jacob, F. Baltzer and J. A. Grimaud**. (1996) Heparin decreases the blood clearance of interferon-gamma and increases its activity by limiting the processing of its carboxyl-terminal sequence. *J Biol Chem* **271**: 16139-16143.
273. **J. U. Gutterman, M. G. Rosenblum, A. Rios, H. A. Fritsche and J. R. Quesada**. (1984) Pharmacokinetic study of partially pure gamma-interferon in cancer patients. *Cancer Res* **44**: 4164-4171.
274. **N. Hunzelmann, S. Anders, G. Fierlbeck, R. Hein, K. Herrmann, M. Albrecht, S. Bell, R. Muche, J. Wehner-Caroli, W. Gaus and T. Krieg**. (1997) Double-blind, placebo-controlled study of intralesional interferon gamma for the treatment of localized scleroderma. *J Am Acad Dermatol* **36**: 433-435.
275. **United States Pharmacopeial Convention**. (2006) *USP DI. Drug information for the health care professional*, 26th ed, Thomson Micromedex, Greenwood Village.
276. **A. Grassegger and R. Hopfl**. (2004) Significance of the cytokine interferon gamma in clinical dermatology. *Clin Exp Dermatol* **29**: 584-588.
277. **U. Boehm, T. Klamp, M. Groot and J. C. Howard**. (1997) Cellular responses to interferon-gamma. *Annu Rev Immunol* **15**: 749-795.
278. **E. Falcoff, N. J. Taranto, C. E. Remondegui, J. P. Dedet, L. M. Canini, C. M. Ripoll, L. Dimier-David, F. Vargas, L. A. Gimenez, J. G. Bernabo and et al.** (1994) Clinical healing of antimony-resistant cutaneous or mucocutaneous leishmaniasis following the combined administration of interferon-gamma and pentavalent antimonial compounds. *Trans R Soc Trop Med Hyg* **88**: 95-97.
279. **S. M. Holland, E. M. Eisenstein, D. B. Kuhns, M. L. Turner, T. A. Fleisher, W. Strober and J. I. Gallin**. (1994) Treatment of refractory disseminated nontuberculous mycobacterial infection with interferon gamma. A preliminary report. *N Engl J Med* **330**: 1348-1355.
280. **T. T. Chang and S. R. Stevens**. (2002) Atopic dermatitis: the role of recombinant interferon-gamma therapy. *Am J Clin Dermatol* **3**: 175-183.
281. **B. Pittet, L. Rubbia-Brandt, A. Desmouliere, A. P. Sappino, P. Roggero, S. Guerret, J. A. Grimaud, R. Lacher, D. Montandon and G. Gabbiani**. (1994) Effect of gamma-interferon on the clinical and biologic evolution of hypertrophic scars and Dupuytren's disease: an open pilot study. *Plast Reconstr Surg* **93**: 1224-1235.
282. **J. M. Kirkwood, J. Bryant, J. H. Schiller, M. M. Oken, E. C. Borden and T. L. Whiteside**. (1997) Immunomodulatory function of interferon-gamma in patients with metastatic melanoma: results of a phase II-B trial in subjects with

metastatic melanoma, ECOG study E 4987. Eastern Cooperative Oncology Group. *J Immunother* **20**: 146-157.
283. **M. Pines and A. Nagler**. (1998) Halofuginone: a novel antifibrotic therapy. *Gen Pharmacol* **30**: 445-450.
284. **T. Z. Kirk, M. E. Mark, C. C. Chua, B. H. Chua and M. D. Mayes**. (1995) Myofibroblasts from scleroderma skin synthesize elevated levels of collagen and tissue inhibitor of metalloproteinase (TIMP-1) with two forms of TIMP-1. *J Biol Chem* **270**: 3423-3428.
285. **T. Hasegawa, A. Nakao, K. Sumiyoshi, R. Tsuboi and H. Ogawa**. (2003) IFN-gamma fails to antagonize fibrotic effect of TGF-beta on keloid-derived dermal fibroblasts. *J Dermatol Sci* **32**: 19-24.
286. **E. N. Unemori, E. A. Bauer and E. P. Amento**. (1992) Relaxin alone and in conjunction with interferon-gamma decreases collagen synthesis by cultured human scleroderma fibroblasts. *J Invest Dermatol* **99**: 337-342.
287. **P. W. Gray and D. V. Goeddel**. (1983) Cloning and expression of murine immune interferon cDNA. *Proc Natl Acad Sci U S A* **80**: 5842-5846.
288. **K. Dorsch-Hasler, G. M. Keil, F. Weber, M. Jasin, W. Schaffner and U. H. Koszinowski**. (1985) A long and complex enhancer activates transcription of the gene coding for the highly abundant immediate early mRNA in murine cytomegalovirus. *Proc Natl Acad Sci U S A* **82**: 8325-8329.
289. **P. C. Familletti, S. Rubinstein and S. Pestka**. (1981) A convenient and rapid cytopathic effect inhibition assay for interferon. *Methods Enzymol* **78**: 387-394.
290. **H. M. Cherwinski, J. H. Schumacher, K. D. Brown and T. R. Mosmann**. (1987) Two types of mouse helper T cell clone. III. Further differences in lymphokine synthesis between Th1 and Th2 clones revealed by RNA hybridization, functionally monospecific bioassays, and monoclonal antibodies. *J Exp Med* **166**: 1229-1244.
291. **M. W. Pfaffl**. (2001) A new mathematical model for relative quantification in real-time RT-PCR. *Nucleic Acids Res* **29**: e45.
292. **P. V. Konarev, V. V. Volkov, A. V. Sokolova, M. H. J. Koch and D. I. Svergun**. (2003) PRIMUS: a Windows PC-based system for small-angle scattering data analysis. *Journal of Applied Crystallography* **36**: 1277-1282.
293. **S. K. Jang, H. G. Krausslich, M. J. Nicklin, G. M. Duke, A. C. Palmenberg and E. Wimmer**. (1988) A segment of the 5' nontranslated region of encephalomyocarditis virus RNA directs internal entry of ribosomes during in vitro translation. *J Virol* **62**: 2636-2643.
294. **P. J. Lewis, G. J. Cox, S. van Drunen Littel-van den Hurk and L. A. Babiuk**. (1997) Polynucleotide vaccines in animals: enhancing and modulating responses. *Vaccine* **15**: 861-864.
295. **C. Bello-Fernandez, J. Stasakova, A. Renner, N. Carballido-Perrig, M. Koening, M. Waclavicek, O. Madjic, L. Oehler, O. Haas, J. M. Carballido, M. Buschle and W. Knapp**. (2003) Retrovirus-mediated IL-7 expression in leukemic dendritic cells generated from primary acute myelogenous leukemias enhances their functional properties. *Blood* **101**: 2184-2190.
296. **I. Rutenfranz and H. Kirchner**. (1988) Pharmacokinetics of recombinant murine interferon-gamma in mice. *J Interferon Res* **8**: 573-580.

297. **N. Ulker and C. E. Samuel**. (1985) Mechanism of interferon action: inhibition of vesicular stomatitis virus replication in human amnion U cells by cloned human gamma-interferon. I. Effect on early and late stages of the viral multiplication cycle. *J Biol Chem* **260**: 4319-4323.
298. **Y. P. Zhang, D. L. Reimer, G. Zhang, P. H. Lee and M. B. Bally**. (1997) Self-assembling DNA-lipid particles for gene transfer. *Pharm Res* **14**: 190-196.
299. **W. Yu, A. Shimoyama, T. Uneda, S. Obika, K. Miyashita, T. Doi and T. Imanishi**. (1999) Gene transfer mediated by YKS-220 cationic particles: convenient and efficient gene delivery reagent. *J Biochem (Tokyo)* **125**: 1034-1038.
300. **J. C. Birchall, I. W. Kellaway and S. N. Mills**. (1999) Physico-chemical characterisation and transfection efficiency of lipid-based gene delivery complexes. *Int J Pharm* **183**: 195-207.
301. **T. Minko**. (2006) Colloids. In *Martin"s Physical Pharmacy and Pharmaceutical Sciences*, 5th, P. J. Sinko (eds), Lippincott Williams & Wilkins, Baltimore; p 469-498.
302. **N. Pongcharoenkiat, G. Narsimhan, R. T. Lyons and S. L. Hem**. (2002) The effect of surface charge and partition coefficient on the chemical stability of solutes in O/W emulsions. *J Pharm Sci* **91**: 559-570.
303. **S. J. Eastman, C. Siegel, J. Tousignant, A. E. Smith, S. H. Cheng and R. K. Scheule**. (1997) Biophysical characterization of cationic lipid: DNA complexes. *Biochim Biophys Acta* **1325**: 41-62.
304. **N. Miyazawa, T. Sakaue, K. Yoshikawa and R. Zana**. (2005) Rings-on-a-string chain structure in DNA. *J Chem Phys* **122**: 44902.
305. **Z. Zhang, W. Huang, J. Tang, E. Wang and S. Dong**. (2002) Conformational transition of DNA induced by cationic lipid vesicle in acidic solution: spectroscopy investigation. *Biophys Chem* **97**: 7-16.
306. **N. J. Zuidam, Y. Barenholz and A. Minsky**. (1999) Chiral DNA packaging in DNA-cationic liposome assemblies. *FEBS Lett* **457**: 419-422.
307. **N. J. Zuidam and Y. Barenholz**. (1998) Electrostatic and structural properties of complexes involving plasmid DNA and cationic lipids commonly used for gene delivery. *Biochim Biophys Acta* **1368**: 115-128.
308. **A. J. Geall and I. S. Blagbrough**. (2000) Rapid and sensitive ethidium bromide fluorescence quenching assay of polyamine conjugate-DNA interactions for the analysis of lipoplex formation in gene therapy. *J Pharm Biomed Anal* **22**: 849-859.
309. **C. M. Wiethoff, M. L. Gill, G. S. Koe, J. G. Koe and C. R. Middaugh**. (2003) A fluorescence study of the structure and accessibility of plasmid DNA condensed with cationic gene delivery vehicles. *J Pharm Sci* **92**: 1272-1285.
310. **A. Yaghmur, L. de Campo, A. Aserin, N. Garti and O. Glatter**. (2004) Structural characterization of five-component food grade oil-in-water nonionic microemulsions. *Physical Chemistry Chemical Physics* **6**: 1524-1533.
311. **R. Winter and R. Kohling**. (2004) Static and time-resolved synchrotron small-angle x-ray scattering studies of lyotropic lipid mesophases, model biomembranes and proteins in solution. *Journal of Physics-Condensed Matter* **16**: S327-S352.

312. **S. C. Hyde, K. W. Southern, U. Gileadi, E. M. Fitzjohn, K. A. Mofford, B. E. Waddell, H. C. Gooi, C. A. Goddard, K. Hannavy, S. E. Smyth, J. J. Egan, F. L. Sorgi, L. Huang, A. W. Cuthbert, M. J. Evans, W. H. Colledge, C. F. Higgins, A. K. Webb and D. R. Gill**. (2000) Repeat administration of DNA/liposomes to the nasal epithelium of patients with cystic fibrosis. *Gene Ther* **7**: 1156-1165.
313. **N. J. Caplen, E. W. Alton, P. G. Middleton, J. R. Dorin, B. J. Stevenson, X. Gao, S. R. Durham, P. K. Jeffery, M. E. Hodson, C. Coutelle and et al.** (1995) Liposome-mediated CFTR gene transfer to the nasal epithelium of patients with cystic fibrosis. *Nat Med* **1**: 39-46.
314. **D. A. Godwin, N. H. Kim and L. A. Felton**. (2002) Influence of Transcutol CG on the skin accumulation and transdermal permeation of ultraviolet absorbers. *Eur J Pharm Biopharm* **53**: 23-27.
315. **M. Foldvari, P. Kumar, M. King, R. Batta, D. Michel, I. Badea and M. Wloch**. (2006) Gene delivery into human skin in vitro using biphasic lipid vesicles. *Curr Drug Deliv* **3**: 89-93.
316. **L. Djordjevic, M. Primorac, M. Stupar and D. Krajisnik**. (2004) Characterization of caprylocaproyl macrogolglycerides based microemulsion drug delivery vehicles for an amphiphilic drug. *Int J Pharm* **271**: 11-19.
317. **J. Y. Cherng, N. M. Schuurmans-Nieuwenbroek, W. Jiskoot, H. Talsma, N. J. Zuidam, W. E. Hennink and D. J. Crommelin**. (1999) Effect of DNA topology on the transfection efficiency of poly((2-dimethylamino)ethyl methacrylate)-plasmid complexes. *J Control Release* **60**: 343-353.
318. **P. C. Bell, M. Bergsma, I. P. Dolbnya, W. Bras, M. C. Stuart, A. E. Rowan, M. C. Feiters and J. B. Engberts**. (2003) Transfection mediated by gemini surfactants: engineered escape from the endosomal compartment. *Journal of the American Chemical Society* **125**: 1551-1558.
319. **F. Podlogar, M. Gasperlin, M. Tomsic, A. Jamnik and M. B. Rogac**. (2004) Structural characterisation of water-Tween 40/Imwitor 308-isopropyl myristate microemulsions using different experimental methods. *Int J Pharm* **276**: 115-128.
320. **K. Sugibayashi, S. Nakayama, T. Seki, K. Hosoya and Y. Morimoto**. (1992) Mechanism of skin penetration-enhancing effect by laurocapram. *J Pharm Sci* **81**: 58-64.
321. **S. D. Wettig and R. E. Verrall**. (2001) Thermodynamic Studies of Aqueous m-s-m Gemini Surfactant Systems. *J Colloid Interface Sci* **235**: 310-316.
322. **E. Alami, G. Beinert, P. Marie and R. Zana**. (1993) Alkanediyl-Alpha,Omega-Bis(Dimethylalkylammonium Bromide) Surfactants .3. Behavior at the Air-Water-Interface. *Langmuir* **9**: 1465-1467.
323. **X. D. Chen, J. B. Wang, N. Shen, Y. H. Luo, L. Li, M. H. Liu and R. K. Thomas**. (2002) Gemini surfactant/DNA complex monolayers at the air-water interface: Effect of surfactant structure on the assembly, stability, and topography of monolayers. *Langmuir* **18**: 6222-6228.
324. **E. Dauty, J. S. Remy, T. Blessing and J. P. Behr**. (2001) Dimerizable cationic detergents with a low cmc condense plasmid DNA into nanometric particles and transfect cells in culture. *J Am Chem Soc* **123**: 9227-9234.

325. **B. Mui, Q. F. Ahkong, L. Chow and M. J. Hope**. (2000) Membrane perturbation and the mechanism of lipid-mediated transfer of DNA into cells. *Biochim Biophys Acta* **1467**: 281-292.
326. **N. J. Caplen, E. Kinrade, F. Sorgi, X. Gao, D. Gruenert, D. Geddes, C. Coutelle, L. Huang, E. W. Alton and R. Williamson**. (1995) In vitro liposome-mediated DNA transfection of epithelial cell lines using the cationic liposome DC-Chol/DOPE. *Gene Ther* **2**: 603-613.
327. **T. Nomura, K. Yasuda, T. Yamada, S. Okamoto, R. I. Mahato, Y. Watanabe, Y. Takakura and M. Hashida**. (1999) Gene expression and antitumor effects following direct interferon (IFN)-gamma gene transfer with naked plasmid DNA and DC-chol liposome complexes in mice. *Gene Ther* **6**: 121-129.
328. **D. R. Gill, K. W. Southern, K. A. Mofford, T. Seddon, L. Huang, F. Sorgi, A. Thomson, L. J. MacVinish, R. Ratcliff, D. Bilton, D. J. Lane, J. M. Littlewood, A. K. Webb, P. G. Middleton, W. H. Colledge, A. W. Cuthbert, M. J. Evans, C. F. Higgins and S. C. Hyde**. (1997) A placebo-controlled study of liposome-mediated gene transfer to the nasal epithelium of patients with cystic fibrosis. *Gene Ther* **4**: 199-209.
329. **D. K. Dalton, S. Pitts-Meek, S. Keshav, I. S. Figari, A. Bradley and T. A. Stewart**. (1993) Multiple defects of immune cell function in mice with disrupted interferon-gamma genes. *Science* **259**: 1739-1742.
330. **T. L. McGaha, R. G. Phelps, H. Spiera and C. Bona**. (2002) Halofuginone, an inhibitor of type-I collagen synthesis and skin sclerosis, blocks transforming-growth-factor-beta-mediated Smad3 activation in fibroblasts. *J Invest Dermatol* **118**: 461-470.
331. **A. Kahan, B. Amor, C. J. Menkes and G. Strauch**. (1989) Recombinant interferon-gamma in the treatment of systemic sclerosis. *Am J Med* **87**: 273-277.
332. **R. Hein, J. Behr, M. Hundgen, N. Hunzelmann, M. Meurer, O. Braun-Falco, A. Urbanski and T. Krieg**. (1992) Treatment of systemic sclerosis with gamma-interferon. *Br J Dermatol* **126**: 496-501.
333. **R. P. Polisson, G. S. Gilkeson, E. H. Pyun, D. S. Pisetsky, E. A. Smith and L. S. Simon**. (1996) A multicenter trial of recombinant human interferon gamma in patients with systemic sclerosis: effects on cutaneous fibrosis and interleukin 2 receptor levels. *J Rheumatol* **23**: 654-658.
334. **N. Hunzelmann, S. Anders, G. Fierlbeck, R. Hein, K. Herrmann, M. Albrecht, S. Bell, J. Thur, R. Muche, B. Adelmann-Grill, J. Wehner-Caroli, W. Gaus and T. Krieg**. (1997) Systemic scleroderma. Multicenter trial of 1 year of treatment with recombinant interferon gamma. *Arch Dermatol* **133**: 609-613.
335. **N. Dujardin, P. Van Der Smissen and V. Preat**. (2001) Topical gene transfer into rat skin using electroporation. *Pharm Res* **18**: 61-66.
336. **S. Wang, S. Joshi and S. Lu**. (2004) Delivery of DNA to skin by particle bombardment. *Methods Mol Biol* **245**: 185-196.
337. **Z. Cui and R. J. Mumper**. (2003) Microparticles and nanoparticles as delivery systems for DNA vaccines. *Crit Rev Ther Drug Carrier Syst* **20**: 103-137.
338. **J. M. Carroll, T. Crompton, J. P. Seery and F. M. Watt**. (1997) Transgenic mice expressing IFN-gamma in the epidermis have eczema, hair hypopigmentation, and hair loss. *J Invest Dermatol* **108**: 412-422.

339. **M. T. Lin, F. Wang, J. Uitto and K. Yoon**. (2001) Differential expression of tissue-specific promoters by gene gun. *Br J Dermatol* **144**: 34-39.
340. **D. Schaarschmidt, J. Baltin, I. M. Stehle, H. J. Lipps and R. Knippers**. (2004) An episomal mammalian replicon: sequence-independent binding of the origin recognition complex. *Embo J* **23**: 191-201.